THESIS

SOLID-STATE NMR (^{13}C, ^{27}Al AND ^{29}Si) STUDY OF THE REACTION BETWEEN $AlMe_3$ AND THE SILICA GEL SURFACE

Submitted by

Jianhua Li

Department of Chemistry

In partial fulfillment of the requirements

for the Degree of Master of Science

Colorado State University

Fort Collins, Colorado

Fall 2007

COLORADO STATE UNIVERSITY

April 3rd, 2006

WE HEREBY RECOMMEND THAT THE THESIS PREPARED UNDER OUT SUPERVISION BY JIANHUA LI ENTITLED, "SOLID-STATE NMR (^{13}C, ^{27}Al AND ^{29}Si) STUDY OF THE REACTION BETWEEN $AlMe_3$ AND THE SILICA GEL SURFACE", BE ACCEPTED AS FULFILLING IN PART REQUIREMENTS FOR THE DEGREE OF MASTER OF SCIENCE.

Committee on Graduate work

Adviser

Department Head

ABSTRACT OF THESIS

SOLID-STATE NMR (^{13}C, ^{27}Al AND ^{29}Si) STUDY OF THE REACTION BETWEEN $AlMe_3$ AND THE SILICA GEL SURFACE

The reaction between the silica gel surface and trimethylaluminum ($AlMe_3$) has been studied in this thesis research. We have examined the $AlMe_3$/silica reaction in the following stages: the initial $AlMe_3$-reacted silica surface after it had been treated with $AlMe_3$; the $AlMe_3$-treated surface after it was washed with dry diethyl ether; the ether-washed surface after it was treated, in steps, with limited amounts of H_2O; and finally the H_2O-reacted surface after an excess-H_2O work-up.

Solid-state NMR (^{13}C, ^{27}Al and ^{29}Si) have been used to elucidate the structures of moieties generated on the silica gel surface at each of the stages listed above. Solid-state ^{13}C NMR showed that $Al(Me)_n$ is the major type of moieties generated on the surface in the initial $AlMe_3$/silica reaction and Si-OMe is the second most important moiety generated. After the sample has been washed with dry diethyl ether, strong ether signals were observed by ^{13}C NMR, which implies that diethyl ether is strongly attached to the surface, even after evacuation. There are no significant changes for the other surface moieties after the diethyl ether treatment. In the series of limited-amount H_2O treatments that followed, the $AlMe_n$ signal intensity decreased as more H_2O was added to the

surface. In the sample resulting from the final (excess H_2O) work-up, $AlMe_n$ and Si-OMe moieties are completely gone and peaks corresponding to Si-Me and $Si(Me)_2$ are the only signals left in the ^{13}C NMR spectrum.

In the ^{29}Si NMR spectra, the signal intensity of the $(SiO)_3\mathbf{Si}(OH)$ (Q_3) peak typical of silica dropped after the $AlMe_3$ treatment. Q_3 signal intensity was replaced with a broad peak centered at about –104 ppm, as expected for a conversion in which most of the Si-OH groups on the silica surface have reacted with $AlMe_3$ and turned into Si-O-Al moieties. The formation of Si-Me, $Si(Me)_2$ and $Si(Me)_3$ moieties were also observed in the ^{29}Si spectra. ^{29}Si spectra didn't show significant changes in the sample-treatment stages that follow the initial $AlMe_3/SiO_2$ reaction.

In the ^{27}Al spectra of $AlMe_3$-treated silica samples, 4-, 5- and 6-coordinate Al moieties were observed. In the initial reacted sample, 5-coordinate Al moieties are the major initial products from the reaction. After the samples were washed with diethyl ether, the 5-coordinate Al moieties are still the major moieties. With limited amounts of H_2O introduced onto the surface, the $AlMe_n$ moieties reacted with H_2O, as shown by the ^{13}C spectra; in ^{27}Al NMR spectra, signal intensity of 5-coordinate Al moieties decreased, while that of 4- and 6-coordinate Al moieties increased, which implies that the 5-coordinate Al moieties turned into 4- and 6-coordinate Al moieties as a result of reaction with H_2O. On the final work-up surface, the 4- and 6-coordinate Al moieties are the major Al structures remaining on the surface. This is the first observation of this kind of change of Al

atom coordination on a $AlMe_3$-reacted silica surface. The structures of surface Al moieties are much more complicated than those proposed in previous publications on $AlMe_3$/silica reactions.

In the initial reaction between $AlMe_3$ and silica gel, we also made quantitative measurements aimed at tracking the route of methyl groups in the whole system. The methane generated during the reaction was trapped in a $N_2(l)$-cooled trap and the volume of trapped methane was measured as a gas with the water-displacement method. Unreacted Al-Me groups in the supernatant liquid were measured by the liquid-sample ^{13}C NMR spin-counting method. The amount of methyl groups attached on the silica surface were measured by the solid-state ^{13}C NMR spin-counting method. The total amount of methyl groups tracked in the $AlMe_3$/silica/toluene system is about 108% of the amount of methyl groups present in the initial $AlMe_3$ and is about 90% for the $AlMe_3$/silica/cyclo-hexane system.

Relaxation studies were carried out on both the initial $AlMe_3$-reacted and ether-washed $AlMe_3$/silica samples using ^{13}C CP/MAS NMR. The methyl-group proton T_1 values were measured by the saturation-recovery technique and the cross polarization relaxation time (T^{CH}) and rotating-frame proton spin-lattice relaxation time ($T_{1\rho}$) were measured using variable-contact-time experiments. The $AlMe_n$ moieties in the initial $AlMe_3$-reacted sample showed very long (5 s ~ 7 s) proton T_1 values, which implies that the $AlMe_n$ moieties may be in a very restrained environment. This result supports the existence of 5-coordination Al

structures indicated from ^{27}Al results; in these structures methyl groups are bridged/shared between adjacent $AlMe_n$ moieties. After the initial $AlMe_3$-reacted silica sample was washed with diethyl ether, methyl-group proton T_1 values were reduced by half, which may be due to replacing the methyl bridges with electron-rich centers consisting of the O atoms of the ether molecules introduced by the washing. This interpretation also explains why we have strong ether signals in ^{13}C NMR spectra of the ether-washed sample and in the H_2O-treated samples that followed.

Overall, the moieties generated in the $AlMe_3$/silica reaction have been characterized by solid-state NMR methods in this thesis work. And, methods were developed which quantitatively characterize the fate of all the Al-Me groups added into the reaction system.

Jianhua Li
Chemistry Department
Colorado State University
Fort Collins, Colorado 80523
Fall 2007

Acknowledgement

First, I would like to thank my advisor, Dr. Gary E Maciel, for his ideas and guidance through the whole research work, for his patience and assistance on preparing this thesis manuscript and for giving the opportunities and the financial support for my academic study. Second, I sincerely appreciate the generous help and advice from Dr. Joseph DiVerdi, on both scientific and instrumental aspects. I also want to thank all the other previous group members, Ting Tao, Herman Lock, Mark Seger, Camille Keeler, Jiwen Feng and Shaokuan Zheng, for their help through these years in the laboratory.

I would like to express my deepest appreciation to my mother and father, for the encouragement and the constant support they gave me through my whole life. A very special thanks to my friends, Ni and Linshi, I am so grateful for having you as my best friends. Finally, to my boy friend, Yong, thank you for being with me for these years.

Dedicated to my mother and father. Love you all.

TABLE OF CONTENTS

Chapter 1.

BACKGROUND, INTRODUCTION AND LITERATURE REVIEW OF MODIFICATION/METHYLATION OF THE SILICA GEL SURFACE BY TRIMETHYLALUMINUM

1.1. Historical perspectives on silica gel.

1.1.1. Silica gel and its physical properties.

Silica, which is composed of the two most abundant elements in the earth's crust, silicon and oxygen, is represented by the chemical formula SiO_2. Silica can be found naturally in both crystalline and amorphous forms, and it is usually found in nature as quartz, cristobalite or tridymite crystals[1]. In 1861, silica gel was first synthesized by Sir Thomas Graham, by dialyzing dilute silica sols made from mixing a dilute aqueous solution of sodium silicate with hydrochloric acid. Since then silica gel has become a well-known and very important substance involved in many applications in chemical science, such as in chromatographic science (HPLC, LC, TLC) and catalyst science, etc. In chromatographic science, it has been used as a very polar stationary phase; modified silica gel is commonly used to improve liquid-solid phase separation. In catalyst science, it has been used as a skeleton to support functional groups on its surface to form solid catalysts.

Silica gel is a highly porous, amorphous substance. Internally silica gel is constructed by the cross-linking of Si-O-Si linkages and contains Si-O-H moieties

on the surface. The structure of silica can be represented with the following two-dimensional representation:

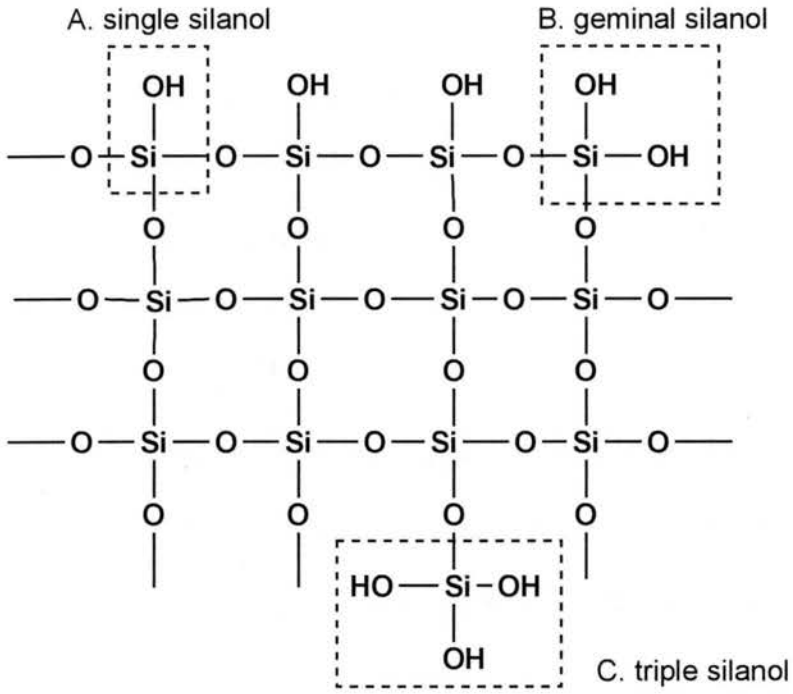

Figure 1.1. Basic framework of silica gel and three kinds of silanols: A) single silanol; B) geminal silanol; C) triple silanol.

The above figure shows the basic framework of silica and surface silanols: single silanols, geminal silanols and triple silanols (very rare). As shown in the figure, the framework of a silica particle consists largely of one silicon atom connected with four oxygen atoms by siloxane (silicon-oxygen-silicon bond) linkage. On the surface of the framework, there are some residual, uncondensed hydroxyl groups left from original synthesis steps.

The surface hydroxyl groups, which are called silanol (-Si-O-H) groups, are what make the surface of silica gel very polar and slightly acidic. Furthermore, it is these hydroxyl groups, and the hydrogen bonds formed between them, which yield the most important chemical properties of silica. These silanols are very

reactive towards chemical reagents to form new surface bonds and give new properties to the modified silica gel for specific purposes (e.g., changes in the surface polarity, or for catalytic purposes).

The physical properties of a silica surface are generally described by:

(i) pore volume or porosity;

(ii) specific surface area;

(iii) particle size;

(iv) size dispersion.[2]

The pore volume or porosity gives an indication of physical strength of the silica gel and the pore size. If the pore volume is large, it indicates that the silica gel has large pore size but its mechanical strength is consequently relatively decreased.[2]

The IUPAC (International Union of Pure and Applied Chemistry) has recommended a classification for porous materials, in which the voids in a material with a pore size less than 2 nm in diameter are termed "micropores"; the voids in a material with a pore diameter between 2 and 50 nm are termed "mesopores", and those with pore size (diameter) greater than 50 nm are termed "macropores". Silica gels have pores with a wide range of diameters – typically between 5 Å and 3000 Å. Silica gels possess pores of all three ranges, but the majority of the pore sizes fall in the mesopore regime, with relatively few micropores. Commonly used mesoporous silica materials with BET surface areas of 100-300 m^2/g and mesopore sizes of 4-15 nm will have pore volumes of 0.2-0.6 cm^3/g.[2]

The surface area dictates the amount of adsorption of small molecules that could occur on the surface.[2] The surface area is generally measured by the BET method.[2] The surface areas of silica gels can vary from 100 m^2/g to 800 m^2/g due to different manufacturing methods and processing conditions. The large surface area makes it possible for silica gel to function as a good absorbent, comparable to other commonly used the absorbents: activated carbon (1100 m^2/g), activated alumina (290 m^2/g).

The particle diameter of a silica is important in determining the packing characteristics of a stationary phase in chromatography; this characteristic is related to column efficiency. The dispersion of the particle size is also important, since it is related with the column packing difficulty.[2] Thus, silica gel particles are typically purchased with a specific particle size distribution. In HPLC practice, the narrower the particle size distribution, the more uniform packing in the chromatographic column can be achieved, and the more efficient the column will be. The presence of larger-size particles effects only the column efficiency, but the presence of very small particles (fines), less than 1 μm, may lead to clogging of the column frit and an increase of the column backpressure.

1.1.2. Silica gel and its chemical properties.

As described above, silanols (Si-OH groups) are the major reactive components on the silica surface after manufacturing. According to the different silicon bonding structures, as seen in Figure 1.1, there can be three major types of silanols on the surface: a *single silanol* is a silicon site with a single hydroxyl group attached and has three siloxane (Si-O-Si) linkages connecting it to the

silica framework. A *geminal silanol* has two hydroxyl groups attached to the same silicon atom, which is connected to the framework by two siloxane linkages. A *triple silanol* (rarely encountered), has three hydroxyl groups attached to the same silicon atom, which is connected to the framework by only one siloxane linkage. The single silanol groups are the most common one on the surface, then the next most common one is geminal silanols. The triple silanols are only rarely observed.

Within the classification, "single silanols", people also use the terms, 'isolated silanol' and 'vicinal silanol' to classify the single silanols. Isolated silanols are single silanols that are sufficiently far apart that they cannot be hydrogen-bonded to other silanols; and vicinal silanols are single silanols which are close enough to be hydrogen-bonded:[3]

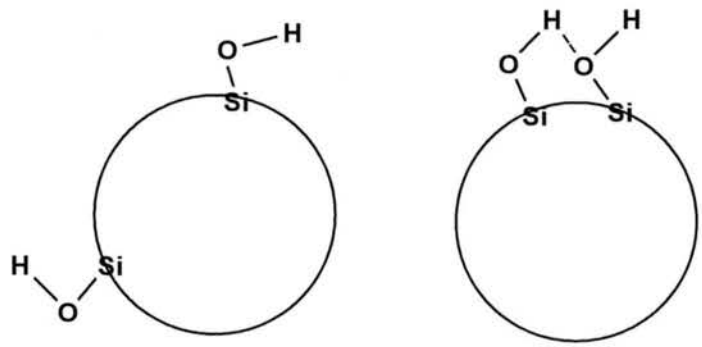

Isolated silanols Vicinal silanols

Figure 1.2. Isolated silanols and vicinal silanols.

It is these surface silanols groups that give silica gel its polar properties (important in adsorption) and chemical reactivity (important in surface modification, e.g., in catalyst supports). Reagents can react with these silanol groups on the surface to form different bonded 'phases'.

Because of surface silanols, one of the most common usages of silica gel is as a dessicant. The polar silanol groups promote the adsorption of water and hold it on the surface. The surface of silica gel is often considered like a sponge, since it can adsorb lots of water. This phenomenon has been seen by many spectroscopic methods, including solid state ^{1}H NMR, etc.[4, 5] It is not surprising that some silanol groups will form hydrogen bonds between each other or with water that is physisorbed on the surface. The surface hydrogen bonding can be represented in the following picture:

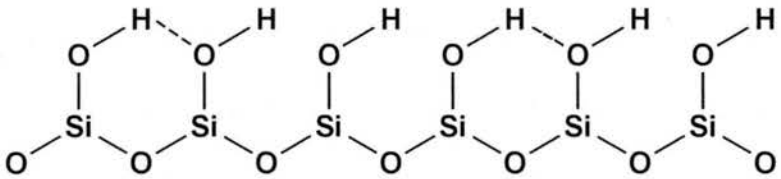

A. Hydrogen bonds between surface silanols.

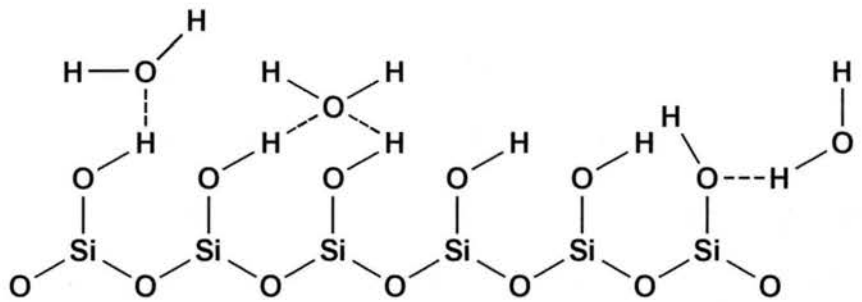

B. Hydrogen bonds between surface silanols and water.

Figure 1.3. Hydrogen bonds formed (A) between surface silanols and (B) between surface silanols and water.

Since essentially all the chemistry that happens on the surface is related with surface silanols, and physisobed H_2O may block the silanols from other reagents, it maybe important to pretreat the surface properly to yield a successful surface reaction. According to Chuang and Maciel's work,[4, 5] an untreated silica gel surface has physisorbed H_2O on the surface and they are hydrogen-bonded

to each other and to surface silanols. When the surface is evacuated at a moderate temperature (25-180 °C), physisorbed H_2O is removed and the silanols which were hydrogen boned only to physisorbed H_2O will become isolated. As the evacuation temperature is increased (above 200 °C), the surface silanols will start to 'dehydroxylate' (splitting out water) and siloxane bridges will start to form on the surface. This process is shown in the following equation:

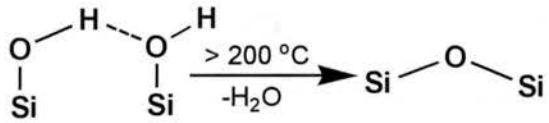

(1.1)

Many studies have shown that the acidity of the surface is related with catalytic activities and selectivities. This makes it very important to quantitatively understand the silanols, especially the concentration of surface hydroxyl groups (by instrumental methods or chemical methods).

The Maciel group has used solid state NMR (^1H, ^{29}Si) spin-counting methods to determine surface silanol concentrations. In ^1H-> ^{29}Si CP-MAS NMR, the spectrum yields a peak at –89 ppm due to $(SiO)_2\mathbf{Si}(OH)_2$ (geminal Q_2) sites, a peak at –99 ppm due to $(SiO)_3\mathbf{Si}(OH)$ (single silanol, Q_3) sites and a peak at –109 ppm due to $(SiO)_4\mathbf{Si}$ (siloxane sites, Q4) at the surface.[6, 7] Thus, these ^{29}Si NMR results show the relative amounts of geminal silanols and single silanols on the surface. Maciel and Liu published quantitative measurements of the concentrations of silanols on silica surfaces, using both MAS-only ^1H NMR and ^1H CRAMPS (combined rotation and multiple-pulse spectroscopy, based on homonuclear dipolar line narrowing with magic-angle spinning (MAS) averaging of the chemical shift anisotropy).[4, 5] Quantitative determination of surface silanol

groups, especially isolated silanols, on the silica surface has also been made by infrared spectroscopy by using suspensions of silica powder in CCl_4[8, 9] or using pellet-sample IR.[10, 11] In the IR spectroscopy of silica, the bands at 3745 cm^{-1} and 3747 cm^{-1} are assigned to isolated and hydrogen-bonded silanols, respectively.[12]

The basis of chemical methods for determining silanol content is reaction with a suitable organometallic reagent. Many organometallic compounds react with compounds that contain active hydrogen to produce H_2 or hydrocarbons. Since silanol groups contain active hydrogens, these kinds of reactions are applicable to silicas. From the results obtained, it is in principle possible to determine the number of hydroxyl groups on the silica surface via the reaction,[13]

$$\text{Si-O-H} + \text{M-R} \rightarrow \text{Si-O-M} + \text{H-R} \qquad (1.2)$$

In the above reaction, M-R could be, for example, MeMgI, MeMgBr, LiMe,[14] triethylborane[13] or dimethylzinc.[15]

On the basis of theoretical calculations, physical measurements and chemical methods, the accepted range of concentrations of silanol groups on a silica gel surface activated at 423K is 4.5 ~ 8.0 OH/nm^2, depending on the type of silica gel.[12]

1.2. Silica gel surface modification.

Although silica gel itself was for many years used as the packing/ stationary phase in chromatography, it is not commonly used now. The most popular use of silica gel now for chromatography is based on *modified* silica gels, which contain different functional groups to serve a specific purpose, such as increasing the surface selectivity for certain solvents or functional groups.[16]

Modification of the silica gel surface accomplishes changing the chemical composition (and properties) of the surface. The surface can be modified by either hydration or dehydration methods, such as thermal or hydrothermal methods, which change the concentration of surface silanols and siloxane bridges, or by other types of chemical methods, which typically attach some kind of pendent groups to the silica surface.

Silica gel has often been used as a catalyst or catalyst support in organic synthesis. The advantages of using silica or analogous inorganic supports, rather than organic catalyst supports such as polymer resins, are:[12]

i. good selectivity,

ii. no swelling,

iii. rapid sorption of metal ions, and

iv. good mechanical stability.

Because of the reactivity and variety of surface silanols, immobilization of various pendent groups (surface modification in general) on the silica surface by various silylating agents (*vide infra*) is often easier than the same kind of surface modification on a polymer resin support. Polymer supports (resins) have a high number of cross-links and typically require longer times to yield a high concentration of surface change. Silica gel has a high specific surface area with constant composition, which makes it easier to analyze and interpret the results. Also, silica gel has great resistance to organic solvents and has very high thermal resistance. For these reasons, silica gel is the most popular substrate and is commercially available with great variety.[12]

Chemical methods to modify the silica gel surface are based on the reaction between surface silanols groups and selectively reacting reagents to form covalently bonded surface species. This can be accomplished in two ways.

The most common method to develop a chemically modified silica surface is to simply immobilize the functional group on the surface by physisorption or by electrostatic interaction, hydrogen bond formation or some other type of non-covalent interaction. Simple impregnation of the solution of modifying reagent or covalent binding into the silica matrix is a popular practice of developing a "functionalized" silica surface. This method is based on the physical interactions between the modifier and silica by either inclusion in the pores of silica or the adhesion process or electrostatic interaction between the two.[12]

The second common method for modifying the silica surface is based on *covalent grafting*. This method involves reaction of active H of surface hydroxyl group with the organosilyl groups of a silane coupling reagent to form a Si-O-Si-C moiety that can modify the surface interactions/properties, e.g.:

$$\text{<Si>-OH} + \text{R-Si-Cl} \rightarrow \text{<Si>-O-Si-R} + \text{HCl} \qquad (1.3)$$

Here, <Si> represents a silicon atom on the surface.

The organosilane reagents are called *silylating agents*. These silylating agents react with the surface silanol groups, with the result that the surface is covered with the desired terminal functional group attached to the silane. Silane reagents with a variety of hydrocarbon chains can make the new surface hydrophobic,[16, 17] or act as precursors for further immobilization of organic molecules on the surface, such as to help introduce basic groups anchored on

the surface.[18, 19] In this route of surface modification, the <Si>–O–Si–C moiety so formed has bifunctional nature, providing firm attachment to the silica matrix (resistant to being lifted off the surface by solvent or a water wash) and allows further surface reactions.[12]

The sol–gel process is another way to modify the silica gel surface by means of covalent grafting. In this method, sol-gel hydrids, a mixture of inorganic oxides (silica) and alkylalkoxysilanes, is prepared and stirred together to result in organically modified silicas (ormosils) with a variety of specific organic groups.[12]

Another covalent grafting method for the preparation of alkyl bonded silica phases is based on binding an organic moiety via a surface silicon site in which a surface –OH has been substituted with halogen atom;[16] the resulting <Si>-Cl moiety on the surface is then treated with Grignard reagent or an organolithium compound:[20]

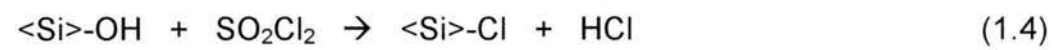

(1.4)

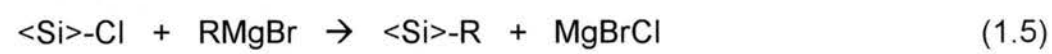

(1.5)

Alternativelly, after treatment of the halogenated surface with $LiAlH_4$, yielding a surface hydride (<Si>-H),[21] the surface can then be coupled with an olefin in the presence of metal catalyst to achieve Si-C bonds on the silica surface:[20]

(1.6)

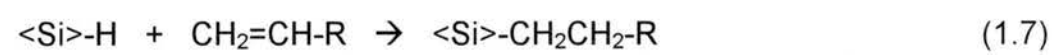

(1.7)

Another approach is to treat the halogenated silica with a amino compound, e.g.[16]

<Si>-Cl + NH_2-R-NH_2 → <Si>-NH-R-NH_2 + HCl (1.8)

Another reason for interest in the surface modification of silica is the grafting of polymer molecules on the silica surface to utilize the miscibility of the polymer with the surrounding fluid medium without detachment from the silica surface. Among the various methods, free radical surface graft polymerization is one approach to covalently bond the polymer chain to the surface with high surface coverage.[12]

1.3. Physical methods of identifying and characterizing the modified silica gel surface.

Most of the interest in the silica gel surface focuses on surface hydroxyl groups and post-reacted hydroxyl groups (after –OH has reacted with other chemicals to form new surface functional groups). Many physical/instrumental methods have been applied to characterize different aspects of the surfaces of silicas and modified silicas.

1.3.1. Chromatographic methods.

For the purpose of improving the functioning of chromatography, the chromatographic properties of silica gel and modified silica gels are often characterized by chromatographic methods, and by measuring such properties as the surface area, packing density and the functional group selectivity in HPLC or LC columns. When a modified silica is to be used as a stationary phase in chromatography, it is important to know the way in which the silica has been modified, such as, the alkyl chain length, bonding density, attachment chemistry

and heterogeneity of the silica surface. Also affecting chromatographic efficiency are the solute structure, temperature and concentration of organic modifier in the mobile phase. All of these variables will affect the configuration and the properties of chemically immobilized chains on the silica.[22]

No single method can characterize all of the properties of a substance. There are many physical/instrumental ways to characterize the surface of modified silica gel, such as FTIR, solid state NMR (^{13}C, ^{29}Si ^{1}H) and the thermal gravimetric method or microscopic methods. Some of these methods can change (damage) the material to be analyzed. To gain maximum advantage in characterizing a chromatographic material, one should analyze the material non-destructively, ideally *in situ* in the chromatographic system, since the separation efficiency is based on the interaction between the analyte, the stationary phase and the mobile phase.[22]

In reported work, the elution sequences of neutral, polar and basic substances have been used to describe the behavior of the stationary phase in terms of the following characteristics: hydrophobicity, silanol activity and shape selectivity of the modified silica stationary phase. On the basis of many published studies, it is suggested that the following factors are best used to characterize the stationary phase for chromatographic effectiveness:[22]

(1) the number of alkyl chains;

(2) hydrophobicity;

(3) steric selectivity;

(4) hydrogen bonding capacity;

(5) ion exchange capacity at pH >7;

(6) ion exchange capacity at pH <3

In chromatography, the following important characteristics can be determined by the behavior of a 'test compound' on the adsorbent: (i) the number and the spacing of the residual silanols on a modified silica gel; (ii) the homogeneity of the surface coverage of chemically bonded phases; (iii) the structure of bonded monomeric, polymeric and oligomeric layers; (iv) the hydrophobicity of the packing materials; and (v) the polar selectivity of the stationary phase.[22] HPLC or LC methods have been used to study various relevant characteristics (e.g., selectivity, hydrophobility and information on residual silanols) of a modified silica as a stationary phase.

1.3.2. The BET method.

The BET method for determination of surface area is named after Brunauer, Emmett and Teller, the three scientists who invented this method and accompanied it with the appropriate theory.[23-25] The BET method is the most common method to measure the surface area and specific pore volume of highly porous or powder samples. It is also known as the 'nitrogen adsorption' technique and has often been used to characterize the texture of modified silica.[25]

The surface area, porosity and the pore-size distribution can be obtained via the BET method. These factors have a significant influence on the successful application of the product of a specific surface modification. Specifically, these

factors are important in chromatography in terms of the ligand (pending group) density, column efficiency and selectivity.[22]

The BET method is a very important and common technique for determining the effective surfaces of solid materials with complicated shapes, such as porous powders, by using adsorbed gas molecules as rulers. The observation of adsorption and desorption isotherms is used to determine the amount of gas molecules adsorbed to a surface. By knowing the size of the adsorbed molecule, one can then calculate the entire effective surface.

It has been accepted that the Type IV adsorption/desorption isotherm shape, showed in Figure 1.4, is the best to describe and interpret the surface of mesoporous materials like silica gel.[26]

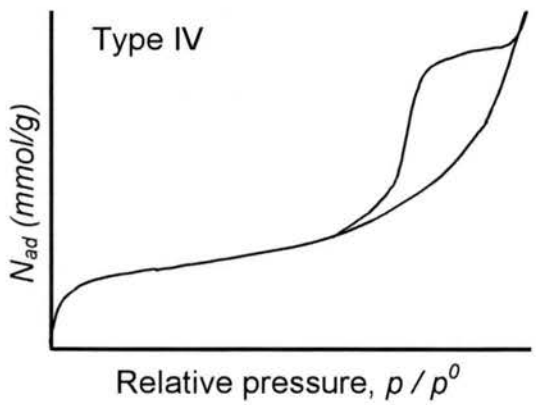

Figure 1.4. Type IV adsorption /desorption isotherm curve.

The geometry of the surface can limit the accessibility of adsorption sites for a gas. Surface hydroxyl groups (silanols) or other surface species are mainly responsible for adsorption properties of silica. Binding a significant amount of functionalizing groups on a silica surface alters the adsorbent geometry of that surface significantly.[12]

Modification of the silica surface involves introducing new functional groups/molecules pendent from the surface. The BET surface area measurement can often indicate the geometry change on a surface by comparing the surface area change from before and after the chemical modification. By measuring the change of pore size and pore volume from gas adsorption/desorption methods, one can often provide information on the configuration of the molecular chains grafted on the surface. Commonly, the decrease of adsorption area, which is reflected as decreasing specific surface area, pore size and pore volume, is observed with increasing extent of surface modification. But exceptions exist; Blitz and coworkers reported that while the BET surface area of all fumed silica samples decreases after surface modification, the pore volume increases after surface grafting of trimethylsilyl and octadecyldimethylsilyl groups. This has been explained by the rearrangment of primary particle swarms during the modification process.[27]

1.3.3. Thermal analysis.

Thermal gravimetric Analysis (TGA) is a thermal analysis technique based on measuring changes in the weight (mass) of a sample as a function of temperature and/or time. The TGA apparatus measures the initial sample weight at room temperature and then continuously monitors changes in sample weight (losses or gains) as heat is applied to the sample.

It is not hard to imagine using TGA as a method to measure the surface silanol concentration, as loss of H_2O via dehydration can occur when the sample temperature is increased. First accounting for the removal of physically adsorbed

water on a silica surface, TGA results indicate that the number of silanol groups on the surface ranges from 4.3 to 6.7 OH/ nm^2 for different types of silicas.[12]

TGA analysis is also a useful and simple tool for determination and characterization of organic groups on a modified silica adsorbent surface. By burning the sample in oxygen, the weight loss tells the amount of chemically bonded phase, provided the loss of other moieties, such as water of condensing silanols, is avoided. The results from differential thermal analysis can be used to calculate the surface area coated.[22]

Differential scanning calorimetry (DSC) is also a useful tool for characterizing chemically modified surfaces. This technique measures the amount of energy (heat) absorbed or released by a sample as it is heated, cooled or held at a constant temperature; differences in the amount of heat required to increase the temperature of a sample and a reference are measured as a function of temperature.[22, 28, 29]

DSC, which is dominated by phase transitions, can help elucidate the association and dissociation of absorbent from the surface of chemically bonded chains. Furthermore, the shape of the DSC curve provides information on the surface porosity and on the structural heterogeneity of a modified silica. Adiabatic calorimetry has also been used to measure the transition entropy and enthalpy, which provides confirmation of models of chemically bonded moieties.[22, 28, 29]

1.3.4. Small Angle Neutron Scattering.

Small angle scattering (SAS) is the collective name given to the techniques of small angle neutron scattering (SANS), X-ray scattering (SAXS)

and light scattering (SALS, or just LS). In each of these techniques radiation is elastically scattered by a sample and the resulting scattering pattern is analyzed to provide information about the size, shape and orientation of some component of the sample.[30] This technique is useful for providing details of pore microstructure on a nanometer scale (1-300 nm).

It is well known that neutron scattering techniques can provide extensive information about the microstructure of porous materials and the properties of adsorbates within the pores.[31] Structural information is obtained from measurements of both coherent and incoherent scattering on the surface. Coherent scattering includes diffraction and small angle scattering (SAS) and has a counterpart in X-ray scattering. Incoherent scattering generates from a unique interaction of the neutron with the atomic nucleus and has no equivalent with either X-ray or light radiation.[31]

By an analysis of different parts of the scattering curve, information on pore size, shape and surface area can be derived. Also pore accessibility can be determined using small-angle neutron scattering experiments in which low-energy neutrons strike the sample and are elastically scattered by pores or other structures.[22] Published work by Ramsay[31] demonstrated the application of SANS to study the adsorption mechanisms of benzene on mesoporous silica and to study the states of water adsorbed on mesoporous silica.

1.3.5. Solid state NMR.

Solid State NMR with magic angle spinning (MAS), high-power ^{1}H decoupling and cross polarization (CP) has been used to investigate the surfaces

of silica gels and modified silica gels.[6, 7, 20, 32-35] The ^{29}Si chemical shift indicates different surrounding chemical groups and also indicates various interactions between surface bonded groups and adsorbed moieties.

In the cross polarization (CP) experiment, proton magnetization is transferred during a distinct CP contact period to dilute heteronuclei, such as ^{29}Si or ^{13}C. The presence of a rigid system and presence of nearby protons leads to an effective magnetization transfer and enhanced signal intensities. Even the flexible moieties of the stationary phase are polarized with a long contact time, and variations of contact time can be used to investigate the dynamics properties of adsorbents.

As shown in the examples in Figure 1.4, ^{29}Si CP-MAS NMR provides useful information about the structure of chemically bonded groups on a silica surface, especially to detect Si-C bond formation as a result of the modification.[20, 32, 33] Maciel and Sindorf used ^{29}Si CP-MAS NMR to obtain the signals characteristic for various features of the silica structure. Single silanols (Q_3) were identified at -100 ppm, siloxane silicons (Q_4) at -109 ppm, and geminal (Q_2) silanols at -90 ppm. ^{29}Si CP-MAS NMR also provides information on changes at the silica surface by showing signals other than Q_2, Q_3 and Q_4, which provide information about the surface modification.[22] Maciel's group has also carried out ^{1}H MAS measurements, some with spin counting, on various silica gels, showing the potential ability of solid state ^{1}H NMR for quantitative measurement.[5]

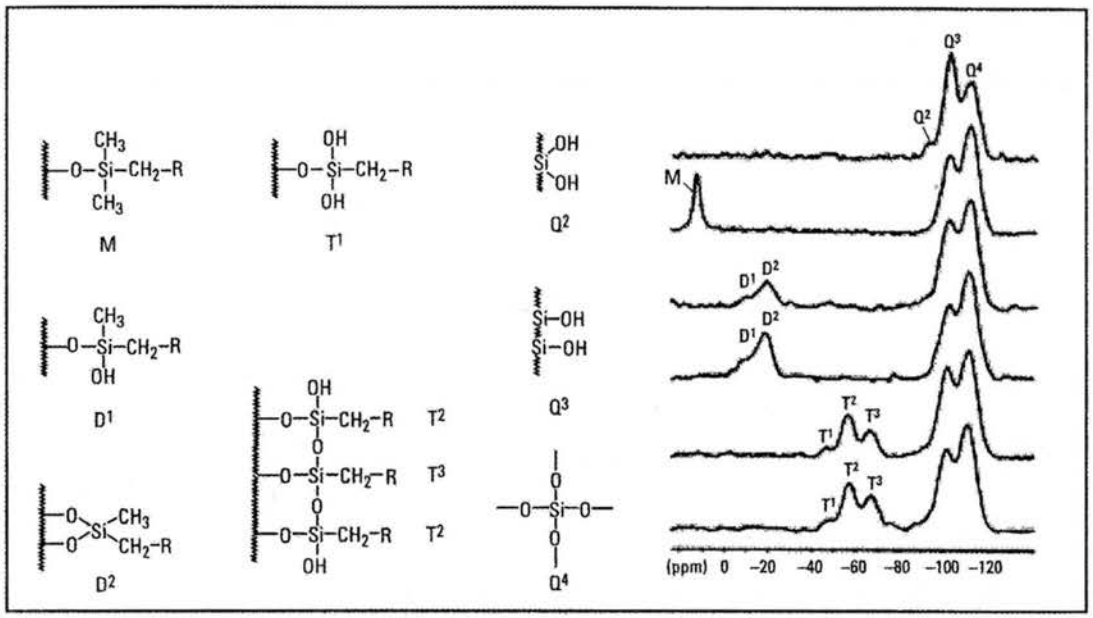

Figure 1.5. ^{29}Si CP-MAS spectra of modified silica surfaces.[36]

In solid state ^{29}Si and ^{13}C NMR, a combination of DP-MAS (direct polarization and MAS spinning) and CP-MAS (cross polarization and MAS spinning) measurements can help elucidate the motional characteristics of the moieties on the surface.[32-36] The ^{29}Si DP-MAS experiment detects mainly the (more abundant) bulk (internal) silicons, while CP-MAS detects mainly the surface silicons, which are emphasized by cross polarization because they are close to silanol protons at the surface. Relaxation time measurements can also provide useful information for describing the motion of surface structures.

1.3.6. Fourier Transform Infrared spectroscopy (FTIR) and Raman spectroscopy.

Fourier Transform infrared spectroscopy (FT-IR) is a technique which measures the absorption of various infrared wavelengths by a material of interest.

The observed infrared absorption bands identify specific molecular components and structures. FTIR has been used to identify typical chemical bonds on the surface, such as those of Si-O, Ti-O, Si-O-Al, Si-O-H, and Si-O-metal moieties.[37-41]

The relative distribution of two classes of hydroxyls in silica gels, one corresponding to physisorbed water and the other due to structural hydroxyls (silanols), never has been completely resolved in thermogravimetric or differential thermal analysis, since, upon heating silica gels, a continuous loss of water occurs over a large temperature range.[14] But in FTIR, the Si-OH moieties can be distinguished as non-hydrogen-bonded Si-OH and hydrogen-bonded Si-OH on the surface, by means of characteristic O-H stretching frequencies. Infrared spectroscopy has been extensively used to study adsorbed species on oxide and on oxide supported metal surfaces. Advantages of the technique are its high sensitivity (in favorable cases <1% of a monolayer can be detected) and ease of sample preparation. By using careful baseline subtraction and baseline linearization, FTIR with signal averaging overcame the problems connected with high 'background' absorption of IR radiation by the internal silica structure and overlapping of the desired signal with the broad and strong background signal.[42]

In contrast, silica gels are relatively poor Raman scatterers and it should be a straightforward matter to obtain low-frequency spectral data for adsorbed species. Some attempts to use Raman spectroscopy have shown that, in general, the sensitivity of the technique is below that of the infrared method.[42] Also, there are other problems, e.g., laser-induced fluorescence (usually associated with traces of hydrocarbon or transition metal ion impurities) and possible thermal

desorption or decomposition due to the laser. As a consequence, Raman spectroscopy up to now has been mainly used to study the interaction of some highly polarizable molecules on various high surface area oxides (SiO_2, Al_2O_3, etc.) and its potential for studying chemisorption has not been greatly utilized.[42]

1.3.7. Fluorescence.

X-ray fluorescence has been used for depth analysis of modified surfaces[43] and X-ray photoelectron spectroscopy has been used for surface analysis to characterize adsorbents.[44] The results of the two techniques give a picture of the differences between the inner pore network and the outer particle surface. Lochmüller suggested that there are three types of fluorescent ligands that can be chemically bonded to a silica support: 1) those located inside micropores or surrounding the alkyl chains where the solvent molecules cannot penetrate between moieties, 2) those "readily accessible to" solvent molecules, and 3) those relatively accessible for solvent molecules but bonded with silanols present on the surface. The type of ligand and the composition of the mobile phase control the polarity of the stationary phase.[22]

1.4. Modification of the silica gel surface with organometallic compounds – chemical aspects.

Modification of chemically and thermally stable support materials such as silica, alumina or zeolites via surface organometallic chemistry attracts lots of interest for possibilities to generate new supramolecular species for both catalysis and materials purposes. Silica gel, as a well-known catalytic material or

catalyst substrate material, receives lots of attention in surface modification with organoaluminum compounds. Trimethylaluminum, the simplest commercially available organoaluminum compound, has been widely used to modify silica gel surfaces for the following reasons:

(i) H-sequestering agents for the quantification of surface silanol groups;

(ii) A source of aluminum to generate catalytically active hydride species (alumination reactions);

(iii) A passivating and/or compatibilizing agent for the immobilization of molecular pre-catalyst species;

(iv) A co-reactant to produce aluminum-containing thin layer materials such as AlN and Al_2O_3.[45]

1.4.1. H-sequestering agents for the quantification of surface silanol groups.

As indicated above, surface silanol groups (Si-OH) are the essential features that are responsible for the most important physical and chemical reactivity and characteristics of silica gel. According to the various methods of silica gel preparation, the structure and concentration of surface silanol groups will vary and affect the physical and chemical behavior of the surface significantly. Having a wide and deep understanding of the surface silanol structure and quantitatively measuring the concentration and coordination of surface silanol groups will help one control the further utilization or chemical modification of silica gels. The surface silanols of silica gel have been regarded as acid-type catalysts.[13] The properties and functions of silanols have been measured in

various ways, such as the gas absorption method, the ion-exchange capacity method, infrared spectra, the chemical titration method and NMR.[13]

The density of surface silanol groups on silicas can be varied according to different methods of preparation. A fully hydroxylated silica gel (no physisorbed H_2O) has been reported to have about 4.5-5.0 hydroxyls/nm^2 and this number is more or less independent of the surface area.[46] For silicas prepared by high temperature hydrolysis, the hydroxyl density is usually lower, being in the range 2.5-3.5 OH/nm^2.[47, 48] The silanol groups on a silica gel surface can have strong interactions via different types of hydrogen bonding, and this interaction strongly affects its surface chemistry.

A normally hydrophilic hydroxylated surface can be modified to a relatively hydrophobic surface by replacing the surface silanol groups by other functional groups. For example, there are many kinds of so-called hydrogen sequestering (HS) agents, MX, which can react with the surface. As described by the following reaction, this process yields a surface with very different adsorption characteristics.[46]

$$SiOH + MX_n \rightarrow SiOMX_{n-1} + HX \qquad (1.9)$$

When the proton sequestering agent contains a trialkylsilyl group (e.g., SiR_3), surface silanols are converted into Si-O-SiR_3; then the surface changes from hydrophilic to relatively inert hydrophobic and might meet various requirements of chromatography, or other purposes. The number of silanols that react with these MX_n reagents will depend on steric factors such as the silanol density and the size of the HS agent.[46] In this reaction model, the extent to which

the silanols react on the surface reflects surface properties such as the silanol density. Using an organometallic compound, such as $AlMe_3$, to measure the concentration of surface silanols might be attractive, since it can be very easily carried out without any sophisticated equipment.[13, 14, 49] In principle, such reactions might follow a simple course, e.g.,

$$AlMe_3 + \text{<Si>-O-H} \rightarrow \text{<Si>-O-}AlMe_2 + CH_4 \quad (1.10)$$

The reactions that occur between the surface hydroxyls of silicas and hydrogen sequestering agents have be investigated by Morrow and McFarlan, using FT-IR, with a view to determining both the concentration and coordination of the surface groups.[13, 48] The sequestering agents most popularly studied are volatile halides (i.e., BCl_3, $SiR_{(4-x)}Cl_x$, $AlCl_3$, etc.). Nucleophilic attack by the surface hydroxyl at the metal (or metalloid) atom leads to a solid reaction product containing chlorine (if n>1).[13]

$$\text{<Si>-OH} + MCl_n \rightarrow \text{<Si>-O-}MCl_{n-1} + HCl \quad (1.11)$$

Most of these reactions between silica gel and proton sequestering agents have been carried out with an excess amount of the vapor-phase agent, and after completion of the reaction, the system is evacuated to remove any unused reagent and any volatile reaction products. *In situ* study by infra-red spectra have shown the disappearance of surface hydroxyls as the reactions proceed.[41, 50-55] This kind of reaction is a nucleophilic attack by a surface hydroxyl, which involves a transition state in which the hydroxyl oxygen atom uses one of its lone pairs to coordinate to the metal atom of the proton sequestering agent. Kunzwicz and Hockey's work[41] noticed that the siloxane bridges that are formed on the surface

when silica is heated at high temperature are more reactive towards hydrogen sequestering agents than are the single surface hydroxyls. The number of these bridges that are reactive depends on the sequestering agent used.[41]

There are various techniques for determining the surface hydroxyl concentration, e.g., by IR spectroscopy,[56-61] by the diborane technique,[62, 63] by exchanging the hydrogen atoms of surface hydroxyl groups with deuterium from heavy water[61, 62, 64-66] and by ^{1}H NMR.[5] The IR method is weak in distinguishing between different types of silanols, such as single or geminal silanols or the silanols of silica-alumina (which has two or more bands attributed to the surface silanols); also the hydroxyl groups connected with Bronsted acidity in silica-alumina can not be distinguished by infra-red spectroscopy.[13] The diborane method gives an error due to evolution of hydrogen from the reaction between the boron compounds added to the reactants and those produced during the reaction.[13] In view of the disadvantages mentioned, it turns out that organometallic compounds appear to be an alternative method worth exploring.

An example used in Sato and Shima's work is represented in the following equation:

$$<Si>\text{-}OH + Al(C_2H_5)_3 \rightarrow <Si>\text{-}O\text{-}Al(C_2H_5)_2 + C_2H_6 \qquad (1.12)$$

In this example, the determination of the number of surface hydroxyl groups on a silica surface was carried out by measuring the volume of ethane (gas) produced from the reaction. It was concluded that, for determining the total amount of surface hydroxyl groups, triethylaluminum is the most convenient reagent, since this compound is very reactive and gives no evolution of other hydrocarbons,

unlike the case of ethyllithium (which yields R-O-Li when the temperature rises; also, ethyllithium might react with ether solvent).[13, 67]

Based on the ideas outlined above, the reaction between the silica gel surface and trimethylaluminum, or similar organometallic compounds, can, in principle, be used to further understand the reactivity of the various surface species (non-hydrogen bonded silanols, hydrogen-bonded silanols and bridged siloxanes on the silica gel surface) towards this kind of hydrogen sequestering reaction.[41] This approach, by using organometallic reagents of different size and reactivity ($TiCl_4$, BCl_3, $AlCl_3$, $AlMe_3$, etc.), has been helpful in evaluating the reactivity and the concentration of different kinds of surface silanol structures.[55]

1.4.2. A source of alumina to generate catalytically active hybrid species (alumination reactions).

Chemical modification of a silica surface can be achieved, as discussed above, by reactions in which the organometallic reagent can be utilized to produce materials (e.g., catalysts) in which the (catalytically) active centers would exist at the surface of the silica support in a discrete array and possibly with a determinable structure and coordination.[55] In the case of a trialkyaluminum reagent, this kind of application is known as an *alumination* reaction on the surface.[45] Reactions suggested in previously published work are shown in the following equations, which represent reactions occurring between $AlMe_3$ and a silica surface:[55]

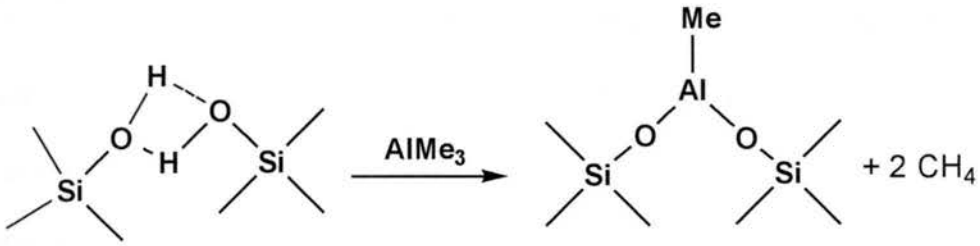

(1.13)

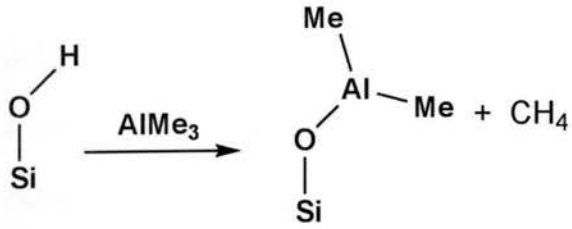

(1.14)

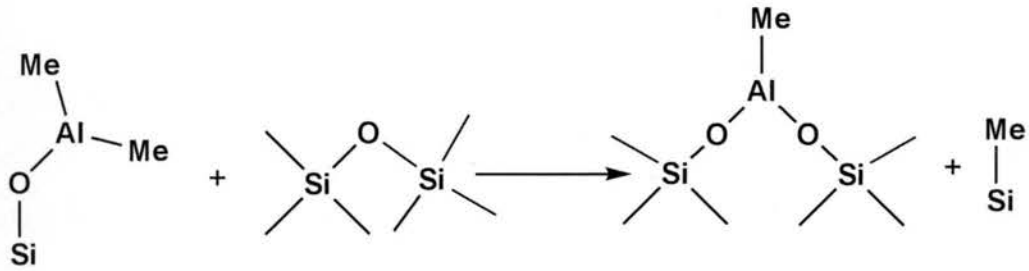

(1.15)

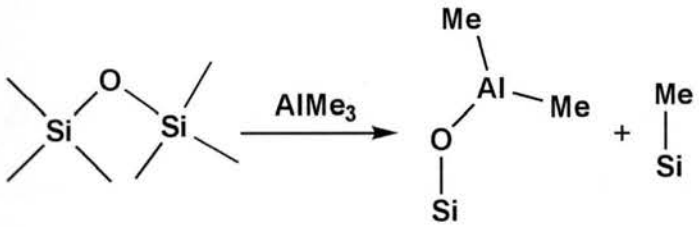

(1.16)

1.4.3. A passivating and/or compatibilizing agent for the immobilization of molecular precatalyst species.

The silica support of a silica-immobilized catalyst is generally thought of as a carrier for the catalytically active phase. Silica gel supported catalysts are currently used to manufacture polyolefins on a multimillion ton scale.[68] The support serves to maximize the active-phase surface area and allows the catalyst to be used in industrially useful reactor processes.

One type of silica-supported polyolefin catalyst is a thermally activated chromium catalyst, for which it is generally recognized that surface-catalyzed chemical reactions are involved. Silica surface hydroxyl (silanol) groups are believed to react to stabilize hexavalent chromium as silyl chromates in the preparation of the catalyst. These silyl chromates then react with ethylene to form active sites. Silica gel surface chemistry thus plays a large role in the study and development of these catalysts.[68]

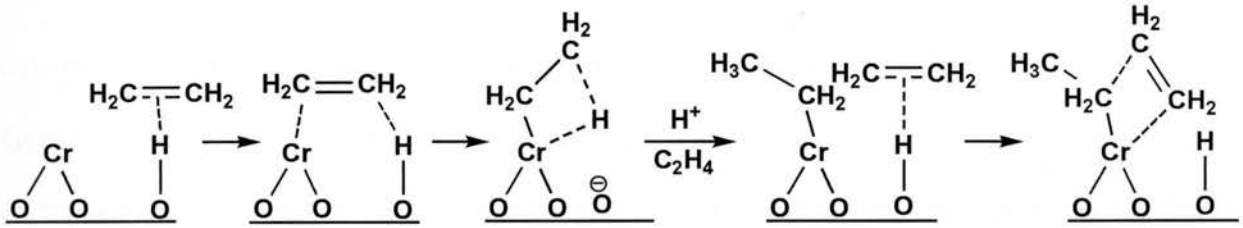

A second type of heterogeneous silica-supported polyolefin catalyst is the Ziegler-Natta catalysts. In their original and simplest form, Ziegler-Natta catalysts consist of the reaction product between a transition-metal halide and a metal alkyl. Ziegler-Natta catalysts are now often supported on silica gel.[68]

Homogeneous Ziegler-Natta catalysts that are derived from metallocene compounds and methylalumoxane co-catalyst combine high activity with excellent stereoregularity in the isotactic polymerization of olefins. The discovery of these catalysts has led to approaches in which an aluminum compound introduces aluminum on the catalytically active surface as a co-catalyst.[69]

One of the most widely used classes of Ziegler-Natta catalysts is based on a mixture containing Ti (e.g., $TiCl_4$), Mg (e.g., dibutylmagnesium), and Al (e.g., triethylaluminum) compounds. These compounds are often immobilized on the

silica gel surface. The following picture shows examples of this kind of catalyst (from $TiCl_4$):[45]

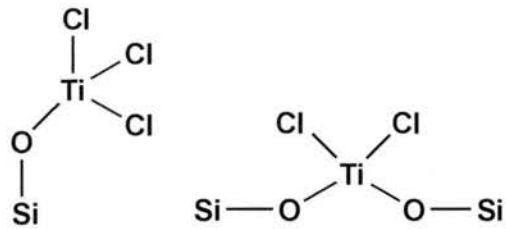

Numerous published reports have considered the reactions of $TiCl_4$ with silica.[40-42, 46, 48, 50] Such reactions can be controlled by appropriate pretreatments consisting of heating the silica, which effectively changes the relative silanols types existing on the surface. An unmodified silica surface, pretreated at 250 °C in N_2 to desorb molecular water, contains both hydrogen-bonded and non-hydrogen-bonded silanols, but no physisorbed water.[70] Titanium tetrachloride reacts with nonhydrogen-bonded silica surface silanols to give single surface linkages, and with hydrogen-bonded silanols to give a "bridged" surface-bonded species.[68]

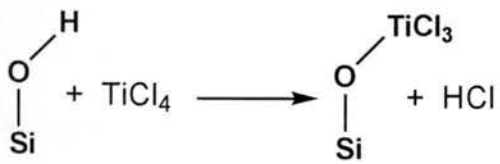

(1.17)

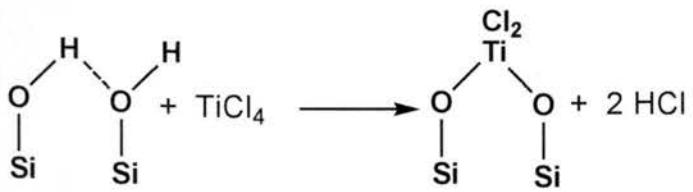

(1.18)

Another example in which the metallocene catalyst is immobilized on the silica surface is in continuous slurry, fluidized-bed gas-phase, or bulk-monomer

synthesis process. In the gas-phase and slurry-phase polymerization process of polyolefins, the soluble homogenous metallocene catalyst generates a fine polymer powder. With a suitable supported heterogeneous metallocene catalyst, the process yields improved control of the product morphology. The supported heterogeneous catalyst helps to create polymer product with shape that is an enlargement of the shape of catalyst particles themselves.[71-73] Various supports have been used for metallocene-alumoxane catalysts, including starches, clays, metals, ceramics, metal halides, polymers and silica gel. The most commonly used supports have been porous inorganic oxides, especially silica gel, represented in the following example.[69, 71]

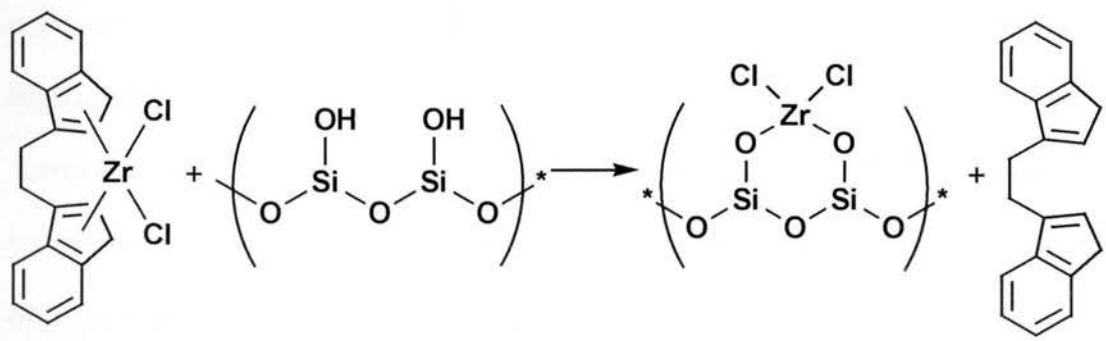

(1.19)

Several strategies have been used to prepare silica-supported metallocene catalysts:

(i) Direct immobilization of the metallocene on the support. The silanol groups on the silica surface react with metal chloride complexes to form Si–O–M functionalities, which can be converted to active catalyst when a co-catalyst is added to the polymerization medium.[74]

(ii) Immobilization of the cocatalyst on the support, followed by reaction with the metallocene compound. In this case, methylaluminoxane

(MAO, the co-catalyst) can be adsorbed on the support or generated *in situ* by hydrolysis of trimethylaluminium (TMA). This hydrolysis process can be carried out in different ways, in which the $AlMe_3$ reacts with water treated on the silica surface or in the gas phase using fluidized bed technology.[75]

(iii) One-step immobilization of the MAO/metallocene complex.[72, 76]

In polymerization reactions based on supported metallocene catalyses, especially ethylene polymerization, supported versions of the well-studied ethylenebis(η^5-indenyl)- and ethylenebis(η^5-tetrahydroindenyl) zirconium dichloride catalysts (see structure above) have been used. In order to obtain high catalytic activity and catalyst stability, the catalyst substrate is pretreated with $AlMe_3$ prior to adsorbing the metallocene compound on it. By changing the surface silanols via reaction between $AlMe_3$ and Si-OH groups, the newly generated surface sites increase the amount of metallocene catalyst adsorbed on the pretreated surface without further decomposition. The above picture is an illustration of this kind of approach.[69]

1.4.4. A co-reactant to produce aluminum-containing thin layer materials such as AlN and Al_2O_3.

Around 1970, the first alumina thin films were grown for electro-luminescent applications by atomic layer epitaxy (ALE), using $AlCl_3$ and H_2O as reactants.[77] Since then, alumina layers have been used as passivating layers or insulators in many different applications. Different compounds, including $AlCl_3$ and aluminum alkoxides, have been studied for growing Al_2O_3 layers. Higashi

and Fleming first described the growth of a Al_2O_3 layer from trimethylaluminum treatment, followed by H_2O hydrolysis. Since then, trimethylaluminum has been used as a precursor compound to introduce Al-based passivating layers on a variety of surfaces. The method has been used not only to grow a single layer, but also to grow multiple layers on the surface.[78]

AlN is a material with a wide band gap, a high thermal conductivity and a thermal expansion coefficient similar to that of silicon. In addition, it is piezoelectric with a high acoustic wave velocity and is transparent in the visible and near-infrared regions. Because of these properties, aluminum nitride should have wide application in microelectronic and optoelectronic devices, as methods are improved that allow it to be grown on surfaces in a crystalline form, at low temperatures, and with high purity.[79]

Because of its attractive thermal, electronic and mechanical properties, AlN has attracted widespread attention in recent years. Applications in microelectronic and sensor technologies, in particular, require thin films of AlN deposited on substrata by using process conditions compatible with the rest of the circuit materials. For this reason, much research interest focuses on the low-temperature deposition of AlN thin films. AlN has been deposited by a variety of sputtering and ion-beam deposition techniques.[80-82] Thermal, plasma-assisted, and photoassisted chemical vapor deposition (CVD) processes have also been employed using reactants such as trimethylaluminum (TMA) (and other alkylaluminum compounds) plus NH_3, TMA plus hydrazine, $AlBr_3$ plus N_2, $AlCl_3$ plus NH_3 and a number of molecular precursors that contain Al-N bonds.[83]

It has been recognized that the reaction between $AlMe_3$ and the silica surface, and the formation on the surface of new species, can perhaps be used as a precusor step for further deposition of N and form Al-N bonds.[84, 85] Several fundamental issues have been noted that are relevant to this possible route for aluminum nitride growth. The effects of the adsorbates must be understood, since they have the potential to enhance or inhibit reactions, undergo side reactions that lead to the incorporation of impurities and affect the morphology of the aluminum nitride film. To address these subjects, the trimethylaluminum/ ammonia/silica system was selected by Rogers and coworkers as the substrate for these reactions because of its transparency to the most relevant infrared wavelengths and the ease of deriving this surface with aluminum alkyls.[78, 79, 83]

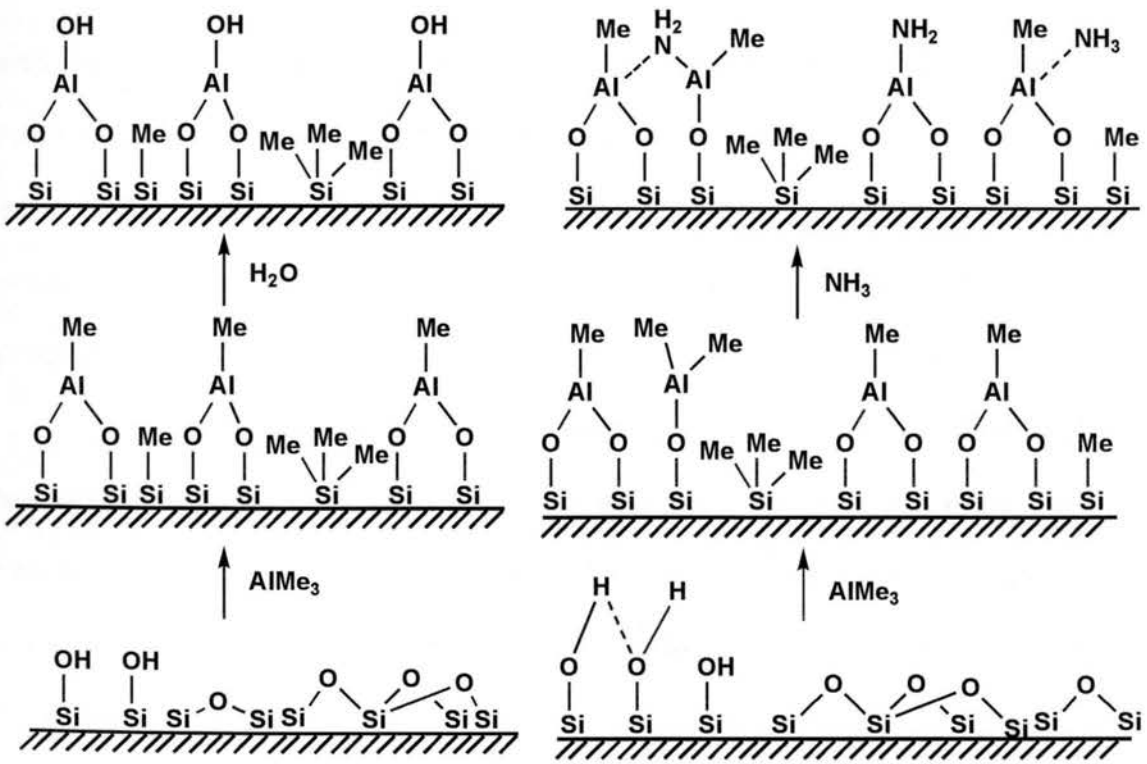

Growth model of Al_2O_3 on a silica surface[77]

Growth model of aluminum nitride on a silica surface[77]

In the implementation of the reactions shown in the above figure,[78] the atomic layer chemical vapor decomposition (CVD) method was used, which is a gas-solid method. The silica substrate was preheated to remove the physisorbed water on the surface; then vaporized trimethyl aluminum in excess amount was applied to the substrate surface to make the reaction between Al-Me and Si-OH moieties occur.[78] Of the many sophisticated technologies currently used in electronic materials growth and processing, perhaps none exhibits a richer, more diverse and perplexing range of chemistries than does CVD.[79]

1.5. Rationale – study of the reaction between the silica gel surface and trimethylaluminum.

As discussed above, modification of the silica surface is a very common and popular area to explore, and it has huge potential in the design of new functionalized materials. Understanding the basic chemistry that happens on the silica surface and mastering the tools of characterizing the surface structure would strengthen the ability to direct the way new materials developments progress.

Published work discusses the reaction between the silica surface and trimethylaluminum.[20, 39-41, 45, 51, 55, 78, 86-89] Trimethylaluminum is one of the very reactive organometallic reagents toward the silica surface and the simple molecular formula makes it promising for elucidating the basic chemistry that happens on the surface.

Ting and Maciel published a study on the solid-liquid interface reaction between silica (and modified silica) and simple organometallic reagents ($AlMe_3$,

$ZnMe_2$, MeMgBr and LiMe) and discussed the reactivities of each kind of silica (unmodified and modified) toward the different organometallic reagents. That work explored the strength of using solid state NMR (^{13}C and ^{29}Si) methods for elucidating the surface structure and new species generated through the modifications.

In Ting and Maciel's work, the samples that were subjected to NMR investigation were fully hydrolyzed after the surface was reacted with the organometallic reagent. Among the four organometallic reagents examined in that work, the results showed that methyllithium is the most reactive reagent; it broke the silica framework of a trimethylsilylated silica sample and generated the largest signal intensity due to Si-Me groups. Methylmagnesium bromide was the second most reactive reagent, after methylithium. Dimethylzinc and trimethylaluminum did not appear to generate substantial Si-Me on the surface, as methyllithium and methylmagnesium bromide did; only very small Si-Me signals were observed in the ^{13}C NMR spectra in the $ZnMe_2$ and $AlMe_3$ cases. However, liquid-sample NMR experiments showed that substantial amounts of $ZnMe_2$ or $AlMe_3$ reacted in the initial reactions with silica. The chemical fates of the methyl groups of $ZnMe_2$ and $AlMe_3$ in the silica reactions remained mysteries in that study. To further study the details of these surface reactions and to gain a deeper understanding of the path of the methyl groups during the whole reaction process of the $AlMe_3/SiO_2$ system is the focus of the present study.

Since $AlMe_3$ is potentially very reactive, it is not hard to imagine that there might be more than one kind of surface moiety generated on the surface in the

initial reaction; and most of these moieties could be unstable when subjected to moisture or air. The "missing" methyl groups in the $ZnMe_2$/silica gel and $AlMe_3$/silica gel reaction could be due to this reason. The surface-structure moieties that were observed in Ting and Maciel's work are only the surface species that are stable after a full hydrolysis treatment. It is not hard to raise questions like: what are the other moieties generated initially on the surface in the reaction between the silica surface and those organometallic reagents? Are these moieties stable or are they extractable when subjected to a polar solvent? And what would happen to these (hypothetical) moieties if only a limited amount of H_2O were introduced on to the surface? The motivation of this thesis study is to try to answer these questions.

This thesis project is focused on the $AlMe_3$/silica system. The emphasis of this thesis project is on understanding the surface reactions between $AlMe_3$ and silica, characterizing quantitatively the moieties generated during the initial reaction and understanding the properties of the initial surface moieties at difference stages (after the initial reaction, after washing with solvent, after treatment with limited amounts of H_2O and after a full work-up). Solid state NMR (^{13}C, ^{1}H, ^{29}Si, ^{1}H) are still the major tools in this study for surface structure elucidation, also assisted by liquid-sample ^{13}C NMR and other analytical methods.

References

1. Scott, R. P. W., *Silica gel and bonded phases: their production, properties, and use in LC*. Wiley: Chichester; New York, 1993; p 1-19.

2. Scott, R. P. W., *Silica gel and bonded phases: their production, properties, and use in LC*. Wiley: Chichester; New York, 1993; p 23-41.

3. Iler, R. K., *The Chemistry of Silica: Solubility, Polymerization, Colloid and Surface Properties and Biochemistry*. John Wiley & Sons: 1979; p 892.

4. Liu, C. C.; Maciel, G. E., The Fumed Silica Surface: A Study by NMR. *J. Am. Chem. Soc.* **1996,** *118*, 5103-5119.

5. Liu, C. C.; Maciel, G. E., Quantitative Analysis of Solids by High-Resolution ^{1}H NMR. *Anal. Chem.* **1996,** *68*, 1401-1407.

6. Sindorf, D. W.; Maciel, G. E., Silicon-29 nuclear magnetic resonance study of hydroxyl sites on dehydrated silica gel surfaces, using silylation as a probe. *J. Phys. Chem.* **1983,** *87*, 5516-5521.

7. Sindorf, D. W.; Maciel, G. E., Silicon-29 NMR study of dehydrated/rehydrated silica gel using cross polarization and magic-angle spinning. *J. Am. Chem. Soc.* **1983,** *105*, 1487-1493.

8. Erkelens, J.; Linsen, B. G., Quantitative determination of hydroxy groups and water for silica. *J. Colloid Interface Sci.* **1969,** *29*, 464-468.

9. Laeufer, S., Quantitative determination of surface groups in silica: IR analysis of isolated silanol groups in pyrogenic silica. *J. Mol. Struct.* **1980,** *60*, 409-414.

10. Gorski, D.; Klemm, E.; Fink, P.; Hoerhold, H. H., Investigation of quantitative silanol determination by the silane treatment of disperse silica. *J. Colloid Interface Sci.* **1988,** *126*, 445-449.

11. McFarlan, A. J.; Morrow, B. A., Infrared evidence for two isolated silanol species on activated silicas. *J. Phys. Chem.* **1991,** *95*, 5388-5390.

12. Jal, P. K.; Patel, S.; Mishra, B. K., Chemical modification of silica surface by immobilization of functional groups for extractive concentration of metal ions. *Talanta* **2004,** *62*, 1005-1028.

13. Sato, M.; Kanbayashi, T.; Kobayashi, N.; Shima, Y., Hydroxyl groups on silica, alumina, and silica-alumina catalysts. *J. Catal.* **1967,** *7*, 342-351.

14. Fripiat, J. J.; Uytterhoeven, J., Hydroxyl content in silica gel "Aerosil". *Journal of Physical Chemistry* **1962,** *66*, 800-805.

15. Nondek, L.; Vyskocil, V., Determination of surface hydroxyl groups on silanized silica gels for reversed-phase liquid chromatography. *Journal of Chromatography* **1981,** *206*, 581-585.

16. Scott, R. P. W., *Silica gel and bonded phases: their production, properties, and use in LC*. Wiley: Chichester; New York, 1993; p 139-156.

17. Schmidt, H.; Bottner, H., Chemistry and Properties of Porous, Organically Modified Silica. In *Chemistry and Properties of Porous, Organically Modified Silica*, Bergna, H. E., American Chemical Society: Washington, DC, 1990; Vol. 234, p 419-432.

18. Prado, A. G. S.; Airoldi, C., Adsorption, preconcentration and separation of cations on silica gel chemically modified with the herbicide 2,4-dichlorophenoxyacetic acid. *Anal. Chim. Acta* **2001,** *432*, 201-211.

19. Price, P. M.; Clark, J. H.; Macquarrie, D. J., Modified silicas for clean technology. *Dalton* **2000**, 101-110.

20. Tao, T.; Maciel, G. E., Reactivities of Silicas with Organometallic Methylating Agents. *J. Am. Chem. Soc.* **2000,** *122*, 3118-3126.

21. Chu, C. H.; Jonsson, E.; Auvinen, M.; Pesek, J. J.; Sandoval, J. E., A new approach for the preparation of a hydride-modified substrate used as an intermediate in the synthesis of surface-bonded materials. *Analytical Chemistry* **1993,** *65*, 808-816.

22. Krupczynska, K.; Buszewski, B.; Jandera, P., Characterizing HPLC stationary phases. *Analytical Chemistry* **2004,** *76*, 226A-234A.

23. Brunauer, S.; Emmett, P. H., Use of van der Waals adsorption isotherms in determining the surface area of iron synthetic-ammonia catalysts. *J. Am. Chem. Soc.* **1935,** *57*, 1754-1755.

24. Brunauer, S.; Emmett, P. H.; Teller, E., Adsorption of gases in multimolecular layers. *J. Am. Chem. Soc.* **1938,** *60*, 309-319.

25. Scott, R. P. W., *Silica gel and bonded phases: their production, properties, and use in LC*. Wiley: Chichester; New York, 1993; p 43-69.

26. Sing, K. S. W., Adsorption methods for the characterization of porous materials. *Adv. Colloid Interface Sci.* **1998,** *76-77*, 3-11.

27. Gun'ko, V. M.; Sheeran, D. J.; Augustine, S. M.; Blitz, J. P., Structural and Energetic Characteristics of Silicas Modified by Organosilicon Compounds. *J. Colloid Interface Sci.* **2002,** *249*, 123-133.

28. Serpinet, J., Gas-chromatographic study of the existence and the physical state of monomolecular films of stationary phases in contact with siliceous supports. Apparent increase of the melting point of the film. *Journal of Chromatography* **1972,** *68*, 9-18.

29. Claudy, P.; Letoffe, J. M.; Gaget, C.; Morel, D.; Serpinet, J., Long-chain alkyl grafts and mixed alkyl-alkane layers at the surface of macroporous silicas. Their gas chromatographic properties below and above the phase transition. *Journal of Chromatography* **1985,** *329*, 331-349.

30. Pethrick, R. A.; Dawkins, J. V., *Modern Techniques for Polymer Characterisation*. John Wiley and Sons Ltd: 1999; p 171-182.

31. Ramsay, J. D. F., Surface and pore structure characterization by neutron scattering techniques. *Adv. Colloid Interface Sci.* **1998,** *76-77*, 13-37.

32. Maciel, G. E.; Sindorf, D. W.; Bartuska, V. J., Characterization of silica-attached systems by silicon-29 and carbon-13 cross-polarization and magic-

angle spinning nuclear magnetic resonance. *Journal of Chromatography.* **1981,** *205*, 438-443.

33. Sindorf, D. W.; Maciel, G. E., Carbon-13 CP/MAS NMR study of molecular motion in n-alkylsilane bonded to the silica surface. *J. Am. Chem. Soc.* **1983,** *105*, 1848-1851.

34. Sindorf, D. W.; Maciel, G. E., Cross-polarization magic-angle-spinning silicon-29 nuclear magnetic resonance study of silica gel using trimethylsilane bonding as a probe of surface geometry and reactivity. *J. Phys. Chem.* **1982,** *86*, 5208-5219.

35. Sindorf, D. W.; Maciel, G. E., Silicon-29 CP/MAS NMR studies of methylchlorosilane reactions on silica gel. *J. Am. Chem. Soc.* **1981,** *103*, 4263-4265.

36. Maciel, G. E.; Sindorf, D. W., Silicon-29 NMR study of the surface of silica gel by cross polarization and magic-angle spinning. *J. Am. Chem. Soc.* **1980,** *102*, 7606-7607.

37. Boiadjiev, V.; Blumenfeld, A.; Gutow, J.; Tysoe, W. T., Infrared and NMR Spectroscopic Studies of n-Alkanethiols Chemically Grafted on Dimethylzinc-Modified Silica Surfaces. *Chem. Mater.* **2000,** *12*, 2604-2613.

38. Kleisner, R. J.; Koeck, B. H.; Phillips, M. R.; Wieland, J. A.; Gutow, J. H.; Boiadjiev, V.; Tysoe, W. T., A system based on metal alkyl species that forms chemically bound organic overlayers on hydroxylated planar surfaces. *Thin Solid Films* **2001,** *381*, 10-14.

39. Puurunen, R. L.; Root, A.; Sarv, P.; Haukka, S.; Iiskola, E. I.; Lindblad, M.; Krause, A. O. I., Growth of aluminium nitride on porous silica by atomic layer chemical vapour deposition. *Appl. Surf. Sci.* **2000,** *165*, 193-202.

40. Kinney, J. B.; Staley, R. H., Reactions of titanium tetrachloride and trimethylaluminum at silica surfaces studied by using infrared photoacoustic spectroscopy. *J. Phys. Chem.* **1983,** *87*, 3735-3740.

41. Murray, J.; Jones, P.; Hockey, J. A., Reactions of silica surfaces with hydrogen sequestering agents. *Trans. Faraday Soc.* **1971,** *67*, 848-853.

42. Morrow, B. A.; Hardin, A. H., Raman spectra of some hydrogen sequestering agents chemisorbed on silica. *J. Phys. Chem.* **1979,** *83*, 3135-3141.

43. Hunnicutt, M. L.; Harris, J. M., Reactivity of organosilane reagents on microparticulate silica. *Analytical Chemistry* **1986,** *58*, 748-52.

44. Lochmuller, C. H.; Colborn, A. S.; Hunnicutt, M. L.; Harris, J. M., Organization and distribution of molecules chemically bound to silica. *Analytical Chemistry* **1983,** *55*, 1344-8.

45. Anwander, R.; Palm, C.; Groeger, O.; Engelhardt, G., Formation of Lewis Acidic Support Materials via Chemisorption of Trimethylaluminum on Mesoporous Silicate MCM-41. *Organometallics* **1998,** *17*, 2027-2036.

46. Morrow, B. A.; McFarlan, A. J., Infrared and gravimetric study of an aerosil and a precipitated silica using chemical and hydrogen/deuterium exchange probes. *Langmuir* **1991,** *7*, 1695-1701.

47. Mathias, J.; Wannemacher, G., Basic characteristics and applications of aerosil. 30. The chemistry and physics of the aerosil surface. *J. Colloid Interface Sci.* **1988,** *125*, 61-68.

48. Morrow, B. A.; McFarlan, A. J., Chemical reactions at silica surfaces. *J. Non-Cryst. Solids* **1990,** *120*, 61-71.

49. Gilman, H.; Benkeser, R. A.; Dunn, G. E., Reaction of butyllithium with some organosilicon compounds. *J. Am. Chem. Soc.* **1950,** *72*, 1689-1691.

50. Murray, J.; Sharp, M. J.; Hockey, J. A., Polymerization of propylene by the $SiO_2/TiCl_4/AlMe_3$ system. *J. Catal.* **1970,** *18*, 52-56.

51. Peglar, R. J.; Murray, J.; Hambleton, F. H.; Sharp, M. J.; Parker, A. J.; Hockey, J. A., Chemical production and trapping of methyl radicals at silica surfaces. *J. Chem. Soc. A* **1970**, 2170-2172.

52. Armistead, C. G.; Hockey, J. A., Reactions of chloromethyl silanes with hydrated Aerosil silicas. *Trans. Faraday Soc.* **1967,** *63*, 2549-2556.

53. Peri, J. B., Infrared study of OH and NH_2 groups on the surface of a dry silica aerogel. *J. Phys. Chem.* **1966,** *70*, 2937-2945.

54. Davydov, V. Y.; Kiselev, A. V.; Zhuravlev, L. T., Surface and bulk hydroxyl groups of silica by infrared spectra and D_2O-exchange. *Trans. Faraday Soc.* **1964,** *60*, 2254-2264.

55. Peglar, R. J.; Hambleton, F. H.; Hockey, J. A., Surface structure and catalytic cracking properties of silicon oxide-boron trichloride, silicon oxide-trimethylaluminum, and silicon oxide-aluminum trichloride systems. I. Infrared and analytical studies. *J. Catal.* **1971,** *20*, 309-320.

56. McDonald, R. S., Study of the interaction between hydroxyl groups of aerosil silica and adsorbed nonpolar molecules by infrared spectrometry. *J. Am. Chem. Soc.* **1957,** *79*, 850-854.

57. Peri, J. B.; Hannan, R. B., Surface hydroxyl groups on g-alumina. *J. Phys. Chem.* **1960,** *64*, 1526-1530.

58. Peri, J. B., Infrared and gravimetric study of the surface hydration of g-alumina. *Journal of Physical Chemistry* **1965,** *69*, 211-219.

59. Basila, M. R., An infrared study of a silica-alumina surface. *Journal of Physical Chemistry* **1962,** *66*, 2223-2228.

60. Carter, J. L.; Lucchesi, P. J.; Yates, D. J. C., The nature of residual OH groups on a series of near-Faujasite zeolites. *Journal of Physical Chemistry* **1964,** *68*, 1385-1391.

61. Uytterhoeven, J.; Christner, L. G.; Keith Hall, W., The hydrogen held by solids. VIII. The decationated zeolites. *Journal of Physical Chemistry* **1965,** *69*, 2117-2126.

62. Weiss, H. G.; Knight, J. A.; Shapiro, I., Change in the ratio of hydroxyl groups attached to silicon and aluminum atoms in silica-alumina catalysts upon activation. *J. Am. Chem. Soc.* **1959,** *81*, 1823-1826.

63. Shapiro, I.; Weiss, H. G., Bound water in silica gel. *Journal of Physical Chemistry* **1953,** *57*, 219-221.

64. Hall, W. K.; Leftin, H. P.; Cheselske, F. J.; O'Reilly, D. E., Hydrogen held by solids. IV. Deuterium exchange and NMR [nuclear magnetic resonance] investigations of silica, alumina, and silica-alumina catalysts. *J. Catal.* **1963,** *2*, 506-517.

65. Lee, J. K.; Weller, S. W., Determination of catalyst water by exchange with deuterium gas. *Analytical Chemistry* **1958,** *30*, 1057-1058.

66. Hindin, S. G.; Weller, S. W., The effect of pretreatment on the activity of g-alumina. I. Ethylene hydrogenation. *Journal of Physical Chemistry* **1956,** *60*, 1501-6.

67. Gilman, H.; Haubein, A. H.; Hartzfeld, H., The cleavage of some ethers by organolithium compounds. *J. Org. Chem.* **1954,** *19*, 1034-1040.

68. Blitz, J. P.; Meverden, C. C.; Diebel, R. E., III, Reactions of Dibutylmagnesium with Modified Silica Gel Surfaces. *Langmuir* **1998,** *14*, 1122-1129.

69. Collins, S.; Kelly, W. M.; Holden, D. A., Polymerization of propylene using supported, chiral, ansa-metallocene catalysts: production of polypropylene with narrow molecular weight distributions. *Macromolecules* **1992,** *25*, 1780-1785.

70. Chuang, I. S.; Maciel, G. E., A Detailed Model of Local Structure and Silanol Hydrogen Bonding of Silica Gel Surfaces. *J. Phys. Chem. B* **1997,** *101*, 3052-3064.

71. Hlatky, G. G.; Upton, D. J., Supported Ionic Metallocene Polymerization Catalysts. *Macromolecules* **1996,** *29*, 8019-8020.

72. Ribeiro, M. R.; Deffieux, A.; Portela, M. F., Supported Metallocene Complexes for Ethylene and Propylene Polymerizations: Preparation and Activity. *Ind. Eng. Chem. Res.* **1997,** *36*, 1224-1237.

73. Abbenhuis, H. C. L., Heterogenization of metallocene catalysts for alkene polymerization. *Angewandte Chemie, International Edition* **1999,** *38*, 1058-1060.

74. Fink, G.; Steinmetz, B.; Zechlin, J.; Przybyla, C.; Tesche, B., Propene Polymerization with Silica-Supported Metallocene/MAO Catalysts. *Chemical Reviews (Washington, D. C.)* **2000,** *100*, 1377-1390.

75. Becker, R.-J.; Guertzgen, S.; Kutschera, D. Process for gas-phase deposition of alkyl aluminoxanes on inert carriers for polymerization process catalysts. 95-102719
EP 672671, 19950225., 1995.

76. Hlatky, G. G., Heterogeneous Single-Site Catalysts for Olefin Polymerization. *Chemical Reviews (Washington, D. C.)* **2000,** *100*, 1347-1376.

77. Suntola, T.; Antson, J. Methods for producing compound thin films. US patent 4058430, 1977.

78. Lakomaa, E. L.; Root, A.; Suntola, T., Surface reactions in Al_2O_3 growth from trimethylaluminium and water by atomic layer epitaxy. *Appl. Surf. Sci.* **1996,** *107*, 107-115.

79. Bartram, M. E.; Michalske, T. A.; Rogers, J. W., Jr.; Paine, R. T., Nucleation and growth of aluminum nitride: self-limiting reactions and the regeneration of active sites using sequential exposures of trimethylaluminum and ammonia on silica at 600 K. *Chem. Mater.* **1993,** *5*, 1424-1430.

80. Gautier, M.; Duraud, J. P.; Le Gressus, C., Electronic structure of an aluminum nitride film produced by ion implantation, studied by electron spectroscopy. *J. Appl. Phys.* **1987,** *61*, 574-580.

81. Kovacich, J. A.; Kasperkiewicz, J.; Lichtman, D.; Aita, C. R., Auger electron and x-ray photoelectron spectroscopy of sputter deposited aluminum nitride. *J. Appl. Phys.* **1984,** *55*, 2935-2939.

82. Hentzell, H. T. G.; Harper, J. M. E.; Cuomo, J. J., Synthesis of compound thin films by dual ion beam deposition. II. Properties of aluminum-nitrogen films. *J. Appl. Phys.* **1985,** *58*, 556-563.

83. Bartram, M. E.; Michalske, T. A.; Rogers, J. W., Jr.; Mayer, T. M., Chemisorption of trimethylaluminum and ammonia on silica: mechanisms for the formation of aluminum-nitrogen bonds and the elimination of methyl groups bonded to aluminum. *Chem. Mater.* **1991,** *3*, 953-960.

84. Hoffman, D. M., Chemical vapor deposition of nitride thin films. *Polyhedron* **1994,** *13*, 1169-1179.

85. Bent, B. E.; Nuzzo, R. G.; Dubois, L. H., Surface organometallic chemistry in the chemical vapor deposition of aluminum films using triisobutylaluminum: b-hydride and b-alkyl elimination reactions of surface alkyl intermediates. *J. Am. Chem. Soc.* **1989,** *111*, 1634-1644.

86. Puurunen, R. L.; Root, A.; Haukka, S.; Iiskola, E. I.; Lindblad, M.; Krause, A. O. I., IR and NMR Study of the Chemisorption of Ammonia on Trimethylaluminum-Modified Silica. *J. Phys. Chem. B* **2000,** *104*, 6599-6609.

87. Uusitalo, A. M.; Pakkanen, T. T.; Kroger-Laukkanen, M.; Niinisto, L.; Hakala, K.; Paavola, S.; Lofgren, B., Heterogenization of racemic ethylenebis(1-indenyl)zirconium dichloride on trimethylaluminum vapor modified silica surface. *J. Mol. Catal. A* **2000,** *160*, 343-356.

88. Bartram, M. E.; Michalske, T. A.; Rogers, J. W., Jr., A reexamination of the chemisorption of trimethylaluminum on silica. *J. Phys. Chem.* **1991,** *95*, 4453-4463.

89. Low, M. J. D.; Severdia, A. G.; Chan, J., Reactive silica. XV. Some properties of solids prepared by the reaction of trimethylaluminum with silica. *J. Catal.* **1981,** *69*, 384-391.

Chapter 2. EXPERIMENTAL SECTION.

2.1. Background of Solid State NMR Techniques.

After about 30 years of theory development, as well as technique and hardware improvements, solid-state NMR shows its strength in the analytical chemistry area. The biggest advantage from solid-state NMR is that it breaks the traditional liquid sample NMR routine, which requires having all samples in the liquid state. The sample remains in the solid form, making it possible to do *in situ* studies, or to study the structure of a sample of interest in the solid form, which can often more faithfully represent the real properties of the sample. In the study reported here, solid-state NMR is used to study/elucidate the structures on the silica gel surface after it has reacted with trimethylaluminum. In the following text, the basic techniques involved in this study are first covered briefly.

2.1.1. Homonuclear and heteronuclear dipole-dipole interactions.

The magnetic dipole-dipole interaction, which is a weak intermolecular interaction between the magnetic dipole moments of nuclei, is one the dominating factors in solid-state NMR spectroscopy. Due to different orientations of the magnetic dipole moments of neighboring nuclei, the local magnetic field varies from point to point over the solid. Since the NMR frequency is strongly sensitive to the local magnetic field, the local magnetic field variation is reflected

in the NMR spectrum and the signal appears as a distribution over a large frequency range, instead of just a single resonance frequency (determined by the chemical shift). This line broadening effect caused by the nuclear magnetic dipole-dipole interaction is called "dipole-dipole broadening". In liquid-sample NMR, due to the fast tumbling motion of the molecules, this dipole-dipole interaction is averaged to zero, being therefore manifested only mainly in terms of relaxation. But, in solid-state NMR, in which there is a lack of the freedom of molecular motion, this dipole-dipole effect can become significant, even dominant.

Dipole-dipole interactions can occur between homonuclear or heteronuclear spin pairs. In ^{1}H NMR, proton-proton homonuclear dipolar interactions are a major factor in the spectrum, since the proton is an abundant spin species and has a large gyromagnetic ratio. Homonuclear ^{1}H-^{1}H dipole interactions in rigid solids can be as large as tens of kilohertz. As demonstrated in this lab before,[1] only if the protons in the sample are very weakly coupled, such as in a dry silica gel or zeolite, can a proton NMR spectrum obtained at a "modest" magic-angle spinning speed (roughly 10 kHz) be entirely successful. In previous published work by Maciel,[2, 3] White[4] and Pfiefer[5-7], MAS ^{1}H NMR was used to investigate the surface hydroxyl groups of zeolite or silica gel surfaces, showing that with a MAS speed of about 11 kHz, the ^{1}H-^{1}H dipole interaction can be largely overcome so that quantitative information on surface hydroxyl groups can be obtained. In ^{13}C and ^{29}Si NMR experiments, since the natural abundance of ^{13}C and ^{29}Si are so small (1.1% for ^{13}C and 4.7% for ^{29}Si), homonuclear dipole pairs are rare. This, and the fact that the magnetic moments of ^{13}C and ^{29}Si are

small, lead to the fact that the homonuclear ^{13}C-^{13}C and ^{29}Si-^{29}Si dipole interactions are so small that they can usually be ignored (or are easily overcome).

In ^{13}C or ^{29}Si NMR, the heteronuclear dipole interaction between an abundant spin species (^{1}H) and a dilute spin species (^{13}C or ^{29}Si) becomes a major concern in the NMR experiment. This heteronuclear (^{1}H-^{13}C or ^{1}H-^{29}Si) dipole interaction can be suppressed by applying a ^{1}H decoupling technique, which is brought about by irradiation at the proton resonance frequency during the acquisition period. The MAS technique is also combined with high-power ^{1}H decoupling to reduce line broadening and will be described in the next section.

2.1.2. Magic angle spinning (MAS).

Another source of NMR line broadening in a solid sample is the chemical shift anisotropy (CSA). CSA is the orientation dependence of the local (shielding) magnetic field generated by electronic currents induced by the static magnetic field, $\mathbf{B_0}$. The local (shielding) magnetic field $\mathbf{B'}$, which is proportional to the applied external field $\mathbf{B}$, can be written as:

$$\mathbf{B'} = -\boldsymbol{\sigma} \cdot \mathbf{B} \qquad (2.1)$$

where $\boldsymbol{\sigma}$ is the "chemical shielding" effect, represented by a second rank tensor. Because of this tensor property the local chemical shift field may differ according to the direction of $\mathbf{B}$. The chemical shift Hamiltonian is written, for the case of $\boldsymbol{B}$ applied along the z axis ($\mathbf{B} = \mathbf{k}B_0 = \mathbf{B_0}$) as:

$$H_c = \sum_i \hbar \sigma_{izz} I_{iz} B_0 \tag{2.2}$$

where *i* represents a particular nucleus. If the symmetric part of the tensor $\boldsymbol{\sigma}_i$ has principle values σ_{i1}, σ_{i2} and σ_{i3} along its principal axes and if θ_{i1}, θ_{i2} and θ_{i3} are the three angles made between each of these axes and the direction of $\mathbf{B_0}$, then

$$\sigma_{izz} = \sigma_{i1} \cos^2 \theta_{i1} + \sigma_{i2} \cos^2 \theta_{i2} + \sigma_{i3} \cos^2 \theta_{i3} \tag{2.3}$$

In the liquid-sample case with rapid and random rotation, angles θ_{i1}, θ_{i2} and θ_{i3} in the above equation vary randomly; then the time average of σ_{izz} is given by:

$$\sigma_{izz} = \frac{1}{3}(\sigma_{i1} + \sigma_{i2} + \sigma_{i3}) = \overline{\boldsymbol{\sigma}_i} \tag{2.4}$$

In the solid-sample case, different sites (orientations) may have different values for the angles, θ_{i1}, θ_{i2} and θ_{i3}. This forms a distribution of local fields and results in a broadened line. If the solid sample is rotated at an angular frequency, ω_r, along an axis having an angle β with respect to the magnetic field $\mathbf{B_0}$ and angles, χ_{i1}, χ_{i2} and χ_{i3}, with respect to the principal axes of a specific particle or component of the sample, then for the *p*th principal axis we have:

$$\cos\theta_{ip} = \cos\beta\cos\chi_{ip} + \sin\beta\sin\chi_{ip}\cos(\omega_r t + \psi_{ip}) \tag{2.5}$$

where ψ_{ip} is the initial azimuthal angle σ_i of the *p* th principle axis with respect to the rotating axis; with Eq. 2.3 and 2.5, one can get:

$$\overline{\sigma_{izz}} = \frac{1}{2}(\sin^2\beta)(\sigma_{i1} + \sigma_{i2} + \sigma_{i3}) + \frac{1}{2}(3\cos^2\beta - 1)\sum_p \sigma_{ip}\cos^2\chi_{ip} \qquad (2.6)$$

where $\overline{\sigma_{izz}}$ is the time average of σ_{izz}. When $(3\cos^2\beta - 1)$ is equal to zero, the chemical shift Hamiltonian is reduced to zero, and the CSA has been eliminated.[8]

As described above, the chemical shift anisotropy (as well as the dipole-dipole interaction) have a factor in which, when the angle between the sample-rotation axis and the external magnetic field $\mathbf{B_0}$ is equal to 54.7°, the effect is reduced to zero. This technique, setting the sample rotating at an axis that makes a 54.7° angle with the external magnetic field direction, can eliminate the line broadening effects brought about by the chemical shift anisotropy (and many nuclear dipole interactions); this technique is called *Magic Angle Spinning*, MAS. The angle, 54.7°, is called the *magic angle*.

2.1.3. Sensitivity enhancement by cross polarization (CP).

The cross polarization technique was first developed during the early 1970's by Pines, Gibby and Waugh.[9] The cross polarization experiment is a double resonance experiment, which transfers the polarization of abundant, higher-magnetogyric-ratio spins (such as ^1H) to insensitive nuclei (such as ^{13}C or ^{29}Si). The cross polarization process in solids can be explained in a thermodynamic way. The proton spins can be considered as a large thermodynamic bath, which can be placed at a lower spin temperature than that of the small thermodynamic bath of ^{13}C spins. When the Hartmann-Hahn condition is met ($\gamma_H B_{1H} = \gamma_C B_{1C}$, where γ is the magnetogyric ratio), heat (energy) can be transferred between the ^1H spin bath and the ^{13}C spin bath through the

heteronuclear ^{1}H-^{13}C dipole interaction. In this experiment, the magnetization of the abundant spins (^{1}H) is first placed in the transverse plane by applying a $\pi/2$ pulse, followed by a spin-locking field. In the Hartmann-Hahn condition, the two spin baths are placed in thermal contact. The ^{13}C spin bath lowers its spin temperature much more than the ^{1}H spin bath temperature increases during the cross polarization period, due to the difference in spin bath sizes (abundant spins and less abundant spins). During cross polarization, transverse magnetization is transferred from ^{1}H spins to ^{13}C spins. In a single exchange, the ^{13}C signal intensity can be enhanced by up to a factor of $\gamma_H / \gamma_C = 3.98$. Furthermore, the abundant spins, ^{1}H, have smaller spin-lattice relaxation times (T_1) than ^{13}C, which permits the process to be repeated faster than a simple single-pulse experiment on ^{13}C nuclei (governed by the ^{13}C T_1).

The CP technique is often combined with the MAS technique, yielding the technique known as CP/MAS NMR, and with high power proton decoupling during data acquisition time to get the best ^{13}C line narrowing (and hence, the best signal-to-noise) spectrum. Figure 2.1 shows the pulse sequence of a typical cross polarization (CP) experiment.

The cross polarization process takes place via ^{1}H-^{13}C dipolar interactions. During the CP period, the proton spins are spin-locked in the x-y plane along the direction of the cross-polarization RF pulse. During this period ^{1}H magnetization decays via rotating-frame ^{1}H spin-lattice relaxation and ^{13}C magnetization grows with a rate controlled by a constant T^{CH}, that reflects the strength of the heteronuclear interaction between ^{1}H and ^{13}C. The stronger the interaction, the

larger the rate constant $(T^{CH})^{-1}$ is. While ^{13}C magnetization is building up, ^{1}H magnetization is also decaying with a rate constant $(T_{1\rho})^{-1}$; there is a balance between the loss of ^{1}H magnetization and growth of ^{13}C magnetization. Thus, the contact time (how long the cross polarization is allowed to occur) must be carefully chosen if one wishes to obtain the maximum ^{13}C signal enhancement. The two rate constants, $(T^{CH})^{-1}$ and $(T_{1\rho})^{-1}$, can be measured directly by variable-contact-time CP experiments (*vide infra*).

2.1.4. Relaxation in NMR.

Not only to obtain the NMR spectrum with the highest signal-to-noise, but also to be able to make quantitative measurements using solid-state NMR, it is necessary to know the relevant relaxation constants in the system studied. With the benefits of signal enhancement and shorter experimental time resulting from cross polarization, the CP/MAS spin counting experiment has received considerable attention in NMR analysis. In the CP/MAS NMR spin counting experiment, corrections from both ^{1}H spin-lattice relaxation (T_1) and for cross polarization behavior (T^{CH} and proton $T_{1\rho}$) must be accomplished in order to get quantitatively reliable measurements.

2.1.4.1. Spin-lattice relaxation in the rotating frame; the measurement of proton $T_{1\rho}$.

As described above, proton $T_{1\rho}$ is the inverse of a rate constant that describes the decay of the ^{1}H magnetization during spin-locking; this parameter is known as the *spin-lattice relaxation time in the rotating frame*. The larger the

proton $T_{1\rho}$ is, the slower is the proton magnetization decay during spin-locking and the easier it is for ^{13}C magnetization to achieve better signal intensity. By setting up a series of CP experiments in which the period of the cross polarization (Hartmann-Hahn) condition (*contact time*) is varied systematically, both proton $T_{1\rho}$ and T^{CH} can be measured; this is referred to as the *variable-contact-time experiment*. The signal intensity obtained for a specific CP contact period (t) is determined by T^{CH} and proton $T_{1\rho}$ according to the following equation:[10]

$$M(t) = \frac{M^{\infty}}{(1 - T^{CH} / T_{1\rho})} \times e^{(-t/T_{1\rho})} \times (1 - e^{-t/T^{CH}}) \qquad (2.7)$$

T^{CH} and proton $T_{1\rho}$ are obtained at the same time when fitting the intensity data of the variable-contact-time experiment to the above equation.

2.1.4.2. Proton spin-lattice relaxation; the measurement of T_1.

In the presence of the RF field, there will be a transfer of spin polarization along the axis of the applied RF fields. Once the RF fields are turned off, the ^1H magnetization will try to rebuild thermal equilibrium along the external magnetic field $\mathbf{B_0}$, The rate at which spins try to rebuild thermal equilibrium along the $\mathbf{B_0}$ axis is described by T_1. Since this process involves an energy exchange between the spins and the lattice, T_1 is called the *spin-lattice relaxation time*. In pulsed FT NMR in general (including CP), one wants to let the relevant spin magnetization reach equilibrium along the $\mathbf{B_0}$ axis before initiating the next cycle (repetition), in order to obtain maximum magnetization/signal. In pulsed FT NMR, increasing the signal-to-noise ratio by signal averaging depends on carring out a large number

of repetitions of the basic experiment. How fast one can repeat the basic experiment depends on the relevant spin-lattice relaxation time (T_1), and this is a crucial factor in optimizing the CP/MAS experiment. The process of the z-component of spin magnetization relaxing back from zero to equilibrium parallel to the external magnetic field ($\mathbf{B_0}$) can be described in the following equation:

$$M(t) = M^0(1 - e^{-t/T_1}) \tag{2.8}$$

where M^0 is the equilibrium magnetization along $\mathbf{B_0}$, and M(t) is the magnetization after a given relaxation period, t.

The T_1 value can be measured by various kinds of pulsed NMR experiments. The most popular experiment for measuring T_1 is the inversion-recovery experiment, which has a pulse sequence of [180° - t - 90° – acquire - wait]. Figure 2.2 shows the pulse sequence of a single-channel inversion-recovery experiment and a double-channel ^1H T_1 measurement via the ^{13}C CP/MAS-detected ^1H inversion-recovery experiment. The observed signal intensity follows the equation:

$$M(t) = M^0 \times (1 - 2e^{-t/T_1}) \tag{2.9}$$

where M(t) is the magnetization observed at given waiting time t between the 180° and 90° pulses. M^0 is the equilibrium magnetization. By fitting the intensity data into this equation, the T_1 value can be derived.

Another popular method used in this study to obtain the proton T_1 values of a sample is the *saturation-recovery* experiment. In this technique, many short pulses are applied first to saturate the magnetization; then, after a wait a time t to

let the magnetization grow along $\mathbf{B_0}$, a 90° 'interrogation' pulse is applied and data are acquired. Figure 2.3 shows a pulse sequence for a single-channel saturation-recovery experiment and a pulse sequence for a double-channel ^{13}C CP/MAS-detected ^{1}H T_1 saturation-recovery experiment. The intensity of the magnetization follows the following equation:

$$M(t) = M^0 \times (1 - e^{-t/T_1}) \tag{2.10}$$

where M(t) is the magnetization observed for a given waiting time, t, between the last saturation pulse and the 90° 'interrogation' pulse. M^0 is the equilibrium magnetization. By fitting the intensity data to this equation, the T_1 value can be derived.

The inversion-recovery technique is a popular experiment for measuring T_1; how fast one can repeat the complete cycle depends on the T_1 value of the sample studied. Compared to the inversion-recovery experiment, the saturation-recovery experiment can be repeated much faster, regardless of the T_1 value, because, how much magnetization is established along $\mathbf{B_0}$ at the beginning of next cycle doesn't matter, since it will be saturated in the next repetition. Sometimes, when the signals studied overlap with each other, it is most straightforward to use the saturation-recovery experiment, because all the signals obtained are positive and it is easier to do computer deconvolution to obtain the individual signals.

2.2. $AlMe_3$/silica gel reactions.

2.2.1. Preparation of reagents and reaction vessel.

Silica gel (Fisher S679), with a particle diameter range of 100-200 mesh and a surface area of 500 m^2/g, obtained from Fisher Scientific, was heated at 150 °C for 24 hr. at $5x10^{-3}$ torr to remove physisorbed water. Dehydration experiments were carried out in a tube furnace. A certain amount of silica gel was placed in a quartz tube with a stopcock fitting; the stopcock was attached via vacuum tubing to a vacuum line. The quartz tube was placed in a furnace under vacuum ($1x10^{-3}$ torr) at 150 °C for 24 hr. After drying, the silica gel was transferred to a 100 ml, 3-joint, round-bottom flask in a glove box, which was protected with $N_2(g)$ to exclude atmospheric moisture.

Trimethylaluminum ($AlMe_3$, 97%), a pyrophoric and moisture-sensitive material, obtained from Aldrich, was protected under $N_2(g)$ after every use in the original Aldrich Sure-Pac cylinder.

Toluene, purchased from Fisher Scientific, was refluxed over Na metal for 12 hr. with benzophenone; the liquid solution changed color to purple when the solution was free of H_2O. Cyclohexane, purchased from Fisher Scientific, was refluxed over Na metal for 12 hr. with benzophenone; the solution changed color to purple when the solution was free of H_2O. Diethyl ether (anhydrous) was obtained from Fisher Scientific and was stored over 4 Å molecular sieves.

All glassware (vessels, round bottom flasks, condensers, syringes) were heated in an oven at 60 °C for at least 12 hr, before use. All the glass containers were flushed with He(g) for at least 15 min right before use.

2.2.2. Reaction of $AlMe_3$ and silica gel.

A weighed quantity of about 12.0 g of dried silica gel was transferred into a round bottom flask in a glove box protected by N_2(g). Figure 2.4 shows the entire apparatus used for studying the $AlMe_3$/silica reaction. The entire setup was flushed with He(g) for at least 15 min; then 40 ml dry solvent (toluene or cyclohexane) was added to the round bottom flask with a syringe. The entire mixture was mixed by magnetic stirring, while cooling with a water/ice bath for 10 min. Then, a measured quantity (8.0 ml) of $AlMe_3$ (6.0 g), was added by syringe with He(g) protection. The mixture was allowed to react with stirring and under He(g) protection and with water/ice bath cooling for 4 hr. During the reaction, the CH_4 generated was collected in two N_2(l)-cooled traps, which were connected in series (Figure 2.4).

After the reaction proceeded for 4 hr, the mixture was allowed to sit without stirring to let the powder settle on the bottom; then the supernatant liquid was pulled out with a syringe and placed in another He(g)-flushed Erlenmeyer flask. The powder remaining in the round bottom flask was washed with three 20 ml portions of dry solvent (toluene or cyclohexane); each time the supernatant liquid was pulled out with a syringe and placed in the Erlenmeyer flask mentioned above to combine the liquids. About 0.4 ml of the combined liquid was transferred to a dried 5 mm liquid-sample NMR tube (for ^{13}C NMR analysis) under protection of He(g).

The residual powder was subjected to a rough vacuum ($1x10^{-1}$ torr) at room temperature (RT) to remove the bulk of the remaining liquid and then put

under a stronger vacuum ($5x10^{-3}$ torr, RT) for 8 hr. to dry more completely. The resulting solid powder sample (A, about 12 g) is referred to as the "dry sample"; it was weighed in a glove box, and about 2 g of the resulting powder was saved for ^{27}Al, ^{29}Si and ^{13}C NMR, while the remaining powder was transferred back to the round bottom flask to proceed to the next step.

The dry sample (A, above, about 10 g) was washed with three 20 ml portions of anhydrous diethyl ether under He(g) protection. For each wash, the mixture was stirred for about 15 min. A syringe was then used to pull the liquid out from the resulting pasty solid each time. The residual sample was briefly subjected to a rough vacuum ($1x10^{-1}$ torr, RT) to remove most of the diethyl ether, then put under stronger vacuum ($5x10^{-3}$ torr, RT) for 8 hr. for more complete drying. (Heating the sample while evacuating was not applied in order to avoid the possibility of thermal decomposition of surface moieties.) The resulting solid obtained is referred to as the "ether washed sample" (B, about 10 g). The powder sample was weighed in a glove box, and about 2 g powder was saved for ^{27}Al, ^{29}Si and ^{13}C NMR experiments, while the rest (B about 8 g) was packed back to the round bottom flask to proceed to the next step.

From the amount of the Al-CH_3 groups determined by ^{13}C spin-counting (*vide infra*), a quantity of H_2O corresponding to the number of moles of Al-CH_3 counted was added in a H_2O/diethyl ether mixture over 20 min to the "ether washed sample" (B, about 8 g) under He(g) protection, with ice/water cooling. Then, the supernatant liquid was pulled out by syringe and the remaining powder was washed with three 20 ml portions of diethyl ether. The residual powder was

subjected briefly to a rough vacuum ($1x10^{-1}$ torr, RT) to remove most of the diethyl ether and then put on under a stronger vacuum ($5x10^{-3}$ torr, RT) for 8 hr. to more completely dry the solid. The resulting solid sample is referred as "1st H_2O treatment" (C-1, about 8 g). About 2 g of this "1st H_2O treatment" sample was saved for ^{27}Al, ^{29}Si and ^{13}C NMR and the rest (C-1, 6 g) was used in the next step.

The "1st H_2O treatment" procedure was repeated until no further CH_4 evolution was observed into the $N_2(l)$ cold trap. The samples obtained from these H_2O treatments are referred as "2nd H_2O treatment" (C-2) and "3rd H_2O treatment" (C-3). Each such treatment yielded no significant weight change of the sample. About 2 g powder was saved after each H_2O treatment and the remaining powder was used in the next step.

During the "3rd H_2O treatment" no more CH_4 evolution was detected; the "3rd H_2O treatment" sample (C-3, about 2 g) was stirred with 40 ml H_2O for 4 hr. to permit full hydrolysis. The resulting solid sample was washed with 20 ml acetone, 20 methanol and 20 ml H_2O and then vacuum filtered to separate the solid from liquid in the resulting mixture. The resulting powder was dried under vacuum ($5x10^{-3}$ torr, RT) for 8 hr. The solid sample obtained (D) is called the "workup sample" (about 2 g).

Figure 2.5 is a flowchart showing the complete $AlMe_3$/silica gel reaction procedure.

2.3. Methane accounting in $AlMe_3$/silica gel reactions.

2.3.1. Volumetric CH_4.

During the reaction between $AlMe_3$ and silica gel, protecting He(g) was passed through the entire apparatus that includes two N_2(l)-cooled traps (Figure 2.4) to protect the whole reaction mixture from moisture and air. After the reaction apparently stopped (no additional gas evolution observed), the N_2(l)-cooled traps were first closed and disconnected from the reaction vessel and then connected individually to the volume-measuring cylinder at room temperature; the CH_4 trapped in each N_2(l) trap melted, vaporized and expanded at room temperature, expelling water from the measuring cylinder. The volume of CH_4 evolved was measured by the volume (height) of displaced water in the cylinder. This arrangement is show in Figure 2.4.

During the treatments of the $AlMe_3$-reacted silica gel with measured amounts of H_2O (equivalent to the amount of surface attached Al-Me moieties), the CH_4 generated was also monitored with N_2(l) cold traps. These incremental H_2O treatments were stopped when no additional CH_4 appeared to be trapped in the cold traps.

Conversion of the height of water displacement to the volume of CH_4 contained in each trap was made as follows:

Condition 1: trap was at 77.6 K; trap contained solid CH_4 and He(g);

T_1 = 77.6 K

V_1 = trap volume (V^{trap}) = V_1^{He}.

Condition 2: trap warmed to room temperature; the He(g) in the trap expanded and the CH_4 solid turned to gas and expanded at room temperature (RT). These gases expanded into the volume of displaced water in the measuring cylinder and into the original trap.

$T_2 = T^{RT}$ K

V_2 = trap volume (V^{trap}) + $V^{measured} = V_2^{He} + V_2^{CH_4}$

From the ideal gas law, when the amount of gas and pressure are constant,

$V_2 = V_1 (T_2/T_1)$

Then: $V_2^{He} = V_1^{He} (T^{RT}/T_1) = V^{trap} (T^{RT}/T_1)$

$V_2^{CH_4} = V^{measured} + V^{trap} - V_2^{He} = V^{measured} + V^{trap} (1 - T^{RT}/T_1)$

$= V^{measured} - V^{trap} (T^{RT}/T_1 - 1)$

2.3.2. ^{13}C NMR of solutions.

After the $AlMe_3$/silica gel reaction, the supernatant liquid and the washes (toluene solution or cyclohexane solution, depending on the reaction system) were combined together and prepared under He(g) flow for liquid ^{13}C NMR, which was carried out on a 400 MHz Varian Inova spectrometer.

^{13}C relaxation times of toluene methyl carbons, cyclohexane methylene carbons and the methyl groups of unreacted Al-Me species in solution were measured by inversion-recovery experiments; then the recovery time of the liquid sample NMR experiments was set long enough to let all the spins fully relax, so that correction for spin-lattice relaxation is not necessary in the quantitative analysis.

2.4. ^{1}H MAS experiments.

The dried silica gel sample was prepared in a tube furnace as described in Section 2.1. After the drying procedure, each sample was packed into a MAS rotor in a N_2(g)-protected glove box to exclude atmospheric moisture.

^{1}H MAS experiments for assessing surface hydroxyl contents were performed at a ^{1}H frequency of 360 MHz, using a Chemagnetics CMX-II NMR system. A roughly 14~15 mg silica gel sample was packed into a 4 mm zirconia Pencil Rotor™ with snuggly fitting Teflon caps at both ends of the sample chamber. In order to reduce RF field inhomogeneity, the volume of the sample was limited to a cylinder about 4 mm long and 2.5 mm in diameter. The MAS stator material used in the MAS spinning system was Kel-F in order to minimize the proton background signal. The sample was spun at 12.5 kHz with air as both the bearing and driving gas. All the ^{1}H MAS spectra were acquired using a 62.5 kHz ^{1}H B_1 field (4 μs ^{1}H 90° pulse) with a 30 s recovery time. polydimethylsiloxane (PDMS) was used as a reference sample (23.0 mg packed in a separate spinner), via sample substitution.[3]

In order to evaluate this ^{1}H MAS spin counting method, a control experiment was carried out in advance. Three accurately weighed 1,3,5-trimethoxybenzene samples were prepared with weight obtained on an analytical balance (about 16 mg). Experiments of the types described above were carried out, but replacing the silica gel sample with these weighed 1,3,5-trimethoxybenzene samples. The amount of each 1,3,5-trimethoxybenzene sample can in principle be obtained from the NMR signal intensity. The ^{1}H MAS

spin counting method was evaluated by comparing the NMR results with the gravimetric measurements.

2.5. ^{29}Si CP-MAS experiments.

^{29}Si CP-MAS experiments were performed at a ^{29}Si frequency of 39.7 MHz and a ^{1}H frequency of 200 MHz, using a Chemagnetics CMX-II NMR system. Each sample was packed in a 9 mm zirconia pencil rotor with Teflon end pieces, each of which has three O-rings for sealing from air at both ends; see Figure 2.6. The sample was spun at 3.5 kHz in a home-built MAS probe based on a Chemagnetics 9 mm Pencil Rotor™ MAS module. All the ^{29}Si CP-MAS spectra were acquired at a 41.7 kHz B_1 field for the ^{1}H 90° pulse (6 μs 90° pulse), a 35.7 kHz ^{29}Si field and 39.2 kHz ^{1}H field during the 5 ms CP mix time, with 38.5 kHz ^{1}H decoupling during detection, MAS spinning at 3.5 kHz and a 2 s recovery time.

2.6. ^{27}Al MAS experiments.

^{27}Al MAS experiments were performed at a ^{27}Al frequency of 156 MHz, using a Chemagnetics CMX-Infinity 600 MHz NMR system. Each sample was packed in a 4 mm zirconia pencil rotor with snuggly fitting Teflon caps at both ends. The sample was spun at a MAS speed of 16.5 kHz in a home-built single-channel MAS probe based on a 4 mm Chemagnetics Pencil Rotor™ MAS system. All the ^{27}Al MAS spectra were acquired with a 15° ^{27}Al pulse of 0.44 μs and a 0.5 s recovery time. This small tip angle is used because it has been shown that it is more straightforward to use small tip angles with quadrapolar nuclides, if quantitative analysis is desired.[11, 12]

2.7. ^{13}C NMR of solids.

2.7.1. CP-MAS experiments.

^{13}C CP-MAS experiments were performed at a ^{13}C frequency of 90 MHz, using a Chemagnetics CMX-II 360 system. Each sample was packed in a 9 mm zirconia Pencil Rotor™ with Teflon caps, each having three O-rings to seal both ends from air. The sample was spun at 3.6 kHz in a home-built double-channel MAS probe based on a 9mm Chemagnetics Pencil Rotor™ MAS system. All the ^{13}C CP-MAS spectra, except those of relaxation measurements, were acquired at a ^{1}H B_1 field of 50 kHz for the 90° pulse (5 μs ^{1}H 90° pulse), a 38.5 kHz ^{13}C B_1 field and a 42.1 kHz ^{1}H B_1 field during the 5 ms cross polarization time, and a 45 kHz ^{1}H field for decoupling during detection, spinning at 3.6 kHz and using a 3 s recovery time.

2.7.2. Relaxation measurements.

^{1}H spin-lattice relaxation (T_1) measurements on the reference sample, hexamethylbenzene (HMB), were obtained via ^{13}C CP/MAS-detected ^{1}H inversion-recovery experiments[13] at a ^{1}H B_1 field of 50 kHz for the ^{1}H 90° pulse (5 μs ^{1}H 90° pulse), a 38.5 kHz ^{13}C B_1 field and a 42.1 kHz ^{1}H B_1 field for cross polarization and a 45 kHz ^{1}H field for decoupling, with a 5 ms cross-polarization time and a 3 s recovery time.

^{1}H spin-lattice relaxation measurements of $AlMe_3$-reacted silica gel samples were obtained via ^{13}C CP/MAS-detected ^{1}H saturation-recovery experiments at a ^{1}H B_1 field of 50 kHz (5 μs ^{1}H 90° pulse), a 38.5 kHz ^{13}C B_1 field

and a 42.1 kHz ^1H B_1 field for cross polarization and a 45 kHz ^1H field for decoupling, with a 5 ms cross-polarization period and a 0.5 s recovery time.

The cross polarization parameters, proton $T_{1\rho}$ and T^{CH}, of both the reference compound (HMB) and $AlMe_3$-reacted silica gel samples were measured by variable-contact-time ^{13}C CP-MAS experiments[8] at a ^1H B_1 field of 50 kHz for the ^1H 90° pulse (5 μs ^1H 90° pulse), a 38.5 kHz ^{13}C B_1 field and a 42.1 kHz ^1H B_1 field during the 5 ms cross polarization period, and a 45 kHz ^1H field for decoupling, with MAS spinning at 3.6 kHz and a 5 s recovery time.

2.7.3. MAS rotor design.

In order to avoid exposing the sample to air or moisture, the 9 mm zirconia pencil rotors were capped with Teflon pieces at each end, each cap having three O-rings to seal the sample from air. Figure 2.6 shows the diagram of the O-ring/ Teflon cap arrangement.

2.7.4. Spin counting.

Solid-state ^{13}C NMR spin-counting experiments were performed at a ^{13}C NMR frequency of 90 MHz, using a Chemagnetics CMX-II NMR system, as described above. Data on the reference compound, hexamethylbenzene (HMB), were acquired under exactly the same conditions as used for $AlMe_3$/silica samples, before and after each spin counting experiment on reacted silica gel samples. The amounts of surface methyl groups were derived from the spin counting data, using correction factors for proton T_1 relaxation and for cross-polarization dynamics, according to the following equations:

$$M(t) = M^0 \times (1 - e^{-t/T_1}) \tag{2.11}$$

$$M(t) = M^\infty \times \frac{1}{1 - T^{CH} / T_{1\rho}} \times e^{(-t/T_{1\rho})} \times \left[1 - e^{-t/T^{CH}}\right] \tag{2.12}$$

In Eq. 2.11, *M(t)* is the intensity at a spin recovery time *t* and M^0 is the intensity when the recovery period is infinity (spins fully relaxed). In Eq. 2.12, *M(t)* is the magnetization at a given contact time *t* and M^∞ is the ^{13}C intensity that would be achieved if $(T^{CH})^{-1}$ and proton $T_{1\rho}$ were both infinite.

References

1. Dec, S. F.; Bronnimann, C. E.; Wind, R. A.; Maciel, G. E., Comparison of the proton NMR analysis of solids by the CRAMPS and MAS-only techniques. *J. Magn. Reson.* **1989,** *82*, 454-466.

2. Liu, C. C.; Maciel, G. E., The Fumed Silica Surface: A Study by NMR. *J. Am. Chem. Soc.* **1996,** *118*, 5103-5119.

3. Liu, C. C.; Maciel, G. E., Quantitative Analysis of Solids by High-Resolution ^{1}H NMR. *Anal. Chem.* **1996,** *68*, 1401-1407.

4. Wang, X.; Coleman, J.; Jia, X.; White, J. L., Quantitative Investigations of Acidity, and Transient Acidity, in Zeolites and Molecular Sieves. *J. Phys. Chem. B* **2002,** *106*, 4941-4946.

5. Freude, D.; Hunger, M.; Pfeifer, H.; Schwieger, W., Proton MAS NMR studies on the acidity of zeolites. *Chem. Phys. Lett.* **1986,** *128*, 62-66.

6. Freude, D.; Hunger, M.; Pfeifer, H., Study of Broensted acidity of zeolites using high-resolution proton magnetic resonance with magic-angle spinning. *Chem. Phys. Lett.* **1982,** *91*, 307-310.

7. Pfeifer, H.; Freude, D.; Hunger, M., Nuclear magnetic resonance studies on the acidity of zeolites and related catalysts. *Zeolites* **1985,** *5*, 274-286.

8. Stejskal, E. O.; Memory, J. D., *High resolution NMR in the solid state: fundamentals of CP/MAS*. Oxford University Press: New York, 1994; p 111-112.

9. Pines, A.; Gibby, M. G.; Waugh, J. S., Proton-enhanced NMR of dilute spins in solids. *J. Chem. Phys.* **1973,** *59*, 569-590.

10. Mehring, M., *Principles of High-Resolution NMR in Solids*. Springer-Verlag: Berlin; Heidelberg; New York, 1983; p 152-154.

11. Samoson, A.; Lippmaa, E., Excitation phenomena and line intensities in high-resolution NMR powder spectra of half-integer quadrupolar nuclei. *Physical Review B: Condensed Matter and Materials Physics* **1983,** *28*, 6567-6570.

12. Gore, K. U.; Abraham, A.; Hegde, S. G.; Kumar, R.; Amoureux, J.-P.; Ganapathy, S., ^{29}Si and ^{27}Al MAS/3Q-MAS NMR Studies of High Silica USY Zeolites. *J. Phys. Chem. B* **2002,** *106*, 6115-6120.

13. Breitmaier, E.; Voelter, W., *^{13}C NMR spectroscopy: methods and applications*. Verlag Chemie: Weinheim, Bergstr., 1974; p 51-54.

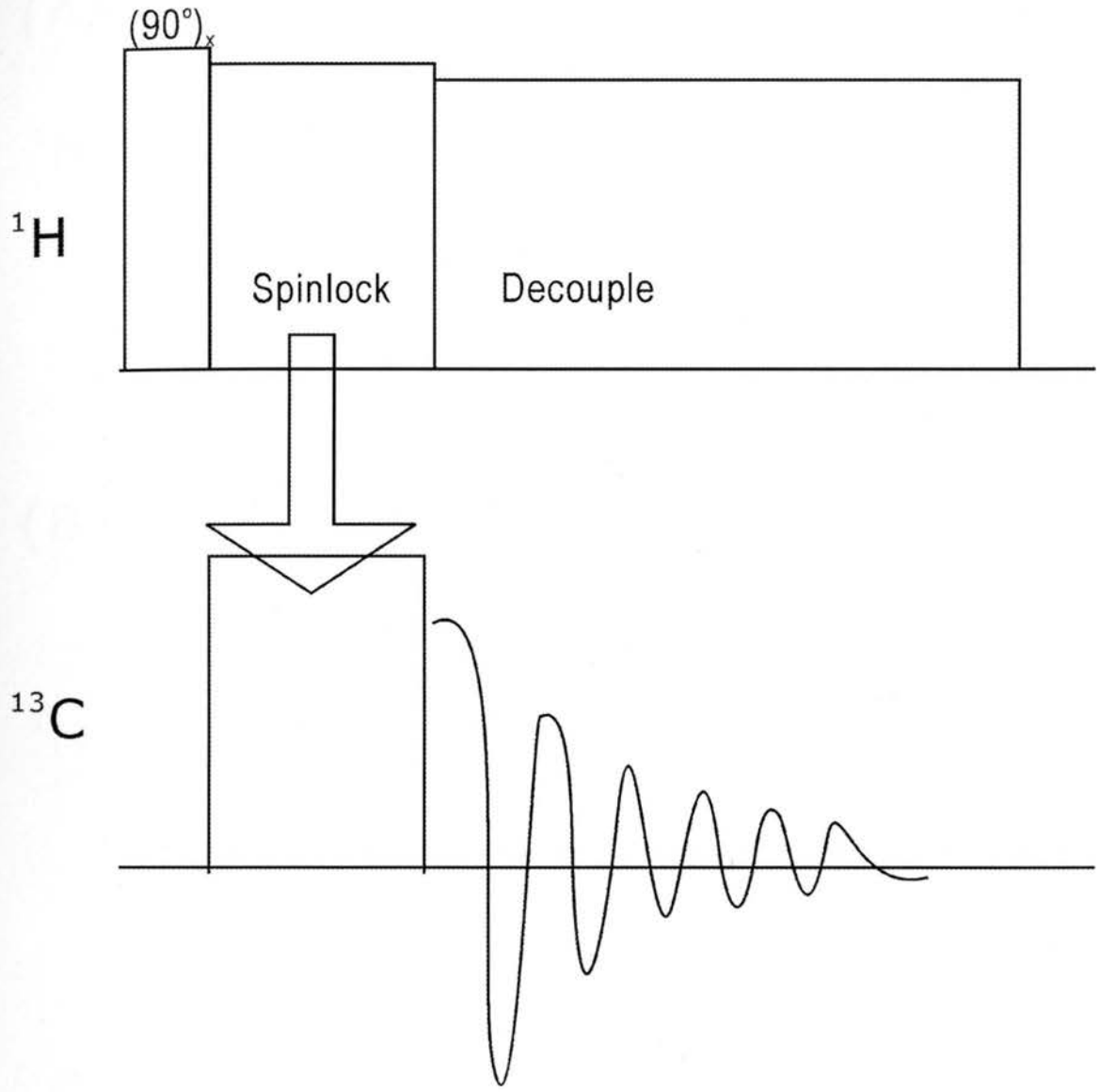

Figure 2.1. Pulse sequence of a typical 1H-13C cross polarization (CP) experiment.

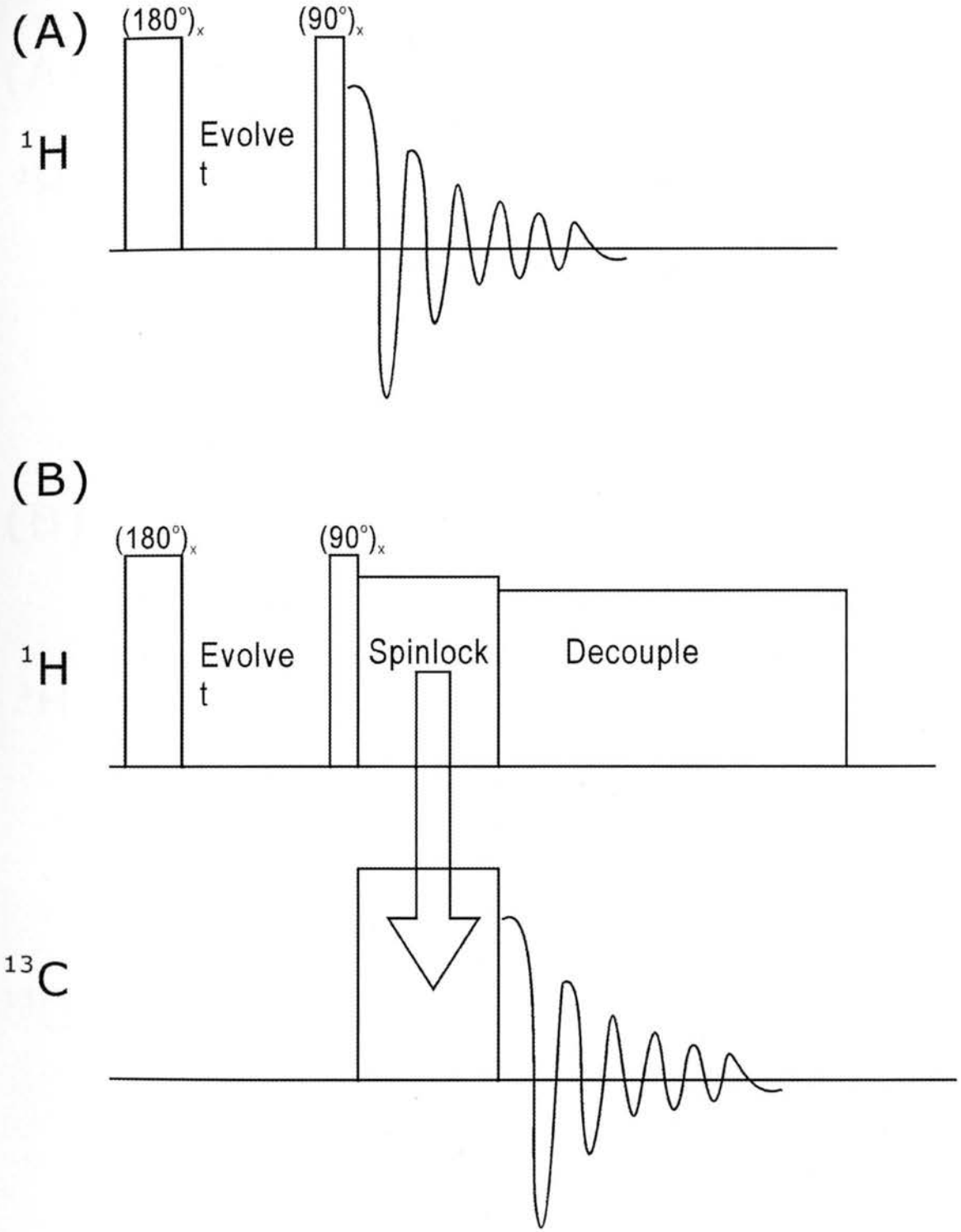

Figure 2.2. Pulse sequence for (A) a single channel inversion-recovery experiment and (B) a ^{13}C CP/MAS-detected ^{1}H T_1 inversion-recovery experiment.

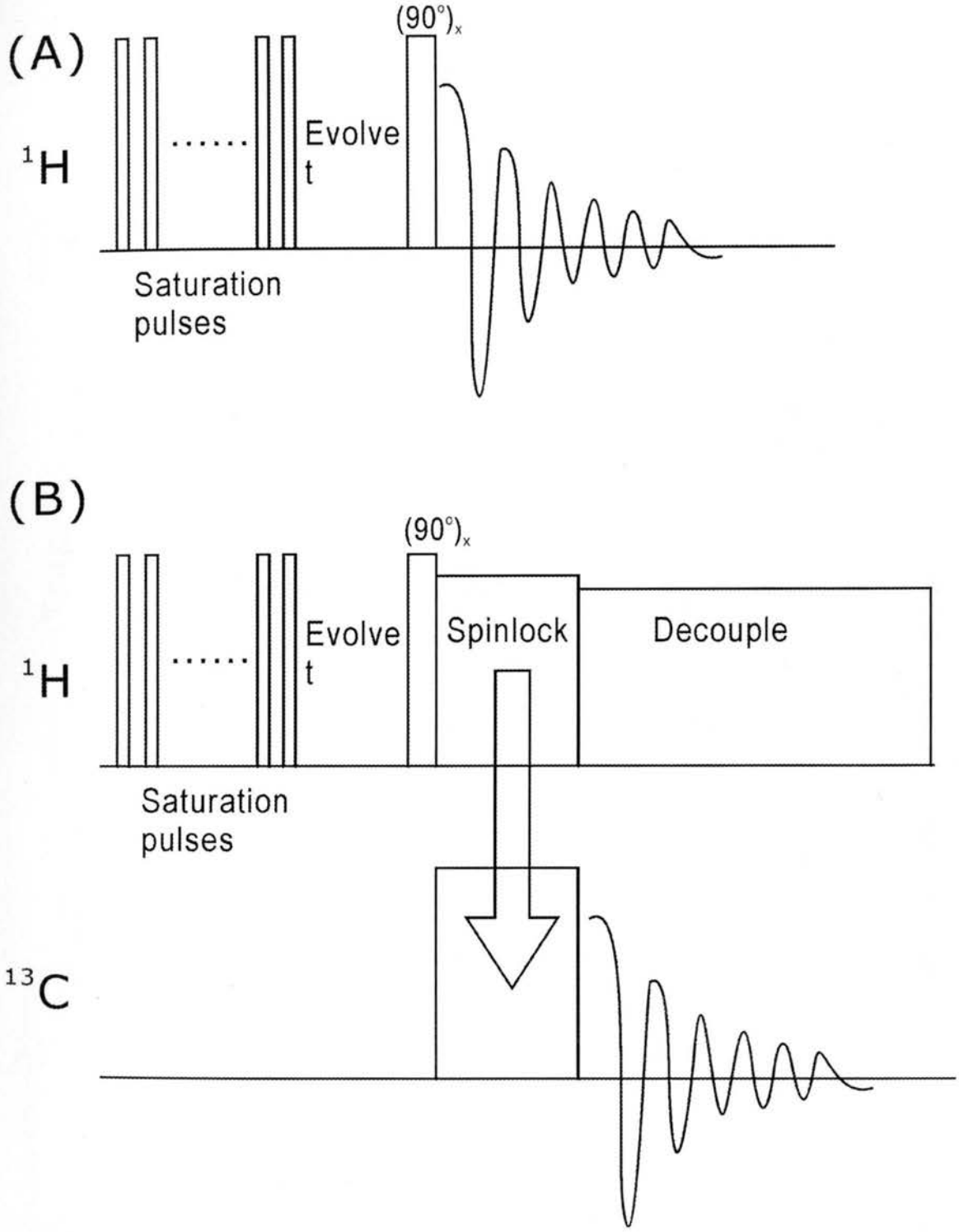

Figure 2.3. Pulse sequence for (A) a single channel saturation-recovery experiment and (B) a ^{13}C CP/MAS-detected ^{1}H T_1 saturation-recovery experiment.

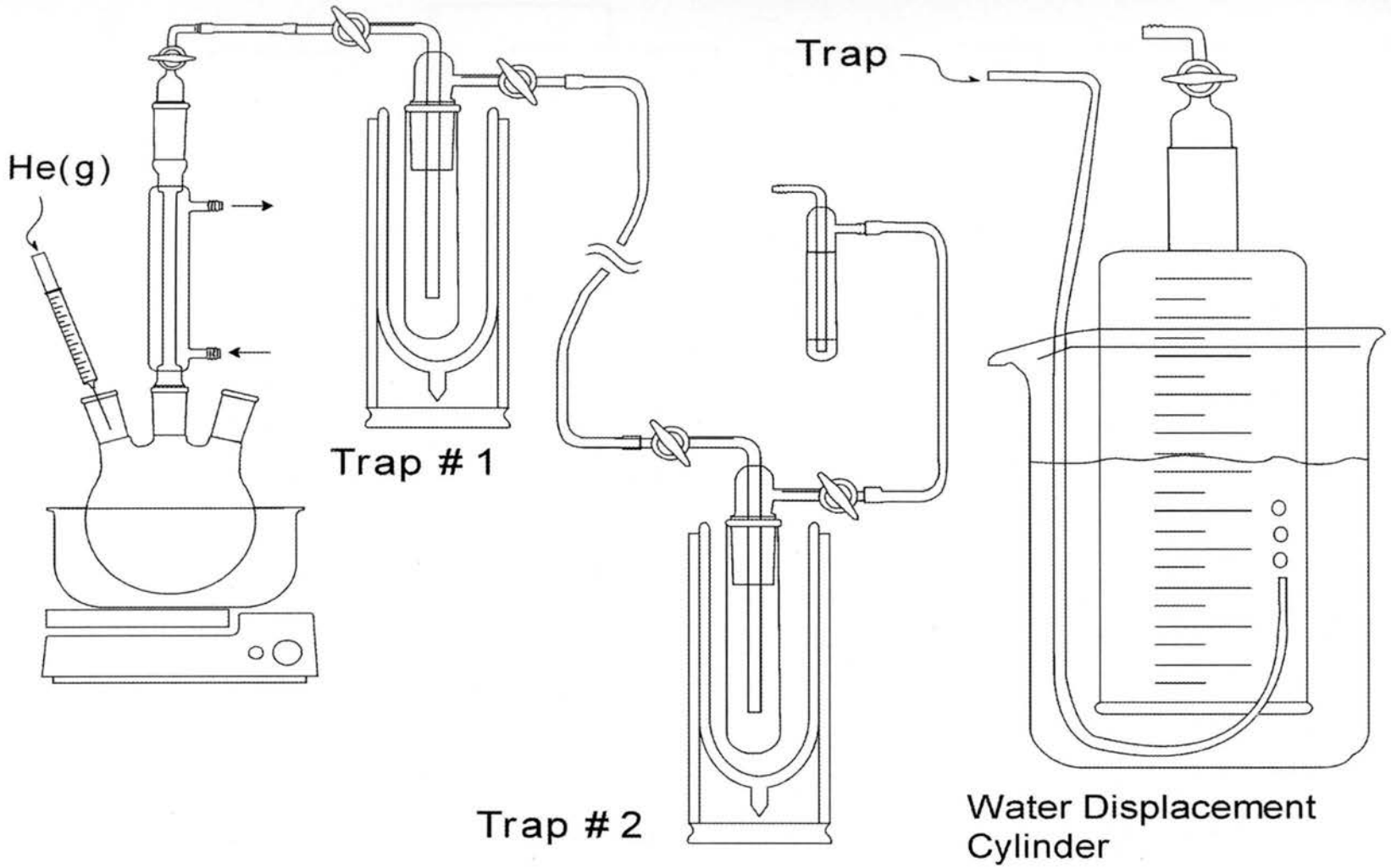

Figure 2.4. AlMe3/silica gel reaction setup, with water replacement cylinder.

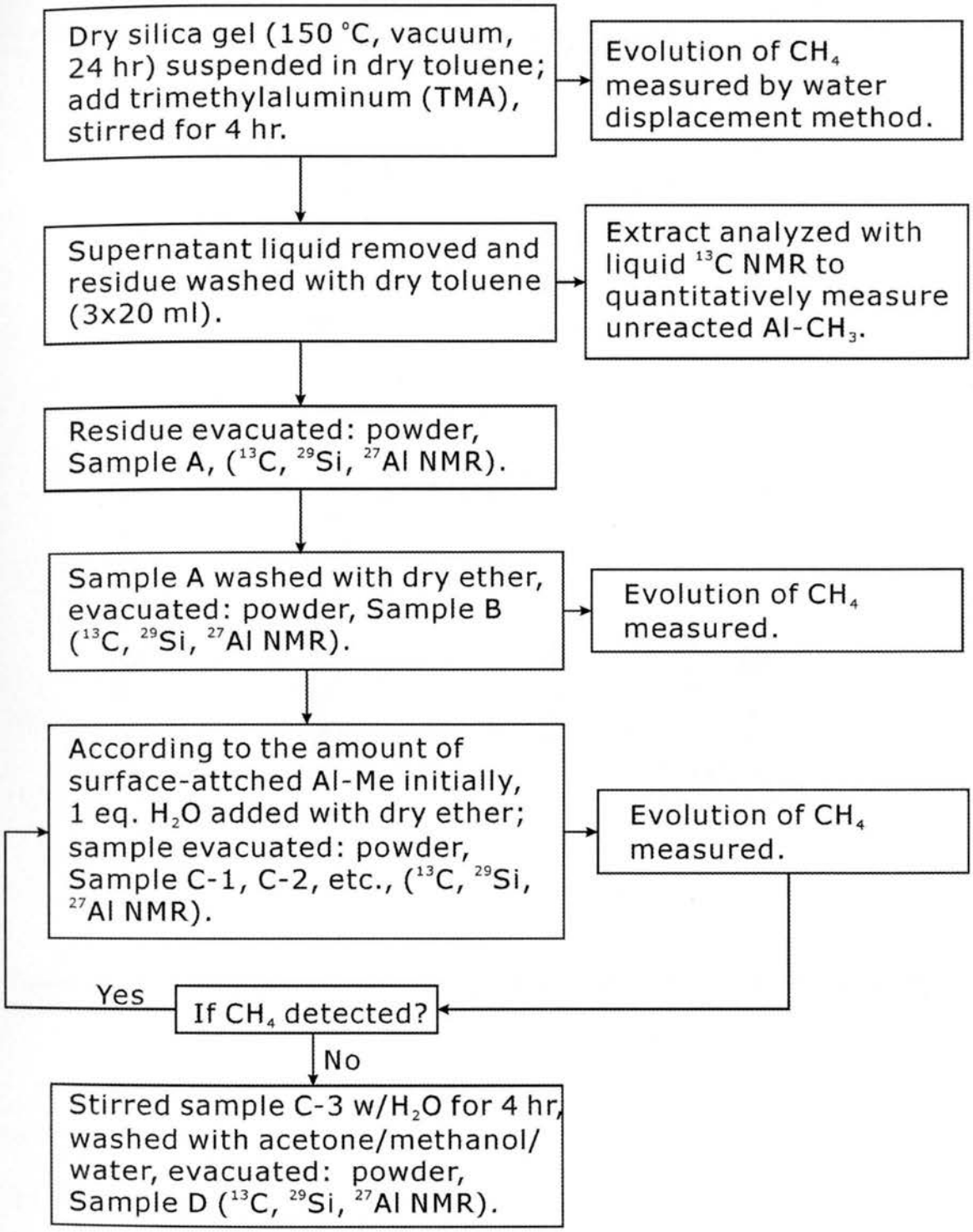

Figure 2.5. Flowchart of $AlMe_3$/silica gel experiment.

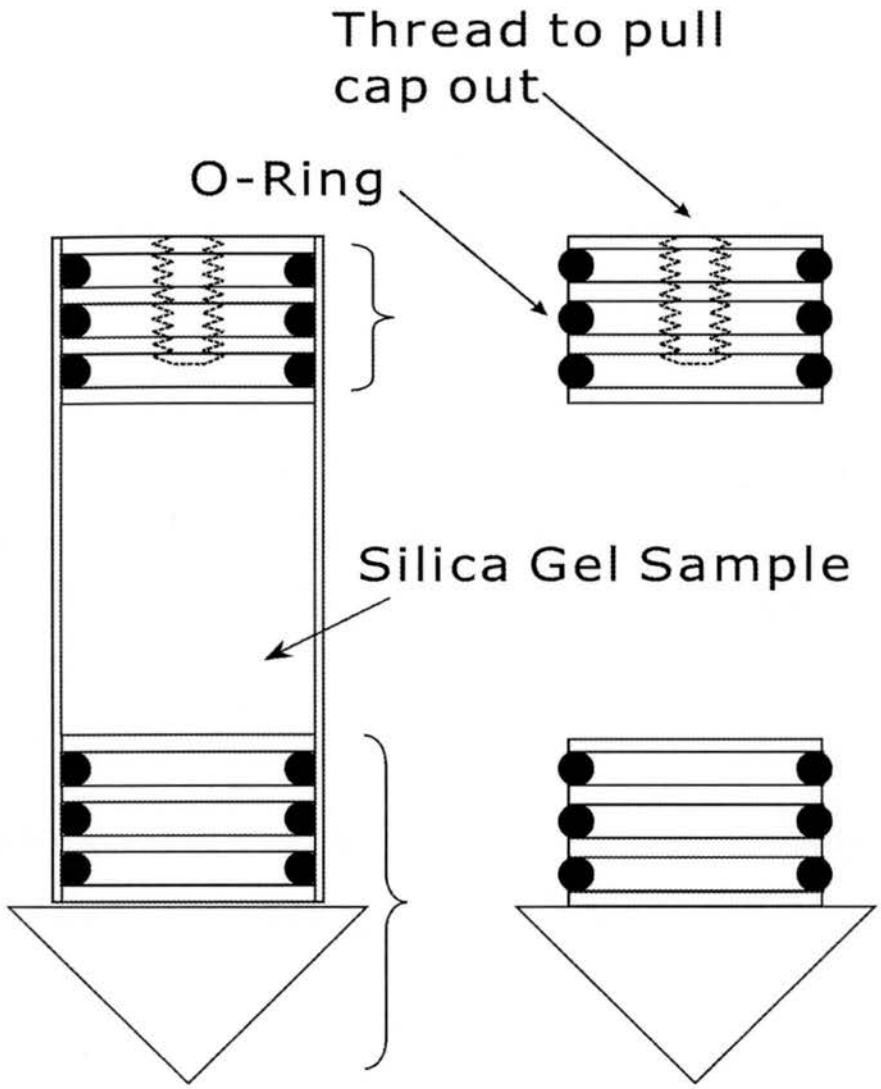

Figure 2.6. 9 mm rotor, with three O-rings on each end cap to seal the sample from moisture and air.

Chapter 3. RESULTS.

3.1. Error analysis.

3.1.1. Definitions

In this thesis, we use the following definitions to analyze error propagation or represent the error associated with results.

The standard deviation, σ, of *n* measurements is given by:

$$\sigma = \sqrt{\frac{\sum_i (x_i - \bar{x})^2}{n-1}} \tag{3.1}$$

where x_i is individual measurement and $\bar{x}$ is the mean of n measurements.

The relative standard deviation (R.S.D) is given by:

$$R.S.D = \frac{\sigma}{\bar{x}} = \frac{\sqrt{\frac{\sum_i (x_i - \bar{x})^2}{n-1}}}{\bar{x}} \times 100\% \tag{3.2}$$

The discrepancy of a measurement is given by:

$$err = |x_i - x_0| \tag{3.3}$$

Where x_0 is the reference/known value of the measurement. The relative discrepancy of a measurement is given by:

$$err\% = \frac{|x_i - x_0|}{x_0} \times 100\% \tag{3.4}$$

The standard error of a sample with *n* measurements is given by:

$$st.\ error = \frac{\sigma}{\sqrt{n}} \tag{3.5}$$

where σ is the standard deviation of these *n* measurements. Relative standard error is calculated as:

$$st.\ error\% = \frac{st.\ error}{\bar{x}} \times 100\% \tag{3.6}$$

Where $\bar{x}$ is the mean of these n measurements.

3.1.2. Error estimate for signal integrals.

In the normal procedures of quantitative analysis, measurements should be done many times under exactly the same experimental conditions and then the data can be analyzed using normal statistical methods (e.g., calculate the standard deviation over a series measurements). In this situation, the consequences of random instrument error can be reduced by repeating the experiments many times. But in this study, as in many instrumental measurements, to repeat experiments numerous times is not realistic. Then, for the quantitative work represented in this study, we need a way to estimate the error in a single measurement.

For a given signal (peak) in the NMR spectrum, the integral is defined as the area *A* under the signal curve, which can be calculated as:

$$A = \sum_{i=1}^{m} \delta \cdot h_i = \delta \cdot \sum_{i=1}^{m} h_i \tag{3.7}$$

where h_i is the intensity of each data point of the signal, $(\delta \cdot m)$ is the width of the integration range of the peak = $w = \delta \cdot m$, *m* is number of data points to represent the peak and *h* is the intensity of the highest point in the peak. One can

approximate the sum $\sum h_i$ as $(mh/2)$, so the approximate relationship, $A \approx (w \cdot h/2)$, can be written. The main approximation in this relationship is treating the area of the peak as the area of a triangle with height of *h* and base width of *w*.

In the NMR data processing program (Varian Spinsight), since the range of a signal integration is counted point-by-point, there is no *random* error associated with this width *w*. Then, the only random error one needs to consider is the random error associated with *h*, which is caused by the noise in the spectrum (a single measurement) and in the stability of the spectrometer. From error propagation theory, the relative standard deviation of a peak integral (area, A) in a single measurement can be written as:

$$\frac{\sigma_A}{A} = \frac{\sigma_h}{h} = \frac{noise_{rms}}{h} = \left(\frac{S}{N}\right)^{-1} \tag{3.8}$$

where $noise_{rms}$ is defined as the root-mean-square of noise intensity over the indicated peak range of the spectrum. The S/N ratio (signal-to-noise ratio) is a number used to evaluate how 'good' the signal is.

Eq. 3.8 expresses the relative standard deviation of an individual measurement (one spectrum) due to the noise in the detection. What we are trying to estimate is the relative standard deviation in the context of repeated measurements (spectra), as if we had obtained repeated spectra. This quantity consists of two components:

$$\frac{\sigma_s}{S} = \sqrt{\left(\frac{\sigma_a}{a}\right)^2 + \left(\frac{\sigma_A}{A}\right)^2} = \sqrt{\left(\frac{\sigma_a}{a}\right)^2 + (S/N)^{-2}} \tag{3.9}$$

where σ_S/S is the relative standard deviation of the final result (from a series of spectra), the component σ_a/a is the relative random error due to spectrometer

instability over a series of measurements and the component σ_A/A is the relative random error of a single measurement (single signal). From Eq. 3.9, one can see that for a strong signal (large *S/N*), σ_a/a is the dominant part, which means the relative standard deviation of the measurements comes from instrument instability; for a very weak signal (very small S/N), σ_A/A can be the dominant part. Two series of measurements were carried out to determine the contribution σ_a/a.

For single-pulse MAS ^{1}H experiments, polydimethylsiloxane (PDMS) was used as the standard sample and repetition experiments were carries out over a range of time to evaluate instrument instability. Table 3.1 shows the integrals of PDMS signals in these repetition experiments. Statistical analysis of the data shows that the instrument variation causes a relative standard deviation of 5% for ^{1}H MAS experiments.

For ^{13}C CP-MAS experiments, hexamethylbenzene (HMB) was used as the standard sample and the repetition experiments were carried out on HMB over a range of time to evaluate the instrument instability. Table 3.2 shows the integral/intensity results for peaks with various heights (strong signals and weak signals). Excluding the results for a very small peak (a spinning sideband at 25 ppm) from these results, one can estimate a relative standard deviation of 5% for the instrument variation.

Table 3.3 shows peak characteristics in the single-pulse MAS ^{1}H spectra of polydimethylsiloxane (PDMS), 1,3,5-trimethoxybenzene and silica and in the ^{13}C CP/MAS spectra of hexamethylbenzene (HMB) and a $AlMe_3$/silica sample. These are the main kinds of signals of interest in this study. The S/N ratio is the

σ_A/A part in the error propagation equation, Eq. 3.9. The table shows that, for most of the signals in the spectra of the samples of interest, the error due to noise in a single measurement is small enough to be ignored in the error estimation. In the dry $AlMe_3$/ silica/toluene spectrum, the peaks at 54 ppm, -3 ppm and –7 ppm have σ_A/A (N/S) values that are larger than the σ_a/a estimate of 5%, because they are very weak signals. In these cases from Eq. 3.9 we get σ_S/S values up to about 10%.

From Table 3.3, one can conclude that, for the intense or relatively intense signals of the spectra of interest in this study, the σ_A/A part in Eq. 3.9 is small enough to be ignored for most signals, yielding a σ_S/S estimate of about 5%. These intense or relatively intense signals include: all the peaks of interest in ^1H MAS spectra and the ^{13}C CP/MAS spectra of HMB and signals at 49 ppm, 0 ppm and –12 ppm in ^{13}C CP/MAS spectra of $AlMe_3$/silica samples. For the weak signals, which are signals at 54 ppm, -3 ppm and –7 ppm in $AlMe_3$/silica spectra, we estimate σ_S/S to be as large as 10%.

3.1.3. Error analysis in relaxation time studies

In the data analysis part of the relaxation study, in which the individual peak intensity (peak integral) is plotted *vs* evolution time, the parameters of interest (e.g., M^0, M^∞, proton T_1, proton $T_{1\rho}$ and T^{CH}) were obtained by computer curve fitting to the proper equation, using the regression procedure in Origin 6.1 software. The error represented in the relaxation result was calculated as standard errors by this curve-fitting software.

3.2. ^{1}H results on Si-OH groups.

3.2.1. Control test on the ^{1}H spin counting method.

A control test was carried out to examine the accuracy of the solid state ^{1}H MAS NMR spin counting method. In the control test, 1,3,5-trimethoxybenzene was used as a calibration sample (weighed amount about 16 mg) in a 4 mm zircornia MAS rotor.

3.2.1.1. ^{1}H MAS spin-lattice relaxation measurements.

In order to apply the appropriate ^{1}H T_1 relaxation corrections for quantitative analysis, the ^{1}H T_1 (spin-lattice relaxation time) of both PDMS (polydimethylsiloxane), the reference compound, and 1,3,5-trimethoxybenzene, the calibration sample, were measured. Figure 3.1 shows the spectra of a ^{1}H saturation-recovery experiment on PDMS; Table 3.4 is the summary of peak integrals of those experiments. The intensity data were fitted into the following single exponential equation:

$$M(t) = M^0 \times (1 - e^{-t/T_1}) \qquad (3.10)$$

where $M(t)$ is the magnetization at recovery time t and M^0 is the magnetization when the recovery time is infinity (spins fully relaxed). Figure 3.2 shows a plot of the peak integral vs. recovery time for PDMS; the curve was obtained by a nonlinear least-squares fit of the integral data to Eq. 3.10, using Origin 6.1 software. The random error was calculated by regression analysis of the software used. The results yield a ^{1}H T_1 value of 1.26(±0.09) s for PDMS, where the

number in parentheses is the standard error given by Origin 6.1 as part of the curve fitting process.

Figure 3.3 shows the spectra of the ^{1}H inversion-recovery experiment on 1,3,5-trimethoxybenzene; Table 3.5 is the summary of peak integrals of those experiments. The integral data were fitted to the following single-exponential equation:

$$M(t) = M^0 \times (1 - 2 \times e^{-t/T_1}) \qquad (3.11)$$

where $M(t)$ is the peak integral at recovery time t and M^0 is the peak integral when the recovery time is infinity (spins fully relaxed). Figure 3.4 shows plots of peak integrals vs. recovery time for 1,3,5-trimethoxybenzene; the curves were obtained by a nonlinear least-squares fit of the integral data to Eq. 3.11. The results yielded a ^{1}H T_1 value of 1.54(±0.01) s for the methoxy group and 2.15(±0.01) s for aromatic protons, where the number in parentheses is the standard error given by Origin 6.1 as part of the curve fitting process.

3.2.1.2. ^{1}H MAS spin-counting of a calibration sample (1,3,5-trimethoxybenzene).

^{1}H MAS spectra of silica gel, PDMS and 1,3,5-trimethoxybenzene were acquired under exactly the same experimental conditions. The PDMS was used as an external reference; reference spectra were obtained before and after acquiring the spectra of 1,3,5-trimethoxybenzene and silica gel, by substituting a PDMS-filled rotor in the probe. On the basis of ^{1}H T_1 measurements described above, a 30 s recovery time was used so that all the spins were fully relaxed and

there was no need for T_1 correction when processing the intensity data. Thus the signal intensity (integral) is proportional to the number of spins:

$$\frac{n_{PDMS}}{n_{TMOB}} = \frac{I(PDMS)}{I(TMOB)} \tag{3.12}$$

where n_{PDMS} represents the number of moles of PDMS (polydimethylsiloxane), the external reference, and n_{TMOB} represents the number of moles of 1,3,5-trimethoxybenzene, the calibration compound; I represents the integrated peak integral in the NMR spectrum of each compound. Since the weight of PDMS is known, by comparing the peak integrals of PDMS and 1,3,5-trimethoxybenzene in the two spectra, one can derive the number of moles of the latter from Eq. 3.12.

Figure 3.5 shows ^{1}H MAS spectra of 1,3,5-trimethoxybenzene and PDMS. Table 3.6 shows the ^{1}H spin counting results on three weighed 1,3,5-trimethoxybenzene samples. The results indicate that, compared to the gravimetric measurement (weight of the 1,3,5-trimethoxybenzene on an analytical balance), the ^{1}H MAS spin counting method gives a relative discrepancy of about 1% to 4%. Thus, the ^{1}H MAS spin counting method can give a satisfactory measurement of the OH concentration of silica.

3.2.2. ^{1}H spin counting of Si-OH on the silica gel surface.

The purpose of applying the solid state ^{1}H NMR technique used here is to quantitatively measure the number of silanol groups on the silica gel surface. There are two benefits obtained by knowing the number of silanol groups on the reacting silica gel surface.

First, it helps to decide how much Al-Me could, in principle, react with a weighed amount of silica gel. This knowledge permits us to control the stoichiometry of the $AlMe_3$/silica reaction mixture, which was just slightly over a 1:1 (**Al**-Me/Si-**OH**) mole ratio in these studies. Controlling the amount of $AlMe_3$ added to the reaction mixture also helps the quantitative measurement and tracking of the methyl groups during the reaction. Furthermore, knowing the number of silanol groups on the silica gel surface helps us to understand the details/path of Al-Me moieties in the overall reaction between $AlMe_3$ and the silica gel surface, especially when combined with results from ^{13}C spin counting and CH_4 tracking, (*vide infra*).

The ^1H solid-state NMR experiments used MAS (magic angle spinning) for line narrowing, with spin excitation by single pulses. Two silica gel samples were investigated by this technique: Fisher S679 silica gels dried under vacuum ($5x10^{-3}$ torr) at 100 °C and 150 °C. Figure 3.6 shows the ^1H MAS spectra and the deconvolved spectra of the two silica gel samples.

From previous published work of this research group,[1, 2] the resonance at 2.0 ppm is due to protons of isolated silanols on the silica gel surface, and the broad feature appearing in the spectrum and centered around 5 ppm is due to OH (mainly silanol) protons in a variety of hydrogen-bonding environments. From these results, there is apparently no physisorbed water, which would appear in the spectrum around 3.5 ppm, left on the Fisher 679 silica gel surface after it has been dried at 100 °C. Many of the silanols on the surface are still in a hydrogen-bonding state in these samples.

^1H T_1 measurement of the 150 °C dried silica gel was made by the ^1H saturation-recovery experiment using MAS, Figure 3.7 shows the spectra of saturation-recovery experiments on 150 °C dried silica gel and Table 3.7 is the summary of corresponding signal integrals. The combined intensity of all of the hydrogen-bonded protons and isolated silanol protons are given together in Table 3.7, since it is only the total amount of these two kinds of protons that is wanted in the analysis. Figure 3.8 shows the plot of combined peak integral *vs* the recovery time for the saturation-recovery data of Table 3.7; the curve was obtained by fitting the intensity data into Eq. 3.10 by a nonlinear least-squares method. The result of this fit is that the ^1H T_1 value of the silanol groups on the surface is around 0.71(±0.02) s. Since the spin counting experiments used a repetition delay of 30 s, all the silanol spins are fully relaxed between each acquisition and no relaxation correction is needed in later calculations. The concentration of silanol groups on the dried silica gel surface can be calculated using the following equation:

$$\frac{n_{PDMS}}{n_{silanol}} = \frac{I(PDMS)}{I(silanol)} \tag{3.13}$$

$$silanol(mmol/g) = \frac{n_{silanol}(mmol)}{W_{silica\ gel}(g)} \tag{3.14}$$

Table 3.8 summarizes the results of ^1H spin counting measurement of 150 °C dried silica gel (Fisher S679). The combined integration represents the total signal from 1 ppm to 10 ppm, which includes all types of silanol groups on the surface, isolated and hydrogen-bonded. The concentration of all kinds of OH groups on the silica gel surface dried at 150 °C was determined to be about

5.2(±0.1) mmol OH/g of silica. The result agrees with other published numbers of silanol hydroxyls of silica gel.[2-6]

3.3. Reactions of silica gel with $AlMe_3$.

3.3.1. Composite of ^{27}Al, ^{29}Si and ^{13}C MAS NMR.

Multi-nuclear solid-state NMR, ^{27}Al, ^{29}Si and ^{13}C, was applied in elucidating the structures present on the surface of $AlMe_3$-modified silica gel. The reaction between surface silanols and $AlMe_3$ is an example of a reaction between an electronic deficient species (Al-Me) and nucleophilic species (Si-O-H). After the initial reaction, Al-Me groups are presumably attached to the surface through Si-O-Al linkages (*vide infra*) and solid-state ^{13}C NMR should be the most important method to investigate the methyl moieties. Reaction of the surface also affects the silica framework, at least at the surface; some Si-OH groups are converted to Si-O-CH_3 moieties and some surface Si-O-Si moieties may be affected by the $AlMe_3$. New moieties attached on the surface and changes in the silica gel framework should also be reflected in the ^{29}Si NMR spectra, which might therefore also provide useful pieces of information to help elucidate reaction(s) on the surface. Another result of the surface reaction is deposition of a 'layer' of Al atoms (along with attached methyl groups) added on top of the silica framework; as indicated above, most of the surface attached Al-containing moieties are presumably attached through Si-O-Al linkages. ^{27}Al NMR should be worth exploring to possibly help elucidate the structures formed on the silica gel surface.

Figure 3.9 shows the combined solid-state ^{27}Al, ^{29}Si and ^{13}C NMR results on $AlMe_3$-reacted silica gel (dried at 150 °C) and the stepwise subsequent behavior (e.g., hydrolysis) of the modified surface. From the bottom to the top of the figure, the following stages are represented:

A. The surface after $AlMe_3$ has reacted;

B. The above surface (A) after washing with anhydrous diethyl ether;

C-1. The above surface (B) after treatment with the first equivalent of H_2O in diethyl ether;

C-2. The above surface (C-1) after treatment with the second equivalent of H_2O in diethyl ether;

C-3. The above surface (C-2) after treatment with the third equivalent of H_2O in diethyl ether;

D. The above surface (C-3) after full hydrolysis with excess H_2O.

In the ^{13}C NMR results shown in Figure 3.9, there are two groups of signals in the spectrum of sample A, from –13 ppm to 1 ppm, and from 47 ppm to 57 ppm. The first group, –13 ppm to 1 ppm, is due to various kinds of methyl groups attached to Al or Si on the surface, such as Al-Me, $Al(Me)_2$, Si-Me, $Si(Me)_2$ and $Si(Me)_3$. The ^{13}C chemical shifts of these species are sufficiently close to each other to cause strong signal overlapping. According to published data, the $Al(Me)_n$ (Al-Me and $Al(Me)_2$) signal should be around –12 ppm; $Si(Me)_3$, $Si(Me)_2$ and $Si(Me)_2$ should be located around 0 ppm, –3 ppm and –7 ppm, respectively.[7-13] The signal at around 49 ppm is due to Si-O-Me groups generated during the surface reaction. More detailed spectral analysis shows that

the weak signals (bumps) around –49 ppm and 27 ppm are spinning sidebands of the signal at –12 ppm, and the peak at 84 ppm is a spinning sideband of the peak at 49 ppm. There are also weak signals at 21 ppm and 130 ppm, which are due to the methyl group and the aromatic carbons of residual toluene, the solvent for the reaction.

In the ^{13}C spectrum of sample B, which was obtained from sample A by washing with anhydrous diethyl ether, there are no dramatic changes in the –12 ppm to 1 ppm and 47 ppm to 57 ppm regions, but additional signals show up around 14 ppm and 69 ppm, which are due to diethyl ether on the surface. In the ^{13}C spectrum of sample C-1, obtained from sample B after treatment with one equivalent of H_2O (according to the amount of surface attached Al–Me groups measured by ^{13}C spin counting, see section 3.4), the major change from the spectrum of sample B is an intensity drop of the signal around –12 ppm, which indicates that the species represented by this signal has at least partially reacted with H_2O added in the treatment.

In the ^{13}C spectrum of sample C-2, which was obtained from sample C-1 after treatment with another equivalent of H_2O, another dramatic drop of intensity of the signal at –12 ppm is observed, which indicates that the additional H_2O added to the surface has again targeted the type of species represented by the signal at –12 ppm, instead of other types of surface moieties. In the ^{13}C spectrum of sample C-3, which was obtained from sample C-2 after treatment with an additional equivalent of H_2O, the signal around –12 ppm has completely disappeared from the spectrum, while all the other signals in the spectrum of

sample C-2 are still present. This indicates that the limited H_2O added to the surface has targeted only the –12 ppm signal, which represents surface-attached species of the type, $Al(Me)_n$.

In the ^{13}C spectrum of sample D, which is fully hydrolyzed material, the signal at 49 ppm (which represents Si-O-Me) and the signal at 0 ppm (which represents $Si(Me)_3$), have disappeared. The only species left on the surface are $Si(Me)_2$ (at –3 ppm) and Si-Me (at –7 ppm).

In the ^{1}H->^{29}Si CP-MAS spectra of Figure 3.9, the main signal appears at –110 ppm, representing the main Si-O-Si (Q_4) structure of the silica gel framework; the apparent absence of Q_2 (-89 ppm) and Q_3 (-100 ppm) intensity in the ^{29}Si spectra A-D support the view that essentially all the surface silanols have reacted with $AlMe_3$ in the $AlMe_3$/silica gel reaction. In addition to the signal around –110 ppm, there are signals with very low intensity (compared to the Q_4 signal) that show up at –60 ppm, -8 ppm and 25 ppm. According to the literature, these signals represent $(O_3SiO)_3$**Si**Me, $(O_3SiO)_2$**Si**$(Me)_2$ and (O_3SiO)**Si**$(Me)_3$ moieties, respectively.[11] The presence of these peaks support the view that species of the $Si(Me)_n$ type are formed in the initial reaction; the corresponding peak integrals (at about –3 and –7 ppm) are relatively low in the ^{13}C NMR spectra and may be overlapped with other, stronger signals due to $Al(Me)_n$ types of moieties.

3.3.2. ^{27}Al NMR results

^{27}Al MAS NMR results in Figure 3.9 show three apparent types of signals in the spectra, at about 6 ppm, 32 ppm and 54 ppm, which likely represent

structures of 6-coordinate, 5-coordinate and 4-coordinate Al species, respectively.[10, 12, 14-16] On the initial $AlMe_3$-reacted silica surface (sample A), 5-coordinate Al is apparently the major Al structure on the surface; 4-coordinate and 6-coordinate Al structures are apparently present in small amounts. With the stepwise addition of H_2O, which reacts with surface $Al(Me)_n$ moieties, the intensity of 5-coordinate Al species decreases, while intensity associated with 4-coordinate and 6-coordinate species increases. In the ^{27}Al spectrum of sample D, after the final workup/hydrolysis step, we see that 4-coordinate Al species (50 ppm to 80 ppm) and 6-coordinate Al species (-10 ppm to 15 ppm) become the major structures on the surface and the 5-coordinate Al population (30 ppm to 40 ppm) on the surface has almost disappeared.[17]

As supplementary information in the ^{27}Al study, a series of experiments was carried out to get a rough quantitative estimation of the number of Al atoms attached on the surface of a dry sample that corresponds to sample A in Figure 3.9. In order to make this estimate, we first wanted to estimate how close the ^{27}Al MAS technique employed is to being quantitative. For this purpose we compared the ^{27}Al NMR integrals and gravimetric number of mmoles of Al present in γ-Al_2O_3, aluminum nitrate ($Al(NO_3)_3 \cdot 9H_2O$) and aluminum lactate ($[CH_3CH(OH)CO_2]_3Al$). The MAS experiments were carried out with the spinning axis a little off the magic-angle axis in order to attenuate the height of spinning sidebands due to satellite transitions.[18] A 0.44 μs pulse was used as the excitation pulse (15°) to get quantitative results.[19, 20] For a comparison between aluminum lactate and γ-Al_2O_3, the experiments were carried out with rapid (16

kHz) sample spinning and the results are shown in Table 3.9. For a comparison between aluminum nitrate and γ-Al_2O_3, the experiments were carried out without sample spinning, in order to get a flat baseline, and the results are also shown in Table 3.9. Results given in Table 3.9 give the ^{27}Al NMR signal integral per number of mmols of Al atoms present in the sample, as determined by gravimetric measurements. Using γ-Al_2O_3 as a reference, the ^{27}Al NMR integral / mmols of Al measured in a (non-spinning) experiment on aluminum nitrate gave a 0.1% relative discrepancy and (spinning) ^{27}Al NMR experiments on aluminum lactate gave a 13.5% relative discrepancy. Thus, it appears that the ^{27}Al NMR technique used in this study is capable of representing the aluminum content of the samples at least semi-quantitatively.

Using γ-Al_2O_3 as a reference sample for comparison with the $AlMe_3$/silica samples, the combined integral of the central-transition peaks of the γ-Al_2O_3 spectrum was measured and compared with the integral of the total central-transition signal (all 4-, 5- and 6-coordinate species integrated together) in a $AlMe_3$/silica sample. This yields an estimate of the number of Al atoms on the silica surface in a $AlMe_3$/silica sample. The results show there are about 1.97 mmol Al atoms / g silica attached on the surface. This result can be compared with the number of Si-**OH** groups (the total of Si-**OH** and Si(**OH**)$_2$ measured with MAS ^1H NMR) on the unreacted silica surface (i.e., 5.2 mmol Si-**OH** / g of silica).

Analogous, albeit less extensive, ^{13}C NMR results on the $AlMe_3$/silica/ cyclohexane system are presented in Figure 3.10.

3.3.3. Solid state ^{13}C NMR spectra.

From the above section and Figure 3.9, we see that, among the three nuclides (^{27}Al, ^{29}Si, ^{13}C), the most useful nuclide in the NMR experiments of this study is probably ^{13}C, since methyl groups are the moieties added on the surface during the $AlMe_3$/silica gel reaction. We expect ^{13}C NMR to reveal substantial valuable information on the structures formed on the surface (*vide infra*; Discussion section).

Due to the relatively low signal intensities observed in the ^{13}C NMR spectra of this project, the background signal caused by the MAS stator of the probe was highly significant and could potentially interfere with interpretation of the spectra. In order to be able to focus on the contributions to spectra due to the real surface structures, we removed the background signal by subtracting a noise-free (computer-simulated) background signal from the experimentally obtained spectrum.

A background spectrum was obtained under exactly the same experimental conditions as employed for the $AlMe_3$/silica samples. The background spectrum thus obtained was then simulated, using a computer program, and a noise-free background spectrum was generated from the simulation. Subsequently, the noise-free background spectrum was subtracted from each $AlMe_3$/silica spectrum, yielding background-free spectra, such as those given in Figure 3.9 and Figure 3.10.

Figure 3.11 shows an example of subtraction of the noise-free background from an acquired spectrum. The spectrum resulting from the background

subtraction shows a good baseline, which signifies that the method is good enough for the purposes mentioned above.

The ^{13}C NMR spectra of Figure 3.9 show that many different kinds of methyl groups are formed on the surface as a result of the $AlMe_3$/silica reaction and that some of the different signals overlap with each other. In order to draw information on different structures in cases of substantial overlap, spectral deconvolution and computer simulation can be applied to separate the overlapping signal. This is especially important for the spectral region from –15 ppm to 1 ppm.

Figure 3.12 shows the deconvolution of the ^{13}C CP-MAS spectrum of the dry $AlMe_3$/silica/toluene reaction sample. Basically, there are six signals that represent methyl moieties added to the surface during the reaction: $Al(Me)_n$ (-12 ppm), Si-Me (-7 ppm), $Si(Me)_2$ (-3 ppm), $Si(Me)_3$ (0 ppm), Si-O-Me (49 ppm) and $Si(OMe)_2$ (54 ppm). Other peaks are due to solvent remaining on the surface or to spinning sidebands (these peak positions varied with the spinning speed used when acquiring the spectrum).

Figure 3.13 shows the deconvolution of the ^{13}C CP-MAS spectrum for the ether washed $AlMe_3$/silica/toluene reaction sample. It shows the six signals mentioned above for the initial dry sample (A) and, in addition to that, signals belonging to diethyl ether are apparent in the spectrum, indicating that quite a bit diethyl ether remains on the surface.

As stated above, diethyl ether peaks showed up in the ^{13}C spectrum of Figure 3.9B (as well as in parts C-1, C-2, C-3 and, to a very small degree, D of

Figure 3.9) due to diethyl ether remaining on the surface, even after drying under vacuum. Of special interest is the apparent relationship between the intensities of the diethyl ether peaks and the intensities of the $Al(Me)_n$ (-12 ppm) species among the B - D samples; as the $Al(Me)_n$ intensity drops, so does the intensity of the diethyl ether peaks. This suggests an interaction between $Al(Me)_n$ moieties and diethyl ether molecules. Such an interaction between $Al(Me)_n$ and ether would not be hard to understand, since $Al(Me)_n$ is an electron deficient species and diethyl ether has unbonded electron pairs on the oxygen.

In comparing ^{13}C spectra from sample A to sample D in Figure 3.9, another interesting observation is the intensity changes of the peak at 49 ppm, which represent Si-O-Me moieties. The intensity of the Si-O-Me peak increases from sample A to sample C-2, yet during these treatments, no CH_3 has been added to the system. This raises the question: where did this additional intensity come from? Is it due to chemical reaction(s) of the surface moieties during the washing by diethyl ether, or it is due to a change in some physical property on the surface, which could manifest itself as changes in NMR spectra (e.g., because of changes in relevant relaxation times). From the ^{27}Al, ^{29}Si and ^{13}C NMR results presented up to this point, it is impossible to answer this question. In order to try to answer this question, further relaxation measurements on the modified silica surface were introduced.

3.3.4. Relaxation data.

As suggested above, the study of relevant relaxation times of the surface moieties might help answer the question of whether physical or chemical

changes of the Si-O-Me moiety on the surface are responsible for the curious intensity changes seen in the ^{13}C spectra in Figure 3.9. It is also necessary to know the relevant relaxation times of the surface moieties in order to quantitatively understand chemical changes on the surface during the reaction of $AlMe_3$ with silica gel. This is an important aspect of tracking down the path of all the methyl groups added to the surface in the $AlMe_3$/silica reaction.

The relevant relaxation issues, in the ^{1}H->^{13}C CP-MAS experiment are the proton spin-lattice relaxation and cross polarization dynamics; these control dominating factors affecting the signal intensity in the spectrum. The proton spin-lattice relaxation time (T_1) is dependent on molecular motion at the proton Larmor frequency, and was measured via ^{13}C, using a CP/MAS-detected saturation-recovery experiment. The intensity data are fitted to the following equation using a nonlinear least-squares fit:

$$M(t) = M^0(1 - e^{-t/T_1}) \tag{3.15}$$

where $M(t)$ is the intensity at a given recovery time (t) and M^0 is the intensity when the recovery time is infinity (spin fully relaxed). The CP (cross polarization) dynamics are controlled by the CP relaxation time (T^{CH}) and the rotating-frame ^{1}H spin-lattice relaxation time (proton $T_{1\rho}$), which were measured by the variable-contact-time CP/MAS technique.

The following four samples were examined by the ^{13}C CP/MAS-detected ^{1}H saturation-recovery relaxation-time technique and ^{13}C CP/MAS variable-contact-time technique: sample A (dry sample of the initial reaction product) and

sample B (ether washed) in both the $AlMe_3$/silica/toluene reaction system and $AlMe_3$/silica/cyclohexane reaction system.

Figure 3.14 shows the ^{13}C CP/MAS-detected ^{1}H saturation-recovery spectra of the dry $AlMe_3$/silica/toluene sample corresponding to sample A in Figure 3.9. The deconvolved peak integrals derived from Figure 3.14 are summarized in Table 3.10. The integral data-vs-recovery time plots and corresponding fitting curves, which were obtained by fitting these data to Eq. 3.15, are shown in Figure 3.15.

In addition to the proton spin-lattice relaxation time T_1, cross polarization dynamics are also important in determining intensities in CP-MAS experiments. The following equation describes the ^{1}H->^{13}C cross polarization dynamics in a variable-contact-time CP/MAS experiment in terms of the cross polarization relaxation time (T^{CH}) and the rotating-frame proton spin-lattice relaxation time ($T_{1\rho}$):

$$M(t) = M^{\infty} \times \frac{1}{1 - T^{CH} / T_{1\rho}} \times e^{(-t/T_{1\rho})} \times \left[1 - e^{(-t/T^{CH})}\right] \qquad (3.16)$$

where *M(t)* is the magnetization for a given CP contact time *t* ms and M^{∞} is the ^{13}C intensity that would be achieved if $(T^{CH})^{-1}$ and the proton $T_{1\rho}$ were both infinite. The proton $T_{1\rho}$ is the proton spin-lattice relaxation time in the rotating frame under the influence of the applied RF field (with infinite $T_{1\rho}$, proton magnetization would not decay) and T^{CH} is the cross polarization time constant that represents the coupling between the ^{1}H spin reservoir and ^{13}C spin reservoir. The stronger the ^{1}H-^{13}C dipolar interaction, the smaller the T^{CH} is. T^{CH} and proton $T_{1\rho}$ can be

measured via a variable-contact-time CP-MAS experiment and fitting the intensity data to Eq. 3.16 to obtain the two relaxation parameters (and M^{∞}). Intensity correction factors due to ^{1}H spin-lattice relaxation and due to CP dynamics are given in the following two equations:

$$\frac{M^{0}}{M(t)} = \frac{1}{1 - e^{-t/T_{1}}} \tag{3.17}$$

$$\frac{M^{\infty}}{M(t)} = \frac{1 - T^{CH}/T_{1\rho}}{e^{(-t/T_{1\rho})} \times (1 - e^{(-t/T^{CH})})} \tag{3.18}$$

where t in Eq. 3.17 is recovery period (s) and in Eq. 3.18 is the CP contact time (ms).

We define the total correction factor as

$$C = \frac{M^{\infty}}{M(5ms)} \cdot \frac{M^{0}}{M(3s)} = \frac{M*}{M(5ms,3s)} \tag{3.19}$$

since all the spectra of $AlMe_3$/silica samples were obtained with a CP contact time of 5 ms and pulse delay of 3 s. M* is the theoretical maximum magnetization.

Figure 3.16 shows the variable-contact-time ^{13}C CP/MAS spectra of a dry $AlMe_3$/silica/toluene sample corresponding to sample A in Figure 3.9. The deconvolved intensities (integrals) derived from Figure 3.16 are summarized in Table 3.11. Plots of the integrated intensity data vs. contact time and the corresponding curves obtained by fitting these data to Eq. 3.16 are shown in Figure 3.17. Table 3.12 summarizes the relaxation times and corresponding correction factors (from Eq. 3.17, Eq. 3.18 and Eq. 3.19) derived from the curve fitting shown in Figure 3.15 and Figure 3.17.

Corresponding results on a dry $AlMe_3$/slica/cyclohexane sample (corresponding to sample A in Figure 3.10) are given in Figure 3.18, Table 3.13 and Figure 3.19 for proton T_1 measurements and in Figure 3.20, Table 3.14 and Figure 3.21 for proton $T_{1\rho}$ and T^{CH} measurements. The relaxation times and corresponding correction factors (from Eq. 3.17, Eq. 3.18 and Eq. 3.19) derived from the curve fitting are shown in Table 3.15.

Figure 3.22 shows the ^{13}C CP/MAS-detected ^{1}H saturation-recovery spectra of the ether washed $AlMe_3$/silica/toluene sample corresponding to sample B in Figure 3.9. The deconvolved intensities (integrals) derived from Figure 3.22 are summarized in Table 3.16. The intensity vs. recovery time plots and corresponding curves, obtained by fitting these data to Eq. 3.15, are shown in Figure 3.23.

Figure 3.24 shows the variable-contact-time ^{13}C CP/MAS spectra of the ether washed $AlMe_3$/silica/toluene sample corresponding to sample B in Figure 3.9. The deconvolved intensities (integrals) derived from Figure 3.24 are summarized in Table 3.17. Plots of peak integrals vs. contact time and corresponding fitting curves obtained by fitting these data to Eq. 3.16 are shown in Figure 3.25. Table 3.18 summarizes the relaxation times and corresponding correction factors (from Eq. 3.17, Eq. 3.18 and Eq. 3.19) derived from the curve fitting shown in Figure 3.23 and Figure 3.25.

Corresponding results on an ether washed $AlMe_3$/slica/cyclohexane sample (corresponding to sample B in Figure 3.10) are given in Figure 3.26, Table 3.19 and Figure 3.27 for T_1 measurements, and in Figure 3.28, Table 3.20

and Figure 3.29 for $T_{1\rho}$, and T^{CH} measurements. The relaxation times and corresponding correction factors (from Eq. 3.17, Eq. 3.18 and Eq. 3.19) derived from the curve fitting are shown in Table 3.21.

Table 3.22 is a comparison of proton T_1 values for signals deconvolved from the four different samples, dry (A in Figure 3.9) and ether washed (B in Figure 3.9) samples of the $AlMe_3$/silica/toluene reaction, and analogous samples of the $AlMe_3$/silica/cyclohexane reaction.

Since Si-O-Me (49 ppm) and $Al(Me)_n$ (-12 ppm) are the major ^{13}C signals, corresponding to the most populated/important moieties attached on the surface, as an initial result of the $AlMe_3$/silica reaction, these signals have the most favorable signal-to-noise characteristics, and the relaxation times determined on these two components are the most reliable of the values given in Table 3.12, Table 3.15, Table 3.18 and Table 3.21. Table 3.23 and Table 3.24 put the relaxation times and the correction factors derived from the relaxation times of these two signals side by side for comparison for the four different samples.

In Table 3.23 and Table 3.24, the "total correction" is the ratio of magnetization observed at a given recovery time or contact time to the magnetization one would achieve if the inverse of the proton T_1 were infinite and $(T^{CH})^{-1}$ and $T_{1\rho}$ were each infinite. This correction reflects how much the signal intensity is affected due to the details of spin relaxation. The closer the number is to unity, the closer the measured spectral intensity reflects the real amount of corresponding moiety on the surface and the smaller is the correction needed.

The larger the number is, the more correction is needed in order to draw quantitative conclusions.

When comparing the total correction factors of sample A to those of sample B in Table 3.23 and Table 3.24, one sees that there is no significant difference between the $AlMe_3$-reacted surface (A) and the ether washed surface (B), for both the toluene and cyclohexane systems. This helps to answer the above question on whether the increasing intensity of the Si-O-Me peak from sample A to sample B in Figure 3.9 and in Figure 3.10 is due to chemical change or is due to physical property change(s). From the relaxation results, it appears that this change cannot be attributed to changes in relaxation times; i.e., this change should be due to chemical changes. In comparing the ^{13}C spectra of A and B in Figure 3.9 and in Figure 3.10, one can also see that the intensity of the peak at –12 ppm (which represents $Al(Me)_n$), dropped a little bit after the ether wash. This implies that, during the diethyl ether treatment, surface $Al(Me)_n$ is perhaps partially converted to Si-O-Me, because there is no CH_3 added to the system; the only source of CH_3 is from the CH_3 groups already on the surface.

Comparing the proton T_1 values for the $AlMe_3$-reacted surface (A) to those of the ether-washed surface (B) in the same reaction system (toluene or cyclohexane), one sees that the proton T_1 has dropped upon washing with diethyl ether in both cases.

3.3.5. Error estimation in ^{13}C-detected relaxation studies.

Signals of the ^{13}C spectra of interest in the reacted silica samples are weak, so a large number of repetitions was needed in order to obtain a suitable

spectrum (3000 scans for relaxation studies). Also, the proton T_1 values are large for signals observed in the spectra (from 3 ~ 7 s). These behaviors result in very time consuming experiments for relaxation studies, e.g., more than 72 hr for either variable-contact-time experiments or saturation-recovery experiments. Because of this time scale, all the ^{13}C CP/MAS detected ^1H relaxation experiments (with various evolution times) were carried out only once.

As described in section 3.3.4, intensity correction factors due to ^1H spin-lattice relaxation and due to CP dynamics are given in the following equations:

$$\frac{M^0}{M(t)} = \frac{1}{1 - e^{-t/T_1}} \tag{3.20}$$

$$\frac{M^\infty}{M(t)} = \frac{1 - T^{CH}/T_{1\rho}}{e^{(-t/T_{1\rho})} \times (1 - e^{(-t/T^{CH})})} \tag{3.21}$$

where in Eq. 3.20, t is the recovery time (s), M^0 is the maximum magnetization that can be achieved when the spins are fully relaxed in terms of spin-lattice relaxation. In Eq. 3.21, t is the particular CP contact time (ms) used and M^∞ is the maximum magnetization that could be achieved if the proton $T_{1\rho}$ and $(T^{CH})^{-1}$ were each infinity.

In the $AlMe_3$/silica spectra, since the experimental CP contact time = 5 ms and the pulse delay = 3 s, the total correction factor is defined as

$$C = \frac{M^\infty}{M(5ms)} \cdot \frac{M^0}{M(3s)} = \frac{M^*}{M(5ms,3s)} \tag{3.22}$$

where M* is the theoretical maximum magnetization if all types of relaxation effects were 'ideal' (optimum). Then, the estimated relative standard deviation of

the correction factor C that is due to the calculation of M^0, M^∞, M(5 ms) and M(3 s), can be written as:

$$\frac{\sigma_C}{C} = \sqrt{\left(\frac{\sigma_{M^0}}{M^0}\right)^2 + \left(\frac{\sigma_{M^\infty}}{M^\infty}\right)^2 + \left(\frac{\sigma_{M(5ms)}}{M(5ms)}\right)^2 + \left(\frac{\sigma_{M(3s)}}{M(3s)}\right)^2} \qquad (3.23)$$

The relative standard error of M^0, M^∞, M(5ms) and M(3s) are calculated from the standard error given by the curve fitting process; they vary from 3% (for strong signals) to 6% (for very weak signals, such as those at 54 ppm, –3 ppm and –7 ppm). From Eq. 3.23, the estimated relative standard error for the final correction factor is calculated to be 6% for strong signals and 12% for weak signals (such as those at 54 ppm and –3 ppm and -7 ppm).

3.4. ^{13}C spin counting results.

For the reasons mentioned above, in order to draw quantitative conclusions on how the populations of CH_3 groups on the surface change during the reaction, we need knowledge of how much surface-attached CH_3 moieties formed on the surface in the $AlMe_3$/silica reaction. As established previously in our lab,[21] the solid state ^{13}C NMR spin counting technique can be used as a quantitative analytical method for this purpose, if proper account is taken of the relevant spin dynamics.

A crucial part in NMR spin counting is to study the relevant relaxation times of the samples. This has already been introduced in section 3.3.4. For ^{13}C spin counting, in addition to the relaxation times of the samples of interest, we also need the relevant relaxation times of an intensity reference compound, HMB (hexamethylbenzene) in the present case. Proton T_1 measurements on HMB

were carried out by the ^{13}C CP/MAS-detected ^{1}H inversion-recovery experiment; the resulting spectra are shown in Figure 3.30. Table 3.25 summarizes the signal integrals corresponding to Figure 3.30. The intensity data of Table 3.25 were fitted to Eq. 3.11, using a nonlinear least-squares fit. Plots of signal integrals vs. recovery time and the corresponding fitting curves are shown in Figure 3.31. The proton T_1 detected via methyl carbons in HMB is 627(±16) ms and for aromatic carbon detection is 642(±27) ms, where the number in parentheses is the standard error given by Origin 6.1 as part of the curve fitting process.

T^{CH} and the proton $T_{1\rho}$ of HMB were measured via the variable-contact-time CP/MAS method. Figure 3.32 shows the variable-contact-time ^{13}C CP/MAS spectra of HMB. The signal intensity data are summarized in Table 3.26 and were fitted to Eq. 3.16 using a nonlinear least-squares method. Figure 3.33 shows plots of signal intensity vs. contact time and the fitting curves. The T^{CH} values of HMB were determined to be 1.81(±0.27) ms for methyl carbons and 3.74(±0.43) ms for aromatic carbons. Proton $T_{1\rho}$ values of HMB are determined to be 208(±29) ms for methyl carbon detection and 130(±22) ms for aromatic carbon detection.

The reference sample for ^{13}C spin counting was a known weight of HMB in the rotor, which has the same dimensions for both the rotor and sample as used with reacted silica gel samples. The HMB reference spectra were obtained, before and after the acquisition of each reacted silica gel spectrum, using exactly the same experimental parameters. Table 3.12 summarizes results of relaxation

corrections for each deconvolved signal of the ^{13}C CP-MAS spectrum of the dry $AlMe_3$/silica/toluene reaction sample corresponding to sample A in Figure 3.9.

Ideally, these is a simple relationship between measured integrals and the number of moles of corresponding species, relative to methyl carbon of a hexamethylbenzene (HMB) reference:

$$\left(\frac{n_{species}}{I_{species}}\right)_{AlMe_3-silica} = \left(\frac{n_{Me}}{I_{Me}}\right)_{HMB} \tag{3.24}$$

Table 3.27 is a summary of repetition data on six $AlMe_3$/silica/toluene samples, from six different runs, corresponding to sample A in Figure 3.9. For each of the six samples, the table lists the appropriate relaxation correction and the amount of each surface species detected through ^{13}C NMR spin counting. Corresponding results for six $AlMe_3$/silica/cyclohexane runs are summarized in Table 3.28, using the relaxation corrections from Table 3.15.

The spin-counting experiment for each sample was carried out only once due to the time scope of the experiment. The estimated standard deviation for the spin-counting result ($n_{AlMe_3/silica}$) is propagated from the other three numbers shown in Eq. 3.24, assuming the random error (relative standard deviation) propagated from the integral of the peak of interest (5%), the integral of the reference HMB sample (5%) and the correction factor obtained from relaxation studies (6% for the strong signals at 49 ppm, 0 ppm and –12 ppm; 10% for the weak signals at 54 ppm, -3 ppm and –7 ppm); this error is estimated as a relative standard deviation of 9.3% for the strong signals at 49 ppm, 0 ppm and –12 ppm; 13.9% for the weak signals at 54 ppm, -3 ppm and –7 ppm.

3.5. Accounting for CH_3 groups.

Besides the quantitative analysis of surface-attached CH_3 groups, two other pieces of information on the fate of CH_3 moieties were investigated in this study: 1) CH_4 gas generated during the reaction and 2) Al-Me groups remaining in the supernatant liquid (or easily washed from the surface). CH_4 gas monitoring/ measuring was carried out by two cold traps and the water displacement (volume) method (*vide supra*). Al-Me analysis in solution was done by liquid-sample ^{13}C NMR spin counting.

3.5.1. $CH_4(g)$ evolution during the reaction.

As described in the experimental section, the collection of $CH_4(g)$ was done by connecting two $N_2(l)$ cold traps with the reaction system, by flushing the reaction system with He(g), collecting the $CH_4(g)$ generated during the reaction as a solid in the cold traps and subsequently measuring the amount of the subsequently gasified $CH_4(g)$ by the water-displacement (volume) (see Figure 2.4). Table 3.29 summarizes the CH_4 generation results for six $AlMe_3$/silica reactions carried out in toluene. Table 3.30 shows the CH_4 generation results for six $AlMe_3$/silica reactions carried out in cyclohexane. The results of both sets of reactions show that roughly 40 mmol of $CH_4(g)$ was measured during each reaction with about 12 g silica gel (about 62 mmol Si-**OH**, *vide supra*), starting with about 75 mmol of $AlMe_3$. According to the total amount of Al-Me groups introduced initially to the reaction system (roughly 210 to 240 mmol Al-**Me** added via $AlMe_3$), the 40 mmol $CH_4(g)$ indicates that only a small fraction of the Al-me groups were converted to $CH_4(g)$. Since we assume that the entire reaction

system is essentially free of water, then these 40 mmol of CH_4(g) all came from the reaction of Al-Me moieties with Si-OH groups on the surface.

Repetitive experiments were carried out on both $AlMe_3$/silica/toluene and $AlMe_3$/silica/toluene cyclohexane reaction systems. The error presented in Table 3.29 and Table 3.30 are the relative standard deviation of these repetitive measurements, respectively.

3.5.2. Al-Me remaining in the supernatant liquid, determined by liquid-sample ^{13}C NMR.

^{13}C liquid-sample NMR spin counting was used to determine the amount of CH_3 groups remaining in the liquid phase after the $AlMe_3$/silica reaction (or loosely adsorbed at the surface and easily removed by washing). Similar to the case of the solid-state NMR spin counting method, in liquid-sample NMR spin counting the relevant relaxation time is a very important part of getting quantitative results. Consequently, measurements of the ^{13}C T_1 values of the essential species present in the liquid phase were carried out by the ^{13}C inversion-recovery technique. The intensity data were then fitted to Eq. 3.11 using a nonlinear least-squares fit to obtain ^{13}C T_1 values. Figure 3.34 shows the ^{13}C inversion-recovery spectra obtained on a supernatant liquid (including the toluene washes) from an $AlMe_3$/silica/toluene reaction. Table 3.31 summarizes the intensity data of methyl groups of toluene and of Al-Me, derived from Figure 3.34. Figure 3.35 shows plots of signal intensity vs. recovery time and the curves obtained by fitting the data to Eq. 3.11. Corresponding results for the supernatant

liquid from an $AlMe_3$/silica/cyclohexane reaction are shown in Figure 3.36, Table 3.32 and Figure 3.37.

The ^{13}C T_1 value derived from Figure 3.35 for the CH_3 group of toluene is 11.9(±1.7) s; for Al-Me groups in toluene solution it is 11.1(±2.5) s. The ^{13}C T_1 value derived from Figure 3.37 for CH_2 of cyclohexane is 19.7(±1.1) s and for Al-Me groups in cyclohexane solution it is 15.6(±1.3) s. The ^{13}C T_1 values are rather long in these sample, at least in part because each sample was prepared under He(g) protection (O_2 minimized). Therefore, in the spin counting experiments for supernatant liquid samples, the recovery time was set to 60 s to let (almost) all the spins fully relax; a small relaxation correction is still needed for the Al-Me groups in the $AlMe_3$/silica/cyclohexane sample.

The solvent (toluene or cyclohexane) signals are the dominant signals in the spectra shown in Figure 3.34 and Figure 3.36; the solvent signal (the methyl signal of toluene and the methylene signal of cyclohexane) can be used as an internal reference, to calculate the amount of Al-Me in the liquid. When all the spins in the sample are fully relaxed between each acquisition (or a suitable correction is made), the signal intensity is proportional to the amount of spins present in the sample. From the volume of the supernatant liquid extracted from the reaction system, the amount of Al-Me can be derived from the equation:

$$\frac{n_{AlMe}}{n_{solvent}} = \frac{I(AlMe)}{I(solvent)} \tag{3.25}$$

where n represents the number of moles of a specific substance and I represents the corresponding signal intensity (integral).

The random error associated with $n_{Al\text{-}Me}$ is propagated from the other three numbers shown in Eq. 3.25. The integral I has an estimated relative standard deviation of 5% and the volume of solvent has an estimated relative standard deviation of 10%. Then the estimated relative standard deviation of n_{AlMe} that is propagated from these measurements is about 11%.

3.5.3. Summary of methyl group counting in $AlMe_3$/silica reactions.

Figure 3.38 and Figure 3.39 collect ^{13}C CP-MAS spectra corresponding to the various stages of six sets of $AlMe_3$/silica/toluene and of six sets of $AlMe_3$/silica/cyclohexane reaction systems, respectively, together with corresponding results of CH_4, surface-CH_3 and solution-CH_3 determinations. In the toluene reaction system, about 70% of the total CH_3 added to the reaction as $AlMe_3$ was detected in the supernatant liquid. In the cyclohexane reaction system about 45-55% of the total CH_3 added to the reaction as $AlMe_3$ was detected in the supernatant liquid. The 'limiting reagent' in these systems is apparently surface silanols, which are present to the extent of about 30% of the initial Al-Me moieties (on a molar basis).

The results in Figure 3.38 and Figure 3.39 show that, for the toluene reaction system, the CH_3 measurements tracked roughly (more than!) (108.0±9.7)% of the initial amount of CH_3 in the system - on the solid surface, in the liquid phase and in the gas phase, where the number in parentheses is the standard deviation. Considering the estimated error of these repetitive results, all the methods together employed in this study are capable to track all the methyl groups and resulted with reasonable quantitative calculation, which helped to

understand the fate of the methyl groups in the whole $AlMe_3$/silica reaction system. In the cyclohexane reaction system, up to roughly (87.7±8.4)% of the initial amount of CH_3 can be accounted for, where the number in parentheses is the standard deviation; this experimental deficiency is most likely due to problems in the liquid-sample ^{13}C NMR spin counting experiment. Al-Me is very reactive toward moisture and it is possible that we need a better experimental technique to protect the sample during the sampling of the reaction mixture, during NMR sample preparation and during NMR experiments.

The results summarized in Figure 3.38 show that, for each $AlMe_3$/silica/toluene run, about 40 mmol of CH_3 groups were detected on the reacted surface. About 60% of the surface-attached CH_3 groups detected are $Al(Me)_n$ (–12 ppm) and about 12% belong to the Si-O-Me moiety (49 ppm).

The results summarized in Figure 3.39 show that about 60 mmol of CH_3 groups were detected on the reacted silica gel surface (about 12 g) in each $AlMe_3$/silica/cyclohexane run. About 70% of the methyl groups detected on the surface of sample A correspond to the signal at –12 ppm ($AlMe_n$), about 10% correspond to the 49 ppm signal (Si-O-Me) and about 10% correspond to the signal at 0 ppm ($SiMe_n$).

The total number of methyl groups tracked is the sum of the methyls detected in each stage. Here we define the fractional (percentage) number in the methyl groups tracked as follows:

$$Me\% = \frac{total\ amount\ of\ methyl\ groups\ tracked\ (mmol)}{initial\ amount\ of\ methyl\ group\ present\ in\ AlMe_3\ (mmol)} \times 100\% \qquad (3.26)$$

The random error (relative standard deviation) associated with Me% is propagated from the random error of the total amount of methyl groups tracked and the random error in the initial amount of methyl groups present in the initial $AlMe_3$. The initial amount of methyl groups present in $AlMe_3$ (mmol) is calculated based on the volume of $AlMe_3$ added to the reaction. The volume of $AlMe_3$ used in the reaction is 7.0±0.2 ml. This uncertainty in the volume measurement corresponds to a 5.7% estimated relative standard deviation of the initial amount of methyl groups present in $AlMe_3$ (mmol).

The total amount of methyl groups tracked (mmol) in the reaction system is calculated based on the following equation, corresponding to the measured volume of CH_4 evolved, the results of methyl group analysis by liquid-sample ^{13}C NMR and the results of solid-state ^{13}C NMR spin counting on the $AlMe_3/SiO_2$ product:

$$total\ amount\ of\ Me\ tracked(mmol) = CH_4 + Me(liq.) + Me(surface) \tag{3.27}$$

The error associated with the total amount of Me tracked is propagated from each measurement represented in Eq. 3.27. The error propagation is:

$$\sigma_{tracked\ Me} = \sqrt{\left(\sigma_{CH_4}\right)^2 + \left(\sigma_{Me(liq.)}\right)^2 + \left(\sigma_{Me(surface)}\right)^2} \tag{3.28}$$

Based on the standard deviation of the total amount of methyl groups tracked, as calculated from Eq. 3.28, the *relative* standard deviation of the total amount of methyl groups tracked can be calculated as 7.5% for the $AlMe_3$/silica/toluene system and 8.0% for the $AlMe_3$/silica/cyclohexane system.

From Eq. 3.26, the relative standard deviation of the methyl groups accounted for, σ_{Me}/Me, can be calculated as:

$$\frac{\sigma_{Me}}{Me} = \sqrt{\left(\frac{\sigma_{tracked\ Me}}{tracked\ Me}\right)^2 + \left(\frac{\sigma_{initial\ Me}}{initial\ Me}\right)^2} \qquad (3.29)$$

The relative standard deviations for Me accounted for, calculated from Eq. 3.29, are 9.7% for the $AlMe_3$/silica/toluene system and 9.5% for the $AlMe_3$/silica/cyclohexane system.

Finally, we conclude that (108.0±9.7)% of the initial amount of methyl in $AlMe_3$ is tracked in the $AlMe_3$/silica/toluene reaction system, and (87.8±8.4)% of the initial amount of methyl in $AlMe_3$ is tracked in the $AlMe_3$/silica/cyclohexane reaction system.

3.6. Summary of the stepwise fate of CH_3 moieties.

From the result shown above, based on ^{27}Al, ^{29}Si and ^{13}C NMR spectra, as well as gas-volume measurements, one can make the following observations and generalizations:

1. CH_3 groups attached on the surface via different kinds of bonds and linkages (Si-O-Me, Si-Me, $Si(Me)_2$, $Si(Me)_3$, Al-Me, and $Al(Me)_2$ moieties) are the major products formed on the surface during the initial reaction.

2. The amount of CH_3 attached on the surface is roughly equal to the amount of Si-OH on the initial silica surface in the $AlMe_3$/silica/cyclohexane experiments. Surface-attached methyl groups found in the $AlMe_3$/silica/toluene experiments account for only about 60% of the Si-OH groups of the initial silica surface.

3. The amount of CH_4 generated during the toluene reaction is about equal to the amount of surface-attached CH_3 detected in the initial product. In the

$AlMe_3$/silica/cyclohexane runs, the CH_4 generated is substantially less than the amount of CH_3 found on the surface.

4. For the toluene reaction system, most of the CH_3 groups (70%) added initially into the reaction system as $AlMe_3$ are present in the supernatant liquid after the initial reaction and about 40% of the initially added Al-Me was found in the liquid form for the cyclohexane reaction system.

5. Al-Me groups are the most reactive, among the surface attached moieties, toward H_2O. With the addition of a small amount of H_2O, Al-Me species are the only ones for which there is an intensity drop in the ^{13}C NMR spectra.

6. After the Al-Me moieties have reacted with limited amounts of H_2O, Si-O-Me (49 ppm) and $Si(Me)_3$ (0 ppm) are the next targets for H_2O.

7. As a result of the final hydrolysis reaction, all Si-O-Me and Al-Me species disappeared from the ^{13}C NMR spectra; the only CH_3 groups left on the surface are Si-Me and $Si(Me)_2$.

References

1. Liu, C. C.; Maciel, G. E., The Fumed Silica Surface: A Study by NMR. *J. Am. Chem. Soc.* **1996,** *118*, 5103-5119.

2. Liu, C. C.; Maciel, G. E., Quantitative Analysis of Solids by High-Resolution ^{1}H NMR. *Anal. Chem.* **1996,** *68*, 1401-1407.

3. Jal, P. K.; Patel, S.; Mishra, B. K., Chemical modification of silica surface by immobilization of functional groups for extractive concentration of metal ions. *Talanta* **2004,** *62*, 1005-1028.

4. Morrow, B. A.; McFarlan, A. J., Infrared and gravimetric study of an aerosil and a precipitated silica using chemical and hydrogen/deuterium exchange probes. *Langmuir* **1991,** *7*, 1695-1701.

5. Zhuravlev, L. T., Concentration of hydroxyl groups on the surface of amorphous silicas. *Langmuir* **1987,** *3*, 316-318.

6. Armistead, C. G.; Tyler, A. J.; Hambleton, F. H.; Mitchell, S. A.; Hockey, J. A., Surface hydroxylation of silica. *J. Phys. Chem.* **1969,** *73*, 3947-3953.

7. Yamamoto, K.; Tatsumi, T., Remarkable improvement in hydrothermal stability of MCM-41 by surface modification with Grignard reagents. *Chem. Lett.* **2000**, 624-625.

8. Lakomaa, E. L.; Root, A.; Suntola, T., Surface reactions in Al_2O_3 growth from trimethylaluminium and water by atomic layer epitaxy. *Appl. Surf. Sci.* **1996,** *107*, 107-115.

9. Puurunen, R. L.; Root, A.; Haukka, S.; Iiskola, E. I.; Lindblad, M.; Krause, A. O. I., IR and NMR Study of the Chemisorption of Ammonia on Trimethylaluminum-Modified Silica. *J. Phys. Chem. B* **2000,** *104*, 6599-6609.

10. Puurunen, R. L.; Root, A.; Sarv, P.; Haukka, S.; Iiskola, E. I.; Lindblad, M.; Krause, A. O. I., Growth of aluminium nitride on porous silica by atomic layer chemical vapour deposition. *Appl. Surf. Sci.* **2000,** *165*, 193-202.

11. Uusitalo, A. M.; Pakkanen, T. T.; Kroger-Laukkanen, M.; Niinisto, L.; Hakala, K.; Paavola, S.; Lofgren, B., Heterogenization of racemic ethylenebis(1-indenyl)zirconium dichloride on trimethylaluminum vapor modified silica surface. *J. Mol. Catal. A* **2000,** *160*, 343-356.

12. Anwander, R.; Palm, C.; Groeger, O.; Engelhardt, G., Formation of Lewis Acidic Support Materials via Chemisorption of Trimethylaluminum on Mesoporous Silicate MCM-41. *Organometallics* **1998,** *17*, 2027-2036.

13. Bartram, M. E.; Michalske, T. A.; Rogers, J. W., Jr., A reexamination of the chemisorption of trimethylaluminum on silica. *J. Phys. Chem.* **1991,** *95*, 4453-4463.

14. Lartiges, B. S.; Bottero, J. Y.; Derrendinger, L. S.; Humbert, B.; Tekely, P.; Suty, H., Flocculation of Colloidal Silica with Hydrolyzed Aluminum: An ^{27}Al Solid State NMR Investigation. *Langmuir* **1997,** *13*, 147-152.

15. Okuno, M.; Shimada, Y.; Schmuecker, M.; Schneider, H.; Hoffbauer, W.; Jansen, M., LAXS and ^{27}Al MAS NMR studies on the temperature-induced changes of non-crystalline single phase type mullite precursors. *J. Non-Cryst. Solids* **1997,** *210*, 41-47.

16. Temuujin, J.; MacKenzie, K. J. D.; Jadambaa, T.; Namjildorj, B.; Olziiburen, B.; Smith, M. E.; Angerer, P., Effect of mechanochemical treatment on the synthesis of calcium dialuminate. *J. Mater. Chem.* **2000,** *10*, 1019-1023.

17. MacKenzie, K. J. D.; Smith, M. E., *Multinuclear solid-state NMR of inorganic materials*. Pergamon: Oxford; New York, 2002; p 273.

18. Ganapathy, S.; Schramm, S.; Oldfield, E., Variable-angle sample-spinning high resolution NMR of solids. *J. Chem. Phys.* **1982,** *77*, 4360-4365.

19. Gore, K. U.; Abraham, A.; Hegde, S. G.; Kumar, R.; Amoureux, J.-P.; Ganapathy, S., ^{29}Si and ^{27}Al MAS/3Q-MAS NMR Studies of High Silica USY Zeolites. *J. Phys. Chem. B* **2002,** *106*, 6115-6120.

20. Samoson, A.; Lippmaa, E., Excitation phenomena and line intensities in high-resolution NMR powder spectra of half-integer quadrupolar nuclei. *Physical Review B: Condensed Matter and Materials Physics* **1983,** *28*, 6567-6570.

21. Keeler, C.; Maciel, G. E., Quantitation in the Solid-State ^{13}C NMR Analysis of Soil and Organic Soil Fractions. *Analytical Chemistry* **2003,** *75*, 2421-2432.

Table 3.1. Repeating measurements of ^{1}H single-pulse MAS integrals of polydimethylsiloxane as a reference sample over a range of times to reflect instrument variation.

Experiments	Peak Integral	Peak height (intensity)
1	19.9	4944
2	20.8	4919
3	19.9	4510
4	20.1	4966
5	20.0	4955
6	20.4	5062
7	20.1	4997
8	21.1	5216
9	21.2	5243
10	21.1	5205
11	21.9	5389
12	22.3	5457
13	22.4	5489
14	22.6	5554
15	22.1	5431
16	22.5	5516
Average	21.2	5178
Standard Deviation	1.01	289
Relative standard deviation	4.8%	5.6%

Table 3.2. Results of repeating ^{13}C CP-MAS measurements on HMB over a range of times.

	167 ppm[a]		131 ppm		96 ppm[a]		25 ppm[a]			16 ppm
Experi-ments	Integral	Intensity	Integral	Intensity	Integral	Intensity	Integral	Intensity	Integral	Intensity
1	8.88	6256	4.50	3369	2.25	1845	0.678	669	29.4	18718
2	7.73	5485	3.45	2654	1.90	1608	0.714	624	29.4	18507
3	7.77	5522	3.52	2681	1.95	1611	0.649	596	29.8	18674
4	8.03	5649	3.73	2823	1.99	1674	0.551	586	30.0	19041
5	8.50	5985	4.09	3091	2.12	1751	0.498	600	30.9	19748
6	8.74	6151	4.32	3246	2.17	1815	0.648	659	30.9	19658
7	8.81	6170	4.37	3270	2.18	1822	0.617	654	30.9	19768
8	8.97	6276	4.49	3368	2.19	1839	0.754	679	29.4	18665
9	8.80	6279	4.47	3396	2.23	1829	0.595	632	29.5	18721
Average	8.47	5975	4.10	3100	2.11	1755	0.634	633	30.0	19056
Standard deviation	0.492	332	0.427	303	0.128	98.6	0.079	34.0	0.68	522
Relative standard deviation	5.8%	5.6%	10.4%	9.8%	6.1%	5.6%	12.5%	5.4%	2.3%	2.7%

[a] spinning sideband of the peak at 131 ppm.

Table 3.3. Peak characteristics in the single-pulse MAS ^{1}H spectra of polydimethylsiloxane (PDMS), 1,3,5-trimethoxybenzene and silica and in the ^{13}C CP/MAS spectra of hexamethylbenzene (HMB) and $AlMe_3$/silica sample.

	Signal intensity[a]	$Noise_{rms}$[b]	S/N[c]	$(S/N)^{-1}$ [d]	% SD[e]
PDMS [f]					
0 ppm	65.6	0.1167	562	0.0018	5.0%
1,3,5-trimethoxybenzene[g]					
5.6 ppm	803	0.221	3628	0.0003	5.0%
3.2 ppm	2462	0.221	11123	$9.0x10^{-5}$	5.0%
Silica [h]					
10 ppmto 1 ppm	619	2.47	251	0.0040	5.0%
HMB [i]					
167 ppm	5975	18.7	320	0.0031	5.0%
131 ppm	3100	18.7	166	0.0060	5.0%
96 ppm	1755	18.7	94.0	0.0106	5.1%
25 ppm	633	18.7	33.9	0.0295	5.8%
16 ppm	19056	18.7	1021	0.0010	5.0%
$AlMe_3$/silica [j]					
54 ppm	299	24.7	12.1	0.0824	9.6%
49 ppm	2423	24.7	98.3	0.0102	5.1%
0 ppm	1842	24.7	74.7	0.0134	5.2%
-3 ppm	952	24.7	38.6	0.0259	5.6%
-7 ppm	395	24.7	16.0	0.0624	8.0%
-12 ppm	4910	24.7	199	0.0050	5.0%

[a] Peak height.
[b] $noise_{rms}$ is the root-mean-square of noise height measured over a range in the spectrum.
[c] S/N ratio, S/N=signal height / $noise_{rms}$.
[d] the reciprocal of S/N ratio, which represent the random error due to spectrum noise.
[e] % SD: relative standard deviation, based on Eq. 3.9, with $\sigma_a/a = 5\%$ (see section 3.1.2).
[f] PDMS single-pulse MAS ^{1}H spectrum.
[g] 1,3,5-trimethoxybenzene single-pulse MAS ^{1}H spectrum.
[h] silica gel single-pulse MAS ^{1}H spectrum.
[i] HMB ^{13}C CP/MAS spectrum.
[j] $AlMe_3$/silica ^{13}C CP/MAS spectrum.

Table 3.4. ^{1}H saturation-recovery results (Figure 3.1) on polydimethylsiloxane.

Recovery Time tau (s)	^{1}H MAS signal integral at 0 ppm[a]
0.001	0.777
0.010	0.948
0.100	1.52
0.200	1.97
0.300	2.51
0.500	3.39
0.700	4.17
0.800	4.53
1.000	5.39
2.000	7.83
3.000	9.00
4.000	9.65
5.000	9.95
6.000	10.1
10.000	10.1

[a] Estimated relative standard deviation, 5% (see section 3.1.2).

Table 3.5. ^{1}H inversion-recovery results (Figure 3.3) on 1,3,5-trimethoxybenzene[a].

Recovery time (s)	Peak at 5.6 ppm	Peak at 3.2 ppm
0.001	-0.783	-2.37
0.010	-0.778	-2.32
0.050	-0.735	-2.21
0.100	-0.700	-2.05
0.500	-0.443	-1.01
1.000	-0.186	-0.060
1.500	0.008	0.63
2.000	0.164	1.13
2.500	0.283	1.48
3.000	0.382	1.74
4.000	0.517	2.06
4.500	0.570	2.16
5.000	0.612	2.23
7.000	0.709	2.38
9.000	0.764	2.42
10.000	0.775	2.43
15.000	0.809	2.43
30.000	0.816	2.43

[a] Estimated relative standard deviation, 5% (see section 3.1.2).

Table 3.6. ^{1}H-MAS spin-counting control test result (on test sample 1,3,5-trimethoxybenzene).

		^{1}H–MAS Integral			Integral ratio of test sample to reference	
	EXP.	I (PDMS)[a]	I (OMe)[b]	I (Ar)[c]	I(Me)/ I(PDMS)	I(Ar)/ I(PDMS)
Sample #1	1	20.4	10.1	3.28	0.498	0.163
	2	20.0	9.52	3.05	0.475	0.154
	3	21.2	9.65	3.12	0.456	0.149
	4	21.5	10.1	3.26	0.468	0.153
	5	21.3	9.70	3.07	0.455	0.146
				Average	0.470±0.018[d]	0.153±0.006[d]
				Error [e]	3.74%	4.25%
	Gravimetric Measurement [f]				0.474	0.158
Sample #2	1	20.4	9.49	3.04	0.466	0.151
	2	20.2	9.43	3.01	0.466	0.151
	3	21.2	10.1	3.23	0.475	0.154
	4	22.1	10.1	3.25	0.459	0.149
	5	22.3	10.3	3.30	0.463	0.150
				Average	0.466±0.006[d]	0.151±0.002[d]
				Error [e]	1.29%	1.41%
	Gravimetric Measurement				0.465	0.155
Sample #3	1	20.0	9.56	3.06	0.478	0.155
	2	20.3	9.48	3.04	0.467	0.152
	3	20.6	9.51	3.07	0.461	0.150
	4	22.3	10.1	3.25	0.452	0.147
	5	22.3	10.3	3.31	0.462	0.150
				Average	0.464±0.010[d]	0.151±0.003[d]
				Error [e]	2.05%	1.78%
	Gravimetric Measurement				0.458	0.152

[a] Integral of external reference compound polydimethylsiloxane (PDMS).
[b] Integral of Me group in 1,3,5-trimethoxybenzene, the weight-known sample.
[c] Integral of aromatic group in 1,3,5-trimethoxybenzene.
[d] Random error given is relative standard deviation.
[e] Relative discrepancy of NMR measurement to gravimetric measurement (see section 3.1.1).
[f] Expected integral ratio of known to reference by gravimetric measurement.

Table 3.7. ^{1}H MAS saturation-recovery results (Figure 3.7) on silica gel dried at 150 °C under vacuum.

Recovery time (s)	^{1}H MAS signal integral[a]
0.001	0.018
0.005	0.031
0.010	0.051
0.020	0.080
0.050	0.515
0.100	1.17
0.200	2.32
0.300	3.23
0.400	3.79
0.500	4.57
0.700	5.67
0.900	6.76
1.000	6.91
1.200	7.40
1.500	7.65
1.800	8.34
2.000	8.96
2.200	8.57
2.500	9.13
3.000	8.70
3.500	9.20
4.000	9.31
5.000	8.67
8.000	9.21
10.000	9.09

[a] Intensity of signal from 10 ppm to 1 ppm, all kinds of silanols integrated together. Estimated relative standard deviation, 5% (see section 3.1.2).

Table 3.8. ^{1}H MAS spin-counting results on silanol groups of the silica gel surface (dried at 150 °C).

	I(PDMS)[a] / I(Si-OH)[b]	weight of silica gel sample (mg)	OH mmol /g on silica surface	Average OH mmol /g on silica surface
sample #1	22.46	15.5	5.35	
	23.08	15.5	5.21	
	23.24	15.5	5.17	5.24±0.10[c]
sample #2	23.23	15.5	5.17	
	23.29	15.5	5.16	
	22.46	15.5	5.35	5.23±0.11[c]
sample #3	24.52	14.6	5.20	
	25.32	14.6	5.04	
	25.21	14.6	5.06	5.10±0.09[c]

[a.] Integral of external reference compound polydimethylsiloxane (PDMS). Estimated relative standard deviation, 5% (see section 3.1.2).
[b.] Integral of all types of silanols present on the silica gel surface. Estimated relative standard deviation, 5% (see section 3.1.2).
[c.] Error given is standard deviation.

Table 3.9. ^{27}Al single-pulse spin-counting results on γ-Al_2O_3, aluminum nitrate and aluminum lactate.

Non-spinning integral[a]	I(aluminum nitrate)[b]	I(γ-Al_2O_3)[b]	% error[c]
Exp. 1	100	291	
Exp. 2	111	291	
Exp. 3	111	295	
Exp. 4	113	303	
Exp. 5	114	301	
Average of integrals[d]	110±6	296±6	
Grav.-Al (mmol)[e]	0.169	0.455	
Integral/Al-Grav. [f]	650	651	0.1%
Spinning Integral[g]	I(aluminum lactate)	I(γ-Al_2O_3)	% error[c]
Exp. 1	84.6	236	
Exp. 2	85.7	233	
Exp. 3	85.3	227	
Exp. 4	82.3	228	
Exp. 5	82.2	228	
Average of integrals[d]	84.0±1.7	230±4	
Grav.-Al (mmol)[e]	0.146	0.455	
Integral/ Al-Grav. [f]	575	506	13.6%

[a] Carried out with no spinning.
[b] Integral of the center peak of the signal.
[c] If we let P = Integral / Al-mmol, then:
%error = [P(aluminumnitrate) - P(γ-Al_2O_3)] / P(γ-Al_2O_3) x 100% or.
%error = [P(aluminum lactate) - P(γ-Al_2O_3)] / P(γ-Al_2O_3) x 100%
[d] The average and standard deviation of the experiment results.
[e] Number of mmols of Al in sample based on gravimetric measurement.
[f] Signal integral per mmol of Al presented in the sample.
[g] The experiments were carried out at 16 kHz spinning and a little of magic angle.

Table 3.10. Deconvolved peak integrals in ^{13}C CP/MAS-detected ^{1}H-saturation-recovery experiments (Figure 3.14) on a dry $AlMe_3$/silica/toluene sample corresponding to sample A in Figure 3.9.

	^{13}C CP-MAS deconvolved peak integrals [a]								
Recovery time tau (s)[b]	88 ppm[c]	54 ppm[d]	49 ppm[e]	27 ppm[f]	0 ppm[g]	-3 ppm[h]	-7 ppm[i]	-12 ppm[j]	-49 ppm[f]
0.0001	0.000	0.000	0.000	0.000	0.000	0.000	0.000	0.000	0.000
0.0010	0.000	0.000	0.000	0.000	0.000	0.000	0.000	0.000	0.000
0.0100	0.000	0.000	0.000	0.000	0.000	0.000	0.000	0.000	0.000
0.1000	0.000	0.000	0.000	0.000	0.000	0.000	0.000	0.000	0.000
0.5000	0.000	0.724	1.21	1.03	0.621	0.161	0.110	5.15	0.000
1.0000	0.0590	1.01	2.59	0.209	0.998	1.30	0.299	10.5	1.12
3.0000	0.815	1.20	6.53	0.810	3.07	2.53	0.806	29.0	1.73
5.0000	1.41	1.91	9.76	2.21	4.09	3.50	1.17	40.4	2.16
8.0000	1.90	2.61	12.3	1.46	5.06	4.07	1.05	52.9	1.55
10.0000	2.08	2.54	13.8	2.07	5.67	5.39	1.41	61.3	1.80
15.0000	2.08	2.75	15.9	1.29	6.90	5.41	1.16	70.7	2.75
30.0000	1.98	2.49	18.1	1.68	8.20	6.29	1.22	81.8	3.08
40.0000	2.18	3.02	17.6	1.68	9.06	5.76	1.42	76.2	3.08

[a] Estimated relative standard deviation, 5% for peak at 49 ppm 0 ppm and –12 ppm; 10% for the rest (see section 3.1.2).
[b] The time set by the instrument is accurate to 10^{-9} sec.
[c] Spinning side band of peak at 49 ppm.
[d] $Si(OMe)_2$.
[e] Si-OMe.
[f] Spinning side band of peak at -12 ppm.
[g] $Si(Me)_3$.
[h] $Si(Me)_2$.
[i] Si-Me.
[j] $Al(Me)_n$.

Table 3.11. Deconvolved peak integrals in ^{13}C CP-MAS variable-contact-time experiments (Figure 3.16) on a dry $AlMe_3$/silica/toluene sample corresponding to sample A in Figure 3.9.

	^{13}C CP-MAS integrals of deconvolved signal [a]								
Contact time (ms)[b]	88 ppm[c]	54 ppm[d]	49 ppm[e]	27 ppm[f]	0 ppm[g]	-3 ppm[h]	-7 ppm[i]	-12 ppm[j]	-49 ppm[f]
0.005	0.000	0.000	0.000	0.000	0.000	0.000	0.000	0.000	0.000
0.010	0.000	0.000	0.000	0.000	0.000	0.000	0.000	0.000	0.000
0.020	0.000	0.000	0.000	0.000	0.000	0.000	0.000	4.43	0.000
0.050	0.850	0.626	3.13	0.405	1.02	0.900	0.216	9.39	1.32
0.100	1.53	2.67	3.37	0.000	2.82	2.20	1.01	16.5	0.306
0.240	1.69	3.70	5.53	1.97	2.53	3.08	1.46	24.5	1.02
0.500	1.70	3.77	6.07	1.49	2.79	3.47	1.07	29.3	1.93
0.750	1.49	3.68	6.44	1.93	3.17	3.99	1.36	31.7	1.93
1.000	2.22	3.59	7.31	1.39	3.43	4.45	1.40	34.9	2.09
1.500	1.10	3.49	7.62	2.11	3.64	4.22	1.41	38.1	2.92
2.000	1.34	2.91	7.83	1.76	3.42	4.36	1.46	40.9	2.55
2.500	1.41	3.17	7.44	1.29	3.47	3.87	1.41	43.1	2.96
3.000	0.906	2.69	7.54	1.26	4.01	3.76	1.26	43.0	2.96
5.000	1.19	3.06	7.61	1.60	3.63	4.05	1.38	41.3	2.85
8.000	1.50	2.60	7.67	0.974	3.63	3.55	1.34	42.3	1.80
10.000	1.05	2.09	7.33	0.608	3.77	3.30	1.14	39.9	1.68
15.000	1.06	1.96	7.50	0.608	3.62	3.71	0.768	39.6	1.26

[a] Estimated relative standard deviation, 5% for peak at 49 ppm 0 ppm and –12 ppm; 10% for the rest (see section 3.1.2).
[b] The time set by the instrument is accurate to 10^{-9} sec.
[c] Spinning-side-band of signal at 49 ppm.
[d] $Si(OMe)_2$.
[e] Si-OMe.
[f] Spinning-side-band of signal at -12 ppm.
[g] $Si(Me)_3$.
[h] $Si(Me)_2$.
[i] Si-Me.
[j] $Al(Me)_n$.

Table 3.12. Relaxation times and corrections for ^{13}C CP-MAS experiments on a dry $AlMe_3$/silica/toluene sample corresponding to sample A in Figure 3.9, based on analysis of data from Table 3.10 and Table 3.11 fitted to Eq. 3.15 and Eq. 3.16.

deconvolved ^{13}C signal		^{13}C-^{1}H cross-polarization dynamics time constant from variable-contact-time experiment			^{1}H T_1 from variable-recovery-time ^{13}C CP-MAS experiment		Total Correction
Peak position [a]	Peak Assign-ment	T^{CH} (ms)[b]	$T_{1\rho}$ (ms)[c]	M^{∞}/M(5 ms)[d]	T_1^H (s)	M^0/M(3 s)[e]	M*/M(5 ms, 3 s)[f]
-12 ppm	$Al(Me)_n$	0.207±0.027	73.2±23.3	1.01	4.91±0.27	2.19	2.22
-7 ppm	Si-Me	0.323±0.061	36.0±14.4	1.32	5.89±0.51	2.51	3.31
-3 ppm	$Si(Me)_2$	0.309±0.056	47.4±21.2	1.12	3.20±0.52	1.64	1.84
0 ppm	$Si-(Me)_3$	0.681±0.094	49.7±21.8	1.12	3.27±0.58	1.67	1.87
49 ppm	-Si-O-Me	0.286±0.012	41.8±16.2	1.13	4.89±0.14	2.18	2.47
54 ppm	$Si(OMe)_2$	0.459±0.024	38.6±4.6	1.15	4.44±0.64	2.04	2.35
HMB as external reference							
16 ppm	methyl	1.81±0.27	208±29	1.11	0.642±0.027	1.01	1.12
132 ppm	aromatic	3.74±0.43	130±22	1.44	0.627±0.006	1.01	1.45

[a] Corresponding to sample A of Figure 3.9.
[b] T^{CH} measured in variable contact time ^{13}C CP-MAS experiment, taken from Table 3.11.
[c] Proton $T_{1\rho}$ measured in variable-contact-time ^{13}C CP-MAS experiment derived from Table 3.11.
[d] M^{∞}, maximum magnetization during cross polarization period. M^{∞}/M(5 ms), magnetization correction for cross polarization with a 5 ms contact time. Estimated relative standard error, 4.2% for peaks at 49 ppm, 0 ppm and –12 ppm (strong signals), 8.5% for the rest (weak signals) (see section 3.3.5).
[e] M^0, maximum magnetization when H spins are fully relaxed. M^0/M(3 s), magnetization correction for T_1 relaxation for 3 s recovery time. Estimated relative standard error, 4.2% for peaks at 49 ppm, 0ppm and –12 ppm (strong signals), 8.5% for the rest (weak signals) (see section 3.3.5).
[f] M*, theoretical maximum magnetization. M*/M(5 ms, 3 s), magnetization correction obtained at 5 ms contact time and 3 s recovery time. Estimated relative standard error, 6% for peaks at 49 ppm, 0 ppm and –12 ppm (strong signals), 12% for the rest (weak signals) (see section 3.3.5).

Table 3.13. Deconvolved peak integrals in ^{13}C CP/MAS-detected ^{1}H-saturation-recovery experiments on a dry $AlMe_3$/silica/cyclohexane sample corresponding to sample A in Figure 3.10.

	^{13}C CP-MAS deconvolved signals [a]									
Recovery Time (s)[b]	88 ppm[c]	54 ppm[d]	49 ppm[e]	26 ppm[f]	16 ppm[c]	0 ppm[g]	-3 ppm[h]	-7 ppm[i]	-12 ppm[j]	-49 ppm[f]
0.0001	0.000	0.000	0.000	0.000	0.000	0.000	0.000	0.000	0.000	0.000
0.0010	0.000	0.000	0.000	0.000	0.000	0.000	0.000	0.000	0.000	0.000
0.0100	0.000	0.000	0.000	0.000	0.000	0.000	0.000	0.000	0.000	0.000
0.1000	0.000	0.000	0.000	0.000	0.000	0.000	0.476	0.000	1.47	0.000
0.5000	0.0410	0.000	1.11	0.000	0.000	0.922	0.861	0.000	6.07	0.488
1.0000	0.146	0.380	2.03	0.337	0.017	1.81	1.53	0.087	10.3	0.777
3.0000	0.953	0.776	5.65	0.751	0.152	5.38	3.50	0.252	26.9	1.27
5.0000	1.19	1.01	8.62	1.03	0.148	7.30	5.47	0.732	39.0	1.50
8.0000	1.78	1.39	10.4	0.618	0.278	10.2	6.73	1.52	49.0	1.90
10.0000	2.40	1.69	11.8	0.555	0.278	11.6	7.91	1.45	55.8	2.14
15.0000	2.37	2.01	13.1	0.944	0.332	13.1	8.34	1.58	63.0	2.42
20.0000	2.00	2.02	14.1	1.77	0.332	12.6	9.13	1.88	70.0	2.55
30.0000	2.28	2.02	14.7	1.84	0.518	13.2	9.94	1.69	73.1	3.32

[a] Estimated relative standard deviation, 5% for peaks at 49 ppm, 0 ppm and –12 ppm (strong signals) and 10% for the rest (weak signals) (see section 3.1.2).
[b] The time set by the instrument is accurate to 10^{-9} sec.
[c] Spinning side band of peak at 49 ppm.
[d] $Si(OMe)_2$.
[e] Si-OMe.
[f] Spinning side band of peak at -12 ppm.
[g] $Si(Me)_3$.
[h] $Si(Me)_2$.
[i] Si-Me.
[j] $Al(Me)_n$.

Table 3.14. Deconvolved peak integrals in ^{13}C CP-MAS variable-contact-time experiments on a dry $AlMe_3$/silica/cyclohexane sample corresponding to sample A in Figure 3.10.

	^{13}C NMR deconvolved signal integrals									
Contact Time (ms) [b]	88 ppm [c]	54 ppm [d]	49 ppm [e]	27 ppm [f]	16 ppm [c]	-0 ppm [g]	-3 ppm [h]	-7 ppm [i]	-12 ppm [j]	-49 ppm [f]
0.005	0.000	0.000	0.000	0.000	0.000	0.000	0.000	0.000	0.000	0.000
0.010	0.000	0.404	0.487	0.000	0.000	0.447	0.170	0.061	1.45	0.000
0.020	0.000	0.333	1.30	0.833	0.526	0.276	0.923	0.354	4.86	0.000
0.050	0.670	0.743	2.62	0.296	0.251	1.10	1.04	0.203	9.99	0.665
0.100	0.568	1.34	3.62	0.275	0.872	3.20	1.21	0.533	17.0	0.410
0.240	0.650	1.28	4.35	1.03	0.204	3.96	1.80	0.453	23.1	0.365
0.500	0.713	1.21	5.27	2.02	0.229	2.68	2.53	0.669	30.2	1.75
0.750	0.779	1.03	5.73	1.03	0.433	5.38	2.99	0.548	33.8	1.84
1.000	1.01	1.40	6.16	0.831	0.158	5.78	2.96	0.586	36.0	2.36
1.500	0.954	0.914	6.93	1.28	0.180	6.15	3.09	0.809	38.2	2.08
2.000	1.70	1.09	6.52	1.29	0.342	6.67	3.02	0.575	41.5	3.25
2.500	1.01	1.04	7.25	1.03	0.223	6.04	3.48	0.691	45.0	2.43
3.000	0.846	0.476	7.30	0.990	0.235	5.88	3.81	0.590	46.7	2.56
5.000	0.907	1.00	5.97	1.52	0.314	6.00	3.48	0.553	44.7	2.59
8.000	0.786	1.19	6.15	1.17	0.306	9.03	2.20	0.995	42.8	3.60
10.000	1.08	0.608	6.01	1.46	0.193	5.72	3.36	0.543	42.7	2.31
15.000	1.04	1.90	5.70	1.07	0.156	4.88	3.03	0.197	43.4	2.38

[a] Estimated relative standard deviation, 5% for peaks at 49 ppm, 0 ppm and –12 ppm (strong signals) and 10% for the rest (weak signals) (see section 3.1.2).
[b] The time set by the instrument is accurate to 10^{-9} s.
[c] Spinning side band of peak at 49 ppm.
[d] $Si(OMe)_2$.
[e] Si-OMe.
[f] Spinning side band of peak at -12 ppm.
[g] $Si(Me)_3$.
[h] $Si(Me)_2$.
[i] Si-Me.
[j] $Al(Me)_n$.

Table 3.15. Relaxation times and corrections for ^{13}C CP-MAS experiments on a dry $AlMe_3$/silica/cyclohexane sample corresponding to sample A in Figure 3.10, based on analysis of data from Table 3.13 and Table 3.14 fitted to Eq. 3.15 and Eq. 3.16.

deconvolved ^{13}C signal		^{13}C-^{1}H cross-polarization dynamics time constant from variable-contact-time experiment			^{1}H T_1 from variable-recovery-time ^{13}C CP-MAS experiment		Total Correction
Peak position [a]	Peak Assign-ment	T^{CH} (ms)[b]	$T_{1\rho}$ (ms)[c]	M^{∞}/M(5 ms)[d]	T_1^H (s)[e]	M^0/M(3 s)[f]	M^*/M(5 ms, 3 s)[g]
-12 ppm	$Al(Me)_n$	0.613 ±0.004	210±12	1.03	7.24±0.03	2.95	3.03
-7 ppm	Si-Me	0.320 ±0.094	13.3±3.6	1.49	6.22±2.48	2.61	3.90
-3 ppm	$Si(Me)_2$	0.701 ±0.170	41.8±22.3	1.15	6.58±0.60	2.73	3.13
0 ppm	$Si(Me)_3$	0.258 ±0.044	92±49	1.06	5.59±0.31	2.41	2.55
49 ppm	Si-O-Me	0.400 ±0.039	53.2±11.6	1.11	6.04±0.23	2.55	2.83
54 ppm	$Si(OMe)_2$	0.059 ±0.007	13.1±1.5	1.47	6.70±2.23	2.77	4.08
HMB as external reference							
16 ppm	methyl	1.81±0.27	208±29	1.11	0.642±0.027	1.01	1.12
132 ppm	aromatic	3.74±0.43	130±22	1.44	0.627±0.006	1.01	1.45

[a] Corresponding to sample A of Figure 3.10.
[b] T^{CH} measured in variable contact time ^{13}C CP-MAS experiment, derived from Table 3.14.
[c] Proton $T_{1\rho}$ measured in variable contact time ^{13}C CP-MAS experiment, derived from Table 3.14.
[d] M^{∞}, maximum magnetization during cross polarization period. M^{∞}/M(5 ms), magnetization correction for cross polarization period 5 ms. Estimated relative standard error, 4.2% for peaks at 49 ppm, 0 ppm and –12 ppm (strong signals), 8.5% for the rest (weak signals) (see section 3.3.5).
[e] T_1^H measured in saturation recovery experiment, taken from Table 3.13.
[f] M^0, maximum magnetization when H spins are fully relaxed. M^0/M(3 s), magnetization correction for recovery time of 3 s. Estimated relative standard error, 4.2% for peaks at 49 ppm, 0 ppm and –12 ppm (strong signals), 8.5% for the rest (weak signals) (see section 3.3.5).
[g] M^*, theoretical maximum magnetization. M^*/M(5 ms, 3 s), magnetization correction for signal obtained at 5 ms contact time and 3 s recovery time. Estimated relative standard error, 6% for peaks at 49 ppm, 0 ppm and –12 ppm (strong signals), 12% for the rest (weak signals) (see section 3.3.5).

Table 3.16. Deconvolved peak integrals in ^{13}C CP/MAS-detected ^{1}H-saturation-recovery experiments on an ether washed $AlMe_3$/silica/toluene sample corresponding to sample B in Figure 3.9.

	^{13}C CP-MAS deconvolved integrals [a]										
Recovery time tau (s)[b]	88 ppm[c]	68 ppm[d]	54 ppm[e]	49 ppm[f]	26 ppm[g]	14 ppm[h]	0 ppm[i]	-3 ppm[j]	-7 ppm[k]	-12 ppm[l]	-49 ppm[g]
40.0000	1.97	9.78	2.27	14.3	0.075	9.72	8.03	5.27	1.74	47.3	3.90
30.0000	2.54	10.5	2.63	14.6	0.211	9.65	7.90	5.51	1.54	46.8	4.23
15.0000	2.36	10.5	2.53	13.9	0.399	9.91	8.10	6.14	1.81	45.0	3.06
10.0000	1.83	9.84	2.27	13.1	0.364	8.84	7.30	5.32	1.44	42.7	2.29
8.0000	1.52	9.23	2.04	12.6	0.177	8.35	7.04	5.01	1.29	40.8	1.73
5.0000	1.90	7.60	1.85	13.2	0.313	6.93	5.73	4.24	1.06	42.9	2.36
3.0000	1.05	6.23	1.48	7.82	0.646	5.30	4.32	3.48	0.531	24.9	1.87
1.0000	0.613	2.90	1.04	3.76	0.568	2.00	1.73	1.47	0.400	10.5	1.79
0.5000	0.259	1.70	0.385	2.15	0.649	1.42	0.992	0.798	0.127	6.32	0.819
0.1000	0.000	0.000	0.000	0.000	0.000	0.000	0.000	0.000	0.000	0.000	0.000
0.0100	0.000	0.000	0.000	0.000	0.000	0.000	0.000	0.000	0.000	0.000	0.000
0.0010	0.000	0.000	0.000	0.000	0.000	0.000	0.000	0.000	0.000	0.000	0.000
0.0001	0.000	0.000	0.000	0.000	0.000	0.000	0.000	0.000	0.000	0.000	0.000

[a] Estimated relative standard deviation, 5% for peaks at 49 ppm, 0 ppm and –12 ppm (strong signals), 10% for the rest (weak signals) (see section 3.1.2).
[b] The time set by the instrument is accurate to 10^{-9} s.
[c] Spinning sideband of peak at 49 ppm.
[d] CH_2 of ether.
[e] $Si(OMe)_2$.
[f] Si-OMe.
[g] Spinning sideband of peak at -12 ppm.
[h] Me group of ether.
[i] $Si(Me)_3$.
[j] $Si(Me)_2$.
[k] Si-Me.
[l] $Al(Me)_n$.

Table 3.17. Deconvolved peak integrals in ^{13}C CP-MAS variable-contact-time experiments on an ether washed $AlMe_3$/silica/toluene sample corresponding to sample B in Figure 3.9.[a]

Contact time (ms)[b]	88 ppm[c]	68 ppm[d]	54 ppm[e]	49 ppm[f]	27 ppm[g]	14 ppm[h]	0 ppm[i]	-3 ppm[j]	-7 ppm[k]	-12 ppm[l]	-49ppm[g]
0.005	0.000	0.000	0.000	0.000	0.000	0.000	0.000	0.000	0.000	0.000	0.000
0.010	0.000	0.000	0.000	0.000	0.000	0.000	0.000	0.000	0.000	0.000	0.000
0.020	1.14	1.58	0.779	2.03	0.978	0.719	0.619	0.419	0.266	4.42	0
0.050	1.22	5.36	2.43	5.01	1.40	1.25	1.34	0.451	0.514	9.98	1.27
0.100	1.47	7.00	1.74	7.33	0.501	2.36	3.09	0.802	0.224	20.6	1.69
0.240	2.15	7.39	2.16	9.38	0.170	4.92	4.43	1.54	0.712	27.7	2.53
0.500	1.56	8.31	2.66	9.57	0.695	6.60	5.21	1.76	0.721	30.9	2.17
0.750	2.16	9.25	2.83	11.4	0.182	7.28	6.35	2.04	0.834	35.9	3.06
1.000	1.33	9.45	2.87	12.9	0.009	7.82	5.38	2.55	0.983	39.1	3.68
1.500	1.84	9.22	2.36	12.3	0.446	8.15	6.50	2.36	0.993	38.7	2.30
2.000	1.87	9.19	2.89	12.7	0.936	7.56	6.76	2.23	0.838	35.9	1.64
2.500	1.55	9.32	2.27	12.3	0.572	6.85	5.99	2.31	0.743	35.4	2.94
3.000	1.33	8.84	1.80	12.8	0.558	7.15	6.33	1.96	0.717	37.2	2.16
5.000	1.61	8.64	2.17	12.2	0.600	6.92	5.33	2.05	0.685	35.2	2.18
8.000	0.863	7.51	0.863	12.0	0.022	6.00	5.83	1.61	0.677	35.5	1.70
10.000	1.34	5.82	0.668	11.2	0.334	5.44	5.28	1.39	0.316	33.1	2.98
15.000	0.765	4.70	0.474	9.20	0.198	4.54	4.74	1.59	0.305	28.8	2.17

[a] Estimated relative standard deviation, 5% for peaks at 49 ppm, 0 ppm and –12 ppm (strong signals), 10% for the rest (weak signals) (see section 3.1.2).
[b] The time set by the instrument is accurate to 10^{-9} s.
[c] Spinning side band of peak at 49 ppm.
[d] CH_2- of diethyl ether.
[e] $Si(OMe)_2$.
[f] Si-OMe.
[g] Spinning side band of peak at -12 ppm.
[h] Me- of ether.
[i] $Si(Me)_3$.
[j] $Si(Me)_2$.
[k] Si-Me.
[l] $Al(Me)_n$.

Table 3.18. Relaxation times and corrections for ^{13}C CP-MAS experiments on an ether washed $AlMe_3$/silica/toluene sample corresponding to sample B in Figure 3.9, based on analysis of data from Table 3.16 and Table 3.17 fitted to Eq. 3.15 and Eq. 3.16.

deconvolved ^{13}C signal		^{13}C-^{1}H cross-polarization dynamics time constant from variable-contact-time experiment			^{1}H T_1 from variable-recovery-time ^{13}C CP-MAS experiment		Total Correction
Peak position[a]	Peak Assign-ment	T^{CH} (ms)[b]	$T_{1\rho}$ (ms)[c]	M^{∞}/M(5 ms)[d]	$T_1{}^H$ (s)[e]	M^0/M(3 s)[f]	M* /M(5 ms, 3 s)[g]
-12 ppm	$Al(Me)_n$	0.192 ±0.002	45.4±0.5	1.12	4.02±0.18	1.90	2.13
-7 ppm	Si-Me	0.287 ±0.067	9.50±1.60	1.75	6.04±0.90	2.55	4.46
-3 ppm	$Si(Me)_2$	0.284 ±0.207	24.4±21.3	1.24	3.30±0.28	1.68	2.08
0 ppm	$Si(Me)_3$	0.286 ±0.033	32.1±4.50	1.18	3.96±0.11	1.88	2.22
49 ppm	Si-O-Me	0.124 ±0.005	51.7±3.28	1.10	3.95±0.18	1.88	2.08
54 ppm	$Si(OMe)_2$	0.077 ±0.019	7.67±1.30	1.94	2.98±0.40	1.58	3.05
Ether peaks presented on the surface							
14 ppm	Me	0.276 ±0.034	25.0±3.66	1.24	3.99±0.15	1.89	2.34
68 ppm	CH_2	0.089 ±0.007	23.2±1.67	1.25	3.46±0.16	1.72	2.15

[a] Corresponding to sample B of Figure 3.9.
[b] T^{CH} measured in variable contact time ^{13}C CP-MAS experiment, derived from Table 3.17.
[c] $T_{1\rho}$ measured in variable contact time ^{13}C CP-MAS experiment, derived from Table 3.17.
[d] M^{∞}, maximum magnetization during cross polarization period. M^{∞}/M(5 ms), magnetization correction for a cross polarization period of 5 ms. Estimated relative standard error, 4.2% for peaks at 49 ppm, 0 ppm and –12 ppm (strong signals), 8.5% for the rest (weak signals) (see section 3.3.5).
[e] $T_1{}^H$ measured in saturation CP-MAS recovery experiment, derived from Table 3.16.
[f] M^0, maximum magnetization when H spins are fully relaxed. M^0/M(3 s), magnetization spin-lattice relaxation correction for 3 s recovery time.
[g] M*, theoretical maximum magnetization. M*/M(5 ms, 3 s), magnetization correction for signal obtained at 5 ms contact time and 3 s recovery time. Estimated relative standard error, 6% for peaks at 49 ppm, 0 ppm and –12 ppm (strong signals), 12% for the rest (weak signals) (see section 3.3.5).

Table 3.19. Deconvolved peak integrals in ^{13}C CP/MAS-detected ^{1}H-saturation-recovery experiments on an ether washed $AlMe_3$/silica/cyclohexane sample corresponding to sample B in Figure 3.10.

	^{13}C CP-MAS deconvolved signals [a]										
Recovery Time tau (s)[b]	88 ppm[c]	68 ppm[d]	56 ppm[e]	49 ppm[f]	26 ppm[g]	14 ppm[h]	0 ppm[i]	-3 ppm[j]	-7 ppm[k]	-12 ppm[l]	-49ppm[g]
40.0000	2.36	7.88	5.01	13.8	1.55	8.80	4.98	6.98	3.84	34.0	2.08
30.0000	1.87	7.63	4.99	13.7	1.48	8.47	6.98	6.98	3.25	31.5	2.02
15.0000	3.13	8.02	5.21	13.1	1.46	8.31	6.55	6.55	3.70	32.2	2.03
10.0000	1.89	7.42	5.00	14.1	1.64	7.98	6.25	6.25	3.21	30.2	2.21
8.0000	1.94	7.60	3.98	14.0	1.49	7.75	6.58	6.06	2.85	28.3	1.32
5.0000	1.86	6.52	3.47	12.3	1.14	6.94	5.88	5.34	3.03	24.7	1.23
3.0000	1.39	5.21	3.20	9.51	1.11	5.27	4.89	4.89	1.71	19.3	1.24
1.0000	0.803	2.06	0.970	4.43	0.874	2.12	1.96	1.96	1.01	8.64	1.04
0.5000	0.273	0.931	0.364	2.36	0.213	1.03	0.887	0.887	0.712	5.09	0.807
0.1000	0.000	0.000	0.000	0.000	0.000	0.000	0.000	0.000	0.000	0.000	0.000
0.0100	0.000	0.000	0.000	0.000	0.000	0.000	0.000	0.000	0.000	0.000	0.000
0.0010	0.000	0.000	0.000	0.000	0.000	0.000	0.000	0.000	0.000	0.000	0.000
0.0001	0.000	0.000	0.000	0.000	0.000	0.000	0.000	0.000	0.000	0.000	0.000

[a] Estimated relative standard deviation, 5% for peaks at 49 ppm, 0 ppm and –12 ppm (strong signals), 10% for the rest (weak signals) (see section 3.1.2).
[b] The time set by the instrument is accurate to 10^{-9} s.
[c] Spinning side band of peak at 49 ppm.
[d] CH_2 of ether.
[e] $Si(OMe)_2$.
[f] Si-OMe.
[g] Spinning side band of peak at -12 ppm.
[h] Methyl of ether.
[i] $Si(Me)_3$.
[j] $Si(Me)_2$.
[k] Si-Me.
[l] $Al(Me)_n$.

Table 3.20. Deconvolved peak integrals in ^{13}C CP-MAS variable-contact-time experiments on an ether washed $AlMe_3$/silica/cyclohexane sample corresponding to sample B in Figure 3.10.[a]

Contact time (ms)[b]	88 ppm[c]	68 ppm[d]	54 ppm[e]	49 ppm[f]	27 ppm[g]	14 ppm[h]	0 ppm[i]	-3 ppm[j]	-7 ppm[k]	-12 ppm[l]	-49ppm[g]
0.005	0.000	0.000	0.000	0.000	0.000	0.000	0.000	0.000	0.000	0.000	0.000
0.010	0.000	0.000	0.000	0.000	0.000	0.000	0.000	0.000	0.000	0.000	0.000
0.020	0.330	1.63	1.00	2.60	1.12	0.664	0.962	0.376	0.361	2.55	0.000
0.050	0.297	3.49	1.14	4.68	1.15	1.15	1.22	1.73	0.362	6.59	1.29
0.100	0.849	5.73	2.84	2.73	1.08	2.71	3.26	2.53	1.34	11.0	1.12
0.240	1.31	5.99	3.20	9.02	1.26	3.75	4.05	2.61	1.99	14.1	1.12
0.500	1.61	7.53	4.21	10.3	2.70	5.42	5.14	3.36	2.04	15.5	1.43
0.750	1.59	8.35	4.48	11.2	1.63	5.69	6.35	3.70	2.57	17.3	1.65
1.000	0.725	8.46	4.14	12.9	1.55	6.53	6.42	4.57	2.13	19.4	2.03
1.500	1.65	8.59	4.37	12.6	1.72	7.46	6.79	4.65	3.18	20.1	2.21
2.000	1.72	8.16	4.30	12.2	1.57	7.33	6.91	4.51	3.09	20.0	2.05
2.500	1.17	7.72	4.09	12.4	1.94	6.95	6.24	4.28	2.62	21.5	2.35
3.000	1.59	7.84	3.62	13.0	1.97	7.36	6.67	4.41	2.91	22.1	1.88
5.000	1.45	6.54	3.80	11.9	1.56	6.43	6.13	3.89	2.51	18.1	1.84
8.000	1.19	5.98	2.77	11.7	1.29	7.09	6.05	3.43	2.50	23.2	2.07
10.000	1.19	5.54	2.79	11.3	1.19	6.59	5.64	3.35	2.14	21.9	1.51
15.000	1.15	4.86	2.77	9.70	0.888	5.86	5.13	2.59	1.14	19.8	2.14

[a] Estimated relative standard deviation, 5% for peaks at 49 ppm, 0 ppm and –12 ppm (strong signals), 10% for the rest (weak signals) (see section 3.1.2).
[b] The time set by the instrument is accurate to 10^{-9} s.
[c] Spinning side band of peak at 49 ppm.
[d] CH_2 of ether.
[e] $Si(OMe)_2$.
[f] Si-OMe.
[g] Spinning side band of peak at -13 ppm.
[h] Me- of ether.
[i] $Si(Me)_3$.
[j] $Si(Me)_2$.
[k] Si-Me.
[l] $Al(Me)_n$.

Table 3.21. Relaxation times and corrections for ^{13}C CP-MAS experiments on an ether washed $AlMe_3$/silica/cyclohexane sample corresponding to sample B in Figure 3.10, based on analysis of data from Table 3.19 and Table 3.20 fitted to Eq. 3.15 and Eq. 3.16.

deconvolved ^{13}C signal		^{13}C-^{1}H cross-polarization dynamics time constant from variable-contact-time experiment			^{1}H T_1 from variable-recovery-time ^{13}C CP-MAS experiment		Total Correction
Peak position[a]	Peak Assign-ment	T^{CH} (ms)[b]	$T_{1\rho}$ (ms)[c]	M^{∞}/M(5 ms)[d]	T_1^H (s)[e]	M^0/M(3 s)[f]	M^*/M(5 ms, 3 s)[g]
-12ppm	$Al(Me)_n$	0.273 ±0.004	131 ±7	1.04	3.51±0.24	1.74	1.81
-7 ppm	Si-Me	0.522 ±0.160	15.8 ±5.0	1.42	3.73±0.44	1.81	2.57
-3 ppm	$Si(Me)_2$	0.349 ±0.067	20.9 ±4.0	1.29	3.61±0.51	1.77	2.29
0 ppm	$Si(Me)_3$	0.263 ±0.040	54.8 ±16.7	1.10	2.84±0.22	1.53	1.69
49 ppm	Si-O-Me	0.215 ±0.011	66.1 ±7.5	1.08	2.59±0.11	1.46	1.58
54 ppm	$Si(OMe)_2$	0.132 ±0.039	24.7 ±8.1	1.23	3.92±0.41	1.87	2.30
Ether peaks presented on the surface							
14 ppm	Me-	0.380 ±0.049	76.7 ±28.9	1.07	3.23±0.13	1.65	1.77
68 ppm	$-CH_2-$	0.118 ±0.012	24.8 ±3.06	1.23	2.93±0.16	1.56	1.92

[a] Corresponding to sample B of Figure 3.10.
[b] T^{CH} measured in variable contact time ^{13}C CP-MAS experiment, derived from Table 3.20.
[c] $T_{1\rho}$ measured in variable contact time ^{13}C CP-MAS experiment, derived from Table 3.20.
[d] M^{∞}, maximum magnetization during cross polarization period. M^{∞}/M(5 ms), magnetization correction for cross polarization period of 5 ms. Estimated relative standard error, 4.2% for peaks at 49 ppm, 0 ppm and –12 ppm (strong signals), 8.5% for the rest (weak signals) (see section 3.3.5).
[e] T_1^H measured in saturation recovery experiment, derived from Table 3.19.
[f] M^0, maximum magnetization when ^{1}H spins are fully relaxed. M^0/M(3 s), magnetization correction for T_1 relaxation, 3 s used as recovery time. Estimated relative standard error, 4.2% for peaks at 49 ppm, 0 ppm and –12 ppm (strong signals), 8.5% for the rest (weak signals) (see section 3.3.5).
[g] M^*, theoretical maximum magnetization. M^*/M(5 ms, 3 s), magnetization correction for signal obtained at 5 ms contact time and 3 s recovery time. Estimated relative standard error, 6% for peaks at 49 ppm, 0 ppm and –12 ppm (strong signals), 12% for the rest (weak signals) (see section 3.3.5).

Table 3.22. Comparison of ^{1}H T_1 values (s) in different $AlMe_3$/silica samples.

Samples	^{13}C CP-MAS deconvolved peaks and T_1 (s)[a]					
	54 ppm $Si(OMe)_2$	49 ppm Si-O-Me	0 ppm $Si(Me)_3$	-3 ppm $Si(Me)_2$	-7 ppm Si-Me	-12 ppm $Al(Me)_n$
Tol-A[b]	4.44±0.64	4.89±0.14	3.27±0.58	3.22±0.52	5.89±0.51	4.91±0.27
Tol-B[c]	2.98±0.40	3.95±0.18	3.96±0.11	3.37±0.28	6.04±0.90	4.02±0.18
Cyc-A[d]	6.71±2.23	6.04±0.23	5.59±0.31	6.58±0.60	6.22±2.48	7.24±0.03
Cyc-B[e]	3.92±0.41	2.59±0.11	2.84±0.22	3.61±0.51	3.73±0.44	3.51±0.24

[a.] Error given is the standard error given by Origin 6.1 as part of the curve fitting process.
[b.] Dry sample in $AlMe_3$/silica/toluene reaction system, which corresponds to sample A in Figure 3.9.
[c.] Ether washed sample in $AlMe_3$/silica/toluene reaction system, which is corresponds to sample B in Figure 3.9.
[d.] Dry sample in $AlMe_3$/silica/cyclohexane reaction system, which is corresponding to sample A in Figure 3.10.
[e.] Ether washed sample in $AlMe_3$/silica/cyclohexane reaction system, which corresponds to sample B in Figure 3.10.

Table 3.23. Comparison of relaxation corrections for the peak at 49 ppm in four different $AlMe_3$/silica samples.

Signal at 49 ppm	T_1 (s) [a]	T^{CH} (ms) [a]	$T_{1\rho}$ (ms) [a]	Total correction [b]
Sample A in toluene reaction	4.89±0.14	0.286±0.012	41.8±16.2	2.47±0.15
Sample A in cyclohexane reaction	6.04±0.23	0.400±0.039	53.2±11.6	2.83±0.17
Sample B in toluene reaction	3.95±0.18	0.124±0.005	51.7±3.28	2.08±0.13
Sample B in cyclohexane reaction	2.59±0.11	0.215±0.011	66.1±7.5	1.58±0.09

[a.] Error given is the standard error calculated by Origin 6.1 as part of the curve fitting process.
[b.] Total correction is the ratio of magnetization observed at given recovery time and contact time to the magnetization that would achieved with full spin-lattice relaxation and if $(T^{CH})^{-1}$ and proton $T_{1\rho}$ were both infinite (see section 3.3.5).

Table 3.24. Comparison of relaxation corrections for the peak at -12 ppm in four different $AlMe_3$/silica samples.

Signal at -12 ppm	T_1 (s)[a]	T^{CH} (ms) [a]	$T_{1\rho}$ (ms) [a]	Total correction [b]
Sample A in toluene reaction	4.91±0.27	0.207±0.027	73.2±23.3	2.22±0.13
Sample A in cyclohexane reaction	7.24±0.03	0.613±0.004	210±12	3.03±0.18
Sample B in toluene reaction	4.02±0.18	0.192±0.002	45.4±0.5	2.13±0.13
Sample B in cyclohexane reaction	3.51±0.24	0.273±0.004	131±7	1.81±0.12

[a.] Error given is the standard error calculated by Origin 6.1 as part of the curve fitting process.
[b.] Total correction is the ratio of magnetization observed at given recovery time and contact time to the magnetization that would achieved with full spin-lattice relaxation and if $(T^{CH})^{-1}$ and proton $T_{1\rho}$ were both infinite (see section 3.3.5).

Table 3.25. Peak integrals in the ^{13}C CP/MAS-detected ^{1}H-inversion-recovery experiment on HMB.[a]

Recovery Time (s)[b]	200 ppm[c]	166 ppm[c]	132 ppm	97 ppm[c]	64 ppm[c]	51 ppm[d]	30 ppm[c]	16 ppm	-4 ppm[c]	-18 ppm[d]
0.001	-0.0159	-0.272	-1.46	-0.586	-0.337	-0.499	0.0150	-5.88	-0.0705	-0.0199
0.002	-0.0242	-0.290	-1.45	-0.593	-0.363	-0.527	0.00164	-5.89	-0.115	-0.0302
0.005	-0.0276	-0.292	-1.48	-0.628	-0.364	-0.540	0.0282	-5.86	-0.115	-0.0346
0.008	-0.00602	-0.249	-1.41	-0.560	-0.326	-0.492	0.0783	-5.63	-0.0982	-0.00752
0.010	-0.0119	-0.270	-1.44	-0.596	-0.366	-0.496	0.0715	-5.65	-0.107	-0.0149
0.020	-0.00370	-0.292	-1.46	-0.605	-0.353	-0.503	0.0525	-5.46	-0.141	-0.00463
0.050	-0.00370	-0.221	-1.27	-0.526	-0.296	-0.438	0.0903	-4.80	-0.0983	-0.00463
0.080	-0.0195	-0.243	-1.22	-0.551	-0.314	-0.458	0.0332	-4.38	-0.112	-0.0243
0.100	0.00127	-0.176	-1.00	-0.392	-0.209	-0.308	0.0172	-3.95	-0.0591	0.00159
0.200	-0.0115	-0.145	-0.626	-0.257	-0.152	-0.240	0.0455	-2.31	-0.0853	-0.0144
0.500	0.00758	0.0664	0.395	0.236	0.119	0.173	0.0135	1.38	0.0438	0.00948
0.800	0.0112	0.191	0.995	0.467	0.269	0.358	0.0370	3.66	0.0904	0.0140
1.000	0.0122	0.229	1.26	0.597	0.330	0.437	0.0269	4.66	0.103	0.0152
2.000	0.0260	0.360	1.85	0.862	0.486	0.645	0.0221	6.82	0.158	0.0325
3.000	0.0139	0.212	1.13	0.541	0.301	0.403	0.0249	4.13	0.0987	0.0178
5.000	0.0136	0.387	1.97	0.891	0.499	0.699	0.0291	7.33	0.163	0.0170
10.000	0.00662	0.372	1.98	0.886	0.505	0.686	0.0248	7.32	0.158	0.00828

[a.] Estimated relative standard deviation, 10% for peaks at -18 ppm, 30 ppm and 200 ppm (weak signals), 5% for the rest (strong signals) (see section 3.1.2).
[b.] The time set by the instrument is accurate to 10^{-9} sec.
[c.] Spinning sideband of the peak at 132 ppm, which belongs to the aromatic carbon of HMB.
[d.] Spinning sideband of the peak at 16 ppm, which belongs to the methyl carbon of HMB.

Table 3.26. Peak integrals in the variable-contact-time ^{13}C CP-MAS experiment on HMB.[a]

Contact time (ms)[b]	200 ppmc	166 ppmc	132 ppm	97 ppm[c]	64 ppm[c]	51 ppm[d]	30 ppm[c]	15 ppm	-4 ppm[c]	-18 ppm[d]
0.005	0.0301	0.00689	0.0260	0.00794	0.00813	0.000754	0.00204	0.147	0.00924	0.00165
0.010	0.118	0.0415	0.0155	0.0273	0.00375	0.0107	0.00723	0.0674	0.0182	0.00968
0.015	0.0595	0.0121	0.00904	0.0095	0.0341	0.0216	0.0102	0.216	0.0152	0.0122
0.020	0.00466	0.0466	0.0586	0.0366	0.0175	0.00266	0.00246	0.303	0.00812	0.00271
0.030	0.102	0.0858	0.0901	0.0471	0.0534	0.0158	0.00894	0.603	0.00444	0.00527
0.050	0.109	0.132	0.103	0.0459	0.0439	0.0235	0.0286	1.05	0.00839	0.0170
0.070	0.0210	0.154	0.126	0.0633	0.0783	0.0357	0.0168	1.54	0.00431	0.00435
0.080	0.00514	0.150	0.0740	0.0636	0.0857	0.0277	0.005	1.71	0.00643	0.0202
0.100	0.0201	0.205	0.157	0.107	0.106	0.0374	0.0096	2.17	0.0132	0.0147
0.120	0.0623	0.238	0.150	0.107	0.124	0.0277	0.0365	2.61	0.0215	0.0182
0.240	0.0598	0.484	0.276	0.145	0.151	0.0864	0.0693	4.34	0.0348	0.0203
0.360	0.00535	0.677	0.386	0.228	0.261	0.109	0.0595	5.23	0.0389	0.0222
0.540	0.00579	0.893	0.508	0.245	0.322	0.0609	0.0885	5.41	0.0268	0.0103
0.640	0.164	1.10	0.577	0.322	0.415	0.110	0.109	5.28	0.0340	0.0138
0.750	0.107	1.14	0.660	0.381	0.454	0.0527	0.0917	5.44	0.0323	0.0321
0.900	0.215	1.31	0.729	0.389	0.472	0.0845	0.122	5.67	0.0510	0.0257
1.000	0.172	1.31	0.708	0.394	0.489	0.0943	0.127	5.62	0.0592	0.0121
1.200	0.157	1.43	0.749	0.400	0.522	0.0622	0.140	5.92	0.0524	0.0159
1.500	0.233	1.57	0.829	0.452	0.569	0.0600	0.151	6.18	0.0683	0.00743
2.000	0.233	1.68	0.884	0.506	0.634	0.0968	0.150	6.61	0.0867	0.0408
3.000	0.417	1.96	0.985	0.569	0.723	0.0902	0.178	7.10	0.100	0.0223
5.000	0.477	2.27	1.08	0.639	0.824	0.0698	0.245	7.74	0.0643	0.0223
8.000	0.498	2.52	1.13	0.678	0.849	0.0159	0.251	8.13	0.0437	0.0157
10.000	0.582	2.62	1.23	0.720	0.938	0.0447	0.299	8.38	0.0728	0.0245
15.000	0.362	2.63	1.19	0.696	0.890	0.0444	0.231	8.39	0.0700	0.00248
20.000	0.544	2.70	1.29	0.735	0.978	0.0108	0.225	8.38	0.127	0.0435
30.000	0.468	2.67	1.27	0.704	0.895	0.0201	0.147	8.09	0.130	0.0486
40.000	0.0870	2.42	1.12	0.663	0.838	0.0319	0.129	7.55	0.137	0.0294
50.000	0.0278	2.20	1.09	0.578	0.758	0.0484	0.0396	7.06	0.170	0.0904
60.000	0.112	2.03	1.06	0.545	0.711	0.0371	0.0144	6.58	0.220	0.0643
70.000	0.263	1.78	0.974	0.475	0.621	0.0692	0.0445	6.01	0.180	0.0747
80.000	0.242	1.72	0.942	0.499	0.622	0.0191	0.0137	5.70	0.166	0.0664

[a] Estimated relative standard deviation, 10% for peaks at -18 ppm, 30 ppm and 200 ppm (weak signals), 5% for the rest (strong signals) (see section 3.1.2).
[b] The time set by the instrument is accurate to 10^{-9} sec.

[c.] Spinning sideband of the peak at 132 ppm, which belongs to the aromatic carbon of HMB.
[d.] Spinning sideband of the peak at 16 ppm, which belongs to the methyl carbon of HMB.

Table 3.27. ^{13}C CP-MAS spin-counting results (Me groups on the surface) of dry $AlMe_3$/silica/toluene product from six different runs corresponding to sample A in Figure 3.38.

		Exp. I-A			Exp. II-A			Exp. III-A			Exp. IV-A			Exp. V-A			Exp. VI-A		
Peak position[a]	Peak Assign-ment	Integral[b]	Corr. Integral[c]	C (mmol)[d]	Integral[b]	Corr. Integral[c]	C (mmol)[d]	Integral[b]	Corr. Integral[c]	C (mmol)[d]	Integral[b]	Corr. Integral[c]	C (mmol)[d]	Integral[b]	Corr. Integral[c]	C (mmol)[d]	Integral[b]	Corr. Integral[c]	C (mmol)[d]
-12 ppm	$Al(Me)_n$	94.1	208.8	1.64	128.5	285.1	1.61	151.7	336.6	1.94	129.7	287.8	1.56	143.2	317.6	1.78	163.9	363.6	1.99
-7 ppm	Si-Me	4.73	15.6	0.123	2.59	8.57	0.0484	3.54	11.7	0.0675	7.60	25.1	0.136	4.15	13.7	0.0771	1.61	5.33	0.0292
-3 ppm	$Si(Me)_2$	7.13	13.1	0.103	21.3	39.1	0.221	5.78	10.6	0.0613	12.7	23.3	0.126	12.2	22.4	0.126	11.7	21.6	0.118
0 ppm	Al-Me	12.6	23.6	0.185	25.0	46.8	0.264	23.0	43.0	0.248	25.4	47.5	0.257	15.8	29.5	0.166	14.2	26.6	0.146
15 ppm	SSB[e]	0.756	1.87	0.0147	0.00	0.00	0.00	0.00	0.00	0.00	0.00	0.00	0.00	0.00	0.00	0.00	0.00	0.00	0.00
49 ppm	-Si-O-Me	15.6	38.6	0.303	22.1	54.7	0.309	8.73	21.6	0.125	18.3	45.2	0.245	26.8	66.4	0.373	4.64	11.5	0.0630
54 ppm	$-Si(OMe)_2$	3.55	8.33	0.0653	4.05	9.50	0.0537	0.00	0.00	0.00	0.00	0.00	0.00	4.15	9.73	0.05	0.00	0.00	0.00
88 ppm	SSB[e]	2.19	5.41	0.0424	2.08	5.15	0.0291	0.00	0.00	0.00	1.90	4.70	0.0255	3.65	9.03	0.05	0.00	0.00	0.00
Total non-toluene Me carbon detected				2.47			2.54			2.44			2.35			2.63			2.35
HMB as reference																			
16 ppm	methyl	7.70	8.6		29.7	33.1		29.1	32.5		30.9	34.5		29.8	33.3		30.6	34.1	

[a] Deconvolved ^{13}C CP-MAS signal.
[b] Deconvolved ^{13}C CP-MAS integral. Estimated relative standard deviation, 5% for peaks at 49 ppm, 0 ppm and -12 ppm (strong signals), 10% for the rest (weak signals) (see section 3.1.2).
[c] Calculated theoretical maximum magnetization from experimental integral, using M*/M(5 ms, 3 s), with correction for ^1H T_1 effects and CP dynamics (from Table 2.5). Estimated relative standard deviation, 6.0% for peaks at 49 ppm, 0 ppm and -12 ppm (strong signals), 12.0% for the rest (weak signals) (see section 3.3.5).
[d] Amount of carbon calculated according to the weighed amount of HMB, the external reference. Estimated relative standard deviation, 9.3% for peaks at 49 ppm, 0 ppm and -12 ppm (strong signals), 13.9% for the rest (weak signals) (see section 3.4).
[e] Spinning side band of peak at 49 ppm.
[f] Methyl carbon of HMB.
[g] Aromatic carbon of HMB.

142

Table 3.28. ^{13}C CP-MAS spin-counting results (Me groups on the surface) of dry $AlMe_3$/silica/cyclohexane products from six different runs corresponding to sample A in Figure 3.39.

		Exp. I-A			Exp. II-A			Exp. III-A			Exp. IV-A			Exp. V-A			Exp. VI-A		
Peak position[a]	Peak Assign-ment	Integral[b]	Corr. Integral[c]	C (mmol)[d]	Integral[b]	Corr. Integral[c]	C (mmol)[d]	Integral[b]	Corr. Integral[c]	C (mmol)[d]	Integral[b]	Corr. Integral[c]	C (mmol)[d]	Integral[b]	Corr. Integral[c]	C (mmol)[d]	Integral[b]	Corr. Integral[c]	C (mmol)[d]
-12 ppm	$Al(Me)_n$	156	472	2.59	177	535	3.10	180	544	3.17	158	479	2.81	165	499	2.92	117	355	2.07
-7 ppm	Si-Me	3.34	13.0	0.0710	3.51	13.7	0.0793	6.34	24.7	0.144	3.15	12.3	0.0723	1.16	4.53	0.0264	3.83	14.9	0.0873
-3 ppm	$Si(Me)_2$	18.5	57.8	0.318	5.81	18.2	0.106	11.3	35.5	0.207	14.5	45.3	0.266	12.6	39.5	0.231	19.3	60.6	0.355
0 ppm	$Si(Me)_3$	34.9	88.9	0.488	24.8	63.3	0.367	13.5	34.4	0.201	13.5	34.4	0.202	18.7	47.8	0.279	24.9	63.6	0.372
49 ppm	Si-O-Me	22.0	62.2	0.341	3.53	9.82	0.0571	2.52	7.14	0.0421	12.0	33.9	0.199	7.22	20.3	0.118	16.1	45.6	0.267
57 ppm	$Si(OMe)_2$	0.000	0.000	0.000	0.000	0.000	0.000	0.000	0.000	0.000	0.000	0.000	0.000	0.000	0.000	0.000	0.000	0.000	0.000
88 ppm	SSB[e]	2.26	6.40	0.0351	0.000	0.000	0.000	0.000	0.000	0.000	0.000	0.000	0.000	0.000	0.000	0.000	0.000	0.000	0.000
Total non-toluene Me carbon detected				3.85			3.71			3.76			3.55			3.57			3.16
HMB as reference																			
HMB-Me	methyl	11.0	12.3		28.9	32.3		28.8	32.1		28.6	31.9		28.7	32.0		28.7	32.0	

[a] Deconvolved ^{13}C CP-MAS signal.
[b] Deconvolved ^{13}C CP-MAS integral. Estimated relative standard deviation, 5% for peaks at 49 ppm, 0 ppm and -12 ppm (strong signals), 10% for the rest (weak signals) (see section 3.1.2).
[c] Calculated theoretical maximum magnetization from experimental integral, using M*/M(5 ms, 3 s), with correction for ^1H T_1 effects and CP dynamics (from Table 2.9). Estimated relative standard deviation, 6.0% for peaks at 49 ppm, 0 ppm and -12 ppm (strong signals), 12.0% for the rest (weak signals) (see section 3.3.5).
[d] Amount of carbon calculated according to the weighed amount of HMB, the external reference. Estimated relative standard deviation, 9.3% for peaks at 49 ppm, 0 ppm and -12 ppm (strong signals), 13.9% for the rest (weak signals) (see section 3.4).
[e] Spinning side band of peak at 49 ppm.
[f] Methyl carbon of HMB.
[g] Aromatic carbon of HMB.

Table 3.29. CH_4 generated in the $AlMe_3$/silica/toluene reactions represented in Table 3.27.

Experiment.	I	II	III	IV	V	VI
Silica gel (g)[a]	12.1	10.8	13.2	12.3	12.4	12.7
Si-OH (mmol)[b]	62.9	56.0	68.3	63.7	64.1	66.1
$AlMe_3$ (ml)	7.4	8.0	8.0	8.0	7.0	7.0
$AlMe_3$ (mmol) [c]	75.6	81.8	81.8	81.8	71.6	71.6
Me (mmol) [c]	226.9	245.3	245.3	245.3	214.7	214.7
Atmosphere Pressure (atm)	0.84	0.84	0.84	0.84	0.84	0.84
temperature (K)	292.5	292.5	292.5	292.5	293.5	293.5
trap #1 expanding factor (ml)[d]	62.3	62.3	62.3	62.3	62.6	62.6
trap #2 expanding factor (ml)[d]	34.6	34.6	34.6	34.6	34.8	34.8
during reaction CH_4 in trap #1 (mm)[e]	226	221	257	253	268	257
during reaction CH_4 in trap #1 (ml)	920	898	1055	1037	1102	1055
during reaction CH_4 in trap #1 (mmol)	32.2	31.4	36.9	36.3	38.4	36.8
during reaction CH_4 in trap #2 (mm)	10.0	9.0	10.0	11.0	9.0	10.0
during reaction CH_4 in trap #2 (ml)	8.9	4.5	8.9	13.2	4.3	8.7
during reaction CH_4 in trap #2 (mmol)	0.310	0.158	0.310	0.462	0.152	0.303
Total CH_4 collected (mmol)[f]	32.5	31.6	37.2	36.8	38.6	37.1

[a.] Weight of silica gel added to the reaction.
[b.] Number of silanol (OH) groups on the silica gel surface according to the ^1H-MAS spin-counting results.
[c.] The quantities were calculated based on the volume of $AlMe_3$ used. Estimated relative standard deviation, 5.7%.
[d.] The volume of N_2 to be excluded from the water displacement measurement due to gas expansion from 77.6 K to room temperature.
[e.] The volume measurement at room temperature (reading in terms of length of the measuring cylinder) of collected CH_4 gas during the reaction.
[f.] Relative standard deviation, 10% (see section 3.5.1).

Table 3.30. CH_4 generated in $AlMe_3$/silica/cyclohexane reactions represented in Table 3.28.

Experiment	I	II	III	IV	V	VI
Silica gel (g)[a]	11.4	13.0	11.1	12.0	12.5	12.6
Si-OH (mmol)[b]	59.3	67.3	57.6	62.3	64.9	65.4
Toluene (ml)	40.0	40.0	40.0	40.0	40.0	40.0
$AlMe_3$ (ml)	8.0	8.0	7.0	7.0	7.0	7.0
$AlMe_3$ (mmol) [c]	81.8	81.8	71.6	71.6	71.6	71.6
Me (mmol) [c]	245	245	215	215	215	215
Atmosphere Pressure (atm)	0.84	0.84	0.84	0.84	0.84	0.84
temperature (K)	292.5	292.5	293.5	293	293	293.5
trap #1 expanding volume (ml)[d]	62.3	62.3	62.6	62.5	62.5	62.6
trap #2 expanding volume (ml)[d]	34.6	34.6	34.8	34.7	34.7	34.8
during reaction CH_4 in trap #1 (mm)[e]	236	264	292	249	260.5	249
during reaction CH_4 in trap #1 (ml)	964	1085	1207	1020	1070	1020
during reaction CH_4 in trap #1 (mmol)	33.7	38.0	42.1	35.6	37.4	35.6
during reaction CH_4 in trap #2 (mm)	10.0	9.0	11.0	9.0	10.0	10.0
during reaction CH_4 in trap #2 (ml)	8.85	4.51	13.04	4.43	8.77	8.69
during reaction CH_4 in trap #2 (mmol)	0.310	0.158	0.455	0.155	0.306	0.303
Total CH_4 collected (mmol)[f]	34.0	38.1	42.5	35.8	37.7	35.9

[a.] Weight of silica gel added to the reaction.
[b.] Number of silanol (OH) groups on the silica gel surface according to the ^{1}H-MAS spin-counting results.
[c.] The quantities were calculated based on the volume of $AlMe_3$ used. Estimated relative standard deviation, 5.7%.
[d.] The volume of N_2 to be excluded from the water displacement measurement due to gas expansion from 77.6 K to room temperature.
[e.] The volume measurement at room temperature (reading in terms of length of the measuring cylinder) of collected CH_4 gas during the reaction.
[f.] Relative standard deviation, 10% (see section 3.5.1).

Table 3.31. Liquid-sample ^{13}C NMR inversion-recovery integrals derived from the spectra of Figure 3.34 (the supernatant solution of $AlMe_3$/silica/toluene reaction).

Recovery time (s)	^{13}C signal intensity for methyl in toluene[a]	^{13}C signal intensity for Al-Me[b]
0.250	-1570	-38.5
0.500	-1510	-34.8
1.000	-1370	-30.9
2.000	-1090	-24.0
4.000	-607	-10.3
8.000	144	9.63
16.000	1130	32.4
32.000	1990	58.7
64.000	1997	59.6

[a.] Estimated relative standard deviation, 5% (see section 3.1.2).
[b.] Estimated relative standard deviation, 5% (see section 3.1.2).

Table 3.32. Liquid-sample ^{13}C NMR inversion-recovery integrals derived from the spectra of Figure 3.36 (the supernatant solution of an $AlMe_3$/silica/cyclohexane reaction).

Recovery time (s)	^{13}C NMR intensity for CH_2 of cyclohexane[a]	^{13}C NMR intensity of Al-Me[b]
0.001	-4188	-66.7
0.100	-4135	-61.1
1.000	-3697	-47.7
10.000	-353	20.5
15.000	936	31.8
60.000	4958	97.0
120.000	5417	100

[a.] Estimated relative standard deviation, 5% (see section 3.1.2).
[b.] Estimated relative standard deviation, 5% (see section 3.1.2).

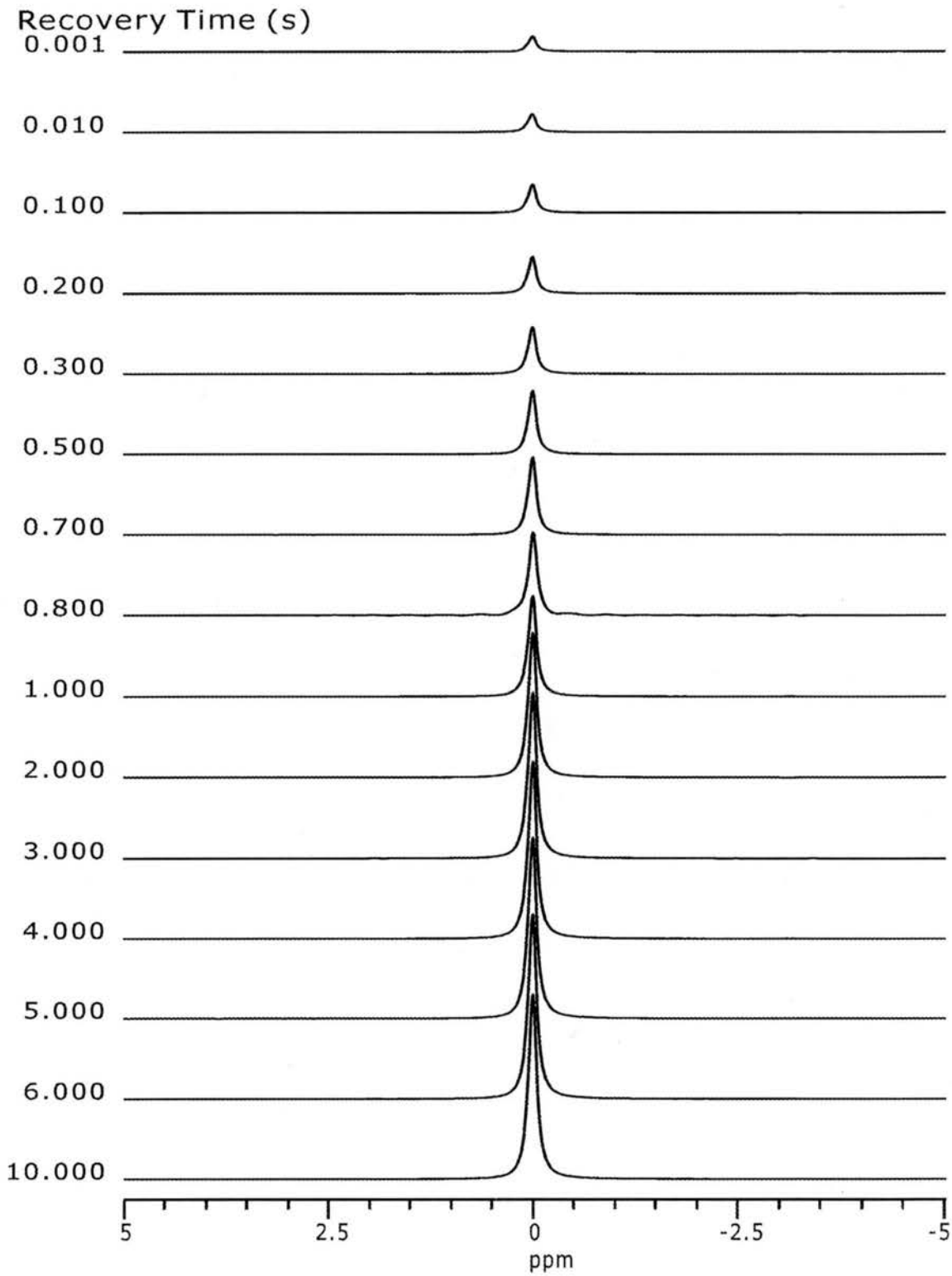

Figure 3.1. ^{1}H MAS saturation-recovery spectra of polydimethylsiloxane.

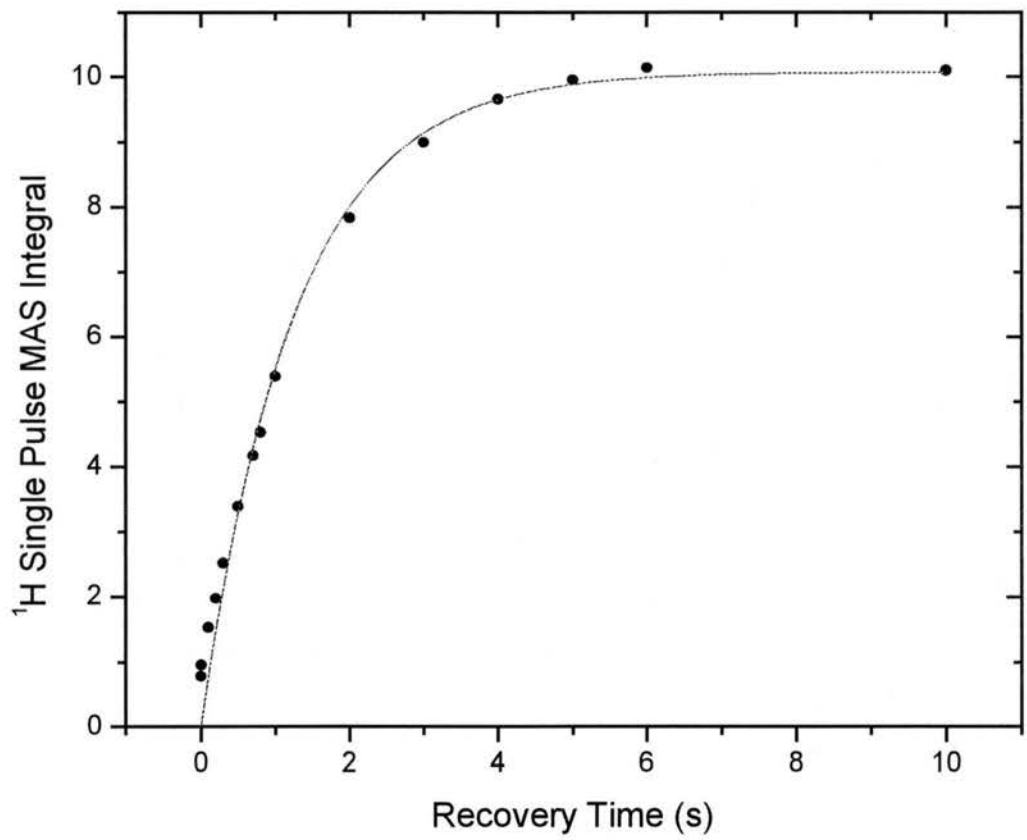

Figure 3.2. Fitting curve of ^{1}H MAS saturation-recovery results for the methyl group in polydimethylsiloxane (PDMS) based on Eq. 3.10.

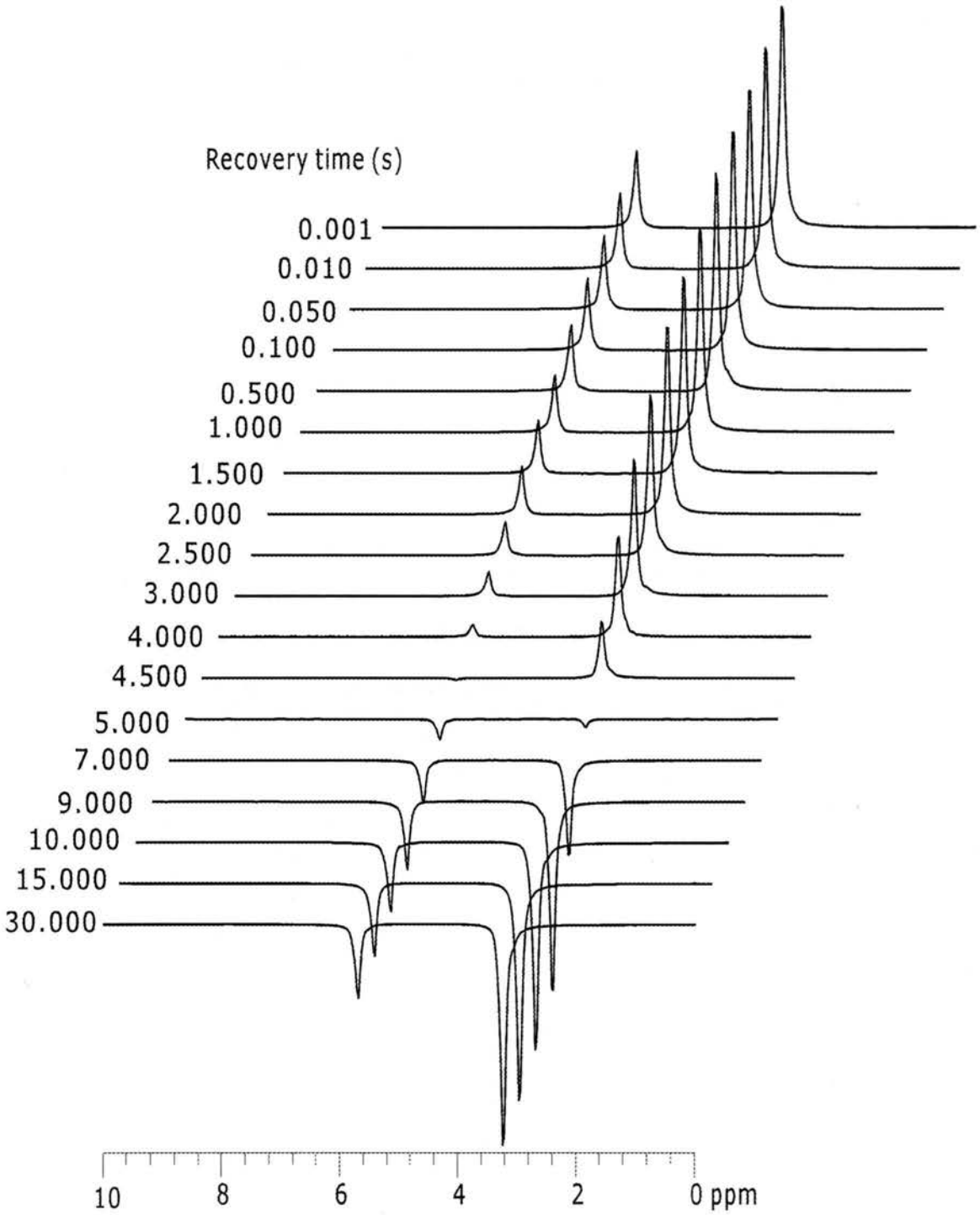

Figure 3.3. ^{1}H MAS inversion-recovery spectra of 1,3,5-trimethoxybenzene.

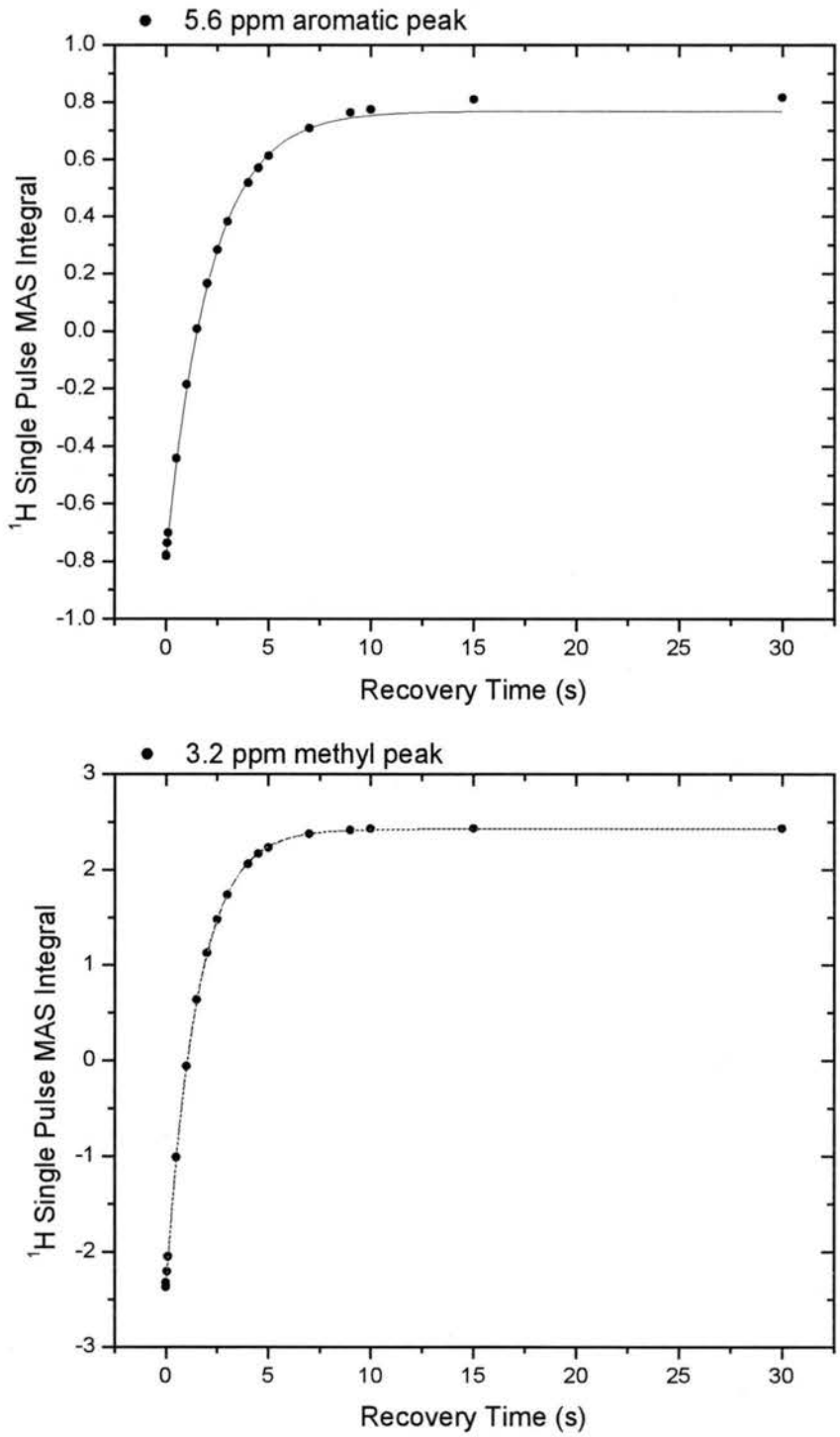

Figure 3.4. Fitting curves of ^{1}H MAS inversion-recovery results for 1,3,5-trimethoxybenzene based on the Eq. 3.11.

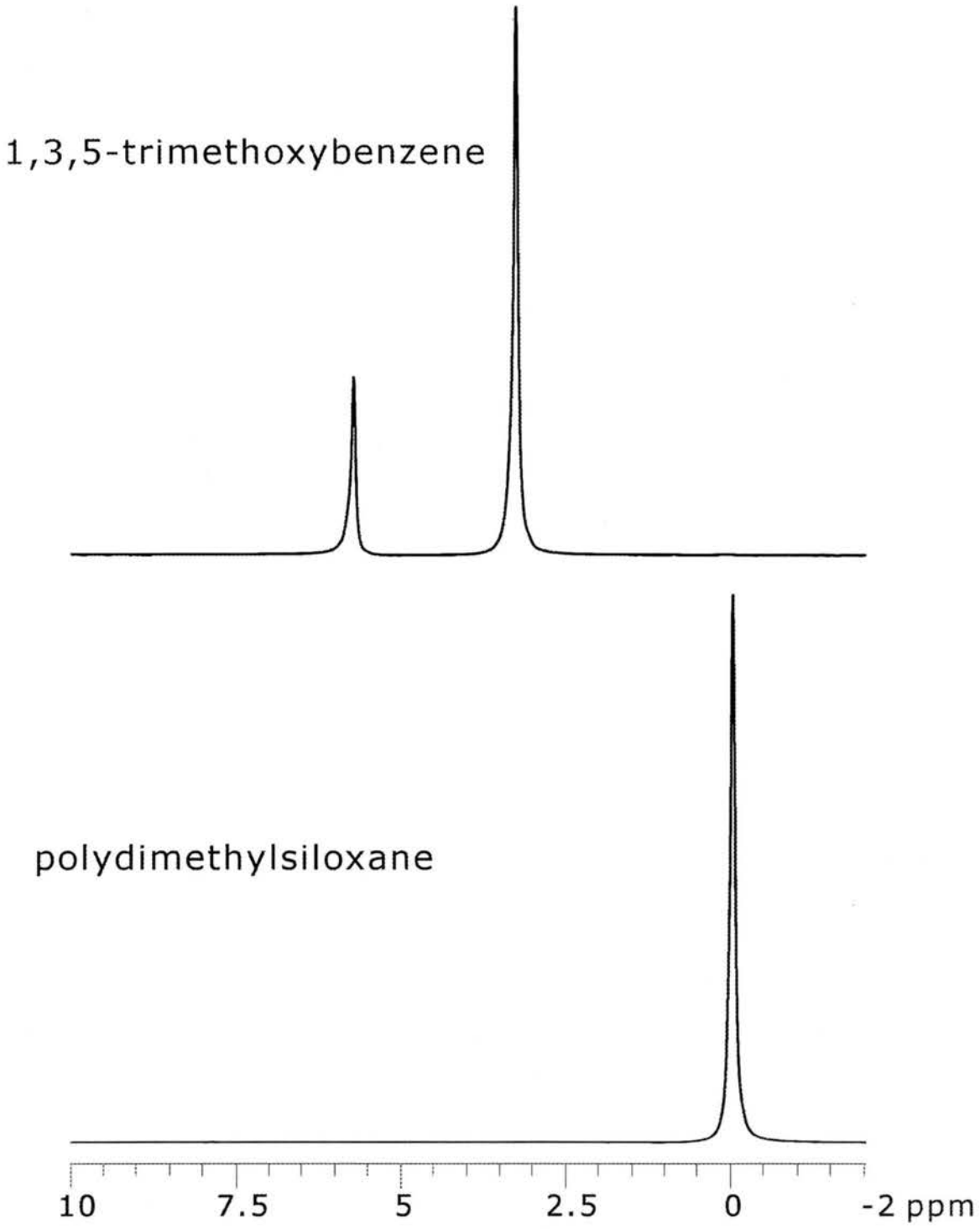

Figure 3.5. ^{1}H MAS spectra of 1,3,5-trimethoxybenzene and polydimethylsiloxane. MAS speed, 12.5 kHz.

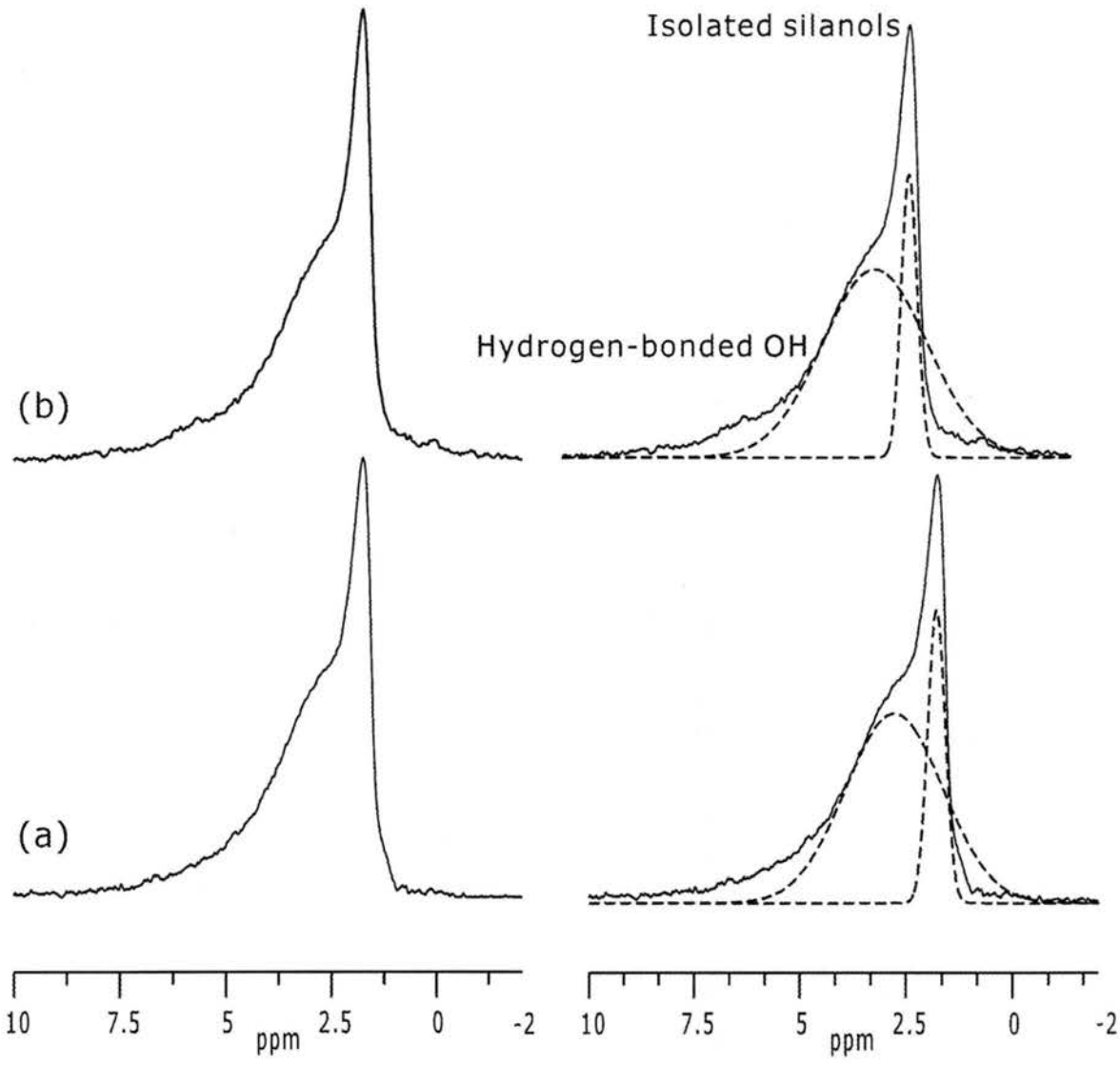

Figure 3.6. 360 MHz ^{1}H MAS spectra of silica gel dried at $5x10^{-3}$ torr and (a) 100 °C and (b) 150 °C silica gel, obtained with a 4 μs ^{1}H 90° pulse and a 12.5 kHz spinning speed, with 64 acquisitions.

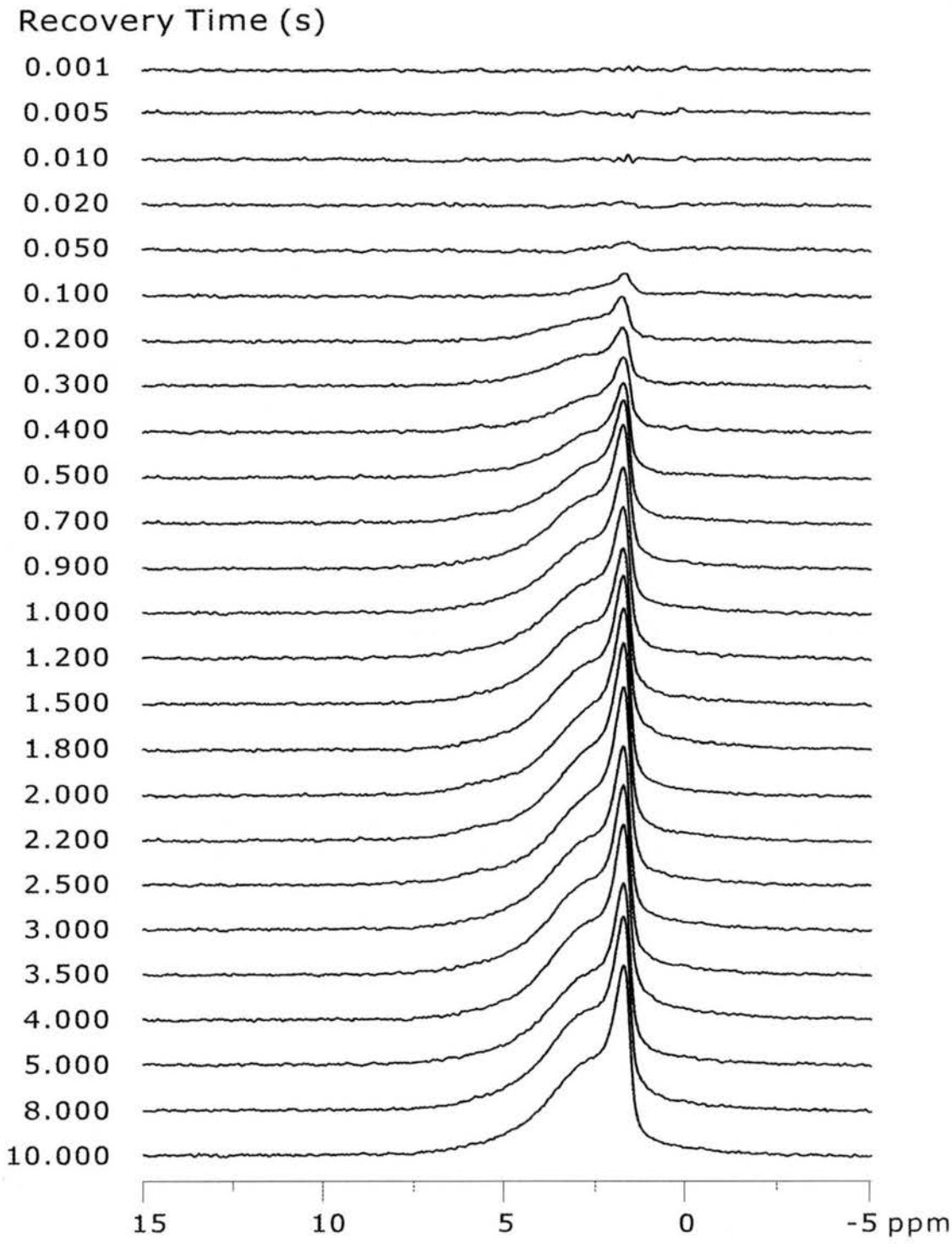

Figure 3.7. ^{1}H MAS saturation-recovery spectra of silica gel dried at 150 °C.

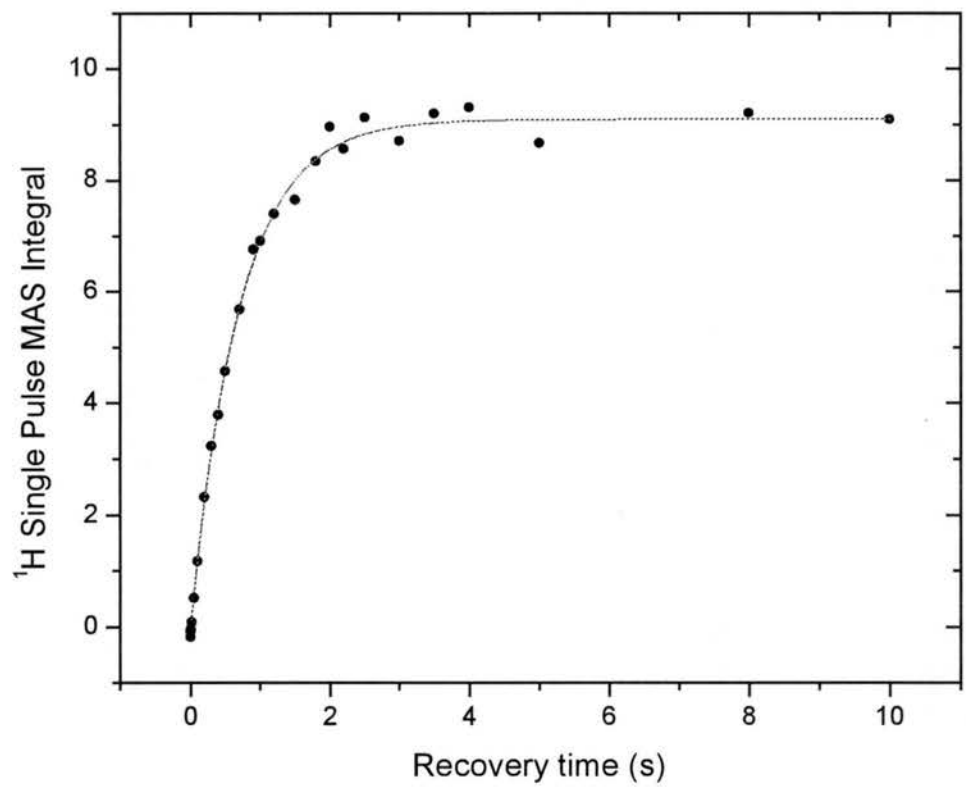

Figure 3.8. Fitting curve of ^{1}H MAS saturation-recovery results on silica gel dried at 150 °C based on the Eq. 3.10. Integral from 10 ppm to 1 ppm, including all types of silanols.

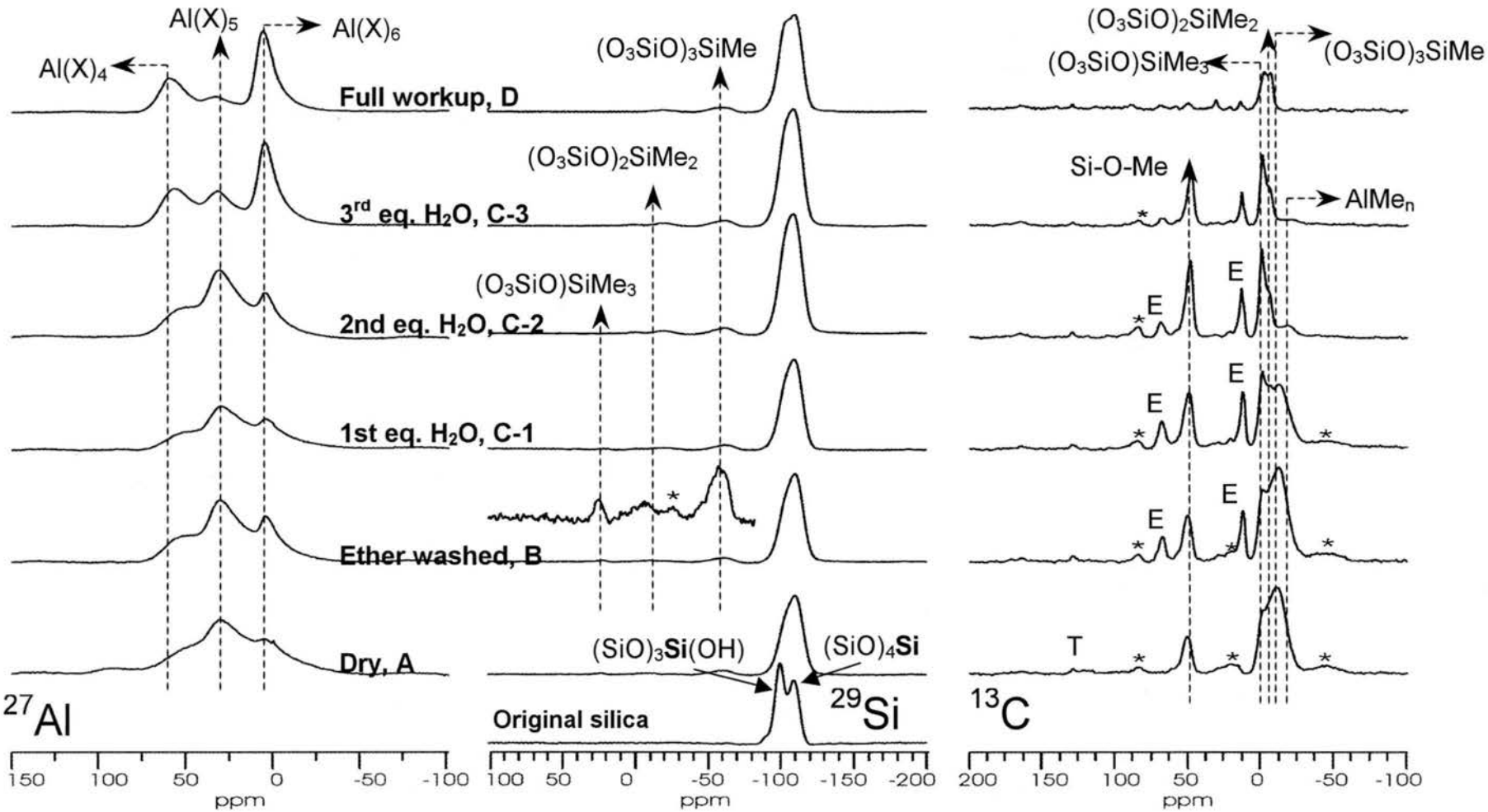

Figure 3.9. Composite of ^{27}Al, ^{29}Si and ^{13}C NMR spectra of $AlMe_3$/silica/toluene reaction samples. The preparation of the sample is described in Section 2.1. The conditions under which ^{27}Al, ^{29}Si and ^{13}C NMR spectra were obtained are described in section 2.6 (^{27}Al), section 2.5 (^{29}Si) and section 2.7 (^{13}C).

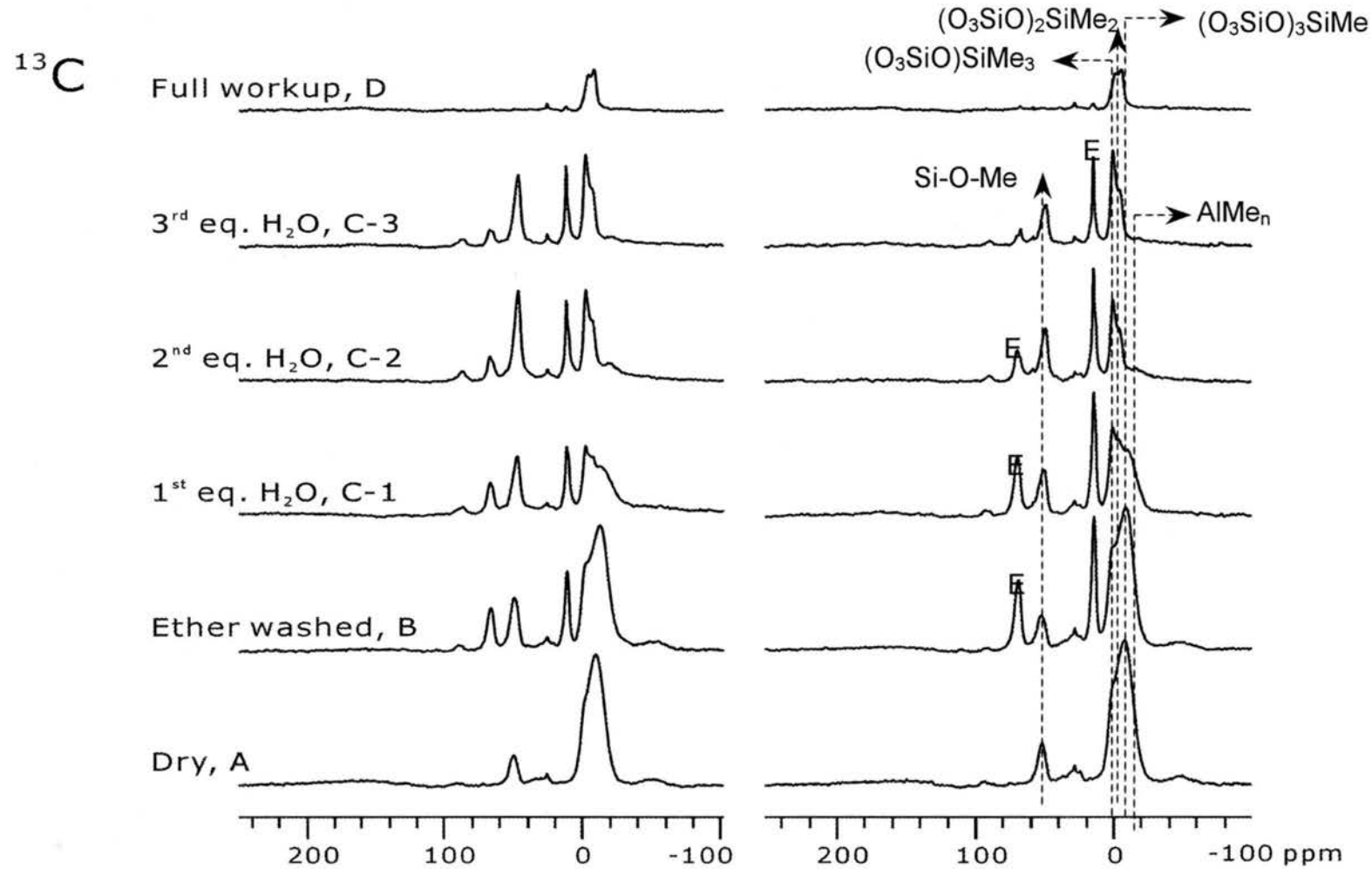

Figure 3.10. ^{13}C NMR spectra of two different runs of $AlMe_3$/silica/cyclohexane reaction samples. The preparation of the sample is described in Section 2.1. The conditions under which the ^{13}C NMR spectra were obtained are described in section 2.6 (^{13}C).

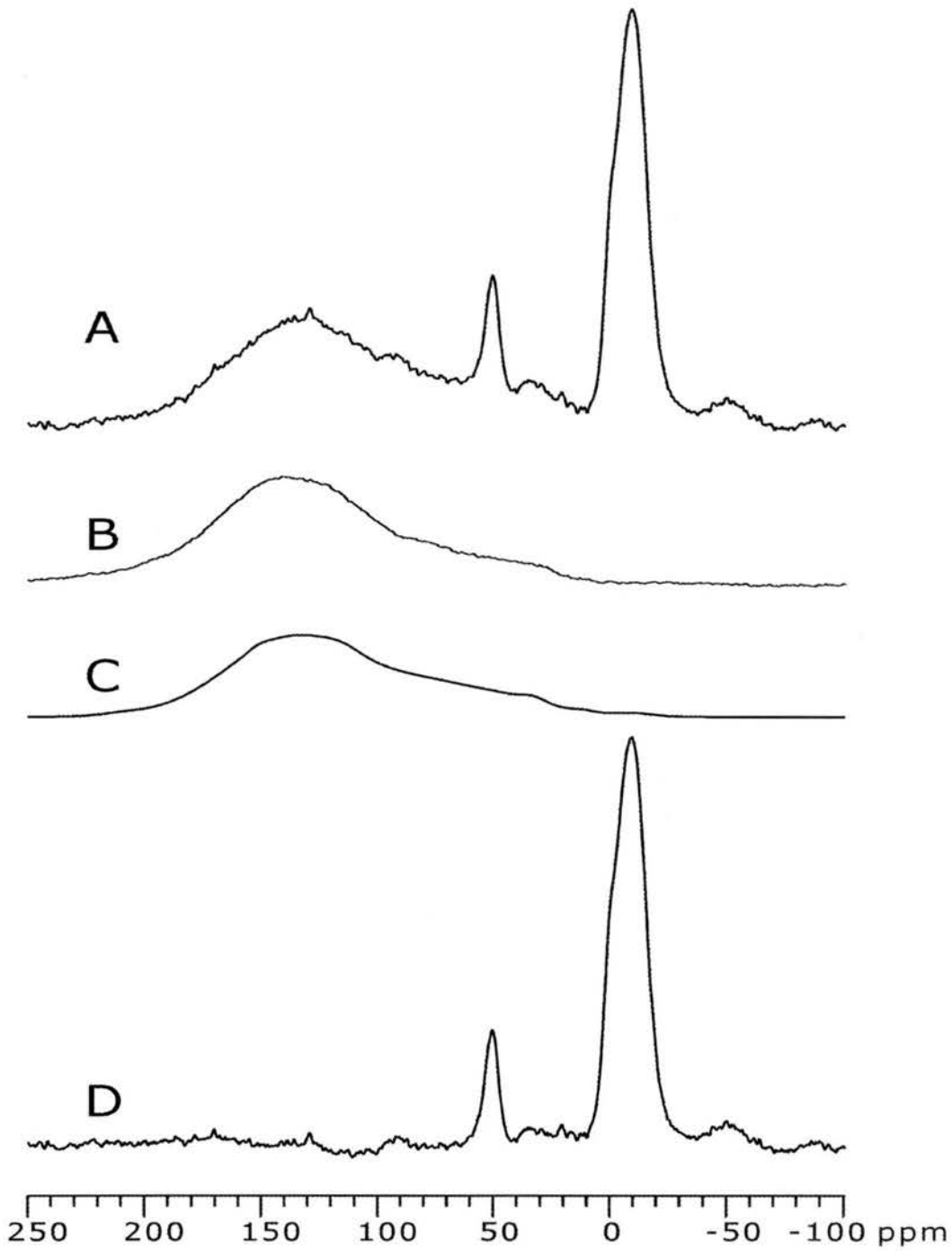

Figure 3.11. ^{13}C NMR spectra of dry $AlMe_3$/silica/toluene sample: (A) original acquired spectrum; (B) background spectrum; (C) computer simulated noise-free background spectrum; (D) spectrum obtained by subtraction of the background spectrum of B from A. ^{13}C spectrum was obtained with the following conditions: ^1H 90° pulse, 5.0 us; CP contact time, 5 ms; ^1H decoupling 45 kHz, 3 s repetition delay; 3.6 kHz spinning speed; and 10000 scans for (A), 100000 repetitions for (B).

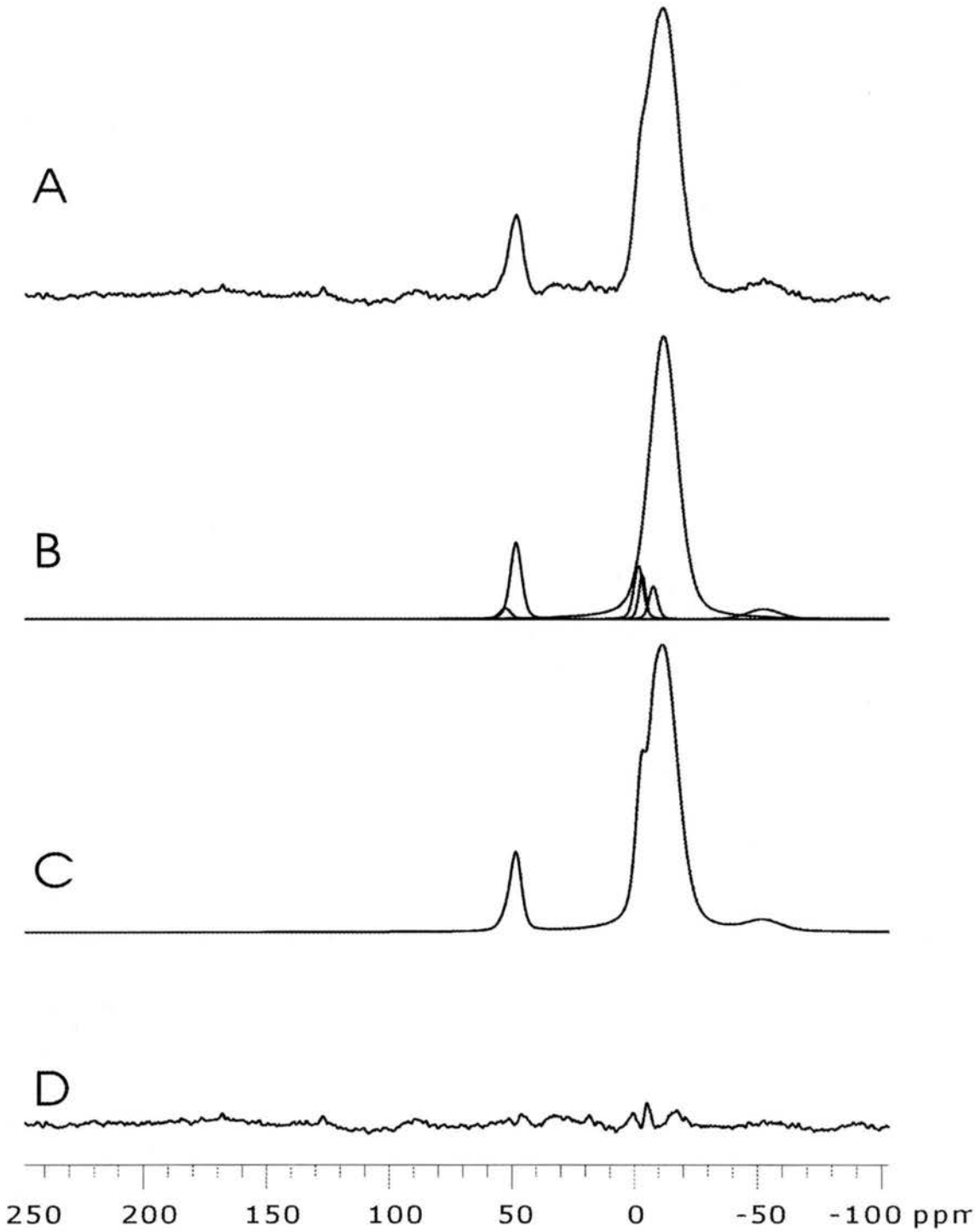

Figure 3.12. ^{13}C spectrum of dry $AlMe_3$/silica/toluene reaction sample: (A) the background-free spectrum; (B) deconvolution of spectrum A, with individual peaks shown; (C) the sum of all the deconvolved peaks, a simulated spectrum of A; (D) the residual of C subtracted from A. ^{13}C spectrum was obtained with the following conditions: ^{1}H 90° pulse, 5.0 us; CP contact time, 5 ms; ^{1}H decoupling 45 kHz, 3 s repetition delay; 3.6 kHz spinning speed; and 10000 repetitions.

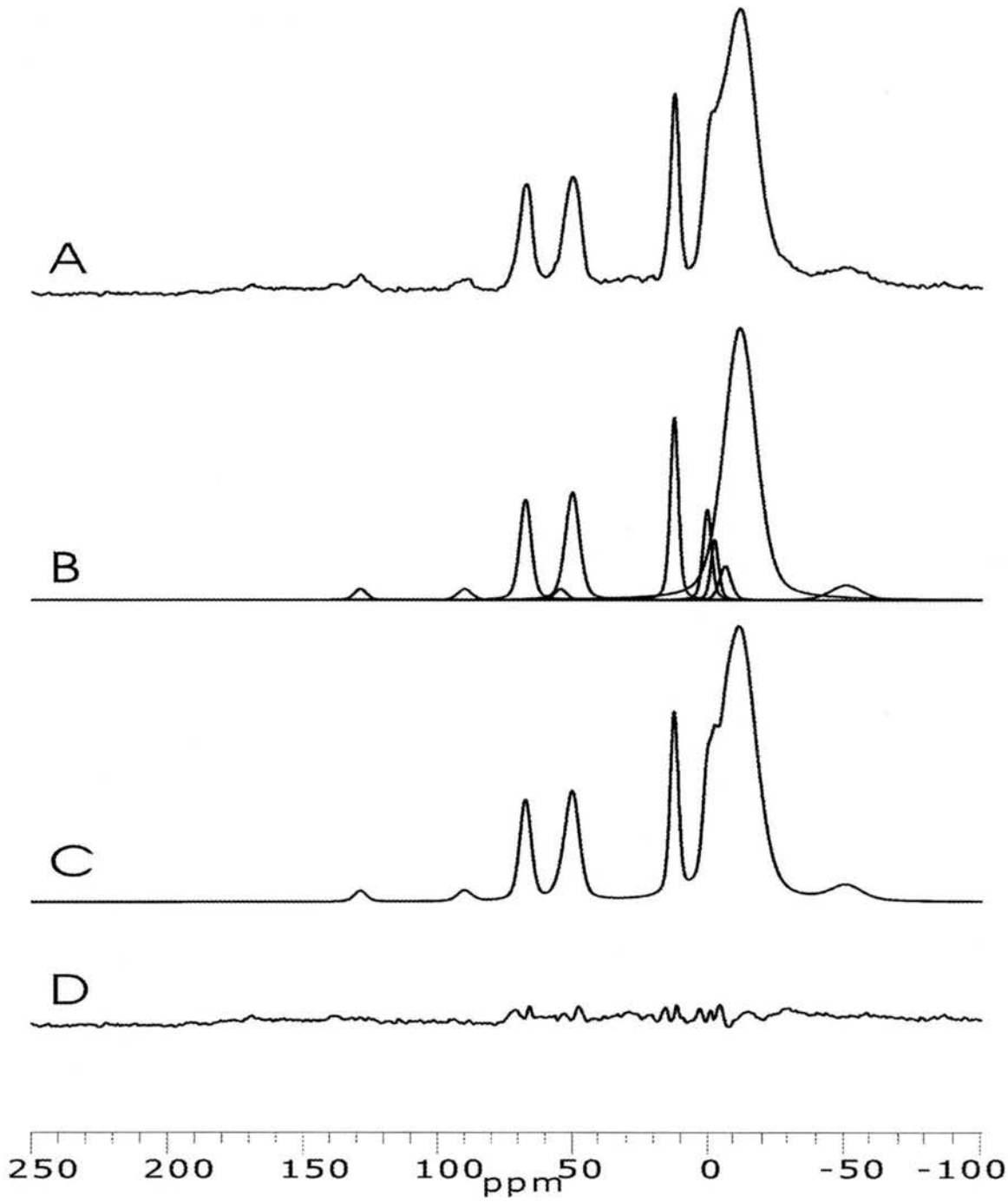

Figure 3.13. ^{13}C spectrum of ether washed $AlMe_3$/silica/toluene sample: (A) the background-free spectrum; (B) deconvolution of spectrum A with individual peaks shown; (C) the sum of all the deconvolved peaks, a simulated spectrum of A; (D) the residual of C subtracted from A. ^{13}C spectrum was obtained with the following conditions: ^{1}H 90° pulse, 5.0 us; CP contact time, 5 ms; ^{1}H decoupling 45 kHz, 3 s repetition delay; 3.6 kHz spinning speed; and 10000 repetitions.

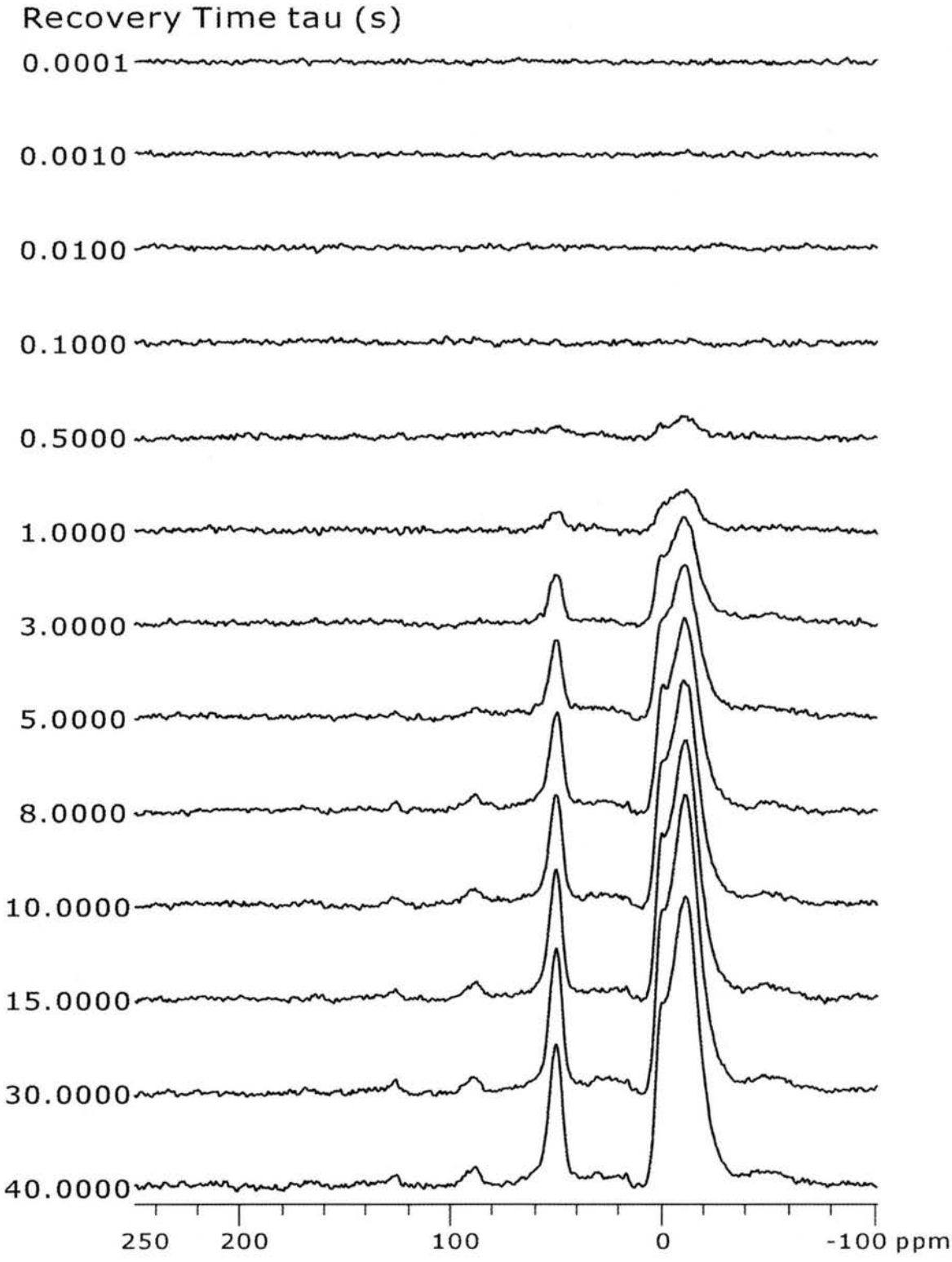

Figure 3.14. ^{13}C CP/MAS-detected ^{1}H-saturation-recovery spectra of dry $AlMe_3$/silica/toluene sample corresponding to sample A in Figure 3.9. Each spectrum is the result of 3000 repetitions.

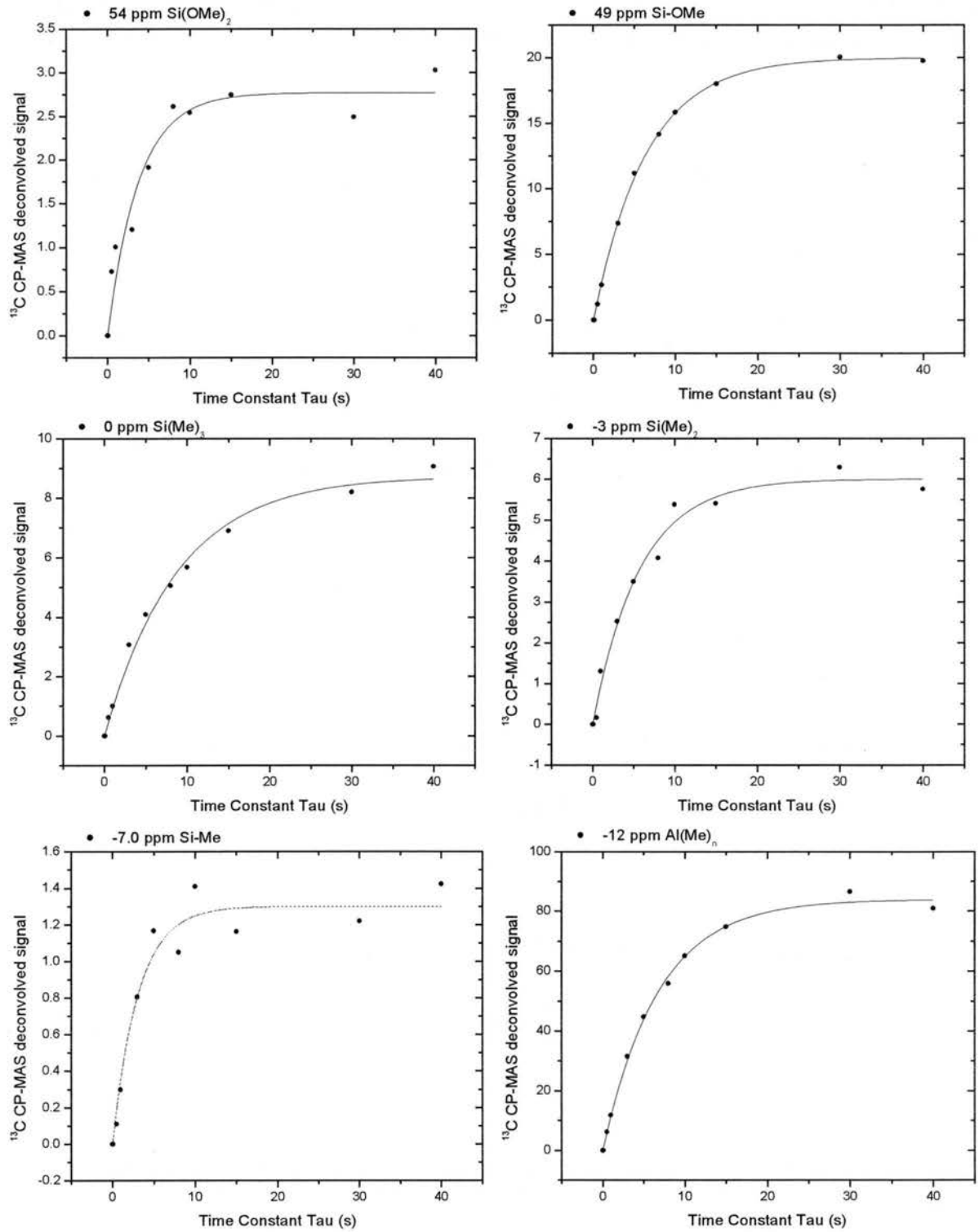

Figure 3.15. Fitting curves of ^{13}C CP/MAS-detected ^{1}H-saturation-recovery results for dry $AlMe_3$/silica/toluene sample corresponding to sample A in Figure 3.9, based on Eq. 3.15.

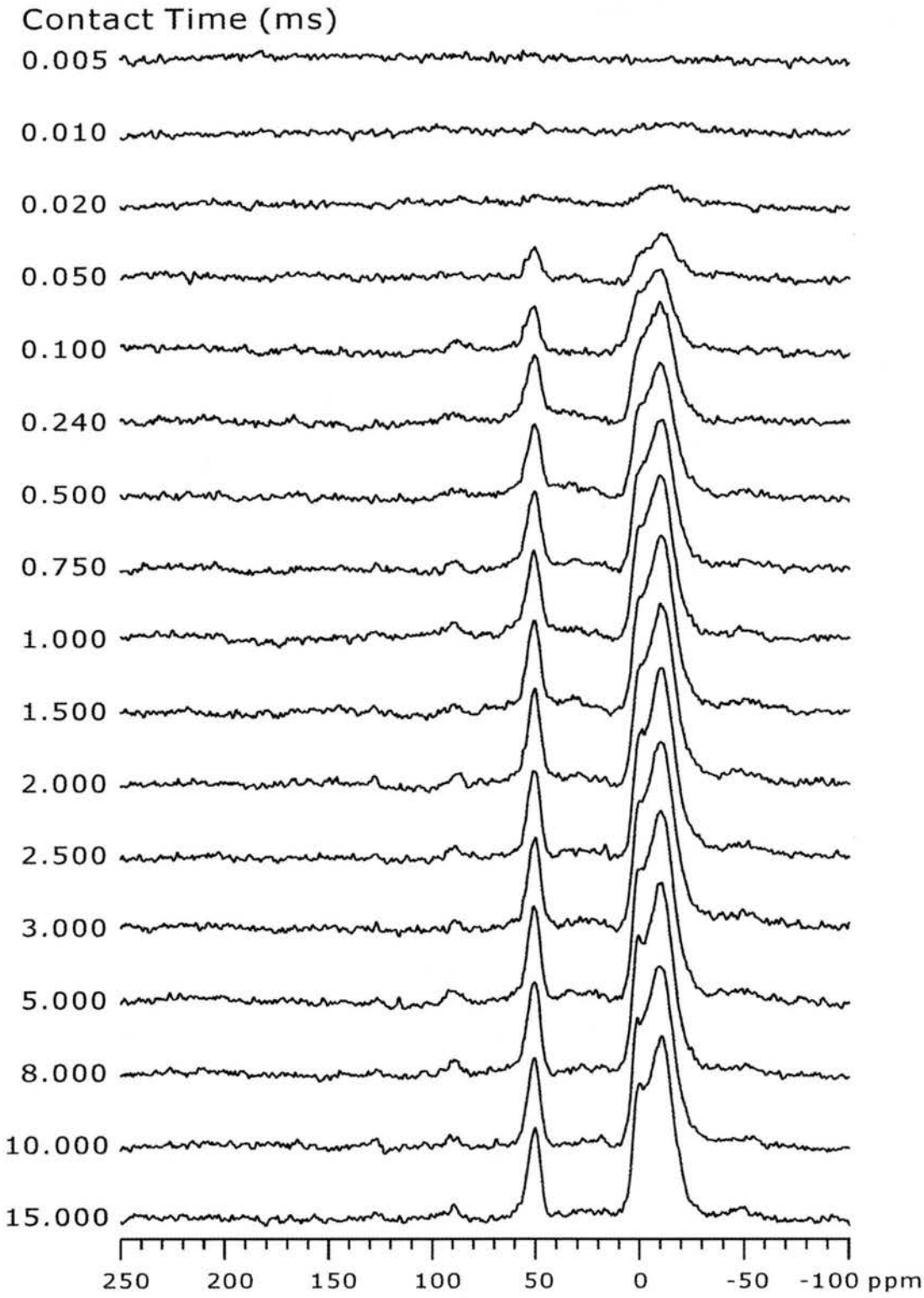

Figure 3.16. ^{13}C CP-MAS variable-contact-time spectra of dry $AlMe_3$/silica/toluene sample corresponding to sample A in Figure 3.9. Each spectrum is the result of 3000 repetitions.

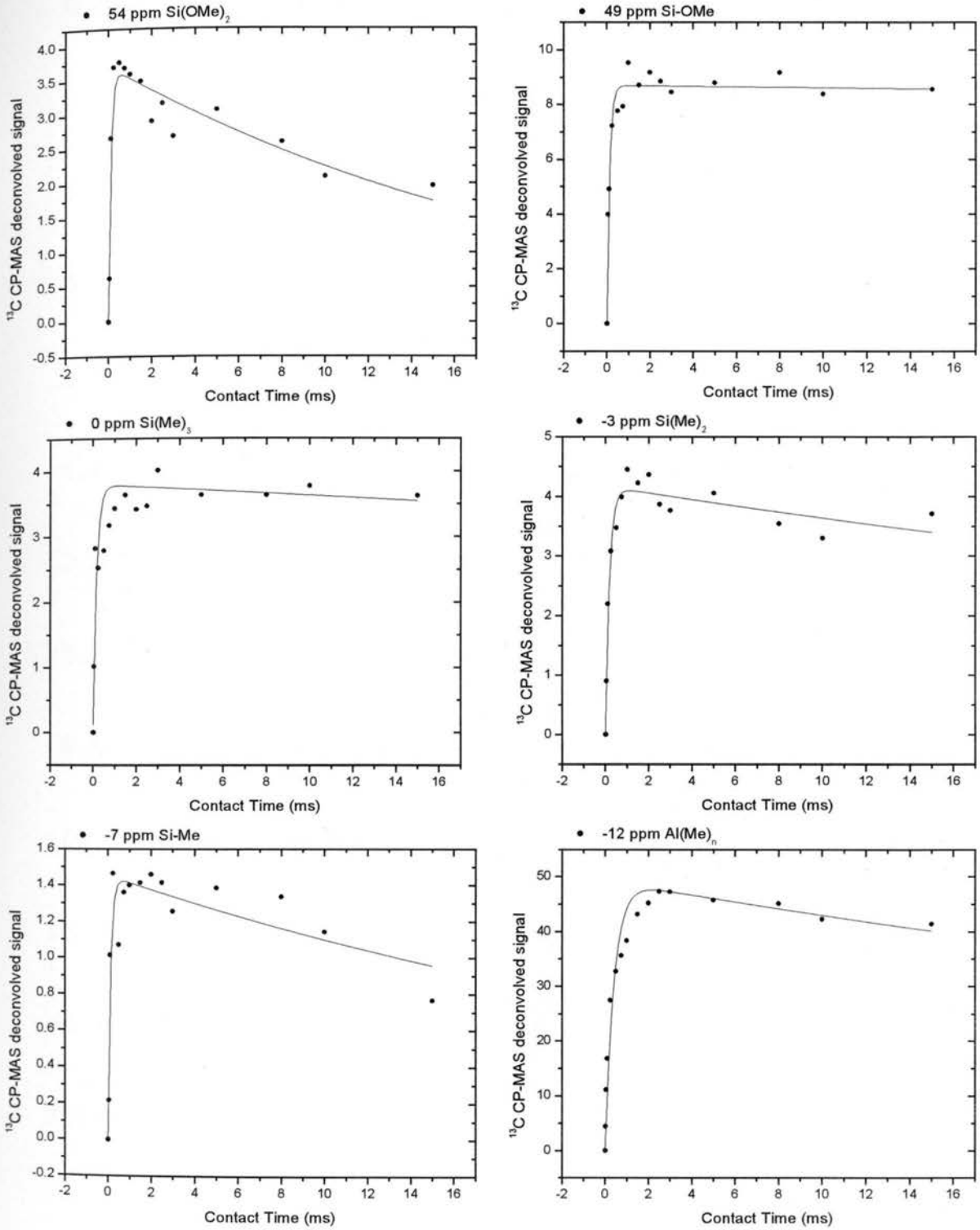

Figure 3.17. Fitting curves of ^{13}C CP-MAS variable-contact-time results for dry $AlMe_3$/silica/toluene sample corresponding to sample A in Figure 3.9, based on Eq. 3.16.

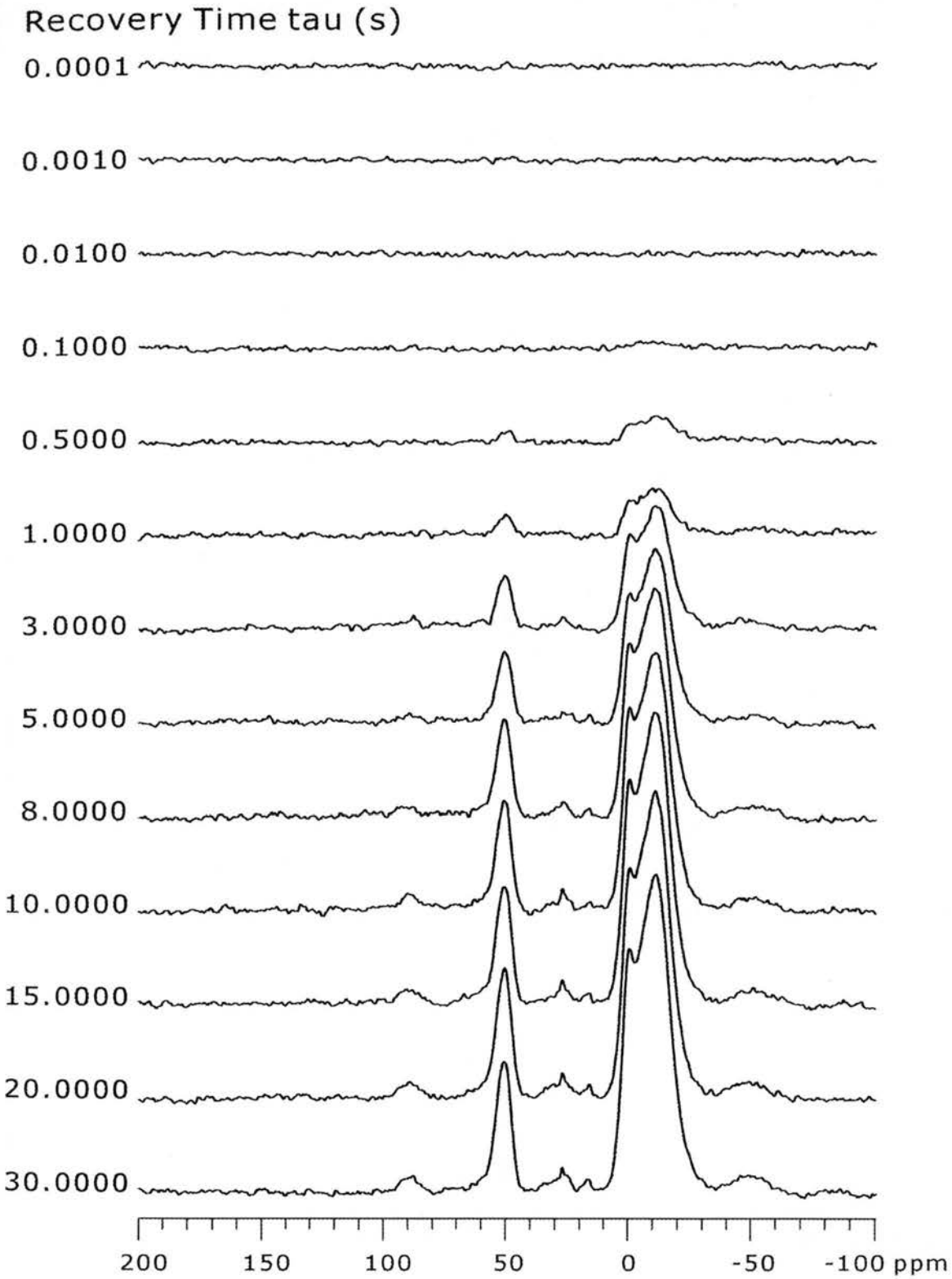

Figure 3.18. ^{13}C CP/MAS-detected ^{1}H-saturation-recovery spectra of dry $AlMe_3$/silica/cyclohexane sample corresponding to sample A in Figure 3.10. Each spectrum is the result of 3000 repetitions.

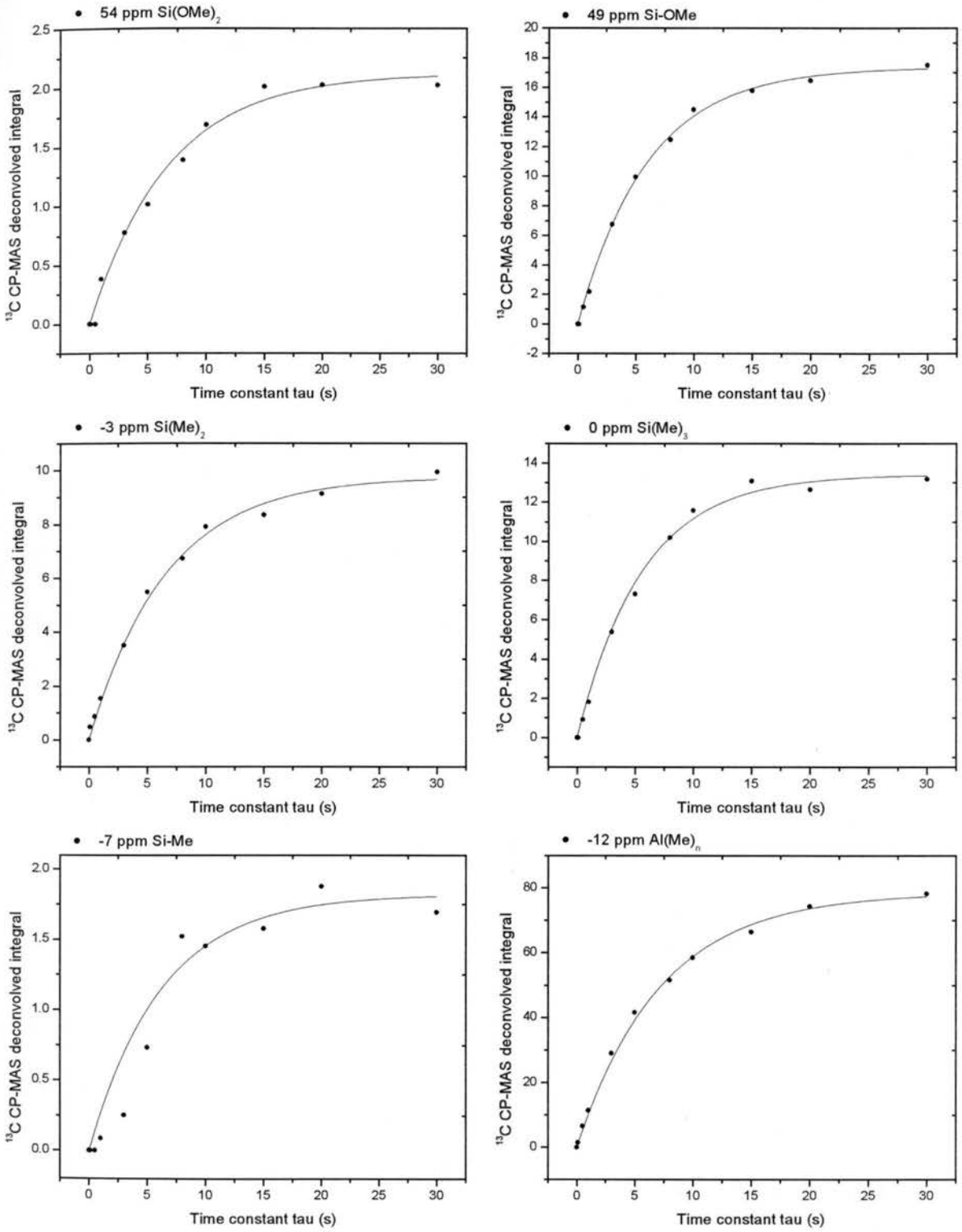

Figure 3.19. Fitting curves of ^{13}C CP/MAS-detected ^{1}H-saturation-recovery results for dry $AlMe_3$/silica/cyclohexane sample corresponding to sample A in Figure 3.10, based on Eq. 3.15.

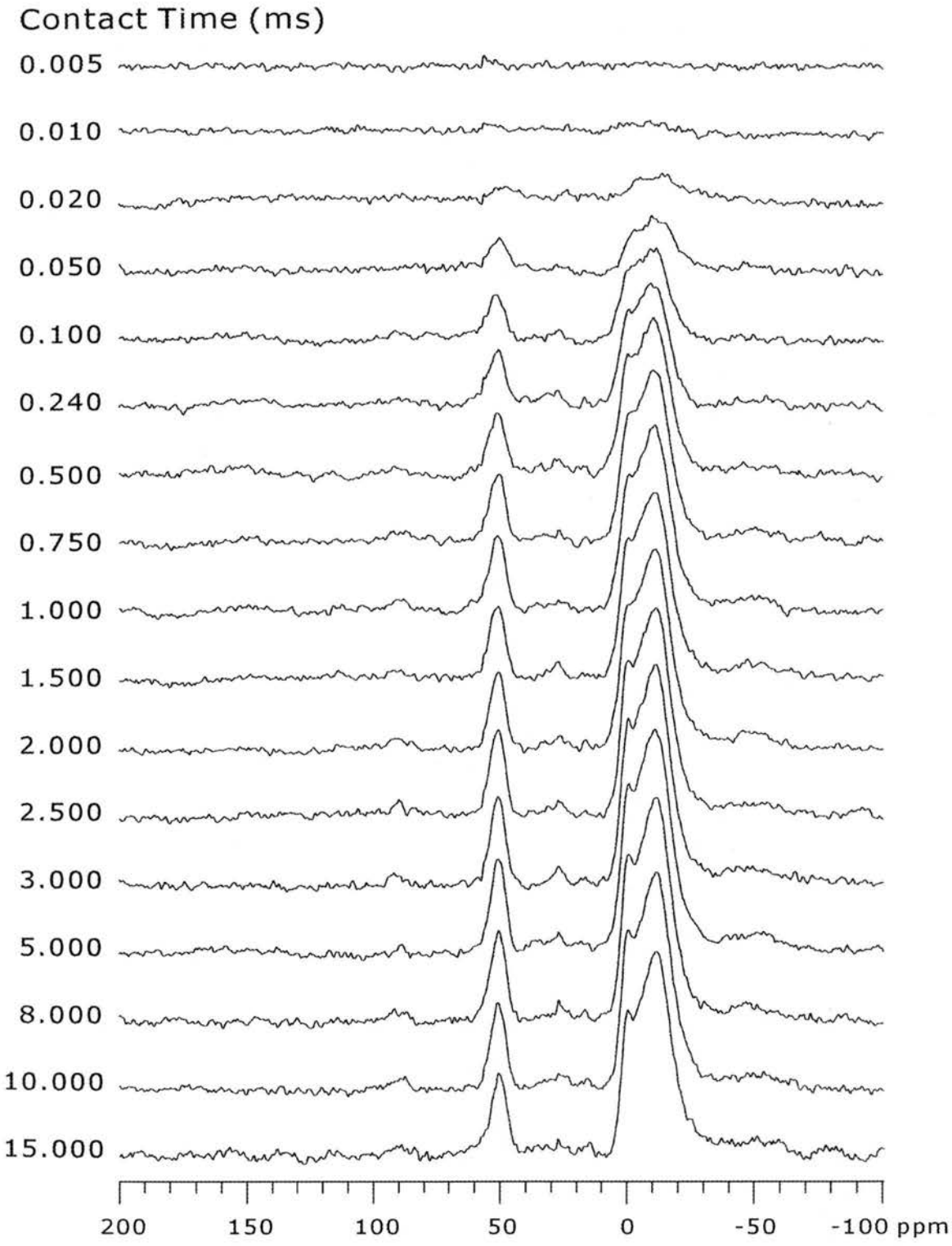

Figure 3.20. ^{13}C CP-MAS variable-contact-time spectra of dry $AlMe_3$/silica/cyclohexane sample corresponding to sample A in Figure 3.10. Each spectrum is the result of 3000 repetitions.

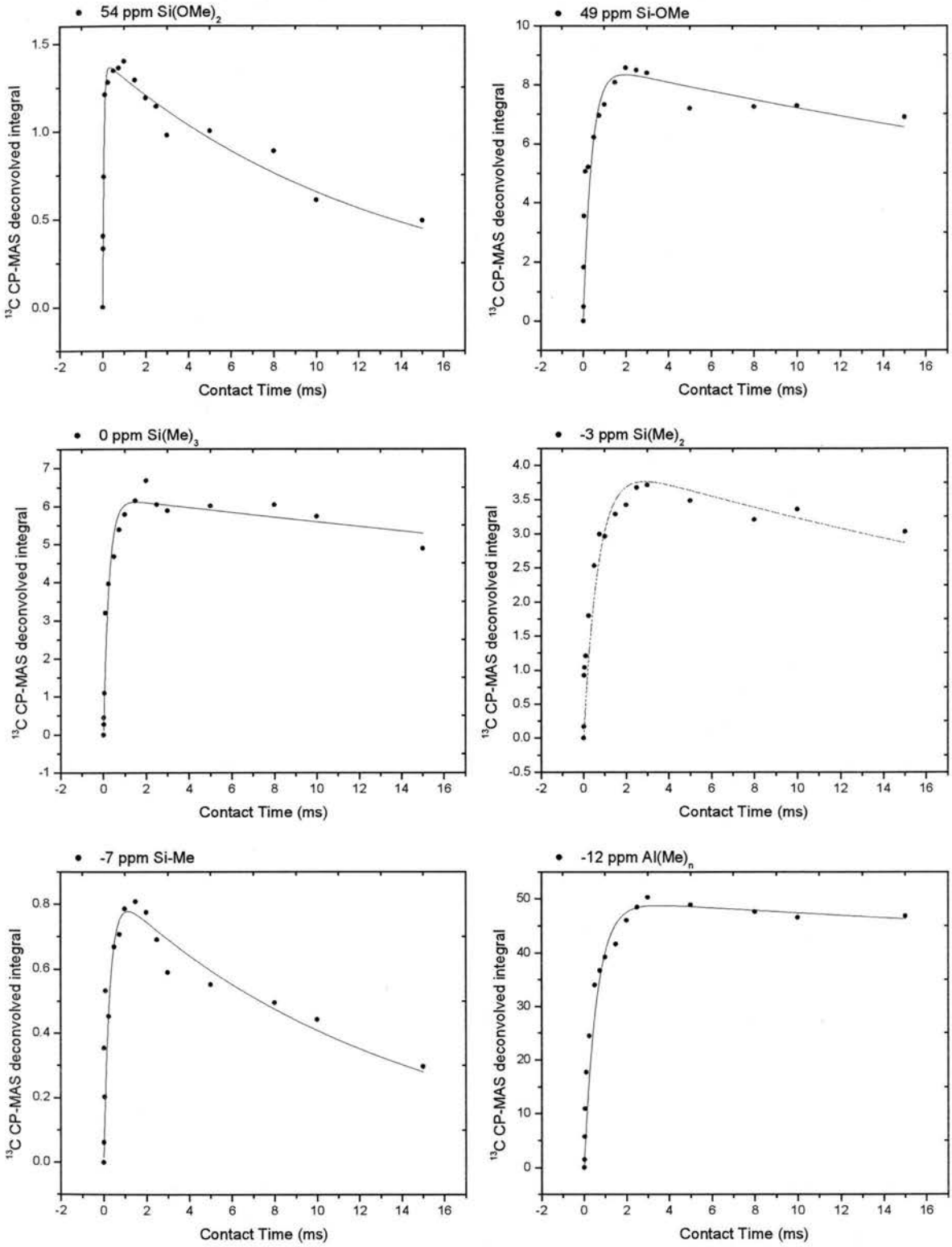

Figure 3.21. Fitting curves of ^{13}C CP-MAS variable-contact-time results for dry $AlMe_3$/silica/cyclohexane sample corresponding to sample A in Figure 3.10, based on Eq. 3.16.

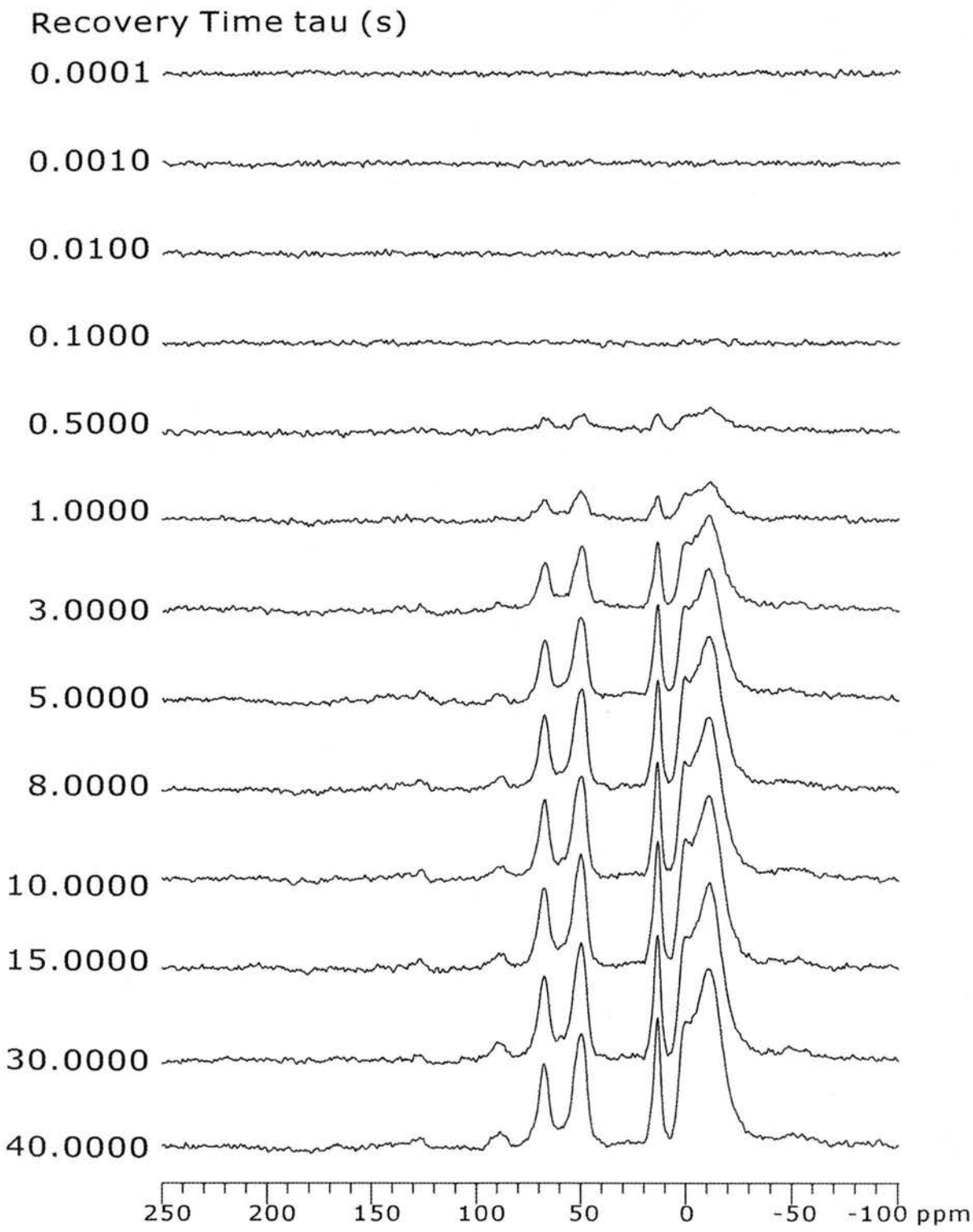

Figure 3.22. ^{13}C CP/MAS-detected ^{1}H-saturation-recovery spectra of ether washed $AlMe_3$/silica/toluene sample corresponding to sample B in Figure 3.9. Each spectrum is the result of 3000 repetitions.

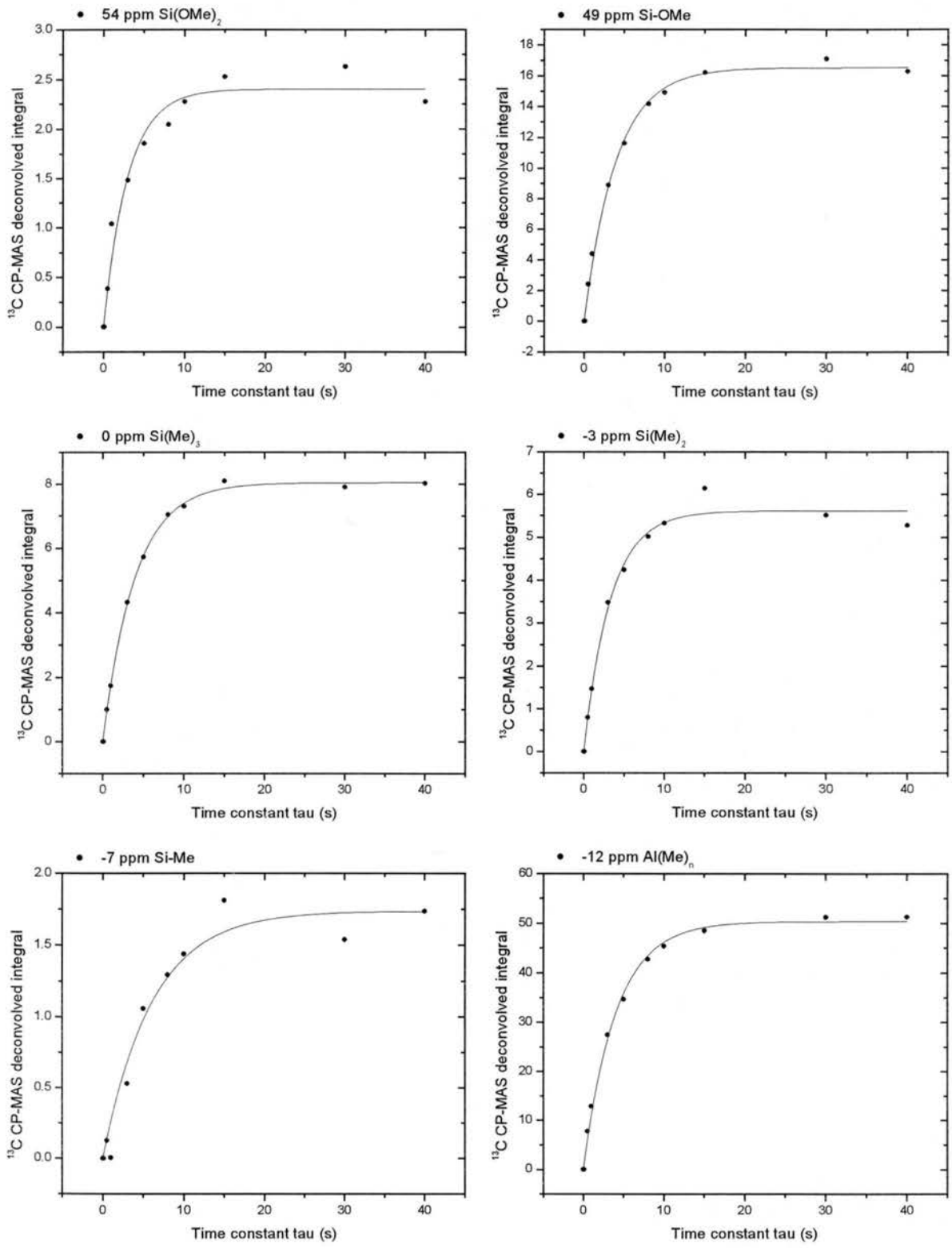

Figure 3.23. Fitting curves of ^{13}C CP/MAS-detected ^{1}H-saturation-recovery results for ether washed $AlMe_3$/silica/toluene sample corresponding to sample B in Figure 3.9, based on Eq. 3.15.

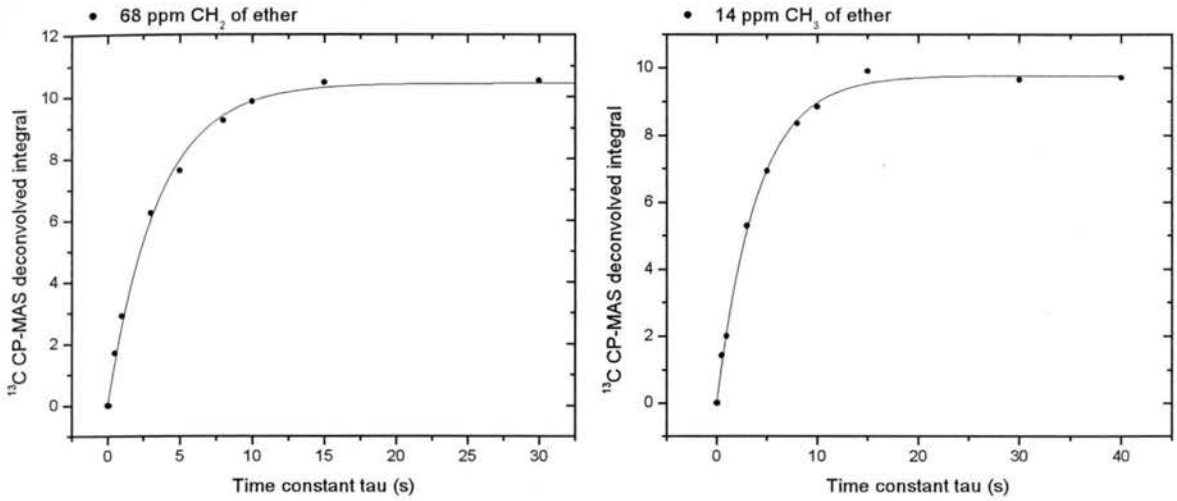

Figure 3.23. (cont.). Fitting curves of ^{13}C CP/MAS-detected ^{1}H-saturation-recovery results for ether washed $AlMe_3$/silica/toluene sample corresponding to sample B in Figure 3.9, based on Eq. 3.15.

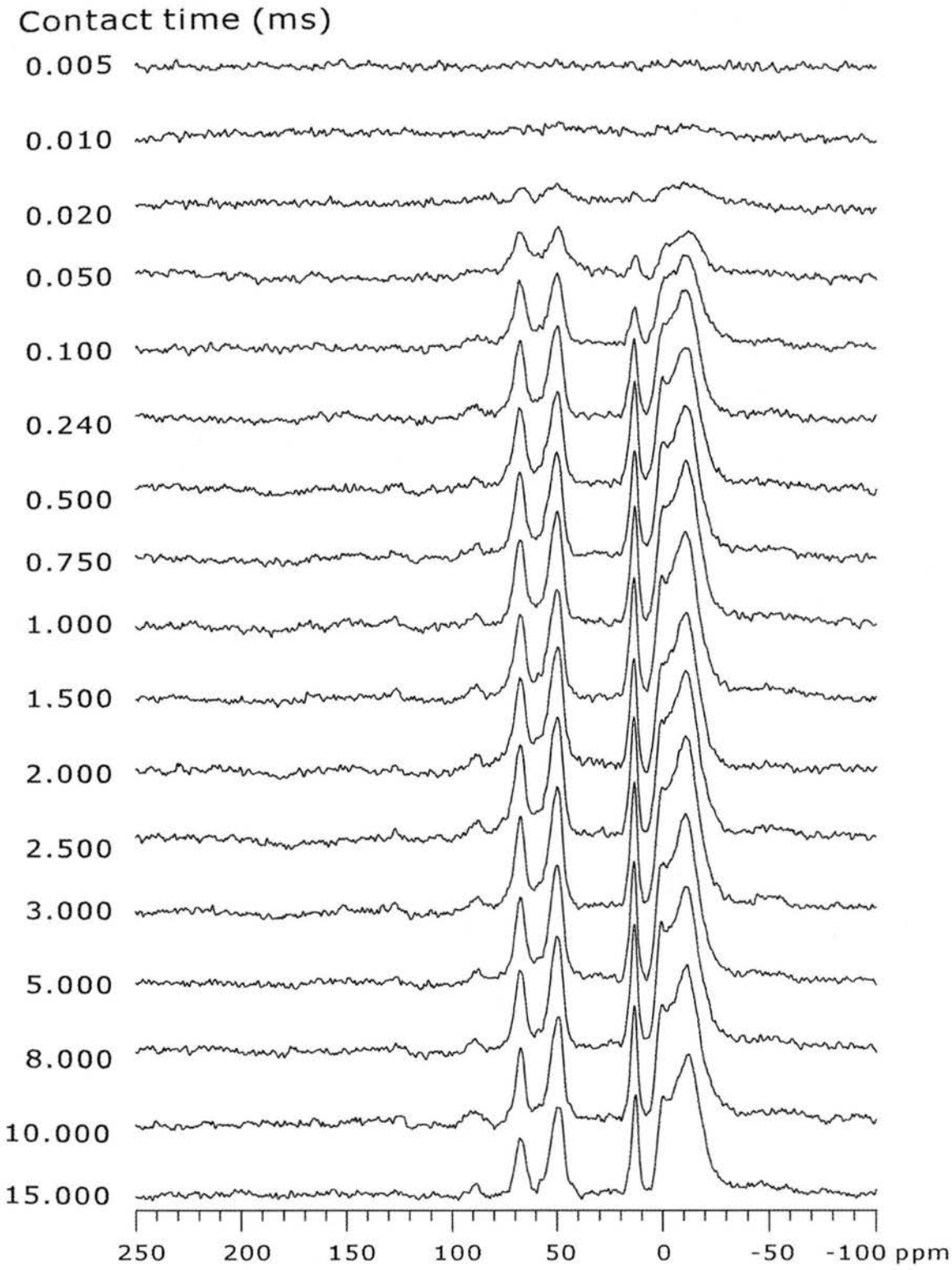

Figure 3.24. ^{13}C CP-MAS variable-contact-time spectra of ether washed $AlMe_3$/silica/toluene sample corresponding to sample B in Figure 3.9. Each spectrum is the result of 3000 repetitions.

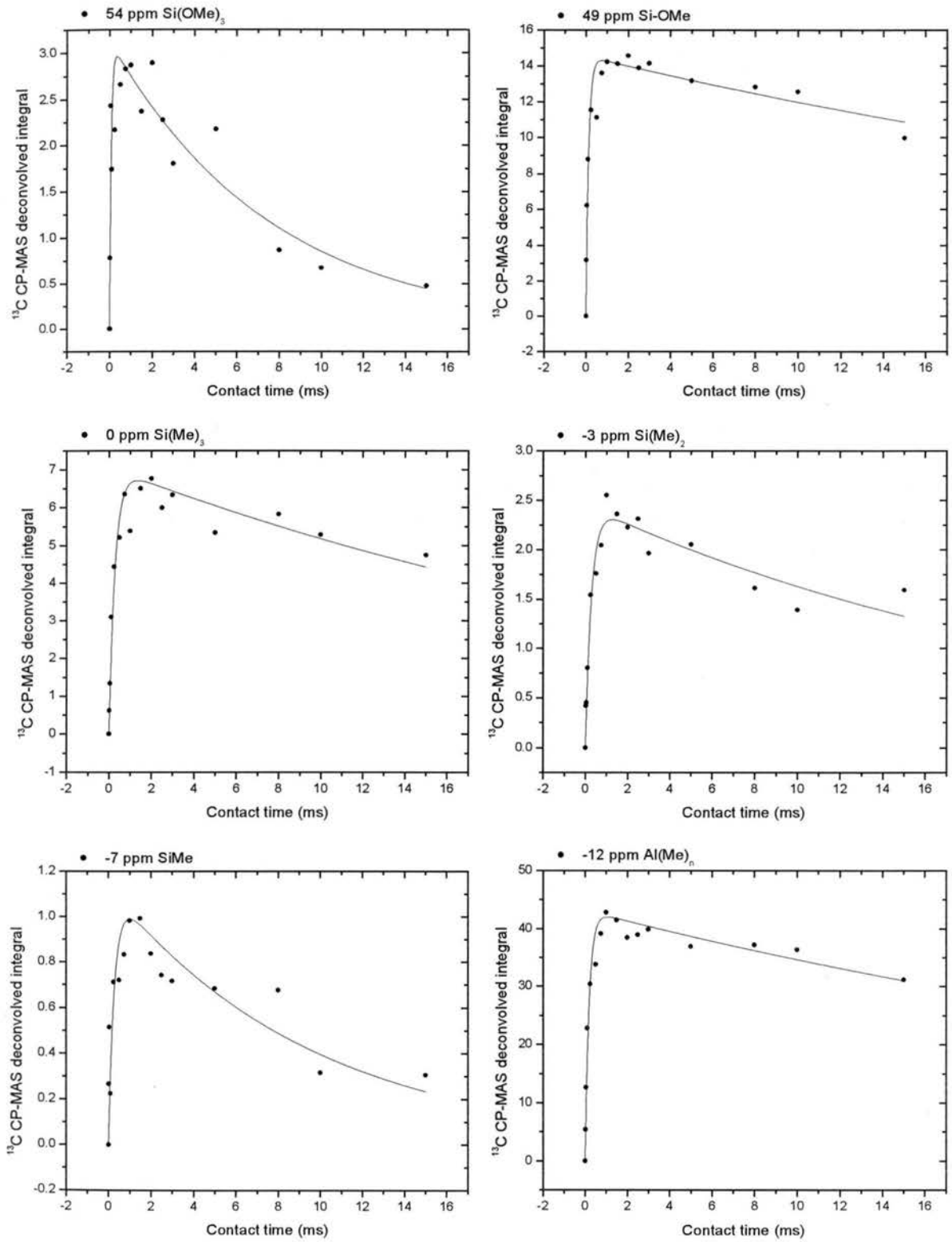

Figure 3.25. Fitting curves of ^{13}C CP-MAS variable-contact-time results for ether washed $AlMe_3$/silica/toluene sample corresponding to sample B in Figure 3.9, based on Eq. 3.16.

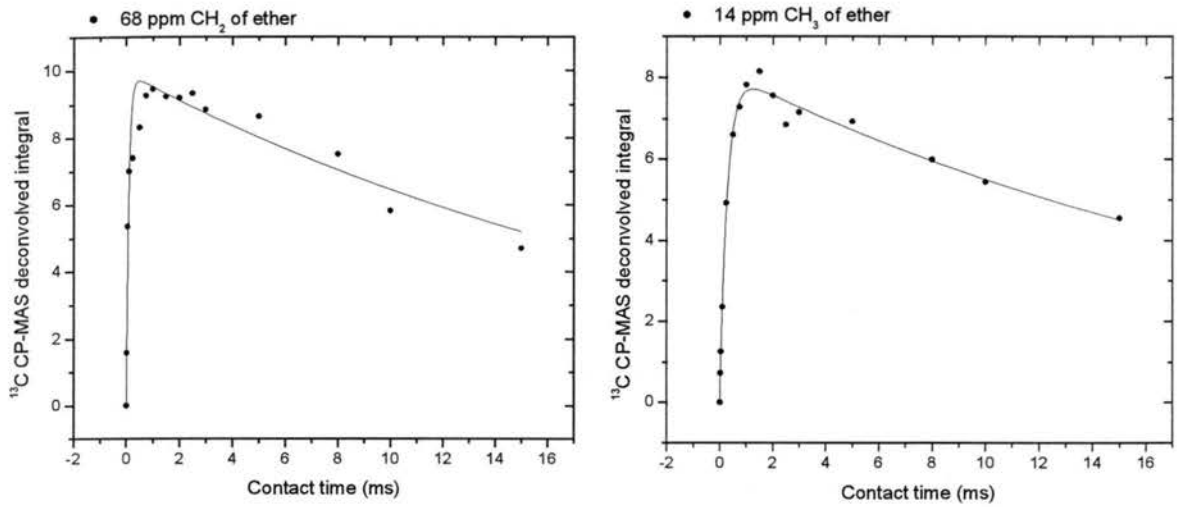

Figure 3.25. (cont.). Fitting curves of ^{13}C CP-MAS variable-contact-time results for ether washed $AlMe_3$/silica/toluene sample corresponding to sample B in Figure 3.9, based on Eq. 3.16.

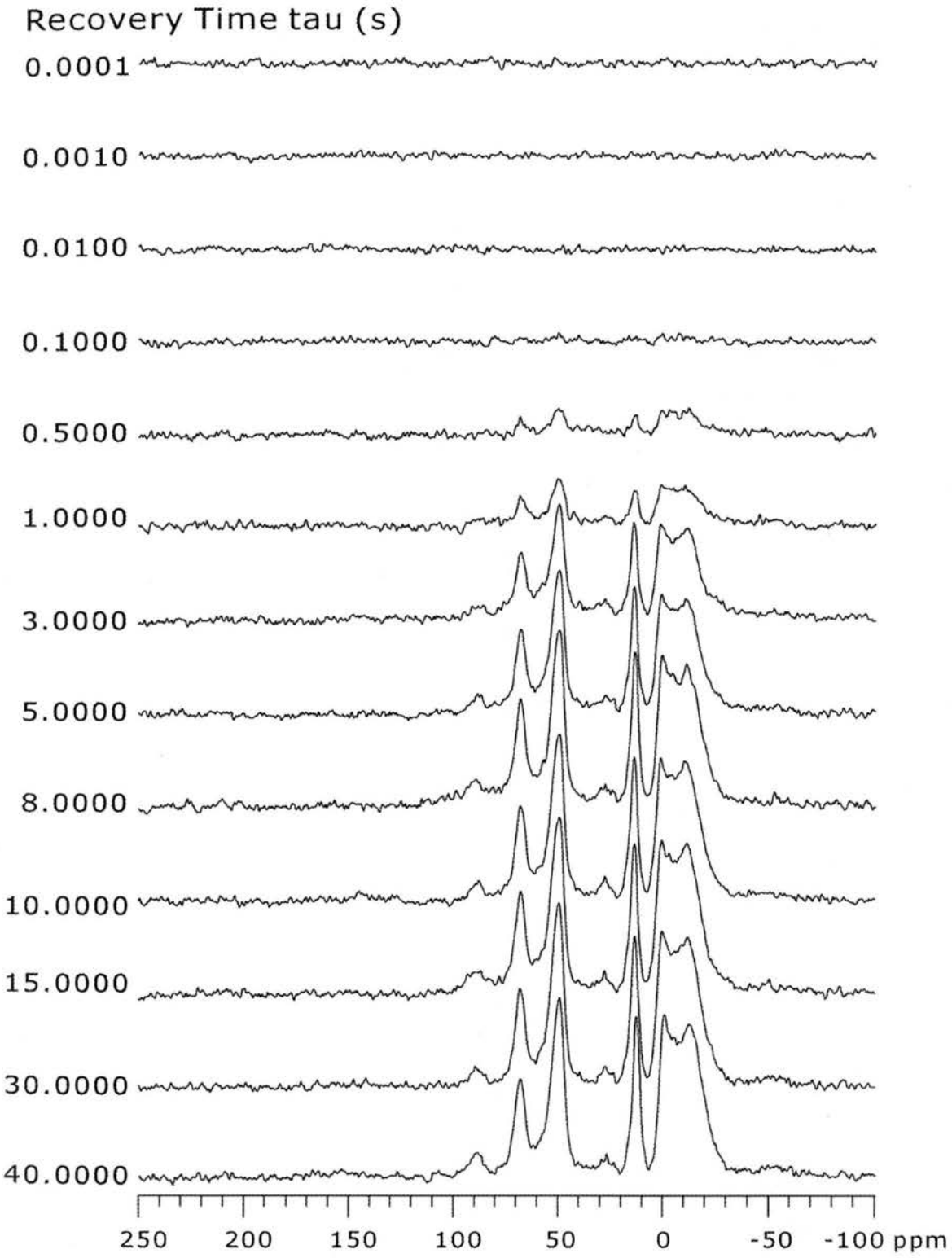

Figure 3.26. ^{13}C CP/MAS-detected ^{1}H-saturation-recovery spectra of ether washed $AlMe_3$/silica/cyclohexane sample corresponding to sample B in Figure 3.10. Each spectrum is the result of 3000 repetitions.

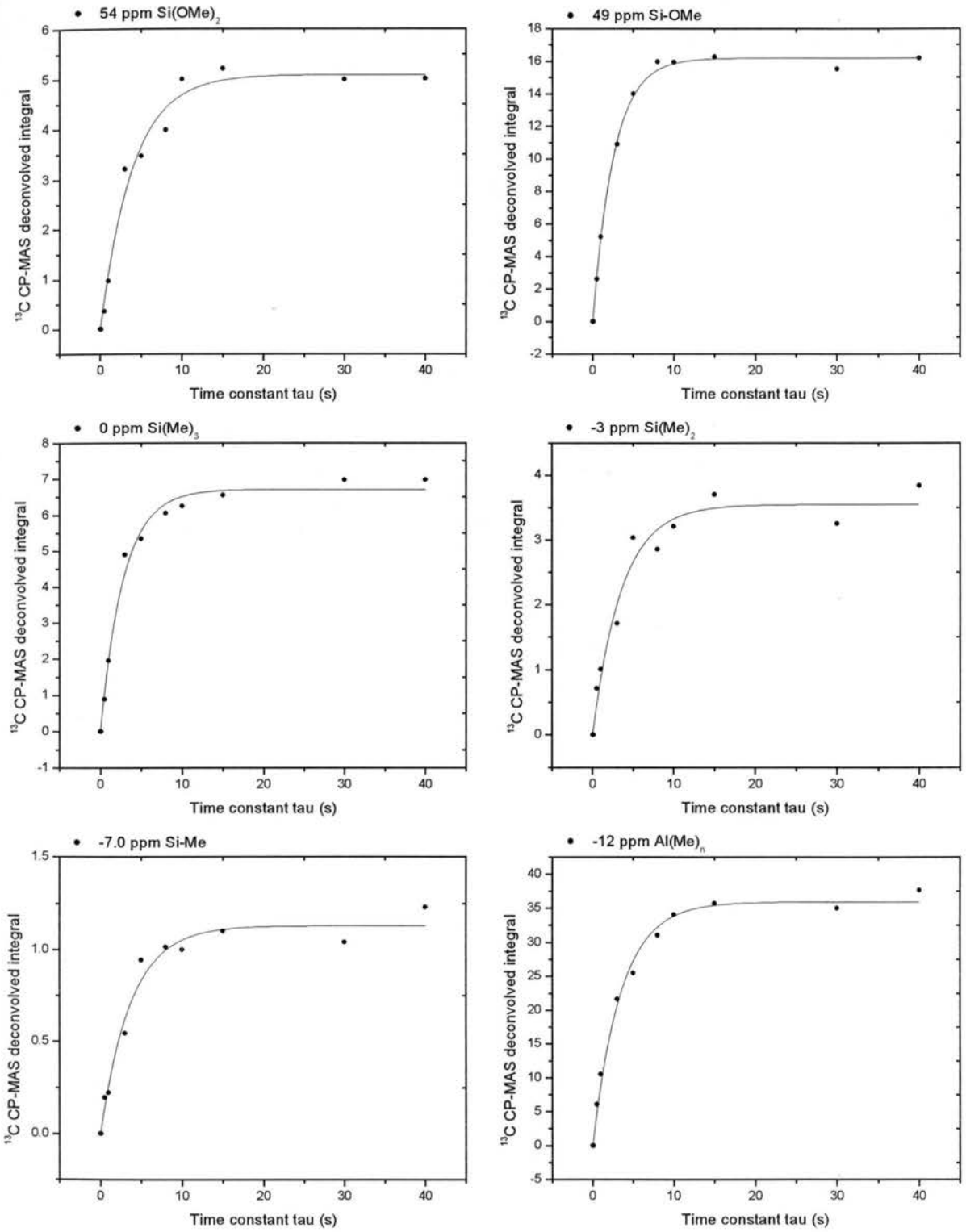

Figure 3.27. Fitting curves of ^{13}C CP/MAS-detected ^{1}H-saturation-recovery results for ether washed $AlMe_3$/silica/cyclohexane sample corresponding to sample B in Figure 3.10, based on Eq. 3.15.

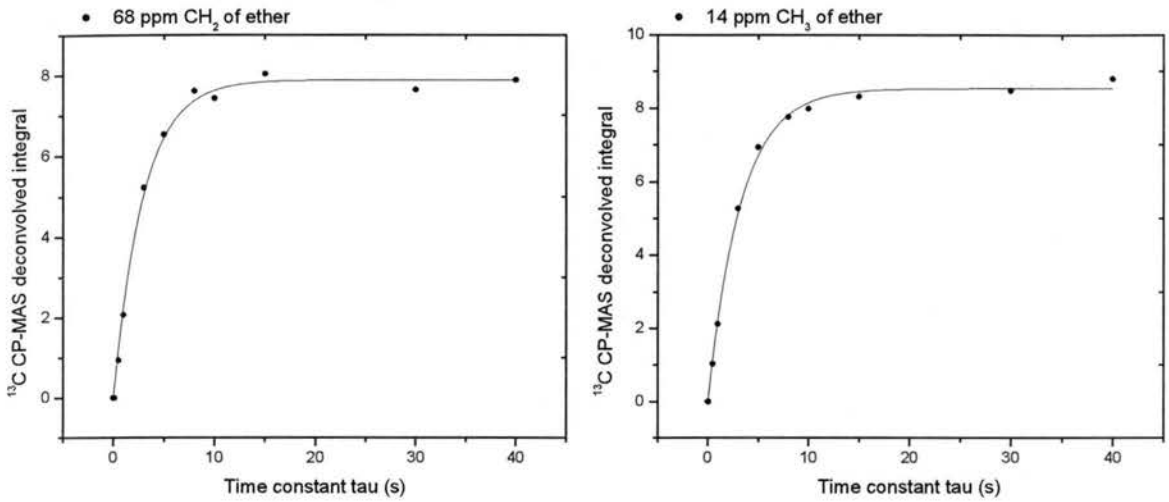

Figure 3.27. (cont.). Fitting curves of ^{13}C CP/MAS-detected ^{1}H-saturation-recovery results for ether washed $AlMe_3$/silica/cyclohexane sample corresponding to sample B in Figure 3.10, based on Eq. 3.15.

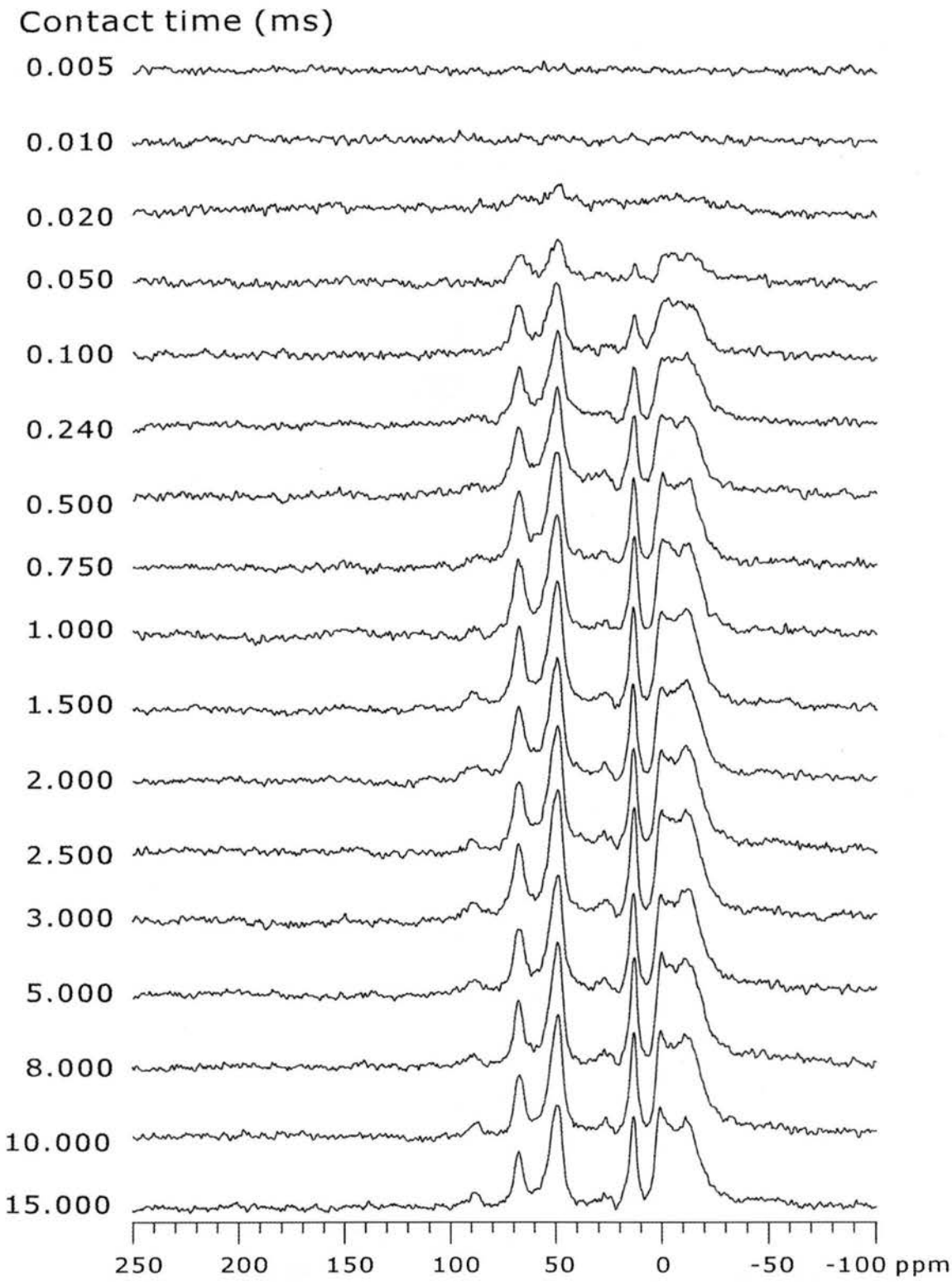

Figure 3.28. ^{13}C CP-MAS variable-contact-time spectra of ether washed $AlMe_3$/silica/cyclohexane sample corresponding to sample B in Figure 3.10. Each spectrum is the result of 3000 repetitions.

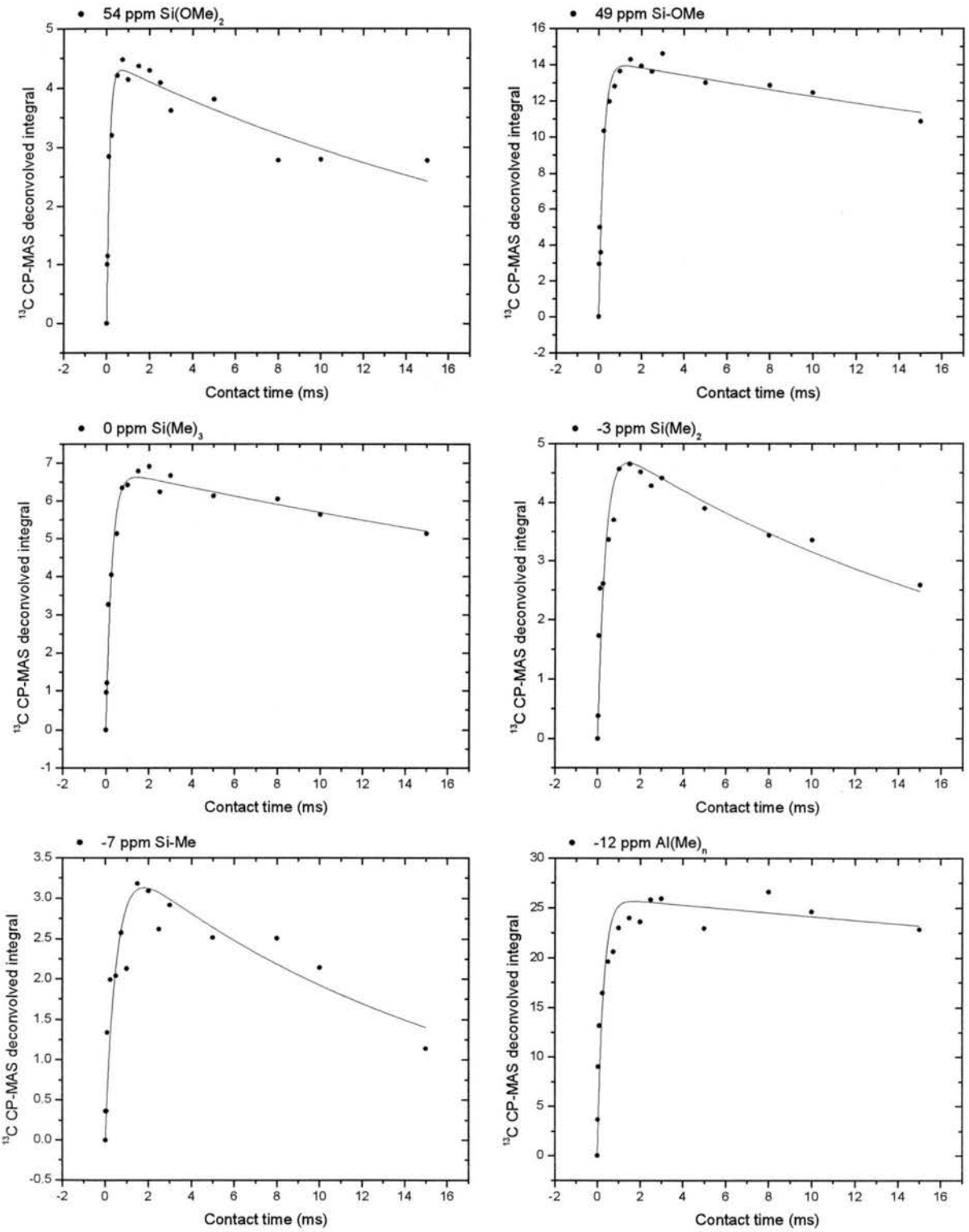

Figure 3.29. Fitting curves of ^{13}C CP-MAS variable-contact-time results for ether washed $AlMe_3$/silica/cyclohexane sample corresponding to sample B in Figure 3.10, based on Eq. 3.16.

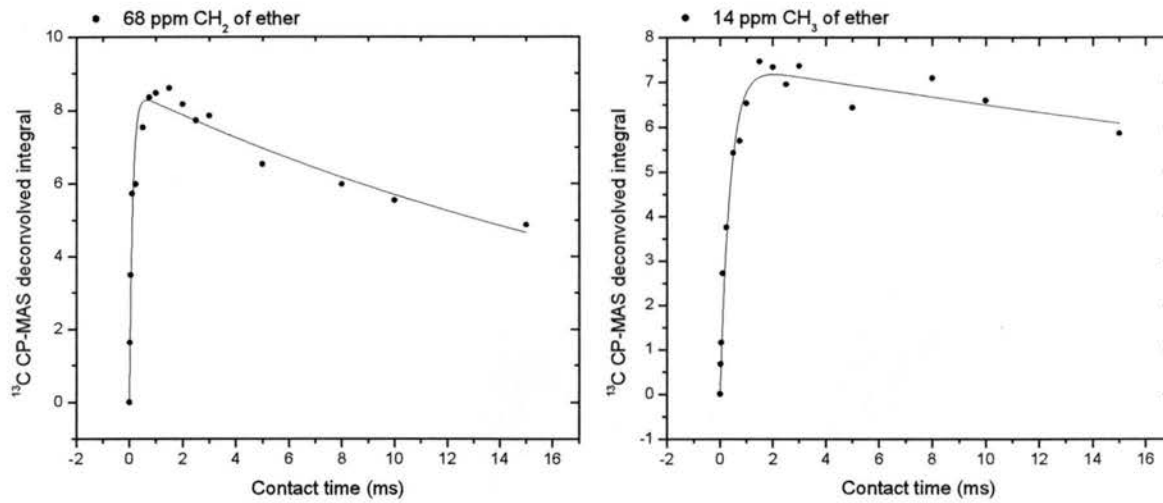

Figure 3.29. (cont). Fitting curves of ^{13}C CP-MAS variable-contact-time results for ether washed $AlMe_3$/silica/cyclohexane sample corresponding to sample B in Figure 3.10, based on Eq. 3.16.

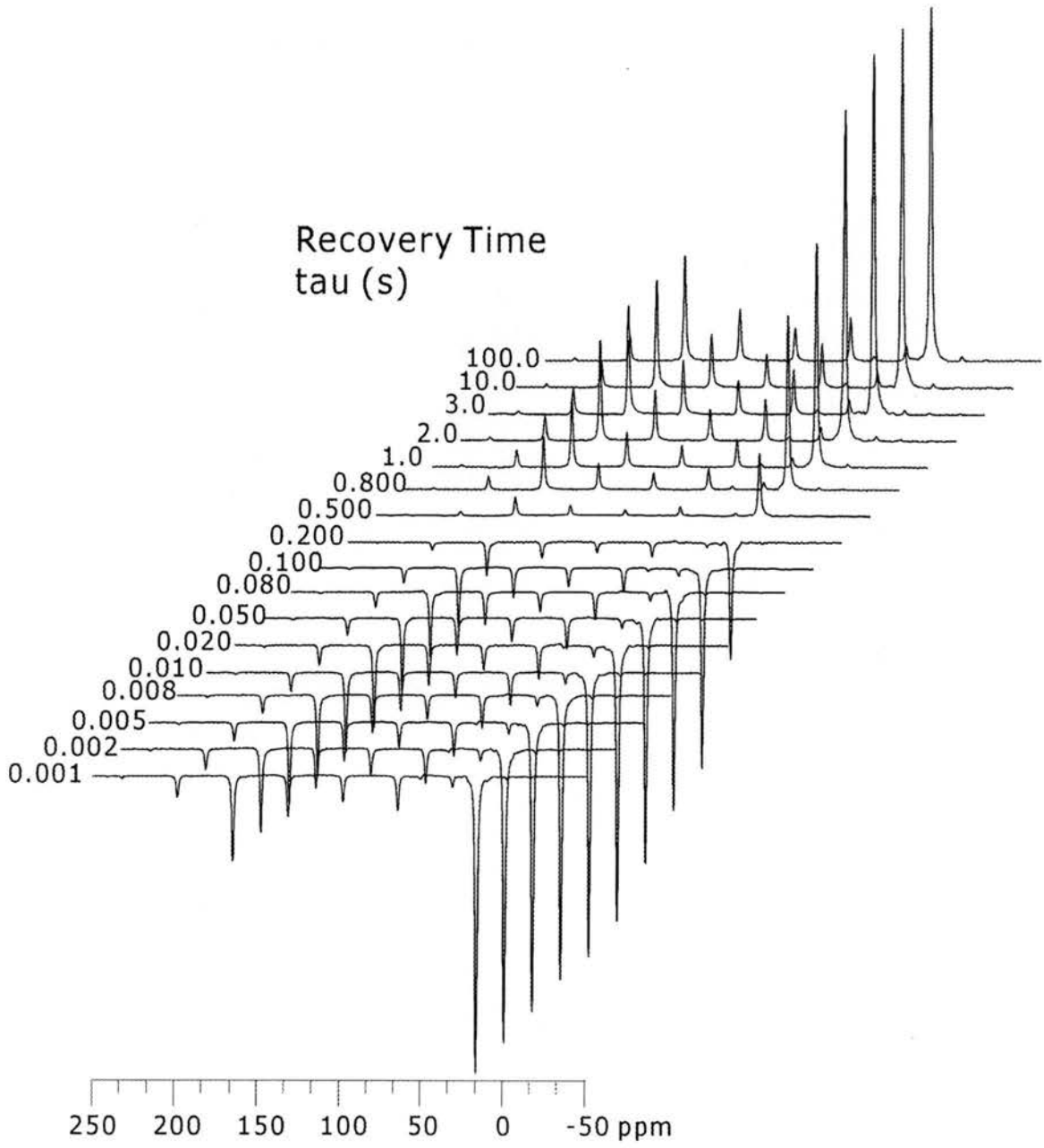

Figure 3.30. ^{13}C CP/MAS-detected ^{1}H-inversion-recovery spectra of HMB. Each spectrum is the result of 36 repetitions.

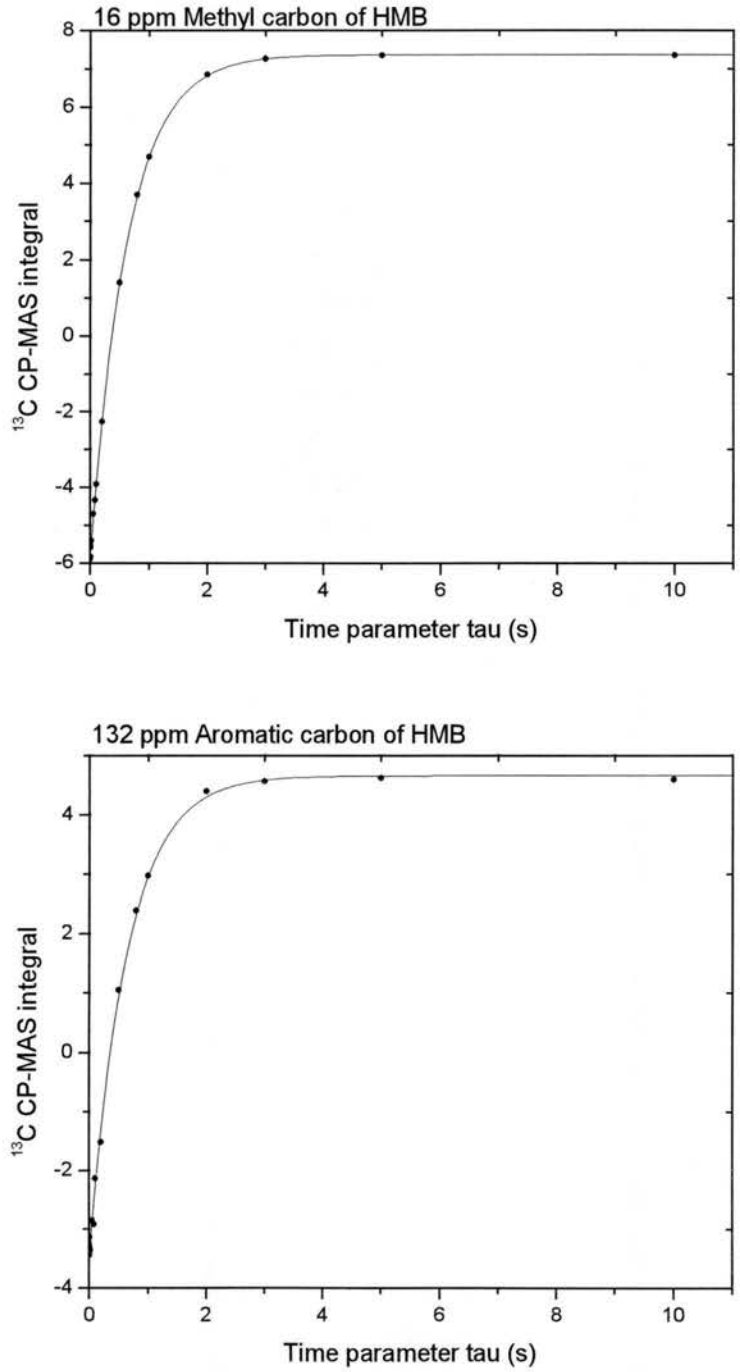

Figure 3.31. Fitting curves of ^{13}C CP/MAS-detected ^{1}H-inversion-recovery results of HMB, based on Eq. 3.11.

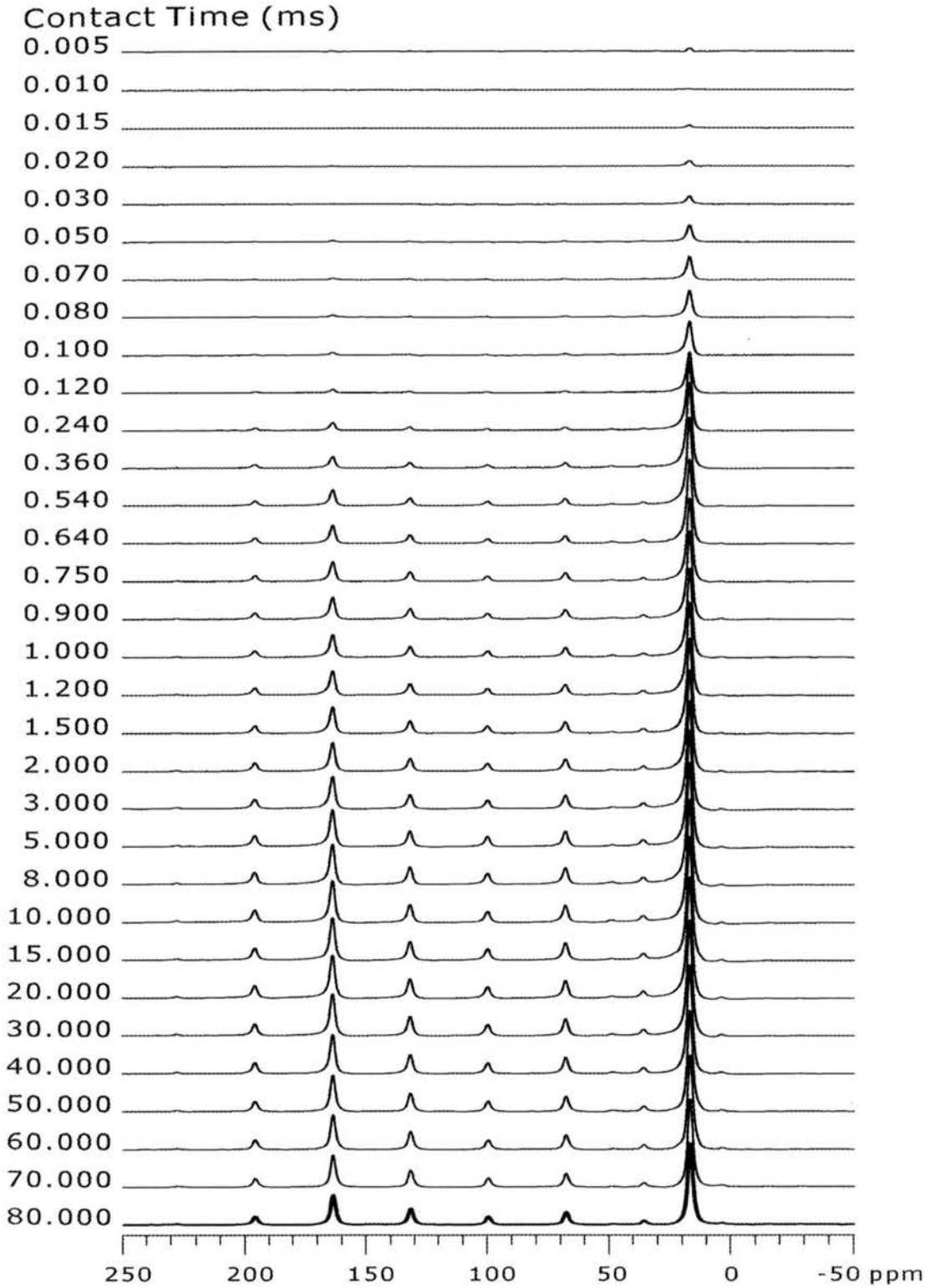

Figure 3.32. ^{13}C CP-MAS variable-contact-time spectra of HMB. Each spectrum is the result of 36 repetitions.

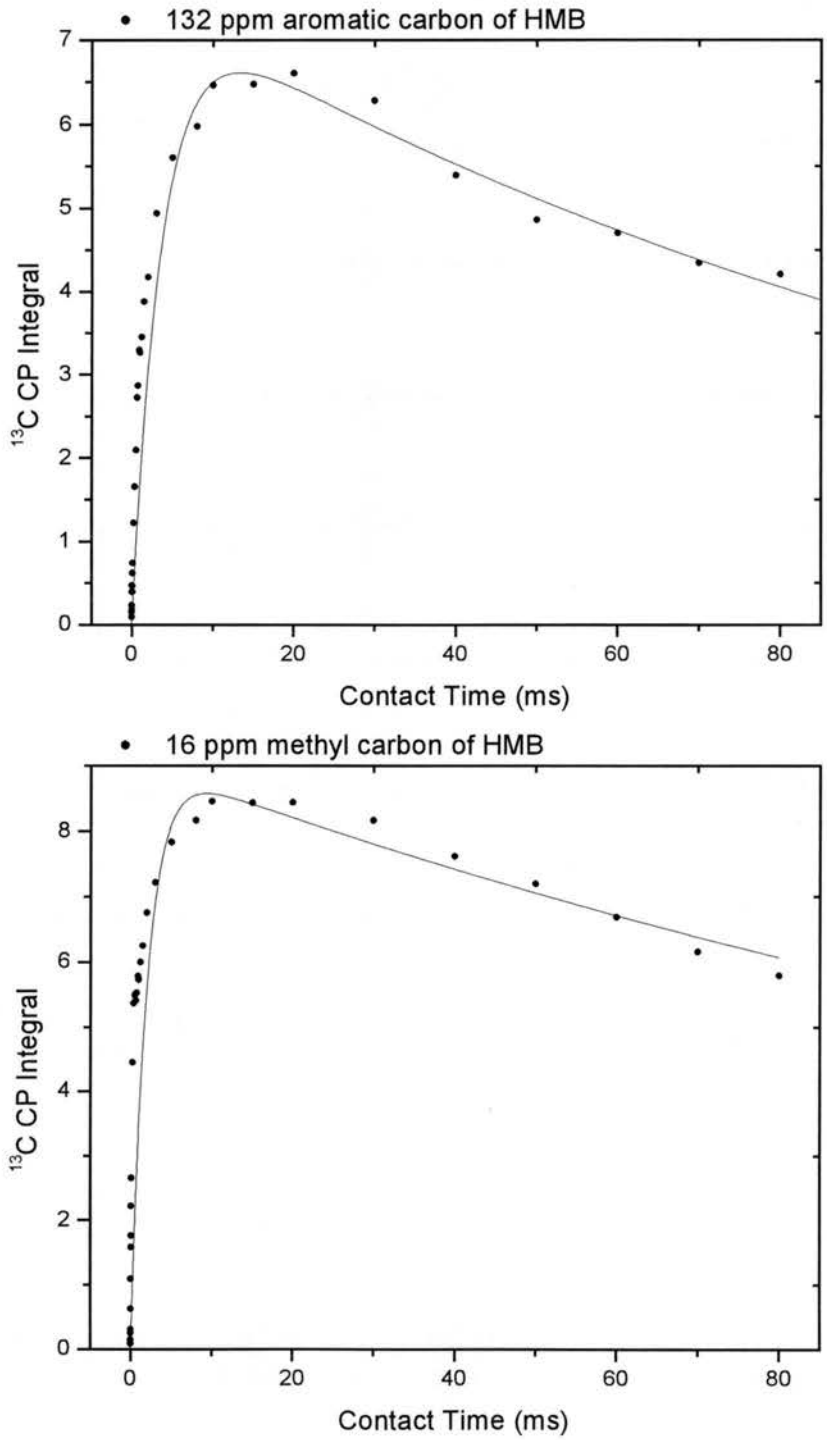

Figure 3.33. Fitting curves of ^{13}C CP-MAS variable-contact-time results (Figure 3.32) of HMB based on Eq. 3.16.

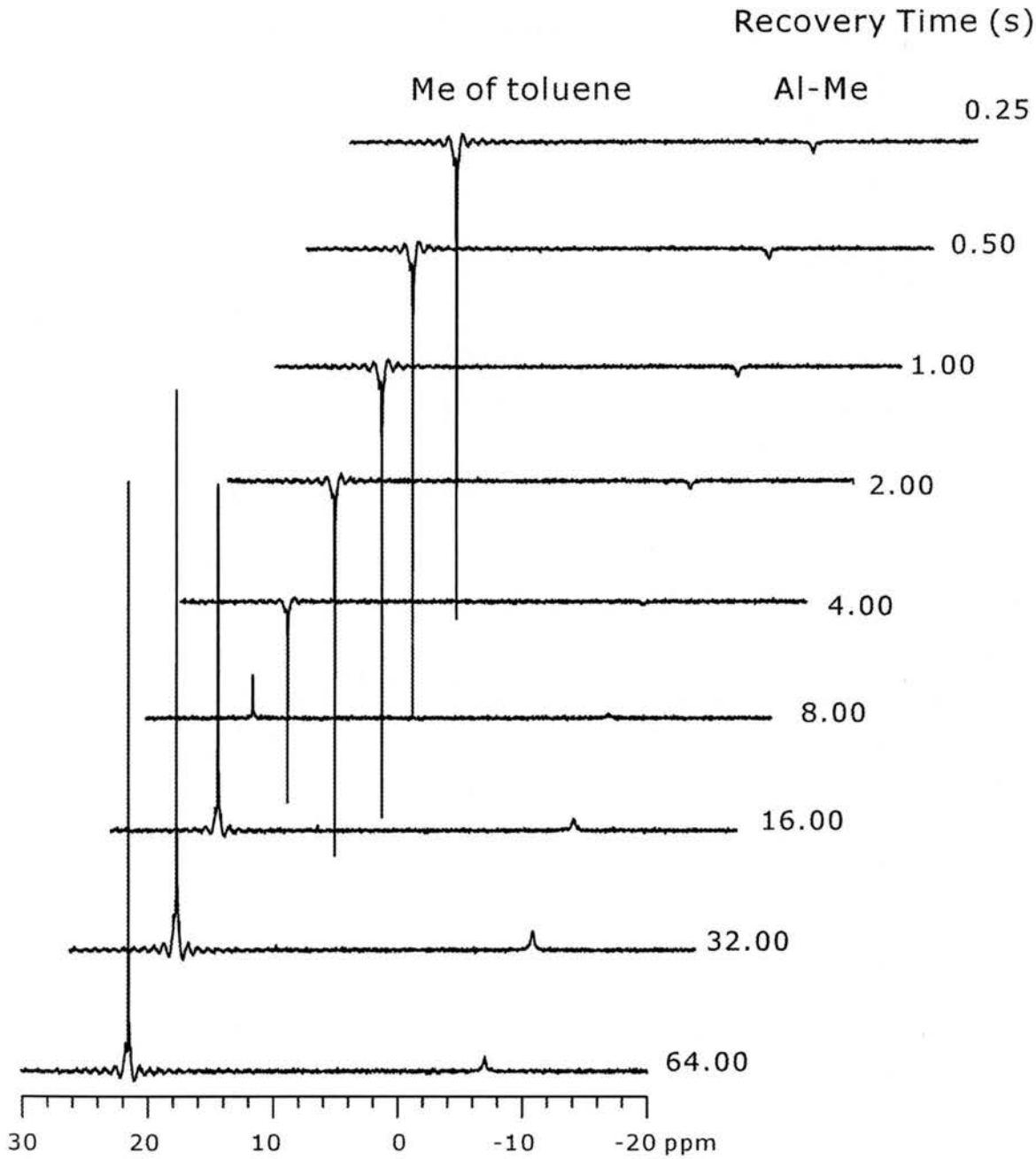

Figure 3.34. Liquid-sample ^{13}C inversion-recovery spectra of a $AlMe_3$/silica/toluene liquid, obtained on a 400 MHz Varian Inova spectrometer.

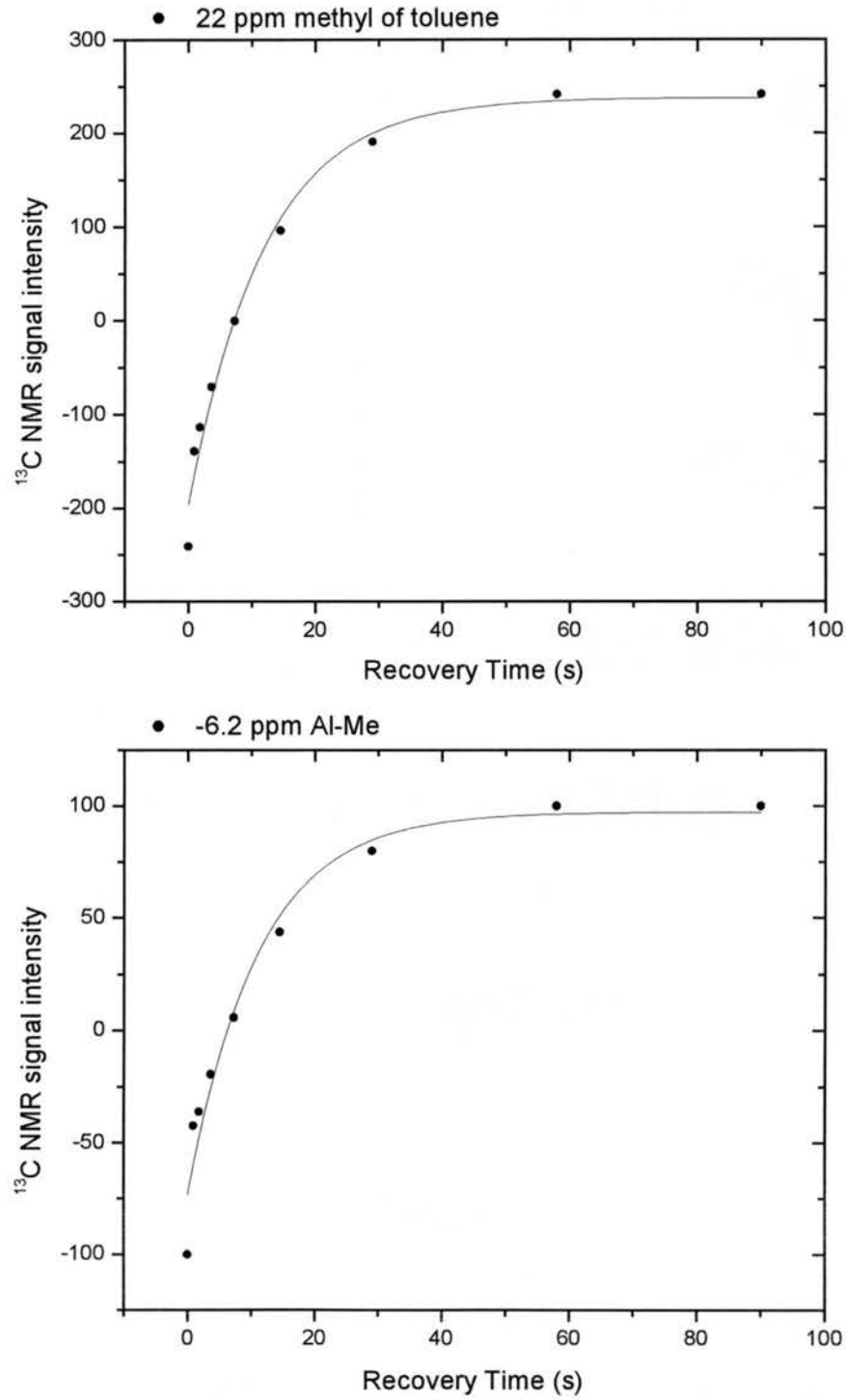

Figure 3.35. Fitting curves of liquid-sample ^{13}C inversion-recovery results (Figure 3.34) of the supernatant solution from an $AlMe_3$/silica/toluene reaction, with curve fitting based on Eq. 3.11.

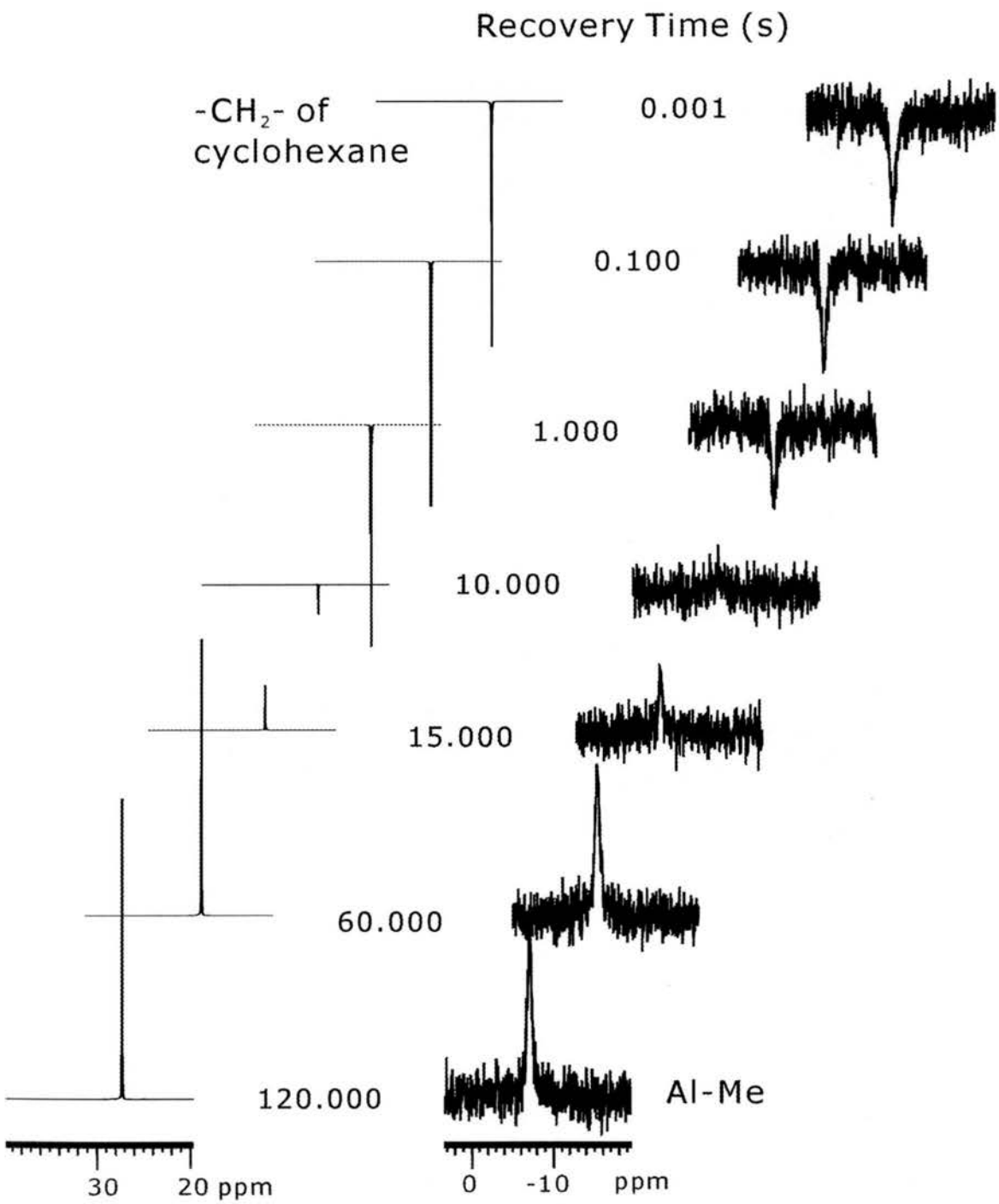

Figure 3.36. Liquid-sample ^{13}C inversion-recovery spectra of a $AlMe_3$/silica/cyclohexane liquid, obtained on a 400 MHz Varian Inova spectrometer. Each spectrum represents 16 repetitions.

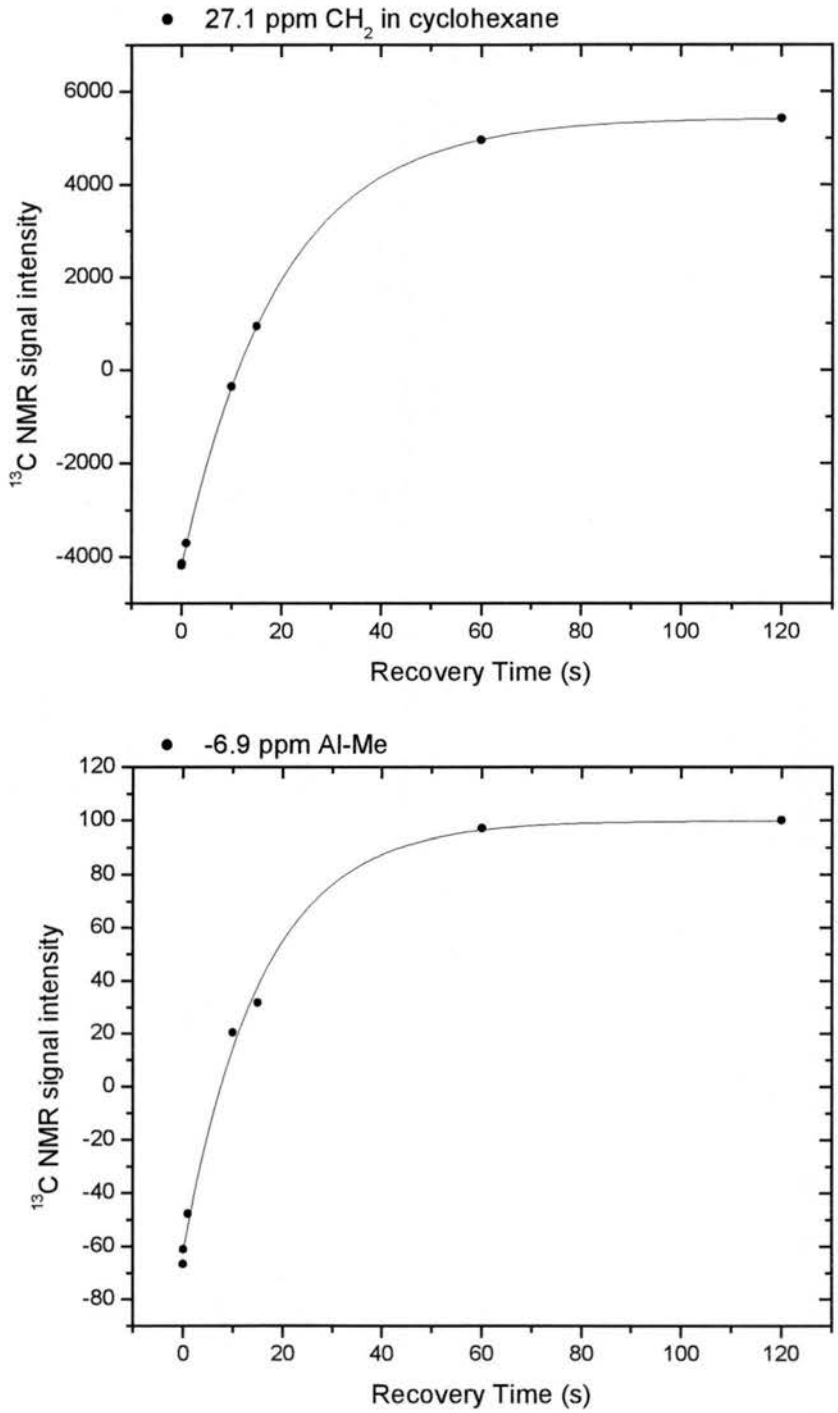

Figure 3.37. Fitting curves of liquid-sample ^{13}C NMR inversion-recovery experiment on the supernatant solution from an $AlMe_3$/silica/cyclohexane liquid (Figure 3.36); curve fitting based on Eq. 3.11.

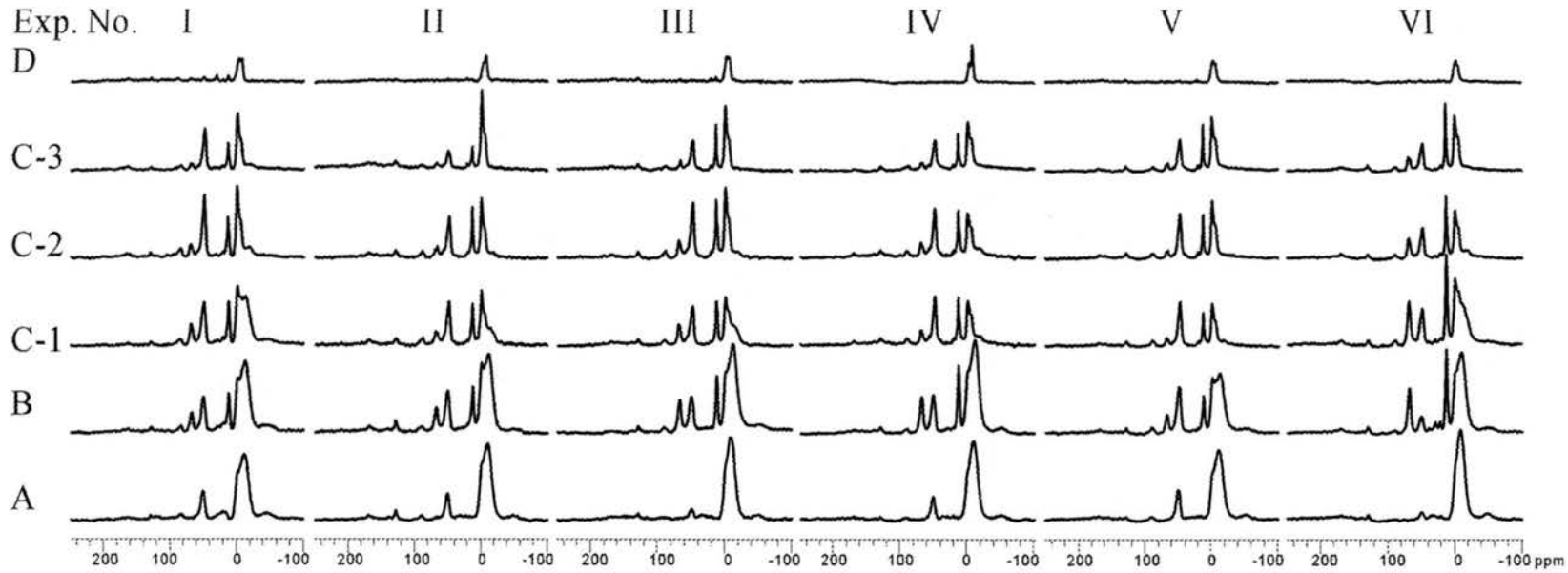

Methyl accounting (mmol)

Si-OH [a]	62	56	68	64	64	66
Al-Me added [b]	243	243	243	243	212	212
CH_4 during reaction [c]	-	31.7	37.8	36.8	38.6	37.3
Al-Me in liquid [d]	-	196.6	170.7	202.6	149.0	162.4
Surface Me [e]	34.7	32.2	38.8	37.3	41.7	43.0
Total Me [f]	-	260	247	275	229	233
%	-	107.2%	101.5%	113.2%	107.7%	109.5%

[a] Determined by ^{1}H MAS spin-counting. Estimated relative standard deviation, 2%.
[b] Determined by the volume of $AlMe_3$ added initially. Estimated relative standard deviation, 5.7%.
[c] Determined by volume measured during the reaction.
[d] Determined by ^{1}H MAS spin-counting in liquid NMR.
[e] Determined by ^{13}C CP-MAS spin-counting.
[f] Estimated relative standard deviation, 10%.

Figure 3.38. ^{13}C CP-MAS Spectra and CH_4/CH_3 counting of $AlMe_3$/silica/toluene reaction systems.

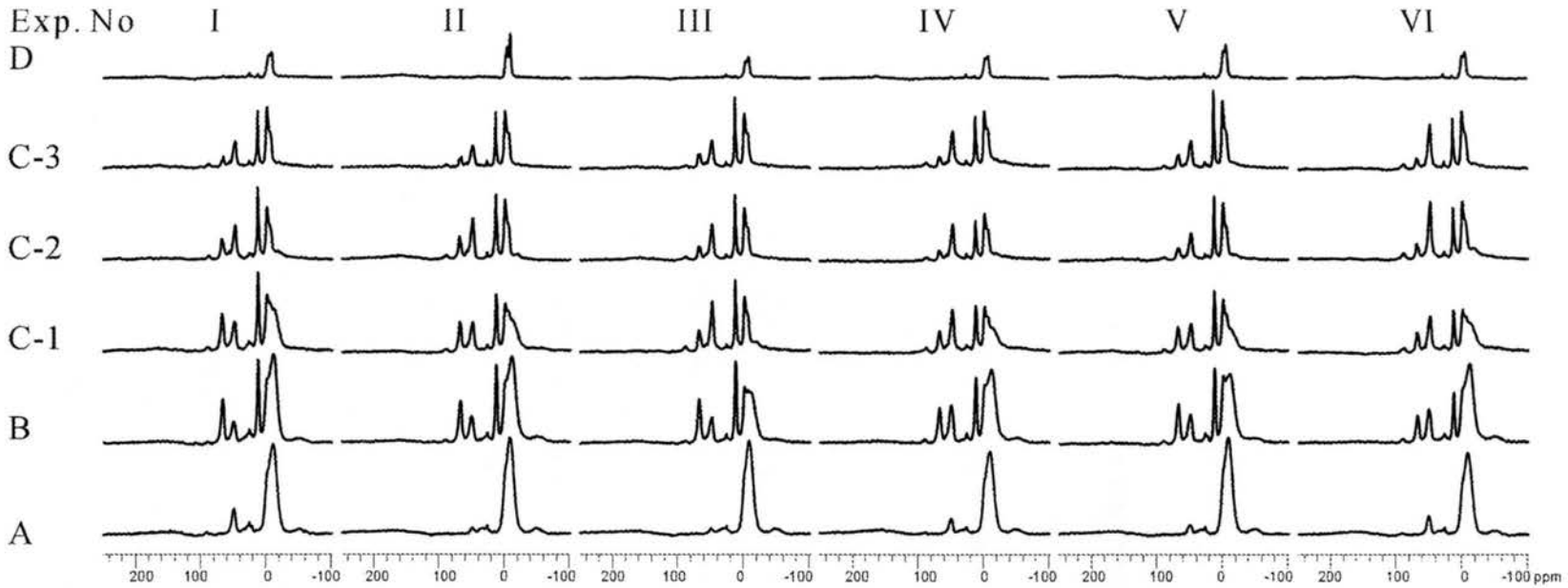

Methyl accounting (mmol)

Si-OH [a]	59	67	66	62	65	66
Al-Me added [b]	243	243	212	212	212	212
CH_4 during reaction [c]	34.1	38.2	42.8	36.0	38.0	36.0
Al-Me in liquid [d]	125.2	135.3	83.4	93.3	94.0	83.4
Surface –Me [e]	57.3	59.6	53.6	54.5	56.2	53.4
Total Me[f]	217	233	180	184	188	173
%	89.2%	96.0%	84.6%	86.5%	88.6%	81.3%

[a] Determined by ^{1}H MAS spin-counting. Estimated relative standard deviation, 2%.
[b] Determined by the volume of $AlMe_3$ added initially. Estimated relative standard deviation, 5.7%.
[c] Determined by volume measured during the reaction.
[d] Determined by ^{1}H MAS spin-counting in liquid NMR.
[e] Determined by ^{13}C CP-MAS spin-counting.
[f] Estimated relative standard deviation, 10%.

Figure 3.39. ^{13}C spectra and CH_4/CH_3 counting of $AlMe_3$/silica/cyclohexane reaction systems.

Chapter 4. DISCUSSION

4.1. Results of relaxation studies.

Besides providing knowledge necessary for carrying out quantitative analysis in the ^{13}C spin counting of surface methyl moieties, a relaxation time study of the surface species also reveals useful information about molecular-level motion. Comparing the proton T_1 values in the same reaction system (toluene or cyclohexane), from sample A to sample B (i.e., for the $AlMe_3$-reacted surface and the diethyl ether-washed surface), one sees that the proton T_1 has dropped upon washing with diethyl ether in both cases. This change might be attributed to some combination of the following potential effects of attaching a diethyl ether moiety to a surface-bonded $AlMe_n$ moiety: 1) alter the mobility of the latter structure by replacing Al-surface interactions or Al-CH_3-Al interactions (both of which should restrict mobility) with Al-$O(Et)_2$ interactions; and/or 2) enhance the concentration of protons near the Al-CH_3 groups being detected. On the initial reaction surface, electron deficient $AlMe_n$ species might interact with each other by sharing methyl groups (form Al-Me-Al bridges), yielding a motionally restrained environment. The introduction of diethyl ether molecules could release some of these kinds of interactions (by replacing the Al-Me-Al bridge with Al-OEt_2 moiety and Al-Me moiety).

Comparing the A sample (initial $AlMe_3$-reacted) of the two different reaction (solvent system), one sees that the methyl groups of $AlMe_n$ species resulting from a reaction carried out in toluene have smaller ^1H spin-lattice relaxation times than the corresponding methyl groups resulting from reactions in cyclohexane. This difference might be explained on the basis that there are weaker interactions between surface $AlMe_n$ moieties and cyclohexane, since cyclohexane is not as "electron rich" (no non-bonded or π electrons) as is toluene. On the $AlMe_3/SiO_2$/toluene surface, toluene has electronic-rich benzene rings, which have the potential to interact with electron-deficient surface species. Interactions between toluene and Al-Me moieties could help reduce the interaction between Al-Me species themselves, which could reduce motional constraints and result in altered relaxation efficiencies.

Further comparing the change from sample A to sample B (ether washed) in the two reaction (solvent) systems, one sees that the effect on proton T_1 of introducing diethyl ether onto the surface is larger for the cyclohexane system than in the toluene system. Since toluene molecules may already participate in some interactions (e.g., with $AlMe_n$ groups) on the surface, the change induced by introduction of diethyl ether molecules might be expected to be less than it is in the cyclohexane case. This scenario is consistent with the view that diethyl ether molecules interact with surface moieties, thereby affecting ^1H T_1 relaxation of the surface species.

4.2. Chemical interpretation of ^{29}Si NMR results.

In the ^{1}H->^{29}Si ^{29}Si CP-MAS spectra of $AlMe_3$-reacted silica in Figure 3.9, the main signals appear around –109 ppm, which is normally where Q_4 silicons (in the silica gel framework at the 'surface') are located. The apparently low signal intensity of Q_3 silicons (which normally appear at about –99 ppm in unreacted silica, the most intense signal) and Q_2 silicons (which normally appear at about –89 ppm in unreacted silica), both of which have hydroxyl groups attached, compared with relative intensities for the unreacted silica gel (bottom spectra), implies that all (or most) of the surface silanols (Si-OH) reacted with $AlMe_3$ (disappearing Q_2 and Q_3 signals). The Si-OH moiety is known to be a very reactive functional group towards reaction with $AlMe_3$; hence, most of the Si-O-H should react and be converted to Si-O-Al linkages in the initial $AlMe_3$/silica reaction. This change, replacement of Si-OH with Si-O-Al linkages, can be observed by comparing ^{29}Si spectrum of the original silica gel with that of the $AlMe_3$-reacted silica (sample A in Figure 3.9), in which the disappearance of the –99 peak is observed. In the ^{29}Si spectrum of sample A in Figure 3.9, the broad peak with a maximum intensity around –109 ppm is consistent with the existence of a peak centered at about –104 ppm that is seriously overlapped with the Q_4 signal at –109 ppm. Even without any computer deconvolution, one can see that there is a roughly 5 ppm shift in intensity from the –99 ppm region to the –104 region in progressing from the original silica spectrum to the ^{29}Si spectrum of sample A in Figure 3.9. Figure 4.1 displays the results of computer deconvolution /simulation, which shows the same intensity shift.

The ^{29}Si chemical shift change of a **Si** atom from the $(SiO)_3$**Si**(OH) moiety to the $(SiO)_3$**Si**(OAl) moiety is not well defined in the current literature; however, it can be estimated from available information. It is useful to consider the **Si**-O-H → **Si**-O-Al change in terms of the following two steps: 1) **Si**-O-H → **Si**-O-**Si** and 2) **Si**-O-**Si** → **Si**-O-Al. For the first step, we already know that, in the silica gel ^{29}Si spectrum, replacing the $(SiO)_3$**Si**(OH) moiety by the $(SiO)_3$**Si**(OSi) moiety changes the ^{29}Si chemical shift of **Si** from –99 ppm to –109 ppm. For the second step, the $(SiO)_4$**Si** moiety and the $(SiO)_3$**Si**(OAl) moiety are the basic structural units in zeolite compounds and the chemical shifts of **Si** in $(SiO)_4$**Si** and $(SiO)_3$**Si**(OAl) are well studied in zeolites.[1]

The following table lists the most relevant ^{29}Si chemical shifts in different zeolites. The zeolites from leucite to chabazite in the table are natural zeolite minerals; and below these are synthetic zeolites.[1-3] One can see that the chemical shift change of **Si** from $(SiO)_4$**Si** to $(SiO)_3$**Si**(OAl) is pretty consistent, averaging around 5 ppm.[1] On this basis it is reasonable to expect the **Si**-OH → **Si**-O-Al chemical shift change in this study to be about: –10 ppm + 5 ppm = –5 ppm, and the ^{29}**Si** chemical shift of the $(SiO)_3$**Si**-O-Al moiety to be about: –99 ppm (for $(SiO)_3$**Si**(OH)) – 5 ppm = -104 ppm.

Table 4.1. ^{29}Si chemical shifts in zeolites.[1]

Type of zeolite	$(SiO)_3$**Si**(OAl) (ppm)	$(SiO)_4$**Si** (ppm)	$\Delta = \delta(SiO)_3$**Si**(OAl) - $\delta(SiO)_4$**Si** (ppm)
Leucite	-97.4	-101	3.6
Heulandite	-99.0	- 108	9.0
Clinoptilolite	-100.5	-112.8	12.3
Stilbite	-101.5	-108	6.5
Chabazite	-104.8	-110	5.2
Omega	-98.8	-103.4	4.6
NaK-L	-101.5	-107.4	5.9
NaK-P1	-102.4	-107	4.6
ZK-5	-103.5	-108.6	5.1
NaK-chabazite	-104.4	-109.5	5.1
Na-mordenite	-105.7	-112.1	6.4
Ferrierite	-105.9	-110.5	4.6
ZSM-11	-105	-113	8
ZK-4	-106.1	-110.7	4.6
ZSM-5	-106	-112	6
ZSM-35	-108	-113	5
TMA-Sodalite	-110.5	-116.2	5.7

It is possible that some silanols (Q_3 silicons at –99 ppm) still remain on the surface after the $AlMe_3$ treatment. This –99 ppm signal might be of very low intensity and seriously overlapped with the strong signal at –104 ppm. To estimate the amount of possible unreacted silanols remaining on the surface, computer simulations of the ^{29}Si spectrum of $AlMe_3$-reacted silica samples (corresponding to sample A in Figure 3.9.) were carried out.

First, the reproducibility of the experimental lineshape was examined. It was found that the ^{29}Si NMR lineshapes obtained on four different preparations of the $AlMe_3$/silica sample A are essentially superimposible. That is, the ^{29}Si NMR results have very good reproducibility of the peak centered at –109 ppm.

Second, computer simulations that include signal intensities of a) unreacted silanols (Q_3, at –99 ppm), b) the postulated Si-O-Al linkages formed in the reaction (-104 ppm) and c) surface siloxane bridges (Q_4, at –109 ppm) were carried out to find out the upper limit of signal due to unreacted silanols in the ^{29}Si NMR spectrum. Figure 4.3 showed the computer simulation results. In Figure 4.3, with the composition of silanols (Q_3, -99 ppm) increasing gradually, the computer-simulated spectra showed more and more shoulder features (centered at –99 ppm) beside the signal centered at –109 ppm. These simulation results indicated that the upper limit for unreacted silanols that might remain on the surface is about 5% (of all the three signals).

In addition to the signal around –109 ppm, there are signals with very low intensity (compared to the Q_4 signal) at about –60 ppm, -8 ppm and 25 ppm. According to the literature, these signals represent $(O_3SiO)_3$**Si**Me, $(O_3SiO)_2$**Si**$(Me)_2$ and (O_3SiO)**Si**$(Me)_3$ moieties, respectively (where the bold **Si** represents the silicon atom on which attention is focused).[3-7] Among these three signals, the $(O_3SiO)_3$**Si**Me signal at –60 ppm is most intense, which indicates that, in the initial reaction $(O_3SiO)_3$**Si**Me moieties are formed more than the other two types of structures. This interpretation can not be supported directly by the ^{13}C

spectra, since the ^{13}C signal intensity of these species would be low and strongly overlapped with signals of more abundant species of the Al-Me type. Based on the fact that the ^{29}Si spectra of the initial reaction product show a small amount of signals intensity at 25 ppm (**Si**$(Me)_3$ moiety), the following process is proposed to rationalized for the formation of this moiety:

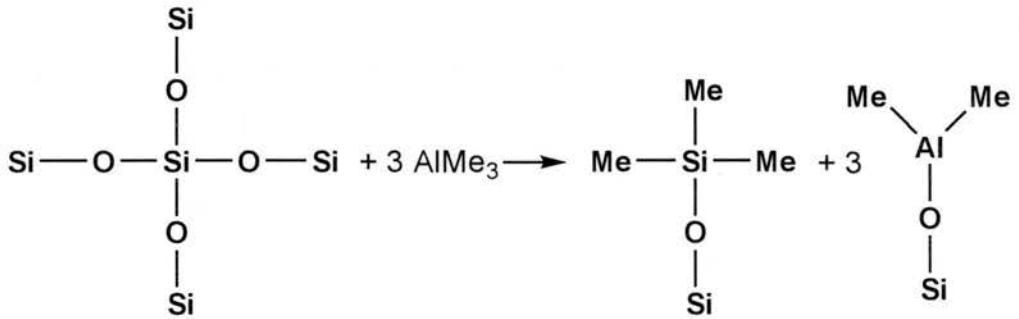

(4.1)

One can visualize this kind of process occurring via the following type of mechanism, in which $(SiO)_3SiMe$ and $(SiO)_2SiMe_2$ moieties are also formed:

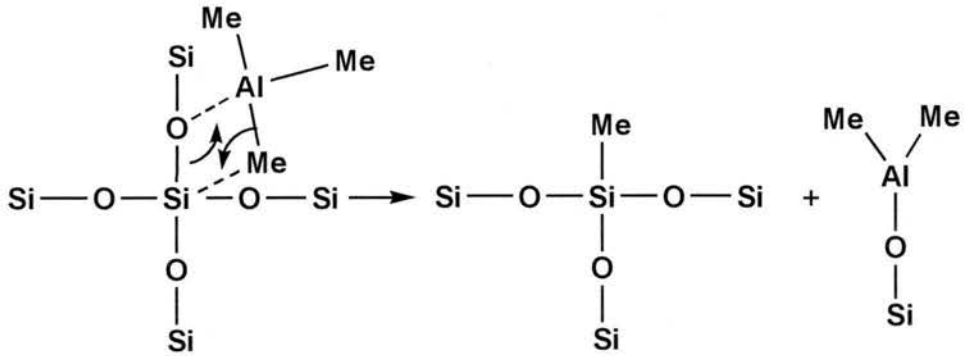

(4.2)

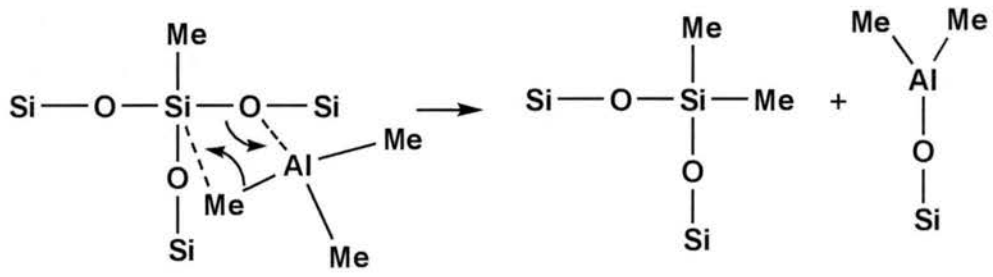

(4.3)

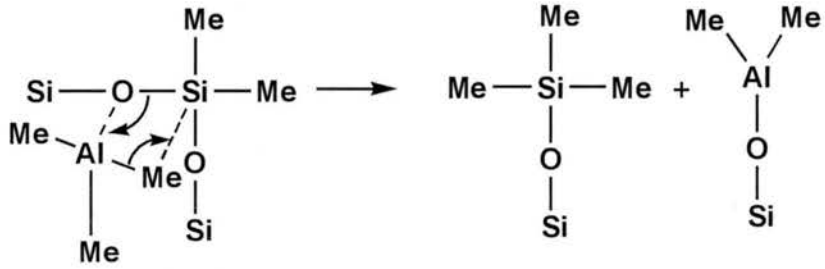

(4.4)

In addition to the reaction shown in Eq. 4.1, the $(SiO)_3$**Si**(OH) moiety might also be involved in the formation of Si-Me moieties on the surface, i.e., through reactions of the following type:

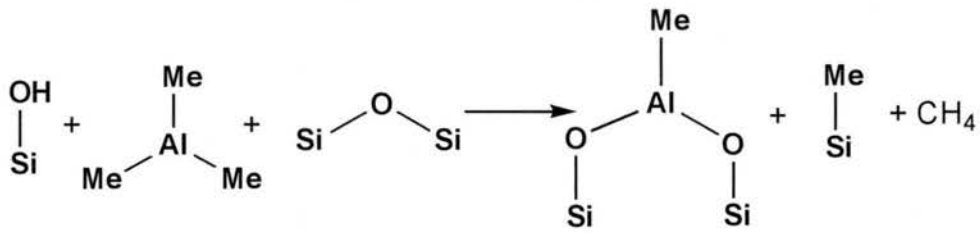

(4.5)

This type of conversion can be rationalized in terms of the following type of mechanism:

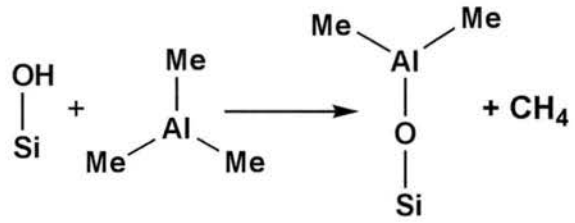

(4.6)

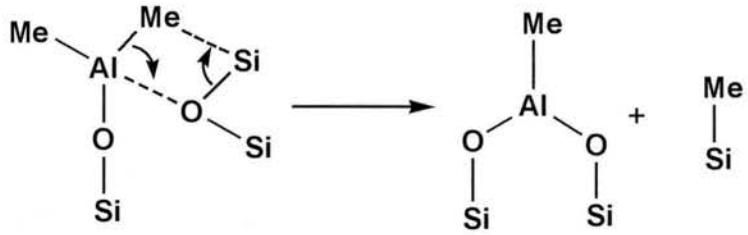

(4.7)

Results of the three-step H_2O treatment, ^{29}Si signals due to $SiMe_n$ peaks didn't show significant change, which indicates that all the H_2O treatments target the surface-attached Al-Me species and don't generate any change in Si-Me species.

According to the literature,[8] structures $(SiO)_3Si$-H and $(SiO)_2(OH)SiH$ would have signal located at –84 ppm and –74 ppm, respectively. None of these signals were observed from our ^{29}Si spectra of $AlMe_3$-reacted silica. Then structures $(SiO)_3Si$-H and $(SiO)_2(OH)SiH$ were not possible product from $AlMe_3$ treatment.

4.3. Chemical interpretation of ^{13}C NMR results.

Previously published $AlMe_3$/silica studies are based almost entirely on reactions occurring with gas-phase reagents, i.e., at a solid/gas interface.[3-7, 9-21]

On the basis of those studies, the following reactions have been suggested in the literature for the $AlMe_3$/silica gel system:

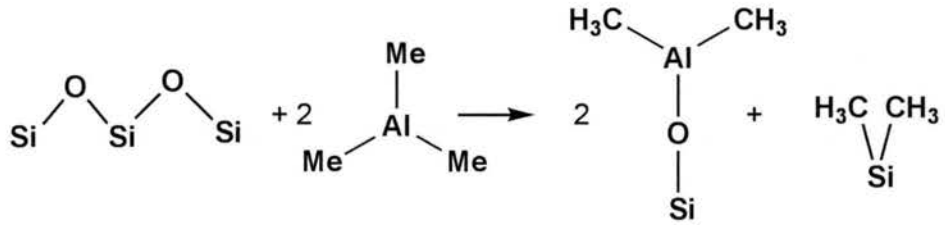

(4.8)

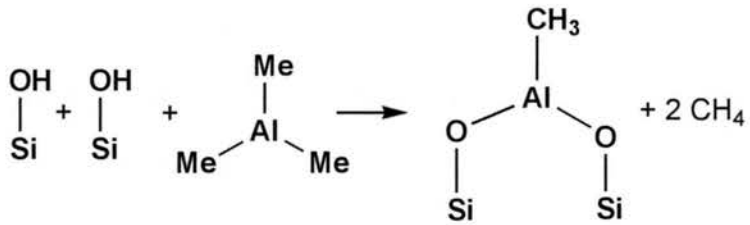

(4.9)

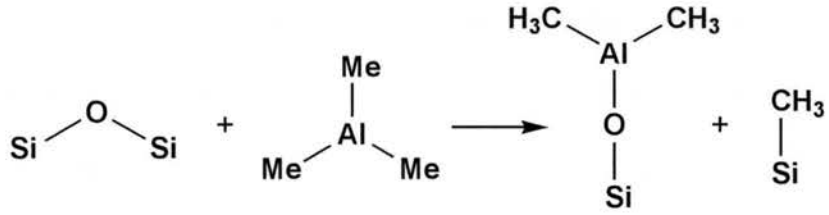

(4.10)

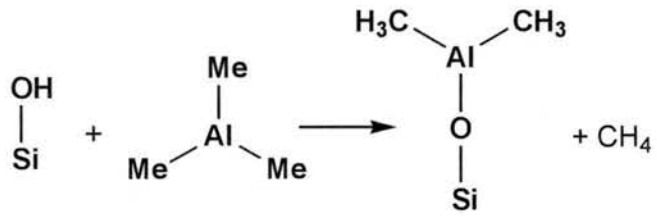

(4.11)

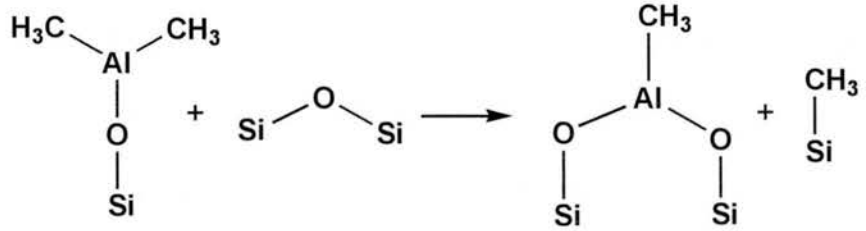

(4.12)

All of these equations show aluminum only in the 3-coordinate form, which is contra-indicated by the ^{27}Al NMR results (*vide infra*). Of course, ^{13}C NMR is not expected to be very sensitive to the Al coordination, so in most of this section we will not imply a specific Al coordination number. Later we will attempt to incorporate the conclusions drawn from the ^{27}Al NMR studies.

As indicated above, the ^{13}C spectra (Figure. 3.9.) show that the most populous carbon-containing moieties on the surface after the initial $AlMe_3$/silica reaction are Al-Me species ($AlMe_n$); this is also the class of structures that shows the most interesting chemistry in the H_2O treatments. The ^{13}C peaks of $Al(Me)_n$ moieties have a very large width (about 12 ppm), compared to the linewidths for other species shown in the spectra. At a MAS speed of 3.6 kHz, which was used in obtaining the ^{13}C spectra, the $AlMe_n$ signal shows substantial spinning sidebands, which indicates that the CSA (chemical shift anisotropy) of the $AlMe_n$ resonance is large. This spinning sideband behavior indicates that the Al-Me species are in a motionally restrained environment (otherwise, much of the CSA effect responsible for the spinning sidebands would be motionally averaged); this can be rationalized in terms of a view in which the Al-Me moieties interact with (e.g., are bonded to) the surface by more than one linkage. The large CSA behavior, which gives rise to large spinning side bands, was also observed for the ^{13}C peak at around 49 ppm (Figure 3.9), which has the second largest intensity among signals of surface methyl groups. This peak is due to Si-O-Me species and it also has substantial spinning sidebands, which indicate that the CSA is relatively large and not largely averaged by atomic-level motion

In the three-step H_2O treatment, the 'residual' ^{13}C peaks associated with diethyl ether do not change dramatically, implying that the residual diethyl ether is hard to remove from the surface. This indicats that the Et_2O moieties might experience some sort of strong interaction with other sites on the surface. Such sites would most probably be of the Al-Me type (with an electron deficient center), especially since the residual diethyl ether moieties are eliminated in the same step (final treatment with excess H_2O) in which Al-Me species are eliminated from the sample.

In the ^{13}C NMR spectra corresponding to the three-step H_2O treatments (Figure 3.9 and Figure 3.10), the peak at –12 ppm, which represent $Al(Me)_n$ moieties, is the peak corresponding to structures that are attacked by H_2O; this is the only ^{13}C peak for which there are substantial changes, in terms of signal intensity, from one sample to another. Only in the final hydrolysis step, in which a large excess of H_2O is used, does the Si-O-Me signal (49 ppm) in the ^{13}C spectra disappear; this implies that excess H_2O reacts with Si-O-Me linkages. The following reactions are suggested to describe chemical changes that occur with addition of H_2O (again, with no implied knowledge of the Al coordination number, which is indicated here as three only for simplicity):

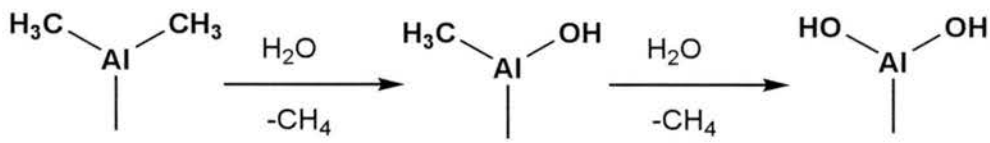

(4.13)

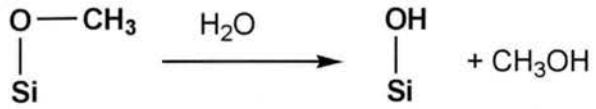

(4.14)

After the final hydrolysis reaction, peaks at 49 ppm and 0 ppm have disappeared; peaks at –2 ppm and –7 ppm are the only signals left in the ^{13}C NMR spectra. These results show that Si-Me and $Si(Me)_2$ species are inert to H_2O and are the only methyl groups remaining from the initial reaction.

Comparing the ^{13}C NMR spectra of sample C-2 (2^{nd} H_2O treatment) and C-3 (3^{rd} eq. H_2O treatment) in Figure 3.9 and Figure 3.10, on sees that the signal intensities due to Si-O-Me (49 ppm) and Al-Me (0 ppm) *both* dropped as a result of the treatment with a 3^{rd} eq. of H_2O; this implies that, after all $Al(Me)_2$ moieties have reacted with H_2O, the reactivities of Si-O-Me and AlMe toward H_2O may be roughly similar.

Comparing the ^{13}C NMR results (Figure 3.9 and Figure 3.10), from sample C-1 to those of sample C-3, along with the corresponding intensity drop for $AlMe_2$ species, the signal intensity due to diethyl ether peaks also dropped upon treatment with H_2O. This implies that it is the $AlMe_2$ species that has a strong interaction with diethyl ether molecules and helps retain them on the surface.

4.4. Chemical interpretation of ^{27}Al NMR results.

4.4.1. Initial reaction products (A).

^{27}Al MAS NMR results in Figure 3.9 show three apparent types of signals in the spectra, with maxima at about 6 ppm, 32 ppm and 54 ppm; these features likely represent structures of the 4-coordinate (tetrahedral Al), 5-coordinate (pentahedral Al) and 6-coordinate (octahedral Al) Al types, respectively [4, 5, 22-25]. On the initial $AlMe_3$-reacted silica, 5-coordinate Al is apparently the major Al structure on the surface; 4-coordinate and 6-coordinate Al structures are apparently present in small amounts. Here we propose that 5-coordinate species might be of types I to VI.

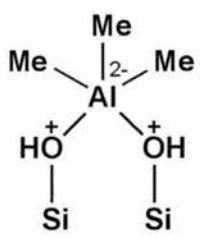

Type I

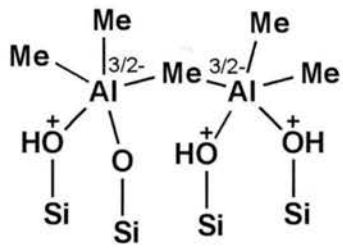

Type II

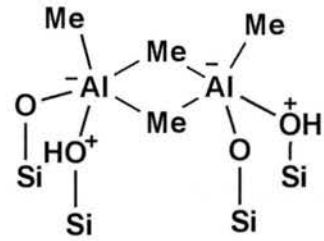

Type III

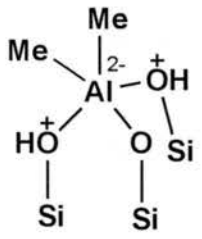

Type IV

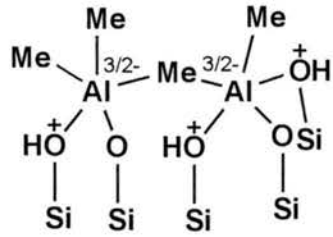

Type V

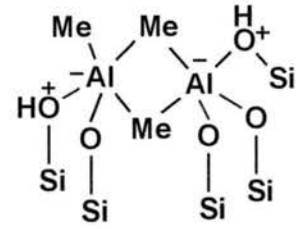

Type VI

Regarding Types IV to VI, in which an Al atom is connected to three O atoms of the silica surface, one might question the possibility of formation of this

kind of structure. The following picture is a top-down representation of 5-coordinate aluminum species on a beta-cristobalite <111> face. This surface is commonly used as a model for single silanols on a silica surface.[26]

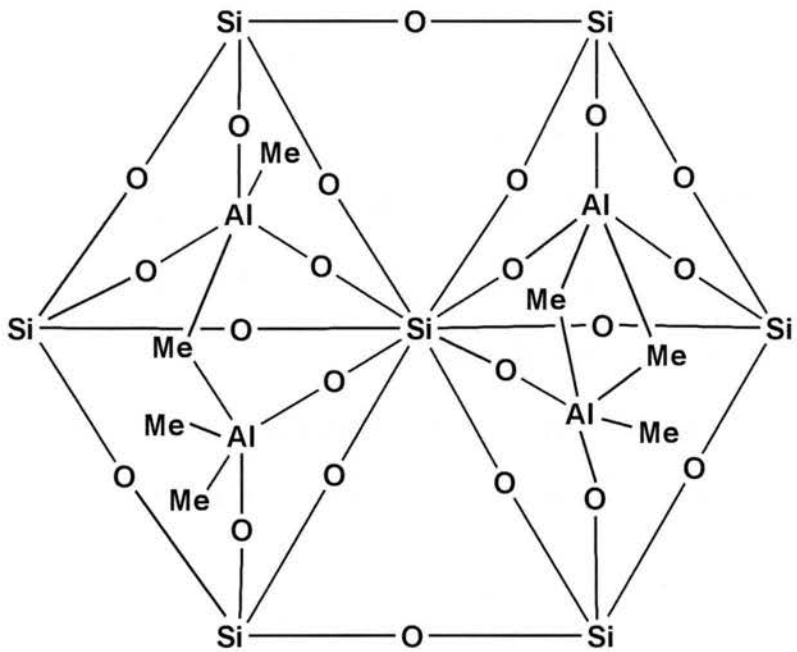

The normal inter-atomic distances represented in the above picture are:[27-35]

Si-Si = 5.04 Å

Si-O = 1.60 Å

Al-O = 1.78 Å

Al-C = 1.97 Å

From geometrical considerations, it appears that formation of the 5-coordinate structures of types I, II and III, each of which has two surface O atoms

attached to each Al atom, should be favorable. 5-coordinate structures of types IV, V and VI, in which three O atoms of silica are attached to an individual Al atom, would likely be very strained, because the possible positions of the Al atom are restricted by three surface Si-O-Al linkages and by the shared-Me linkage. The left part of the picture above simulates the geometry of a type-V structure and the right part of the figure simulates the geometry of a type-VI structure. The C-Al-C angle in the Al-$(Me)_2$-Al bridge (right part of the picture) is about 84.4°, which is a strained angle compared to the C-Al-C angle (102°) in the $AlMe_3$ dimer;[36] but this might still be possible to form. On the basis of only the ^{27}Al spectra, all of the above structures (type I through type VI) are possible; we cannot at this time distinguish among them by just a simple ^{27}Al MAS spectrum.

The ^{13}C relaxation results (see section 3.3.4) concluded that the surface methyl groups in $AlMe_n$ moieties are very immobile. This characteristic might due to the Al-Me-Al bridges formed on the surface. Thus, among the 5-coordinate Al structures proposed above, types II, III, V and VI are likely to be the $AlMe_n$ species responsible for the most intense signal in ^{13}C spectrum (-12 ppm), and these types structure manifest the Al-Me-Al bridging characteristics.

The following are hypothetical reaction schemes that could account, in principle, for all the possible 5-coordinate structures introduced above.

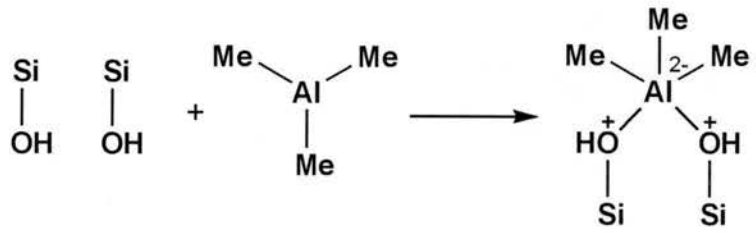

Type I

(4.15)

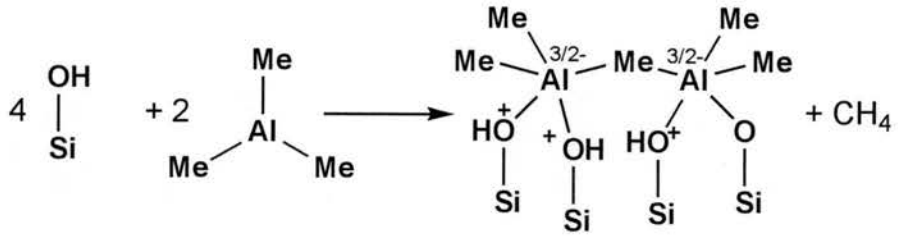

Type II

(4.16)

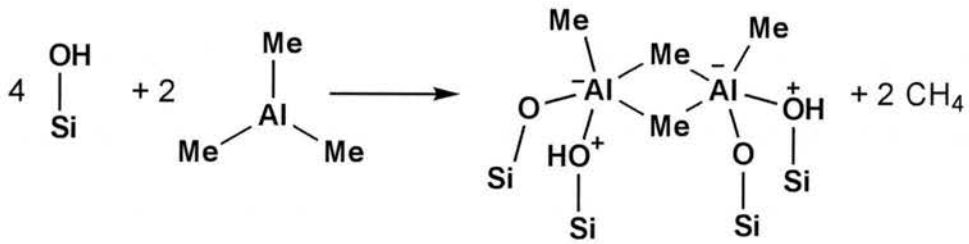

Type III

(4.17)

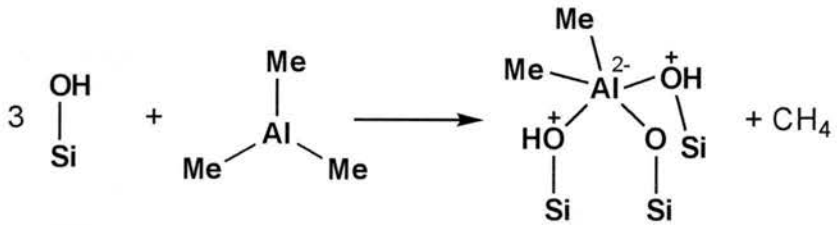

Type IV

(4.18)

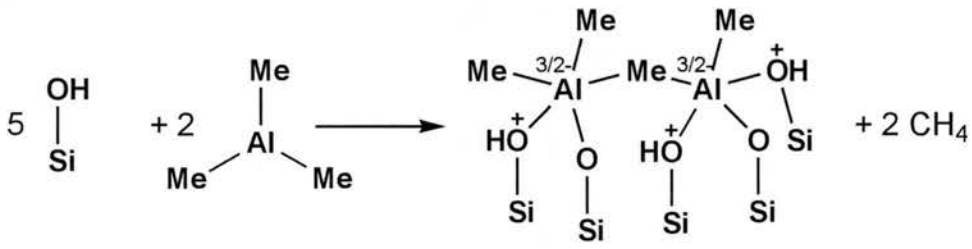

(4.19)

Type V

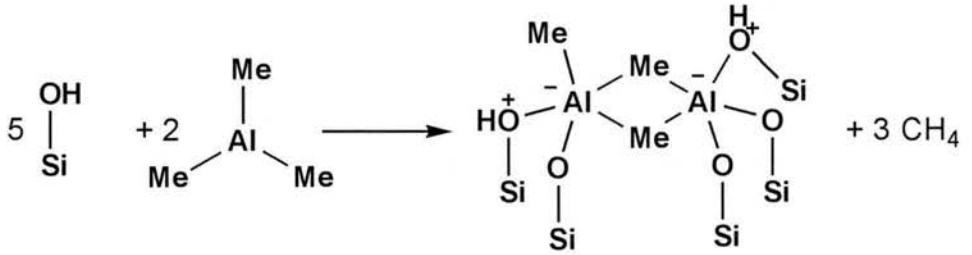

(4.20)

Type VI

In the ^{27}Al spectrum of sample A (Figure 3.9), besides the 5-coordinate resonance shown, there are also weaker signals at 54 ppm and 6 ppm, which represent 4-coordinate and 6-coordinate structures, respectively. This implies that 4-coordinate and 6-coordinate structures are present in the product mix. The following are proposed reaction schemes for the generation of these two types of structures:

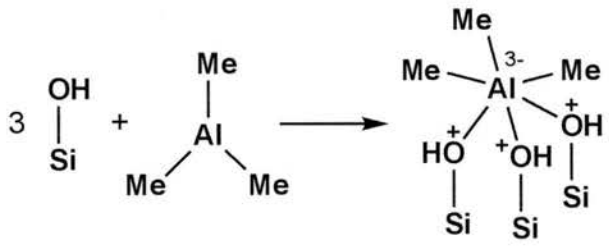

(4.21)

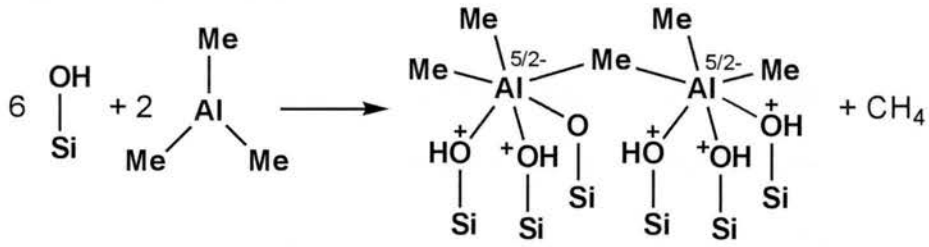

(4.22)

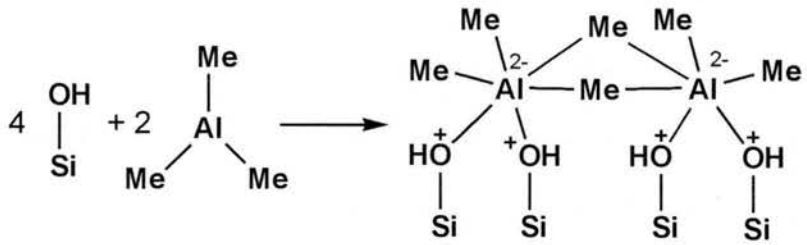

(4.23)

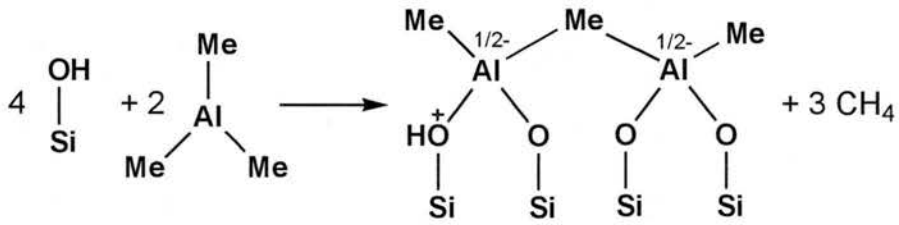

(4.24)

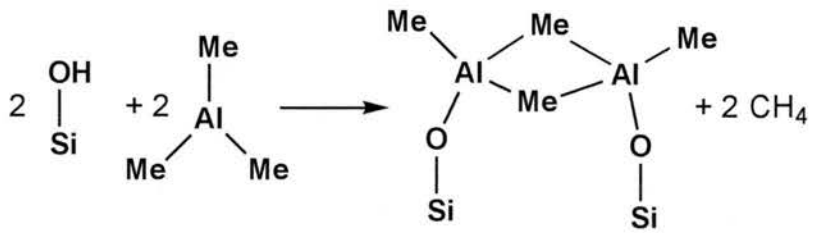

(4.25)

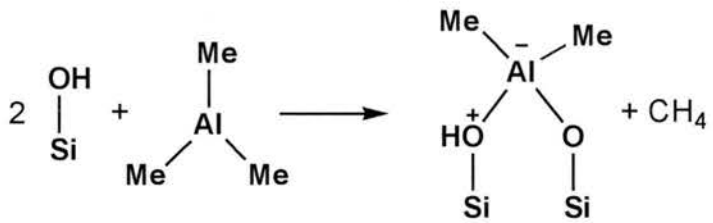

(4.26)

4.4.2. Ether wash product (B).

Surface species of types I through VI would be expected to be substantially reactive toward treatment with potential electron donors, e.g., when the surface is washed with diethyl ether; the O atom of diethyl ether is electron rich and would be able to coordinate with the Al atom or even replace the interaction between the Al atom and methyl in the Al-Me-Al linkage. The changes that might be expected for each of the above 5-coordinate structures as a result of in the ether wash treatment are shown in the following scheme:

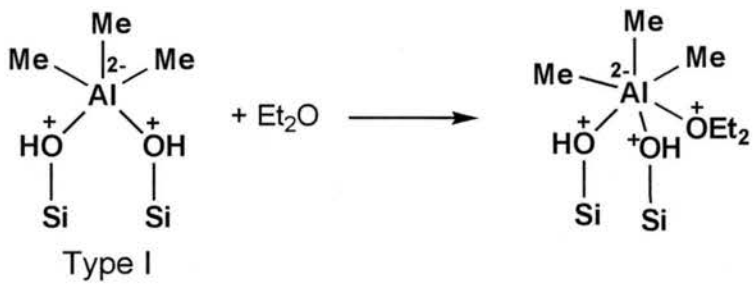

Type I

(4.27)

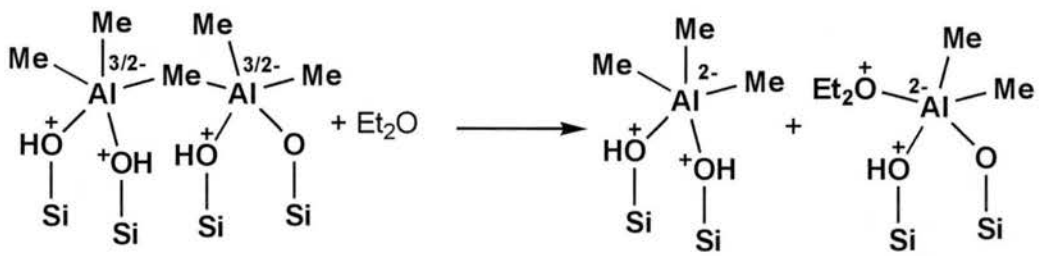

Type II

(4.28)

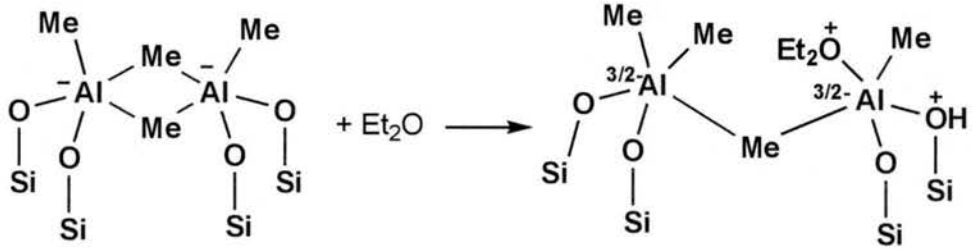

Type III

(4.29)

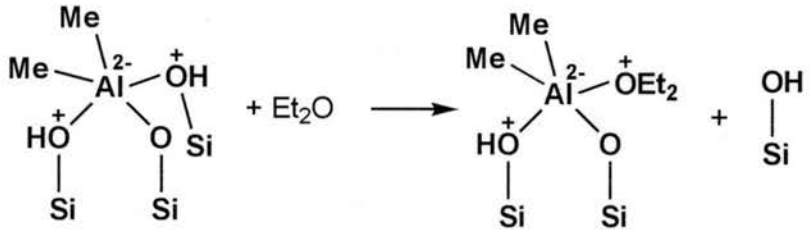

Type IV

(4.30)

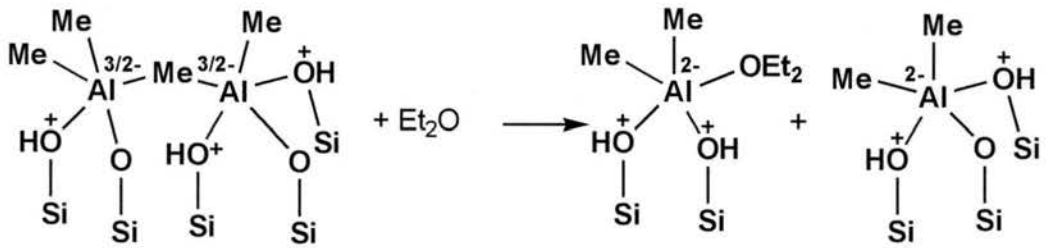

Type V

(4.31)

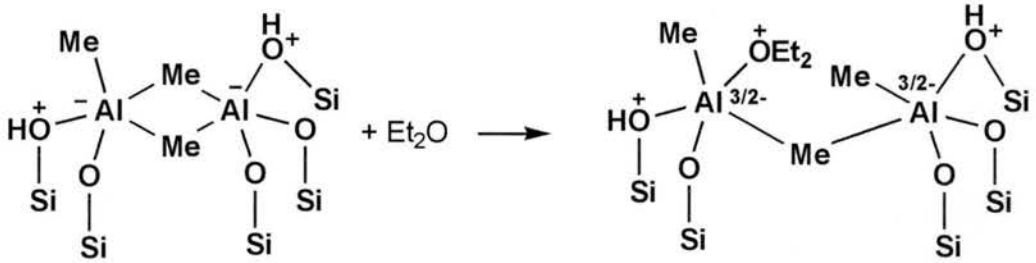

Type VI

(4.32)

The 4-coordinate and 6-coordinate structures might undergo the following kinds of changes:

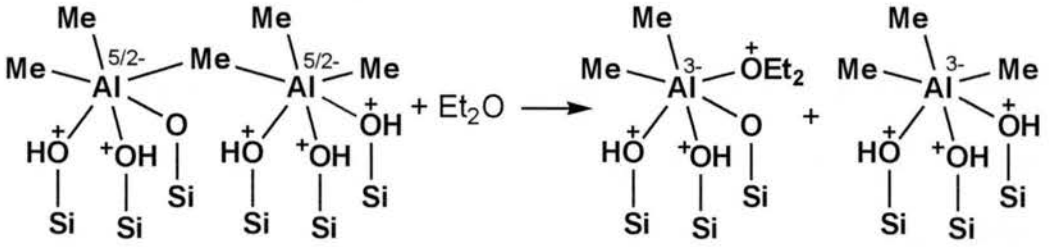

(4.33)

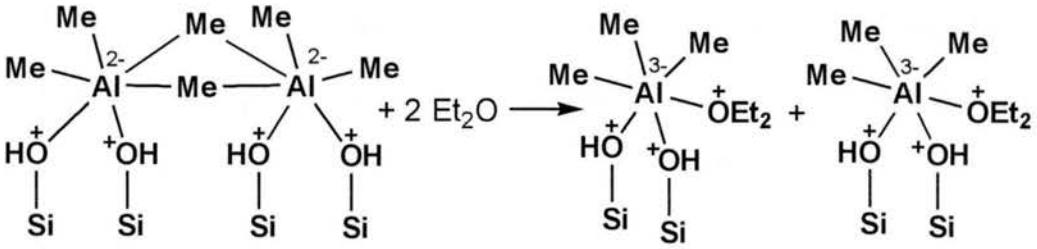

(4.34)

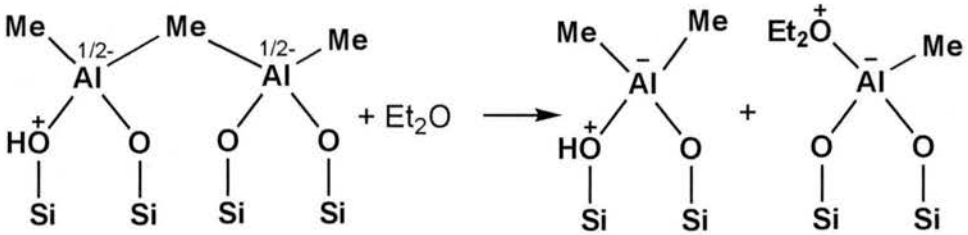

(4.35)

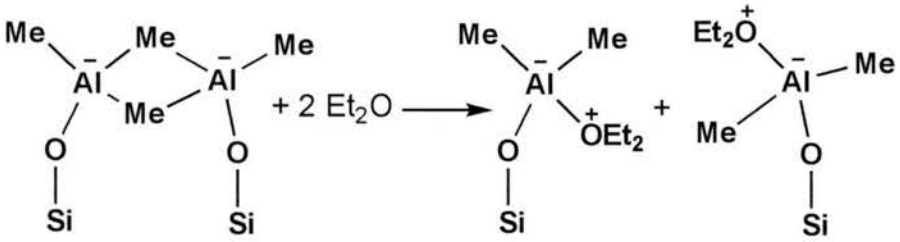

(4.36)

These kinds of transformations would also explain why the ^{13}C spectra of Figure 3.9 show that a significant amount of ether is retained in the ether-washed sample even though it has been "dried" using a 10^{-3} torr vacuum; this ^{13}C NMR result reinforces the argument that there is a strong interaction between ether molecules and the surface species generated in the initial $AlMe_3$/silica reaction

4.4.3. Water treatment products (C and D).

Figures 3.9 and 3.10 show that, with the stepwise addition of H_2O, which would be expected to react with surface $Al(Me)_n$ moieties, the intensity of 5-coordinate Al species decreases, while intensities of 4-coordinate and 6-coordinate species increase. In the ^{27}Al spectrum of sample D, after the final workup/hydrolysis step, we see that 4-coordinate and 6-coordinate Al species become the major structures on the surface and the 5-coordinate Al population on the surface has almost disappeared. These kinds of changes can be rationalized as follows:

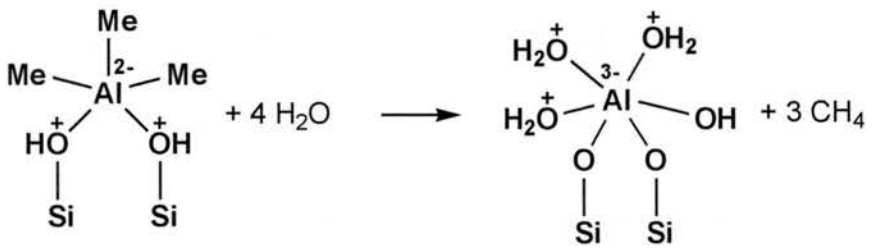

(4.37)

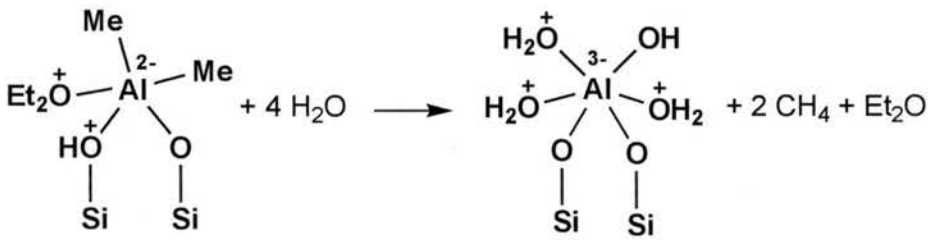

(4.38)

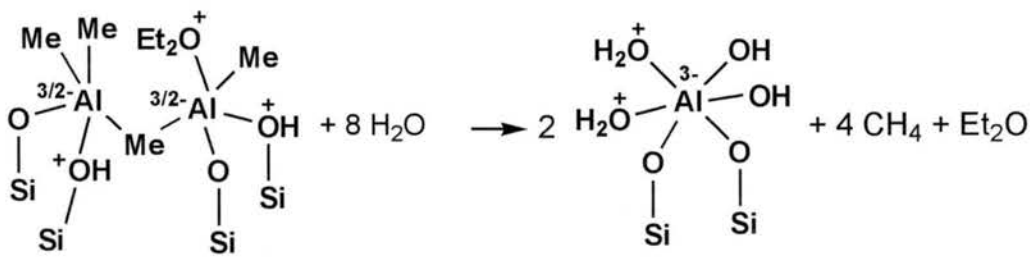

(4.39)

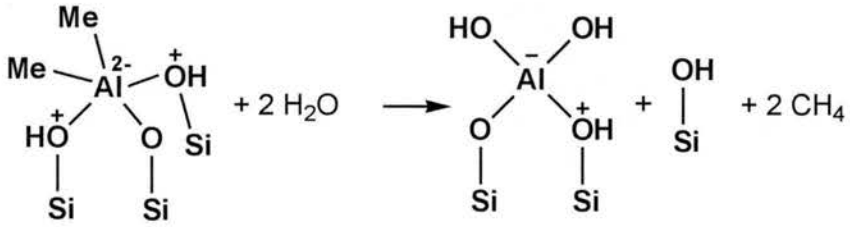

(4.40)

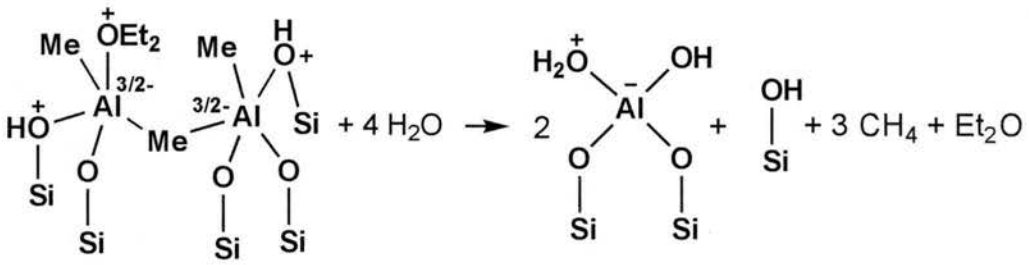

(4.41)

This scheme is consistent with the fact that the 5-coordinate structures of $Al(Me)_n$ species (I, II and III) are converted by water to 4-coordinate and 6-coordinate structures.

Under H_2O treatment, 4-coordinate and 6-coordinate intermediates might undergo the following kinds of changes:

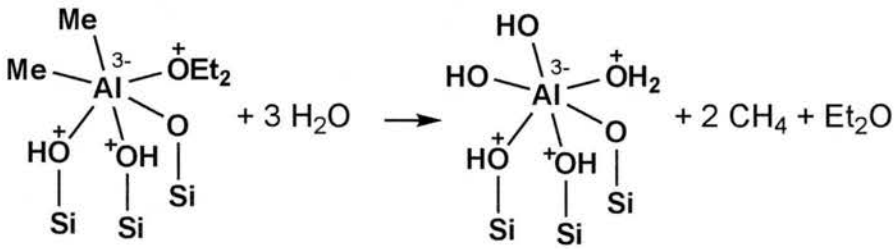

(4.42)

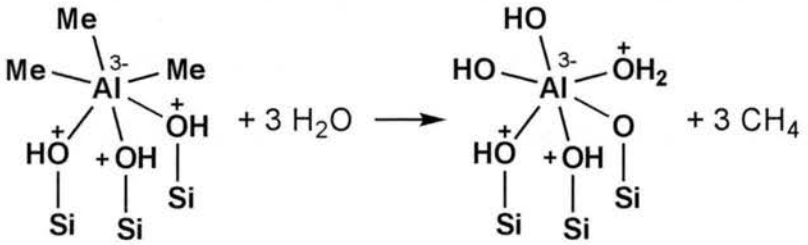

(4.43)

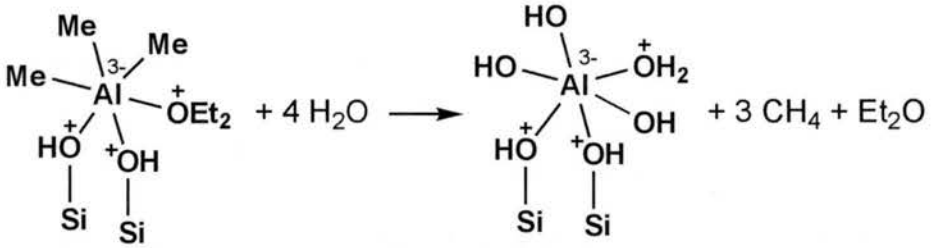

(4.44)

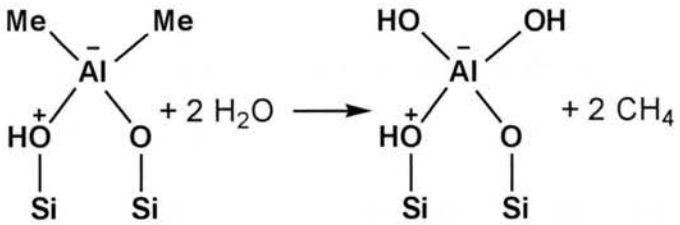

(4.45)

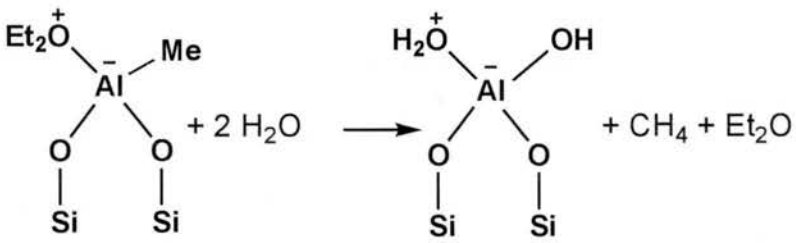

(4.46)

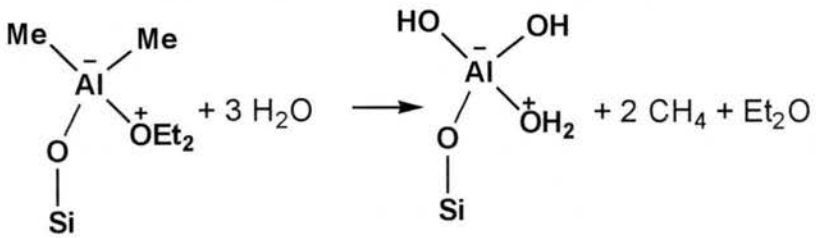

(4.47)

After final hydrolysis, all the $Al(Me)_n$ species turn into Al structures with tetrahedral and octahedral coordinations. These kinds of structures and this kind of transformation have never before been reported for reactions between $AlMe_3$ and silica.

4.5. Spin counting results on surface methyl groups and CH_4 tracking during the initial reaction.

Figure 3.38 and Figure 3.39 summarize the tracking of methyl groups in repetitive experiments on the $AlMe_3/SiO_2$/toluene and $AlMe_3/SiO_2$/cyclohexane systems. The CH_4 released in both reaction systems (toluene or cyclohexane) are about the same, which implies that there is no significant difference in the manner of generating CH_4; when an Al-Me group encounters an active hydrogen, it will release Me-H, methane. But, if one further compares the number of methyl groups observed on (attached somehow to) the surface after the initial reaction, the difference observed between solvent systems implies that there are different solvent effects in attaching and/or keeping the methyl groups on the surface (as detected in ^{13}C NMR).

Among the surface moieties formed in the initial $AlMe_3$/silica reaction, Si-O-Me, $Si(Me)_n$ and $Al(Me)_n$, the ^{13}C spin counting results showed that $Al(Me)_n$ are the most moieties formed in the reaction. The $AlMe_n$ moieties are about 70% of the total amount of surface-attached methyl groups detected in the ^{13}C NMR. The amount of Si-OMe, $Si(Me)_3$ and $Si(Me)_2$ moieties are approximately equal to each other, and together amount to about 30% of the total amount of methyl

groups detected on the surface. These results are consistent with the view that the dominating reactions occurring on the surface are between $AlMe_3$ and Si-OH groups, which generate $AlMe_n$ moieties on the surface.

The silica gel employed in this study was heated only at 150 °C before it was treated with $AlMe_3$. At this temperature, only the physisorbed water on the surface was removed; and most of the surface Si-OH groups remain for the $AlMe_3$ reaction. On this kind of silica surface, the reaction between $AlMe_3$ and surface Si-OH groups would be the most important one, which is consistent with what was observed in the ^{13}C spin counting results.

Since the major reactions occurring on the surface were between $AlMe_3$ and surface Si-OH groups, it is convenient, in examining the role of solvent, to consider the ratio of the number of methyl groups attached to the surface (Me(surface)) to the number of silanols on the unreacted surface. This **Me(surface)**/Si-**OH** ratio is about 0.6 for the toluene reaction and about 0.9 for the cyclohexane reaction. This means that in the toluene reaction each surface Si-O derived from Si-OH group has, on average, about 0.6 Me attached. About 0.9 Me groups, on average, are attached to each surface Si-O group derived from Si-OH in the cyclohexane reaction. This implies that, among the 5-coodinate Al structures introduced above:

1) structures of type I and type II (in section 4.4.1) are not the major products in the initial reaction for either solvent system; each of these two structures has a **Me(surface)**/Si-**OH** ratio >1.

2) structures of type III and V might be the major products in the cyclohexane reaction system, since type III has a **Me(surface)**/Si-**OH** ratio of 1 and type V has a **Me(surface)**/Si-**OH** ratio of 0.8. This conclusion is also consistent with relaxation results from ^{13}C NMR, which indicated that methyl groups in the $AlMe_n$ moieties (with a proton T_1 value as long as 7.2 s) are more likely to be in Al-Me-Al linkage.

3) structures of type IV and VI might be the major products on the surface in the toluene reaction, since type IV has **Me(surface)**/Si-**OH** ratio of 0.67 and type VI has **Me(surface)**/Si-**OH** ratio of 0.6.

From the methyl tracking information in Figures 3.38 and 3.39, one sees that the Al-Me detected by liquid-sample ^{13}C NMR in the cyclohexane system is less than it is for the toluene system. In the $AlMe_3$/silica reaction, $AlMe_3$ was added in excess, based on 'assuming' only one of the three methyl groups will react with Si-OH. As one can see from the results of liquid-sample ^{13}C NMR, there was a large amount of unreacted Al-Me left in the supernatant liquid from the reaction. These unreacted Al-Me species are still chemically reactive; and the Al-Me species in cyclohexane might be more chemically reactive than that is in toluene, because toluene is an electron-rich solvent (compare to cyclohexane) and might be able to stabilize unreacted Al-Me species. In the cyclohexane system, unreacted Al-Me species in the supernatant liquid might undergo chemical changes (e.g., turned to CH_4) before it was examined with liquid-sample ^{13}C NMR. This is our explanation on the fact that there was less Al-Me detected

in the liquid-sample ^{13}C NMR experiment in the cyclohexane reaction case than that was in the toluene case.

In terms of chemical properties, the main difference between toluene and cyclohexane is the presence of the aromatic ring in the toluene case; this is an electron-rich structure, and cyclohexane is a less reactive or interactive molecule, compared to toluene, in this sense. The aromatic ring in toluene might take part in interactions with Al-Me species that are not possible for cyclohexane. This interaction between Al and a benzene ring could partially attenuate the reactivity of Al-containing intermediates generated in the initial $AlMe_3/SiO_2$ reaction, so that some Al-Me groups might not further react with surface Si-OH; instead, some of the $AlMe_3$ might remain in the supernatant liquid. In the presence of toluene, surface Si-O moieties are not the only structures that can provide electrons to (for sharing with) Al-Me species. In contrast, cyclohexane doesn't have this electron donating property, which could result in more reactive Al-Me moieties to attach to the surface (through Si-O); without stabilization from interaction with an electron-donating solvent species, the unreacted Al-Me in the supernatant liquid would therefore be more reactive than in the toluene case.

That the aromatic ring in toluene might take part in interactions with Al-Me species that are not possible for cyclohexane is consistent with the following rationalization of the relaxation results. If one examines the changes in CH_3 proton T_1 values from the initial reacted surface to the ether treated surface, one finds that the proton T_1 values change less in the toluene system than for the

cyclohexane system. This could suggest that toluene molecules might interact with surface species in a manner in which there is not as much Al-Me-Al bridge formation as in the cyclohexane system. Instead of Al-Me-Al bridges, structures of the following type might form in the toluene case:

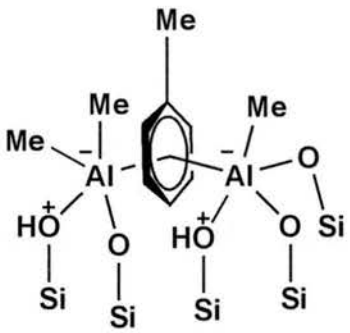

Type V'

This would lead to less Al-Me-Al bridges formed among the surface $Al(Me)_n$ species. Thus, the motional restriction that methyl groups might experience in the $AlMe_3$/toluene-reacted surface is less than it is in the $AlMe_3$/cyclohexane-reacted surface. This may explain why we observed smaller proton T_1 values of $Al(Me)_n$ (about 5 s) in the toluene system than in the cyclohexane system (about 7 s) for the initial $AlMe_3$-reacted sample.

In the ether washed sample, since part of the Al-Me-Al interactions in the $AlMe_3$/toluene-reacted surface already been replaced with Al-toluene-Al interaction, the changes:

$$\text{Al-Me-Al} + Et_2O \rightarrow \text{Al-OEt}_2 + \text{Me-Al} \qquad (4.48)$$

in which result reducing proton T_1 values, were not dramatic in toluene reaction system. In contrast, in the initial $AlMe_3$/cyclohexane-reacted surface, most of methyl groups were involved in Al-Me-Al interactions, since cyclohexane didn't play the same role as toluene did. With introducing ether molecules onto the surface, which released the motion restriction on Me groups according to Eq. 4.48, the change of proton T_1 values was dramatic in cyclohexane reaction system compare to that in the toluene system.

4.6. Overall composite chemical trends in the $AlMe_3$/silica reaction.

In the overall reaction between $AlMe_3$ and the silica surface, surface-attached $AlMe_n$ moieties constitute the major products of the initial reaction and most of those moieties are in a 5-coordination state for aluminum. This coordination number for Al was obtained via the ^{27}Al NMR spectrum and has not been reported in previous publications. The high coordination number for Al atoms (4-, 5- and 6-) on the surface results from the electron-deficient characteristics of $AlMe_3$. With $AlMe_n$ moieties attached, the surface inherits the characteristic of being electron-deficient, which can cause a polarizable solvent (e.g., toluene, ether) to have a substantial interaction with these surface moieties.

The $AlMe_n$ moieties attached on the surface are unstable toward H_2O, even in limited amounts, in the water/ether treatments that follow the ether wash. As a result of H_2O treatments, the initial 5-coordinate surface moieties are converted to 4-coordinate and 6-coordinate Al-O moieties attached on the surface. As represented in Equations. 4.28, 4.31 and Eq. 4.33 ~ Eq. 4.36,

bridged methyl groups in the 5-coordinated Al moiety are released as CH_4 and replaced with O atoms (in the form of OH, or coordinated with Et_2O), which are more electron-rich centers than are methyl groups.

In previously published papers on $AlMe_3$/silica reactions, the formation of Si-O-Me was observed in Lakomaa's paper,[7] in which the atomic layer expitaxy method (solid-gas phase) was used for the reaction between silica and $AlMe_3$. In Lakomaa's work, the formation of Si-O-Me was observed with a relatively low reaction temperature (reaction at 80 °C generated Si-O-Me; reaction at 200 °C did not show Si-O-Me); and the temperature at which the silica surface was preheated did not affect the formation of Si-O-Me (silica preheated at 200 °C or at 800 °C). The reaction time in Lakomaa's work was 2-6 hr. Another study in which the formation of Si-O-Me was observed is Yate's work,[14] based on the solid-gas phase reaction between silica and $AlMe_3$. In Yate's work, the reaction was carried out in a FTIR cell for only a few minutes. Except Lakomaa and Yate's work, other published works about $AlMe_3$/silica reaction (gas/solid phase or liquid/solid phase) did not report the presence of Si-O-Me.[3-6, 9-13, 15-21]

The formation of Si-O-Me was observed in this study. As suggested in previously published work,[14] the formation of Si-O-Me linkages can be rationalized in the following kind of scheme:

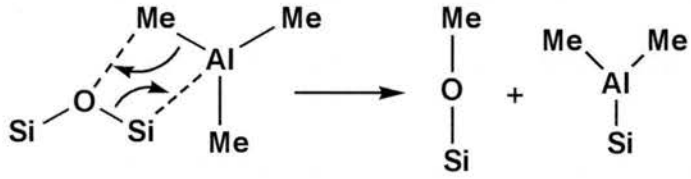

(4.49)

The Al-Si linkage visualized in this hypothesized route for forming Si-O-Me is not distinguished in any of the ^{27}Al, ^{13}C and ^{29}Si NMR spectra of this, or any other, study. No report has been published for unequivocally identifying Al-Si linkages and our NMR results can't verify this Si-Al hypothesis.

A possible reason for seeing more Si-O-Me produced in this study than in previously published work may be the longer reaction time used in this study, four hours compared to about ten minutes in previous work.[3, 4, 6, 13-16]

Another variation in the experimental conditions that might affect the formation of Si-O-Me linkages, is the preparation temperature of the silica gel. In our study, the silica surface was dried at 150 °C, at which temperature only physisorbed H_2O is removed from the surface. We know that at this temperature hydrogen bonding between surface silanols is retained, and no significant dehydration (dehydroxylation-condensation) occurs between surface silanols.[26] In most of the previous work, the silica gel was prepared att 400 °C, or even higher temperatures, which means that the silica surface has been heated very aggressively and only mainly single silanols and Si-O-Si bridges are left on the surface.[3, 4, 6, 7, 13-16] Currently we don't have data on a reaction of a silica surface

that has been prepared more aggressively (at high temperature); this might be an interesting experiment to carry out in the future.

Taken together, all of our result can be interpreted in terms of Eq. 4.1 to Eq. 4.49 to describe the whole pattern of $AlMe_3/SiO_2$ reactions.

4.7. Suggestions for future work.

It would be interesting to look at the reaction between $AlMe_3$ and silica gel samples for which the surface has been dried more aggressively. In this study silica gel was dried under vacuum at 150 °C, which removes only the physisorbed water from the surface; hydrogen bonding between surface silanols still remains and there are no reactive Si-O-Si moieties formed from dehydration between surface silanols.[26] For a silica surface that has been dried more aggressively, such as at 500 °C, all the remaining silanols left on the surface will be 'isolated' (non-hydrogen bonded) silanols and all these silanols will be relatively far from each other. For a silica gel surface that has been dried at about 300 °C, most or all of the hydrogen bonded silanols will have been converted to bridged Q_4 structures. Reaction between $AlMe_3$ and these two kinds of surface sites would be interesting.

In this work, the cyclohexane reaction system was not studied by ^{27}Al and ^{29}Si NMR. Although the chemistry seen in ^{13}C NMR didn't show huge differences from the toluene reaction system, ^{27}Al NMR and ^{29}Si NMR are still worth examining for the additional detail that might be provided.

Relaxation time studies could be extended further to the stepwise H_2O-treated samples (C-1, C-2 and C-3), which might show altered relaxation behavior relative to that of the first two samples. With stepwise H_2O treatment, the relaxation time of $AlMe_n$ moieties would be expected to be smaller than for the species on the initially reacted surface, because any Al-Me-Al linkages, which restrain the motion of Al-attached methyls, would break down to Al-Me and Al-OH or be replaced with Al-Me and Al-OEt_2 (with limited amount of H_2O in diethyl ether) introduced onto the surface.

References

1. Engelhardt, G.; Michel, D., *High-resolution solid-state NMR of silicates and zeolites*. John Wiley & Sons: Chichester, New York, 1987; p 215-217.

2. MacKenzie, K. J. D.; Smith, M. E., *Multinuclear solid-state NMR of inorganic materials*. Pergamon: Oxford; New York, 2002; p 205-207.

3. Uusitalo, A. M.; Pakkanen, T. T.; Kroger-Laukkanen, M.; Niinisto, L.; Hakala, K.; Paavola, S.; Lofgren, B., Heterogenization of racemic ethylenebis(1-indenyl)zirconium dichloride on trimethylaluminum vapor modified silica surface. *J. Mol. Catal. A* **2000,** *160*, 343-356.

4. Anwander, R.; Palm, C.; Groeger, O.; Engelhardt, G., Formation of Lewis Acidic Support Materials via Chemisorption of Trimethylaluminum on Mesoporous Silicate MCM-41. *Organometallics* **1998,** *17*, 2027-2036.

5. Puurunen, R. L.; Root, A.; Sarv, P.; Haukka, S.; Iiskola, E. I.; Lindblad, M.; Krause, A. O. I., Growth of aluminium nitride on porous silica by atomic layer chemical vapour deposition. *Appl. Surf. Sci.* **2000,** *165*, 193-202.

6. Puurunen, R. L.; Root, A.; Haukka, S.; Iiskola, E. I.; Lindblad, M.; Krause, A. O. I., IR and NMR Study of the Chemisorption of Ammonia on Trimethylaluminum-Modified Silica. *J. Phys. Chem. B* **2000,** *104*, 6599-6609.

7. Lakomaa, E. L.; Root, A.; Suntola, T., Surface reactions in Al_2O_3 growth from trimethylaluminium and water by atomic layer epitaxy. *Appl. Surf. Sci.* **1996,** *107*, 107-115.

8. Pesek, J. J. In *Conversion of Oxide Surface to Hydride Surface*, Symposium on Chemically Modified Surfaces, Pesek, J. J.; Leigh, I. E., The Royal Society of Chemistry, Thomas Graham House, Science Park, cambridge; p 1-23.

9. Low, M. J. D.; Severdia, A. G.; Chan, J., Reactive silica. XV. Some properties of solids prepared by the reaction of trimethylaluminum with silica. *J. Catal.* **1981,** *69*, 384-391.

10. Murray, J.; Sharp, M. J.; Hockey, J. A., Polymerization of propylene by the $SiO_2/TiCl_4/AlMe_3$ system. *J. Catal.* **1970,** *18*, 52-56.

11. Peglar, R. J.; Murray, J.; Hambleton, F. H.; Sharp, M. J.; Parker, A. J.; Hockey, J. A., Chemical production and trapping of methyl radicals at silica surfaces. *J. Chem. Soc. A* **1970**, 2170-2172.

12. Murray, J.; Jones, P.; Hockey, J. A., Reactions of silica surfaces with hydrogen sequestering agents. *Trans. Faraday Soc.* **1971,** *67*, 848-853.

13. Peglar, R. J.; Hambleton, F. H.; Hockey, J. A., Surface structure and catalytic cracking properties of silicon oxide-boron trichloride, silicon oxide-trimethylaluminum, and silicon oxide-aluminum trichloride systems. I. Infrared and analytical studies. *J. Catal.* **1971,** *20*, 309-320.

14. Yates, D. J. C.; Dembinski, G. W.; Kroll, W. R.; Elliott, J. J., Infrared studies of the reactions between silica and trimethylaluminum. *J. Phys. Chem.* **1969,** *73*, 911-921.

15. Kinney, J. B.; Staley, R. H., Reactions of titanium tetrachloride and trimethylaluminum at silica surfaces studied by using infrared photoacoustic spectroscopy. *J. Phys. Chem.* **1983,** *87*, 3735-3740.

16. Bartram, M. E.; Michalske, T. A.; Rogers, J. W., Jr., A reexamination of the chemisorption of trimethylaluminum on silica. *J. Phys. Chem.* **1991,** *95*, 4453-4463.

17. Jun, S.; Ryoo, R., Aluminum Impregnation into Mesoporous Silica Molecular Sieves for Catalytic Application to Friedel-Crafts Alkylation. *J. Catal.* **2000,** *195*, 237-243.

18. Kleisner, R. J.; Koeck, B. H.; Phillips, M. R.; Wieland, J. A.; Gutow, J. H.; Boiadjiev, V.; Tysoe, W. T., A system based on metal alkyl species that forms chemically bound organic overlayers on hydroxylated planar surfaces. *Thin Solid Films* **2001,** *381*, 10-14.

19. Boiadjiev, V.; Blumenfeld, A.; Gutow, J.; Tysoe, W. T., Infrared and NMR Spectroscopic Studies of n-Alkanethiols Chemically Grafted on Dimethylzinc-Modified Silica Surfaces. *Chem. Mater.* **2000,** *12*, 2604-2613.

20. Yamamoto, K.; Tatsumi, T., Remarkable improvement in hydrothermal stability of MCM-41 by surface modification with Grignard reagents. *Chem. Lett.* **2000**, 624-625.

21. Tao, T.; Maciel, G. E., Reactivities of Silicas with Organometallic Methylating Agents. *J. Am. Chem. Soc.* **2000,** *122*, 3118-3126.

22. Risbud, S. H.; Kirkpatrick, R. J.; Taglialavore, A. P.; Montez, B., Solid-state NMR evidence of 4-, 5-, and 6-fold aluminum sites in roller-quenched SiO_2-Al_2O_3 glasses. *J. Am. Ceram. Soc.* **1987,** *70*, C/10-C/12.

23. Schneider, H.; Voll, D.; Saruhan, B.; Sanz, J.; Schrader, G.; Ruescher, C.; Mosset, A., Synthesis and structural characterization of non-crystalline mullite precursors. *J. Non-Cryst. Solids* **1994,** *178*, 262-71.

24. Schneider, H.; Saruhan, B.; Voll, D.; Merwin, L.; Sebald, A., Mullite precursor phases. *J. Eur. Ceram. Soc.* **1993,** *11*, 87-94.

25. Okuno, M.; Shimada, Y.; Schmuecker, M.; Schneider, H.; Hoffbauer, W.; Jansen, M., LAXS and ^{27}Al MAS NMR studies on the temperature-induced changes of non-crystalline single phase type mullite precursors. *J. Non-Cryst. Solids* **1997,** *210*, 41-47.

26. Chuang, I. S.; Maciel, G. E., A Detailed Model of Local Structure and Silanol Hydrogen Bonding of Silica Gel Surfaces. *J. Phys. Chem. B* **1997,** *101*, 3052-3064.

27. Atwood, J. L.; Hunter, W. E.; Crissinger, K. D., The synthesis and crystal structure of tetramethylammonium acetatotrimethylaluminate. *J. Organomet. Chem.* **1977,** *127*, 403-414.

28. Hobbs, J. D.; Cygan, R. T.; Nagy, K. L.; Schultz, P. A.; Sears, M. P., All-atom ab initio energy minimization of the kaolinite crystal structure. *Am. Mineral.* **1997,** *82*, 657-662.

29. Liu, W.; Hassan, A.; Wang, S., Novel Oxo-Bridged Blue Luminescent Organoaluminum Complexes: $Al_4(CH_3)_6(\mu_3\text{-}O)_2(dpa)_2$ and $Al_3(7\text{-azain})_4(OCH(CF_3)_2)_2(CH_3)(\mu_3\text{-}O)$ (dpa = Deprotonated Di-2-pyridylamine, 7-azain = Deprotonated 7-Azaindole). *Organometallics* **1997,** *16*, 4257-4259.

30. Thomson, K. T.; Wentzcovitch, R. M.; McCormick, A.; Davis, H. T., A density functional study of sodalite: a new view on an old system. *Chem. Phys. Lett.* **1998,** *283*, 39-43.

31. Gutierrez, G.; Johansson, B., Molecular dynamics study of structural properties of amorphous Al_2O_3. *Physical Review B: Condensed Matter and Materials Physics* **2002,** *65*, 104202/1-104202/9.

32. Turney, J. M.; Sari, L.; Yamaguchi, Y.; Schaefer, H. F., III, The singlet electronic ground state isomers of dialuminum monoxide: AlOAl, AlAlO, and the transition state connecting them. *J. Chem. Phys.* **2005,** *122*, 094304/1-094304/12.

33. Baur, W. H., Silicon-oxygen bond lengths, bridging angles Si-O-Si and synthetic low tridymite. *Acta Crystallographica, Section B: Structural Crystallography and Crystal Chemistry* **1977,** *B33*, 2615-19.

34. Dove, M. T.; Keen, D. A.; Hannon, A. C.; Swainson, I. P., Direct measurement of the Si-O bond length and orientational disorder in the high-temperature phase of cristobalite. *Phys. Chem. Miner.* **1997,** *24*, 311-317.

35. Nyfeler, D.; Armbruster, T., Silanol groups in minerals and inorganic compounds. *Am. Mineral.* **1998,** *83*, 119-125.

36. McGrady, G. S.; Turner, J. F. C.; Ibberson, R. M.; Prager, M., Structure of the Trimethylaluminum Dimer As Determined by Powder Neutron Diffraction at Low Temperature. *Organometallics* **2000,** *19*, 4398-4401.

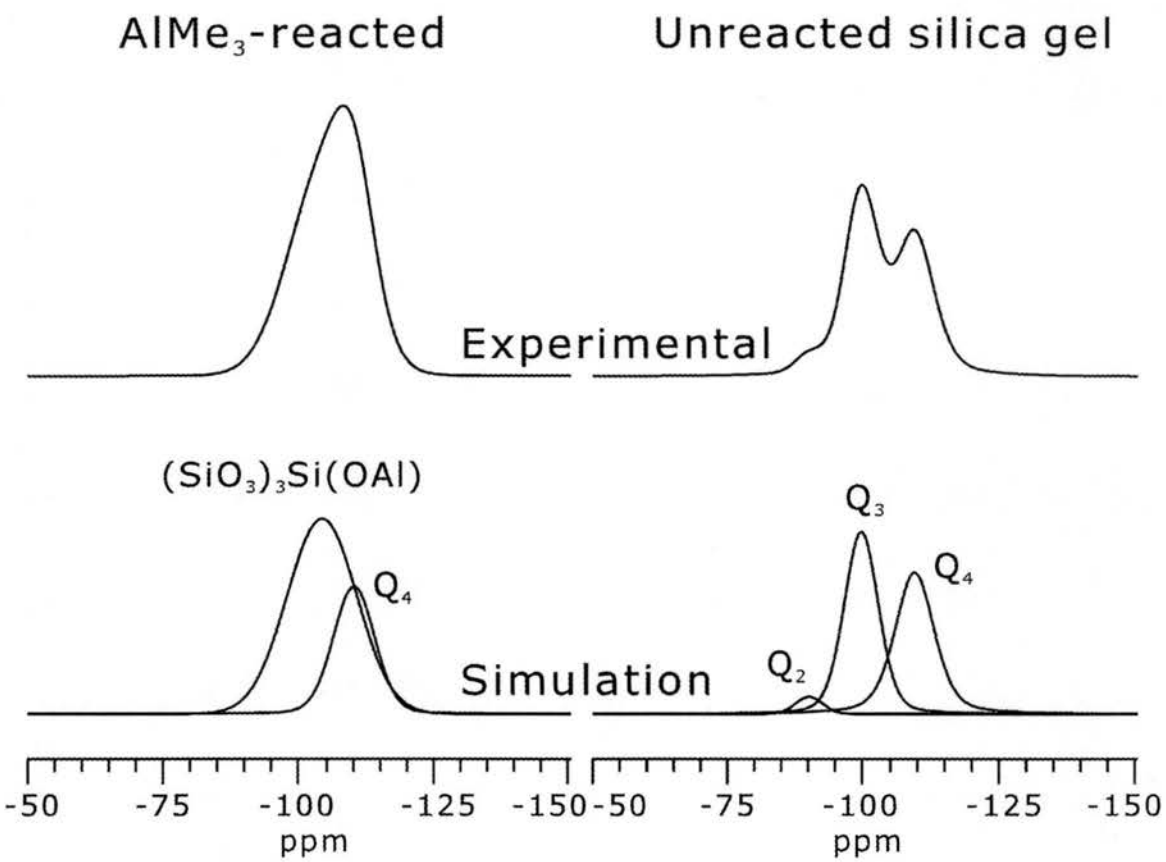

Figure 4.1. ^{29}Si CP/MAS spectra of silica gel and $AlMe_3$-reacted silica and deconvolved/ simulated signals. The $AlMe_3$-reacted silica sample corresponds to sample A in Figure 3.9.

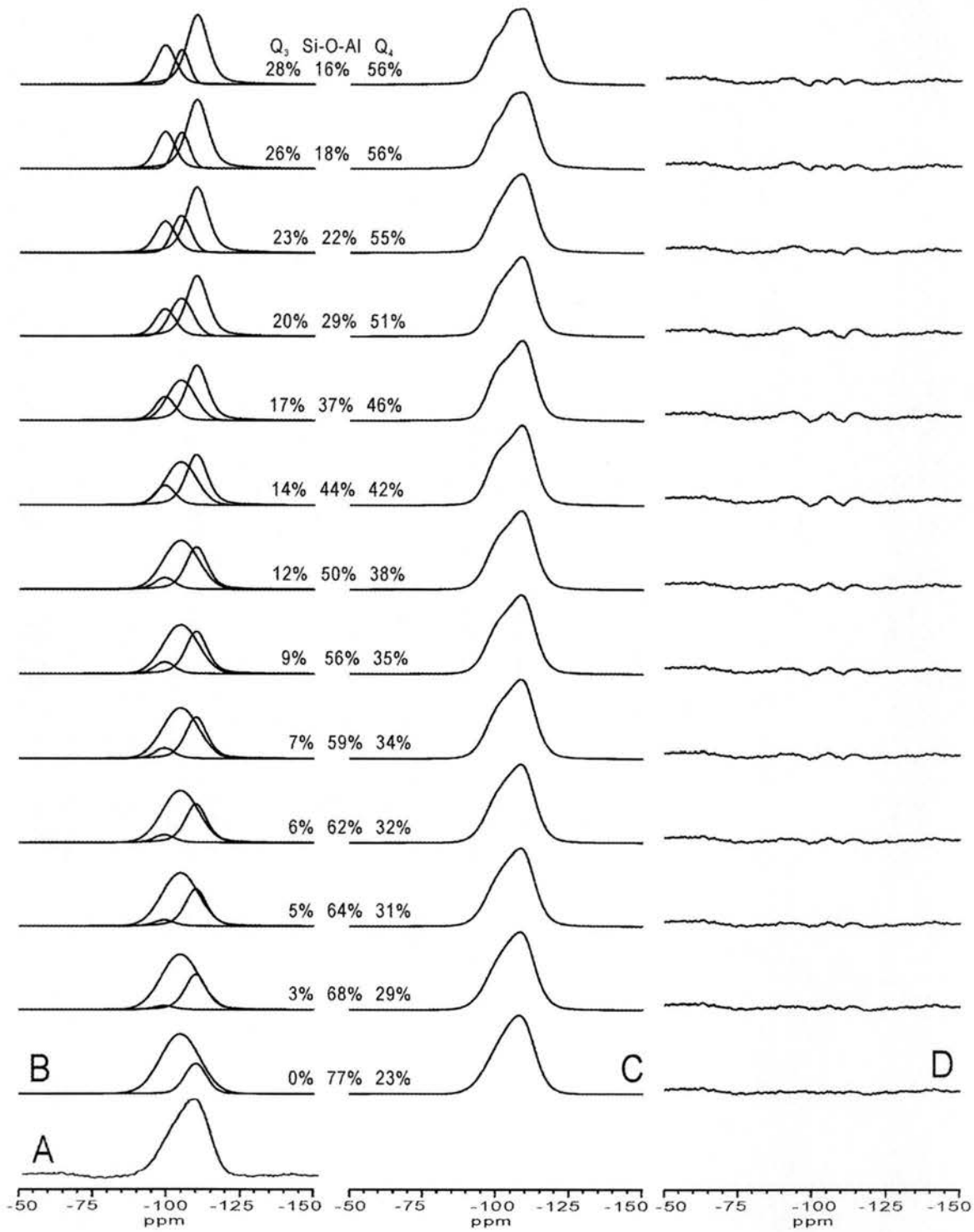

Figure 4.2. Computer simulation of AlMe3-reacted silica: A) experimental spectrum; B) individual components, silanols (-99 ppm), Si-O-Al (-104 ppm) and siloxane (-109 ppm); C) computer simulated spectra; D) difference between simulated and experimental spectra.

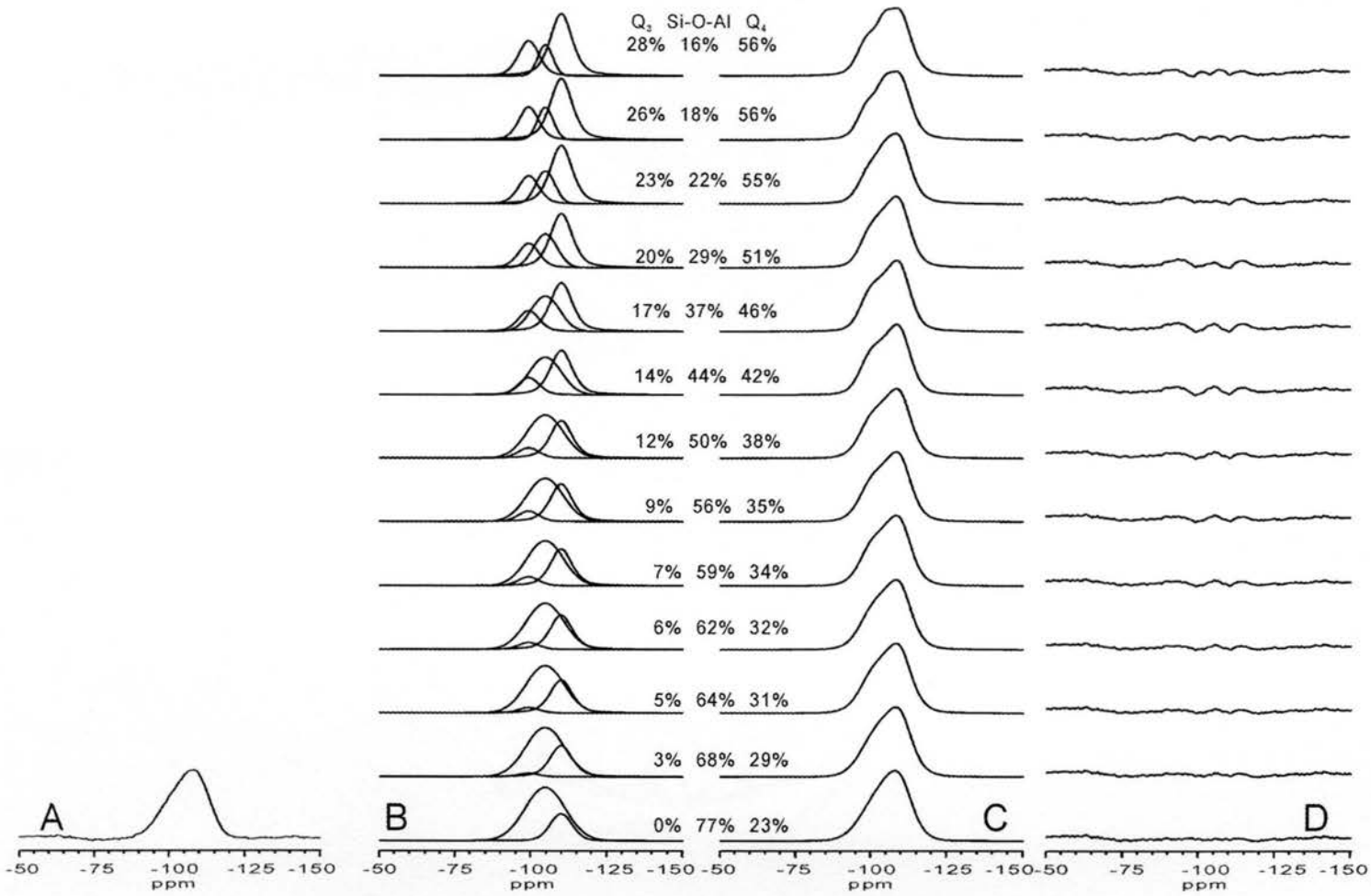

Figure 4.3. Computer simulation of AlMe3-reacted silica: A) experimental spectrum; B) individual components, silanols (-99 ppm), Si-O-Al (-104 ppm) and siloxane (-109 ppm); C) computer simulated spectra; D) difference between simulated and experimental spectra.